A STUDY OF

THE AURORAL ABSORPTION SUBSTORM

A

DISSERTATION

Presented to the Faculty of the

University of Alaska in Partial Fulfillment

of the requirements

for the Degree of

DOCTOR OF PHILOSOPHY

By
Frank Thomas Berkey, B.A., M.S.
College, Alaska
May 16, 1971

A STUDY OF THE AURORAL ABSORPTION SUBSTORM

APPROVED:

R Parthasarathy

Albert E. Belon

Gerald J. Romick for Sd Akasofu

Kenneth W Ruby
Chairman

Roger Sheridan
Department Head

APPROVED: C. J. Schlett DATE: May 17, 1971
Dean of the College of Mathematics, Physical Sciences and Engineering

C. Lee
Vice President for Research and Advanced Study

PLEASE NOTE:

Some pages have indistinct print. Filmed as received.

UNIVERSITY MICROFILMS.

ABSTRACT

The work described herein represents an attempt to better understand the temporal and spatial variations of auroral radiowave absorption. In the first part of this dissertation, the results of an experiment which correlated the variations of auroral light intensity with those in auroral absorption is described. These measurements were carried out over a small angular cone which intercepted an area of less than 400 km^2 at auroral heights. The spatial coherence of auroral absorption and auroral luminosity was examined, as was the correlation of absorption with auroral emission at several wavelengths. It was concluded that the spatial region in which radiowave absorption occurs is of larger dimensions than the visual emitting region. From a large statistical sample, it was demonstrated that absorption correlates best with 4278A auroral luminosity and that the correlation is better during substorm occurrences. The temporal correlation of absorption and luminosity during substorms was illustrated by several examples.

In the second part, a synoptic study of the geographical distribution of auroral absorption during 5 IQSY substorms was undertaken. A cooperative study provided radiowave absorption data from more than 20 observatories in the Northern Hemisphere for this purpose. It was shown that absorption spreads longitudinally from a source located in the midnight sector. The westward expansion of absorption along the auroral oval was documented for the first time. The eastward drift was studied in detail; a differential drift rate with latitude was found, which was also asymmetric with respect to the dawn meridian. The observed drift

rate of precipitation was found to be in agreement with the theoretical calculation of the gradient and curvature drift velocities of energetic electrons in the trapping region. A model of the auroral absorption substorm is proposed.

ACKNOWLEDGEMENTS

There are a large number of people within the Geophysical Institute without whose expertise the completion of this work would not have been possible. Among these people are: Mrs Meg McCoy and the members of the Stenographic Section; Mr Russ Beach and his associates in the Photographic Department; Mrs Shirley Wilson, who prepared many of the drawings, and; the staff of the Data Processing Group, in particular Mr Bob Porter, who initially wrote the data reduction program, and Mr James Dryden who developed the technique for drawing continental outlines on the computer. The assistance and patience of Mr Steve Geller during the development of the contour map program is specially noteworthy. The help of Mrs Jean Lipscomb in many phases of this work must also be noted.

The cooperation of the members of the ESRO Working Group on Auroral Absorption Substorms was essential to the synoptic study of the auroral absorption substorm. It should be noted that for this study the first complete exchange of riometer data was effected. Professor Bengt Hultqvist, of the Kiruna Geophysical Observatory, was instrumental in formulating this exchange and therefore deserves much of the credit for its success. However, considerable work went into the preparation of the riometer data before it could be exchanged and therefore I must acknowledge the following persons: Miss Doris Jelly of the Communications Research Centre, Ottawa; Messers Frank Cowley and Warner Ecklund of the Space Disturbances Laboratory, NOAA; Mr. J. Yliniemi, University of Oulu, Finland; Dr. Olav Holt of the Auroral Observatory, Tromsø; Dr. V. M. Driatsky of the Arctic and Antarctic Scientific Research Institute,

Leningrad; and Mr. Agge Theander of the Kiruna Geophysical Observatory.

I have particularly benefited from the association with, and guidance of Professor S.-I. Akasofu and Professor R. Parthasarathy, as well as many other members of the staff, both past and present, at the Geophysical Institute. Finally, I wish to thank Dr. K. W. Philip for his careful dissection of the manuscript.

The work described in this dissertation has been carried out under the following National Science Foundation grants: GP-947, GP-5540, GA-10127, GA-17663, and GA-11937.

TABLE OF CONTENTS

LIST OF ILLUSTRATIONS

LIST OF TABLES

PREFACE

Of the instrumentation to evolve as a result of the intensive study of the aurora during the IGY, the riometer was perhaps the most elegant. Conceptually simple in design and operation, this instrument can be operated unattended for weeks at a time, yet still provide a continuous measurement of the absorption suffered by a radiowave traversing the ionosphere. Previously, such information could only be obtained from ionospheric soundings, and then only during moderately disturbed periods.

Four distinct categories of absorption phenomena have been recognized: Sudden Cosmic Noise Absorption (SCNA); Sudden Commencement Absorption (SCA); Polar Cap Absorption (PCA); and Auroral Absorption (AA). Whereas SCNA and SCA are infrequent short-lived events associated with either solar flares or sudden commencements, PCA can continue for several days, depending on the intensity of the associated solar proton event. PCA is also characterized by a lack of temporal variation and intense ($\sim$10-30 db) absorption. On the other hand, AA is characterized by the complexity of the temporal variation of the absorption. AA is often defined as that absorption which is not SCNA, SCA, or PCA.

Perhaps the least understood of the four types of absorption phenomena is AA, although the subject has been discussed extensively in the literature (e.g. see review articles by Brown, 1966; Hultqvist, 1966; and Hargreaves, 1969). Recent emphasis in AA studies has been placed on the understanding of the temporal variation of absorption

in terms of the auroral substorm (Akasofu, 1964). In Part I of this thesis, the detailed relationship of auroral absorption and luminosity during a substorm will be examined using photometric, photographic and television techniques. In Part II, we will derive from the geographical distribution of auroral absorption over the northern hemisphere a model of what shall be termed the auroral absorption substorm (AAS). The data for the analysis of the AAS have been made available by the ESRO Working Group on auroral absorption substorms, a consortium of research groups from several countries.

PART I

A STUDY OF THE SPATIAL AND TEMPORAL CORRELATION OF AURORAL ABSORPTION AND LUMINOSITY DURING SUBSTORMS

CHAPTER I

INTRODUCTION

I.1 Historical Review

The anomalous absorption of radio waves in the high latitude auroral ionosphere was first observed by Appleton et al (1933) during the Second International Polar Year. From vertical incidence soundings, Appleton, Naismith, and Ingram (1937) reported that "a 'no-echo' condition was found to accompany magnetic storms and auroral displays at Tromsø, Norway." They concluded that "it is therefore most probable that the effect (of the no-echo condition) is then one of absorption-limitation, the ionizing agency causing the storm being such as to produce ionization at levels below that at which the normal ionization due to ultraviolet light exists."

Harang (1946) was the first to associate radiowave absorption with a specific auroral type; he observed complete absorption during pulsating auroras and attributed the absorption to the lower height (80-95 km) of the "pulsating surfaces". This relationship was investigated more fully by Heppner, Byrne, and Belon (1952) with observations made at College. They found that 72 percent of their ionograms showed complete absorption during pulsating forms of aurora while only 17 percent showed complete absorption during non-pulsating aurora and 13 percent during no-aurora conditions. A similar result was obtained by Major (1954) at Macquarie Island; he found that 62 percent of his ionogram traces recorded during pulsating or flaming auroras showed complete absorption.

Although the vertical incidence sounder technique established a qualitative relationship between the aurora and the absorption of radiowaves, no quantitative relationship was derived until after the application of the cosmic radio noise technique (Dicke, 1946; Machin, Ryle, and Vonberg, 1952) to high latitude radiowave absorption studies (Little, 1954). The riometer (Relative Ionospheric Opacity Meter) is a narrow bandwidth radio astronomy receiver which utilizes the natural background emission of electromagnetic radiation by the galaxy as a stable transmitter whose diurnal variation can be accurately determined. Increases in the ionization of the D-region and hence in the absorption of the galactic radiowave noise, lead to a decrease of the received noise at the riometer. This decrease of noise can be expressed in decibels of ionospheric absorption relative to the undisturbed level (Little and Leinbach, 1959).

The antenna system most commonly employed with a riometer is a three element Yagi (Uda and Mushiake, 1954) directed either toward the zenith or toward the pole star. In the latter case, the diurnal variation can be removed from the cosmic noise signal. The main lobe of the Yagi antenna subtends an elliptical area of roughly 110 by 240 kilometers when projected onto the ionosphere at the 100 kilometer level. While the east-west extent of auroral arcs is generally on the order of hundreds of kilometers, the north-south dimension may be only a few hundred meters (Maggs and Davis, 1968). Thus, an auroral form may fill only a small fraction of the Yagi antenna pattern thereby complicating quantitative studies between the aurora and

Table I

A Summary of Correlated Studies of Auroral Absorption and Luminosity

Reference	Frequency (MHz)	Optical Wavelength (A)	Antenna Half-Power Beamwidth N-S	Antenna Half-Power Beamwidth E-W	Photometer Field of View	Antenna Sidelobe Level	Antenna Type	Photometer Calibration	Corrected Geomagnetic of Latitude Observation	Other Detectors
Little & Leinbach (1958)	30.5	none	15°	60°	-	not given	8 full wave dipole array	-	64.9°	Standard riometer system
Holt & Omholt (1962)	27.6	5577	30°	30°	5°	not given	single Yagi	relative	~66.1	All-sky camera
Graf (1960) Kavadas (1961)[1]	30	none	6.5°	72°	visual observations	6 db	16 element dipole array	-	61.5	-
Johansen (1965)	27.6	5577	30°	30°	5°	not given	single Yagi	absolute	66.1	All-sky camera
Ansari (1965)[1]	36	5577	10°	12°	6°	4-6 db	4x4 Yagi array	reference to dark current	64.9	All-sky camera Magnetometer
Eather & Jacka (1966)	27.6	5577 4861	27°	46°	23°	13 db	4x2 dipole array	absolute	-70.3	All-sky camera Magnetometer 77MHz Riometer/Ionosonde
Berkey (1968)[1]	36	4278 4861 5577	7°	8°	7°	13-14 db	6x8 Yagi array	absolute	64.9	All-sky camera Magnetometer Standard riometer system
Gustafsson (1969)[2]	27.6	5577 6300 4861 4709	30°AZ	25°EL	10°	12.6 db	2x3 Yagi array	absolute ?	64.3	All-sky camera
Reid (1970)[3]	32		45°	3°	-	9 db	28 full wave dipole array	-	-64.6	
Berkey[1]	36	4059 4278 5577 5294	7°	8°	7°	13-14 db	6x8 Yagi array	absolute	64.9	All-sky camera Magnetometer TV System

[1] These experiments used electrically phased arrays to change the main lobe direction

[2] Antenna mounted on rotating boom

[3] Two beams 4° east and west of zenith simultaneously monitored

auroral radiowave absorption. This complication led quite naturally to the construction of large aperture antenna arrays having main lobe beamwidths of only a few degrees; the research groups involved in such studies are listed in Table I.

1.2 *Review of Previous Results*

At College, Little and Leinbach (1958) compared the absorption measured by an array with a beamwidth of 15° by 60° to that measured by a three element Yagi antenna. On the basis of the equality of the absorption as recorded by the two antenna systems, they concluded that "isolated regions of absorption having dimensions of the order 50-150 kilometers did not occur overhead during the period of observation."

Using a 16 element phased array, Graf (1960) was able to monitor the absorption in different directions. He alternately switched his 6.5° by 72° main lobe between a position 3° north of the zenith and 3° south of the zenith. As a result of the high degree of correlation of absorption in the two directions (0.94), he inferred that the north-south extent of the absorbing region exceeded 80 kilometers. He found no relation between auroral absorption and intensity of aurora; in fact he reported several cases in which absorption occurred without visual auroral forms being in the field of view of the antenna pattern. Based on these observations, he suggested that "absorption took place at a height which was appreciably less than the height at which aurora occurred."

Ansari (1963, 1964) conducted the first experiment correlating auroral luminosity and absorption over a spatially limited field of view (10° by 12°). Although his measurements were contaminated by large sidelobe contributions to the cosmic noise signal, he identified two characteristic phases of the auroral storm. He defined category I events, occurring between 20^h and 02^h local time, as those in which the absorption was "limited to luminous regions of the sky." He found a high degree of correlation between the fluctuations of absorption and luminosity during this time, although no statistical relations were given. During category 2 events (after 02^h LT), he observed that the ratio of absorption to luminosity had increased by a factor of 10 to 100 relative to category I events, although again no numerical or statistical relations were derived. Ansari calculated theoretically the absorption produced by electrons having a range of energies; from these calculations, he postulated that category I events were produced by electrons of energy less than 20 kev, while category 2 events were due to electrons with energies from 30-100 kev. No attempt was made to explain how the absorption occurring at 70-90 kilometers resulted from the precipitation of 20 kev electrons. It should also be noted that on the basis of a single example, Ansari (1963) concluded that "pulsating aurora luminosity was not associated with any significant increase in absorption."

The results of Eather and Jacka (1966) observing at Mawson Base (70.3°S CGM) but using an array with a larger field of view (27° by 46°) essentially confirmed the observations of Ansari. They concluded

that "in the breakup and prebreakup phases of auroral activity, absorption takes place only in the region of the sky of the aurora." They observed no cases in which absorption occurred without aurora (as determined by photometer recordings) in the field of view of the riometer antenna. They also found that the ratio of absorption to luminosity increased by a factor of 100 during the post-breakup phase, but provided no examples of such a large increase of this ratio. They derived a correlation coefficient of 0.58 between the absorption and the square root of 5577A luminosity during breakup events and a correlation of 0.31 during the postbreakup phase when the absorption was slowly varying.

At Kiruna (64.7°N CGM), Gustafsson (1969) used a Yagi array mounted on a rotating boom (1 revolution per 2.6 minutes) to investigate the ratio of absorption to the square root of 5577A luminosity. He observed a hardening of the electron spectrum (inferred from the ratio $A(dB)/\sqrt{I_{5577}}$) between 15^h and 05^h LT which he interpreted in terms of the location of Kiruna with respect to the precipitation pattern of soft and hard electrons as observed by satellite. There was, however, no determination of the ratio as a function of antenna azimuth which would support his interpretation.

Johansen (1965) determined the ratio of absorption (as measured using a Yagi antenna) to the 5577A luminosity from a 5° field of view. Although the experimental technique restricted his observations to "cases when most of the sky was covered fairly homogeneously by aurora" he inferred a hardening of the electron spectra between 20^h and 01^h local time (MET).

1.3 Purpose of the Observational Program

The observations of auroral absorption and auroral luminosity to be discussed in this thesis are unique in that the viewed volume is of small angular dimension (~3.5° half-angle). The spatial coincidence allows for a detailed correlation between absorption and luminosity occurring within a small area (~380 km^2) of the auroral ionosphere. In the chapters that follow, auroral substorms which occurred on more than 40 nights during the winter of 1966-67 will be studied in detail. The results from observations made the previous winter (Berkey, 1968) will be referred to where they are pertinent and complement the present work. Using the collection of data resulting from these observations, the following problems will be considered:

(a) the spatial extent of the region in which absorption occurs relative to the region of auroral emission;

(b) the correlation of auroral absorption with various emission lines of the auroral spectrum;

(c) the quantitative relation of absorption to auroral luminosity;

(d) the assumption of quasi-equilibrium in the auroral ionosphere;

(e) the diurnal variation of the precipitated electron spectrum as determined by the ratio $A(db)/\sqrt{I(kR)}$;

(f) the spectral variations during the auroral substorm;

(g) the qualitative relation of absorption to luminosity during various phases of the auroral substorm;

(h) the qualitative relation of absorption and luminosity during the polar magnetic substorm.

An extensive amount of statistical analysis was done with the available data; such analysis provided a basis upon which inferences relative to problems (a) - (e) were drawn. The graphical display of the data in combination with all-sky camera and television data provided information toward a better understanding of those problems listed in (f) - (h).

CHAPTER 2

INSTRUMENTATION AND DATA PROCESSING

2.1 Physical Description of Array

The large aperture antenna array used in this experiment was designed by Ansari (1965) and consists of 48 three-element Yagi antennas arranged in a 6 by 8 configuration. The array was designed so that the main lobe could be switched between two directions in the meridian plane by electrically inserting various lengths of coaxial cable. The half-power beamwidth of the main lobe is 7° in the E-plane and 8° in the H-plane; the first lobes are approximately 13 decibels down from the main lobe peak. Additional parameters of the array are listed in Table II. Figure 2.1(a) illustrates the array pattern in the E-plane; Figure 2.1(b) shows the array pattern when the beam is directed 6° north of the zenith, and Figure 2.1(c) illustrates the array pattern in the H-plane.

2.1.1 Derivation of array pattern

The theoretical array patterns illustrated in Figures 2.1(a), 2.1(b), and 2.1(c) were derived using the principle of pattern multiplication (Kraus, 1950). To analytically express the beam pattern of a three-element Yagi antenna, a typical Yagi pattern (AARL Antenna Handbook, 1968) was scaled at five degree intervals and approximated using a 15 term Fourier expansion. Next, the principle of pattern multiplication was applied; the Fourier expansion of the Yagi pattern was multiplied by the appropriate "array factor" (Kraus, 1950) to obtain the array pattern. This calculation

TABLE II

ANTENNA PARAMETERS

E-plane (N-S pattern)		
Major lobe	half power beam width	7°
	first null beam width	16°
	fraction of power intercepted[1]	62 percent
Largest minor lobe	amplitude below main lobe peak	13.1 dB
	half power beam width	4°
	first null beam width	8°
	fraction of power intercepted[1]	17 percent
Minor lobes	null location	16°, 24.5°, 33.7°, 44°
	peak location	11.5°, 20°, 28.5°, 38°
	amplitude of largest lobe	17.7 dB
H-plane (E-W pattern)		
Major lobe	half power beam width	8°
	first null beam width	17.5°
Largest minor lobe	amplitude below main lobe peak	12.7 dB
	half power beam width	4.5°
	first null beam width	8.6°
Minor lobes	null location	17.5°, 27°, 37.4°, 49.5°
	peak location	12.5°, 22°, 32°, 42.7°
	amplitude of largest lobe	17.1 dB

[1]Calculation assumed circular symmetry of E plane

Figure (2.1a)

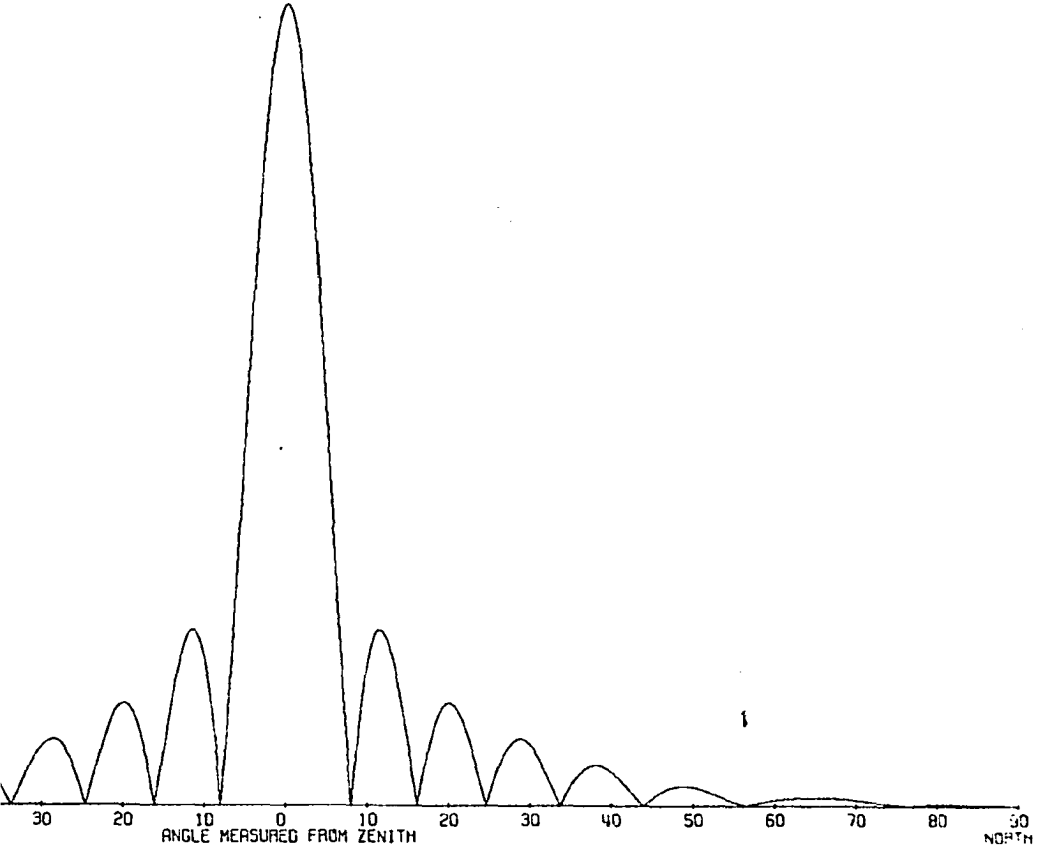

E-plane lobe configuration for 6 x 8 Yagi array with main beam in zenithal position.

Figure (2.1b)

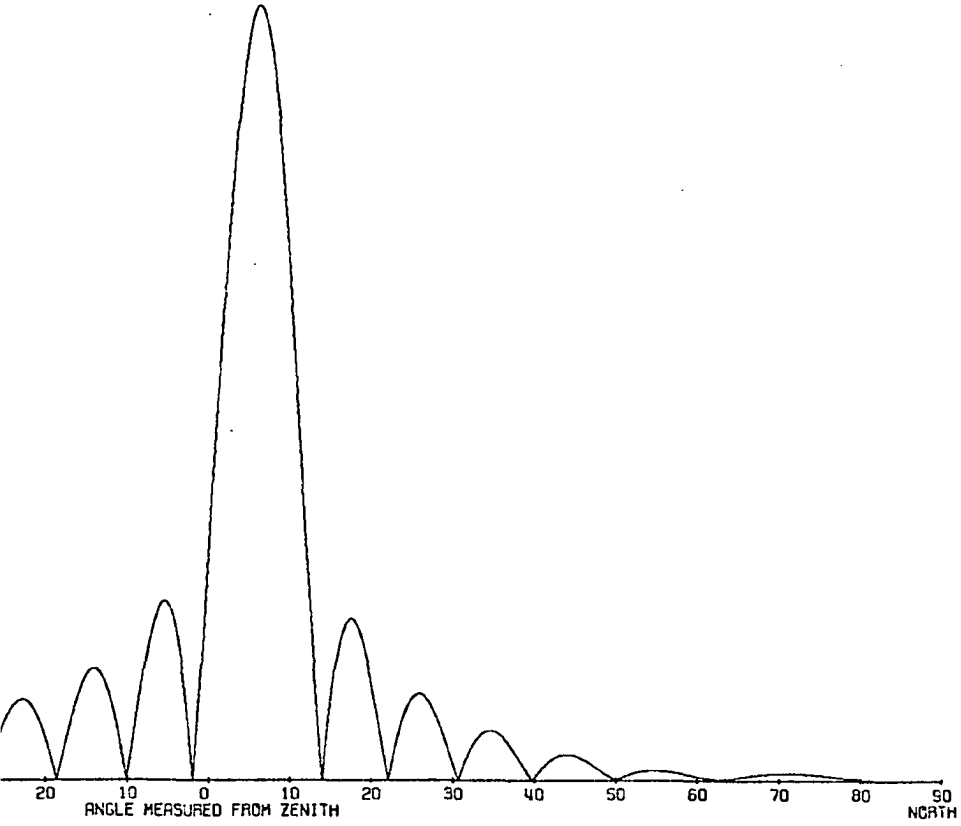

E-plane lobe configuration for 6 x 8 Yagi array with main beam directed 6° North of zenith.

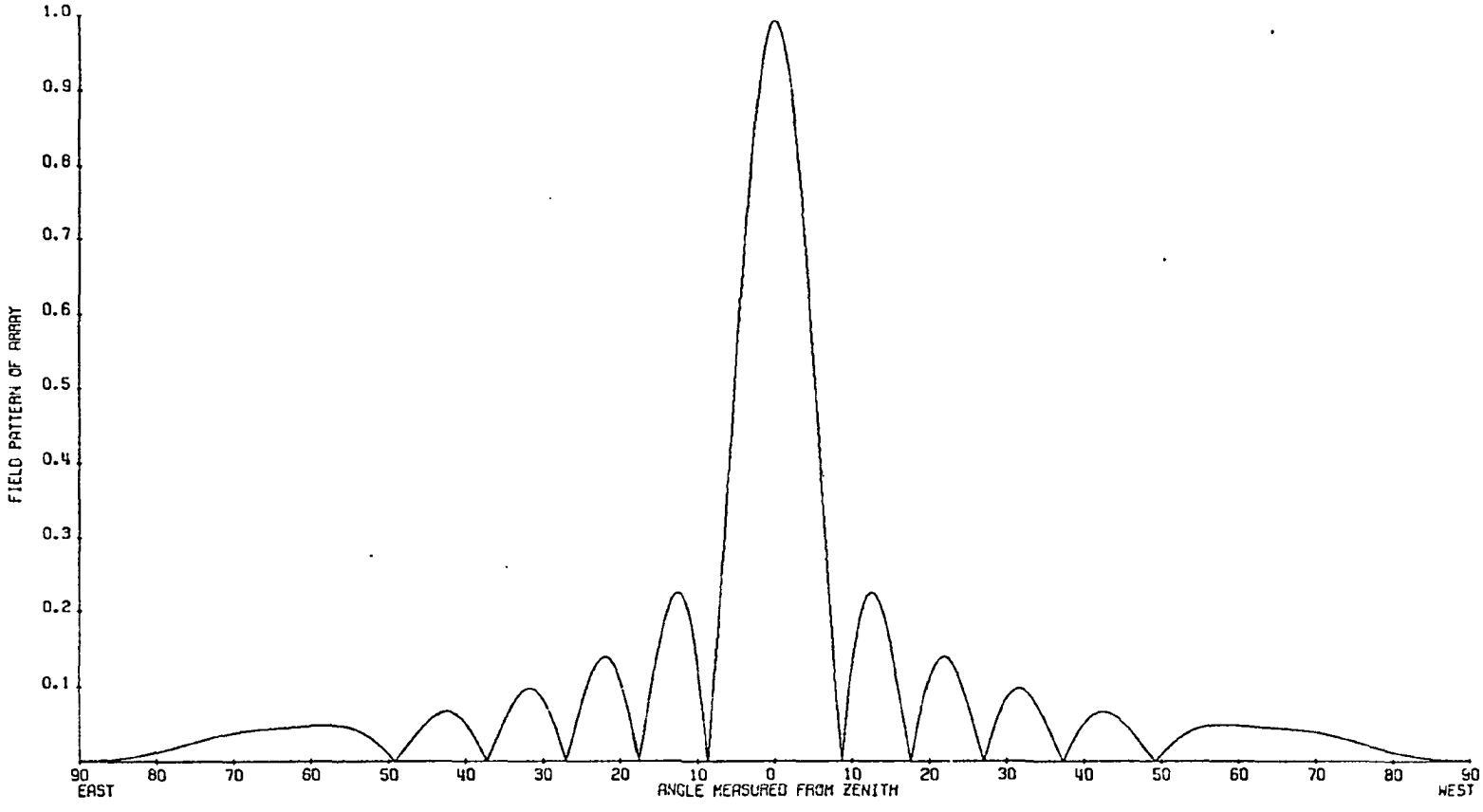

Figure (2.1c) H-plane lobe configuration for 6 x 8 Yagi array.

was carried out in 0.1° steps on a digital computer which was used to generate the array patterns on a CalComp digital increment plotter.

2.1.2 Beam efficiency

An important parameter of large aperture antenna arrays is the beam efficiency factor, which has been defined by Nash (1964) as

$$\eta = \frac{\int_{\Omega_o} F(\theta,\phi)d\Omega}{\int_{4\pi} F(\theta,\phi)d\Omega} \leq 1$$

where $F(\theta,\phi)$ = normalized antenna power pattern, $d\Omega = \sin\theta d\theta d\phi$, Ω_o = main beam solid angle. Assuming circular symmetry of the E-plane, a beam efficiency factor of 0.62 was derived for the main beam of the Yagi array used in this investigation. The percentage of the total power incident on the array and intercepted by the minor lobes is given in Table II.

Although this factor is often neglected in auroral absorption investigations utilizing large aperture arrays, it is the parameter which determines the upper limit to the amount of absorption which can be interpreted as being the contribution from the main lobe. In the case of the 6x8 Yagi array, total absorption occurring within the solid angle of the main beam would result in a recorded absorption of 4.2db by a riometer connected to the array. While it is unlikely that total or infinite absorption would occur solely within the solid angle of the main beam, the ramifications of the beam efficiency on the interpretation of the data are important. Absorption events whose magnitude exceed 4-5db imply that the spatial extent of the absorbing region is greater than the area intercepted by the main lobe. In

other words, the absorbing region obscures minor lobes which are situated at a larger zenith angle than the main beam.

2.1.3 Discussion of small angular measurements of absorption

To emphasize the need of using an antenna beamwidth comparable to the spatial dimensions of the aurora, consider the following situation; assume that a flux of energetic electrons creates D-region ionization which completely absorbs the galactic radiowave emission and at the same time produces an IBC-III aurora (100kR). Next, assume that the riometer system which is monitoring this disturbance is connected to an antenna system the major lobe of which is completely filled by the aurora and which intercepts 80 percent of the total power incident upon the array. At this time, the riometer will record 7db of absorption and the ratio $A/\sqrt{I} = 0.7$. Now, if the geometry of the aurora were to change such that only 50 percent of the antenna beam pattern and the photometer field of view (assumed equal) were filled by the auroral form, the photometer will register 50kR intensity and the riometer will indicate 2.2db absorption. In this case the ratio $A/\sqrt{I} = 0.3$, less than half of the previous value. Thus it is important to note that a change in the ratio $A/\sqrt{I}$ may result from either a change in auroral geometry or variations of auroral intensity or absorption. For small fields of view it is difficult to distinguish between these two causes, particularly during active aurora. However, utilization of as small a beamwidth as practicable is necessary to achieve physically meaningful results.

2.2 Experimental Configuration 1965-1966

During the 1965-66 observing season (hereafter called season I) two identical riometer and photometer systems were operated and the main lobe beam position was alternately switched between the 6° north and 6° south (of zenith) positions. During this period the 4278A, 4861A, and 5577A auroral emission lines were monitored and the ratio $A/\sqrt{I_{5577}}$ derived from the observations. Auroral luminescence was detected by photometers which used IP21 photomultiplier tubes and logarithmic amplifiers. Filter bandwidths were nominally 10A, and the filters were manufactured by Thin Films Corporation.

2.3 Experimental Configuration 1966-1967

The main lobe was fixed in the zenithal position (see Figure 2.2) beginning in September 1966 and remained in that position throughout the 1966-67 observing season (season II). The Second Positive band emission of nitrogen near 4059A and the First Negative band emission of oxygen at 5294A were additional features monitored during this phase of the study. Two 50A bandwidth filters were mounted in series to monitor the 4059A emission, while a single 50A bandwidth filter was used in monitoring the 5294A band emission. The H_β emission of hydrogen at 4861A was not observed during this phase of the study.

Tube type riometers constructed during the IGY were utilized during the greater part of the observations. However, after March 1967, an EMI model 123 riometer, the transistorized version of the IGY riometer, was used.

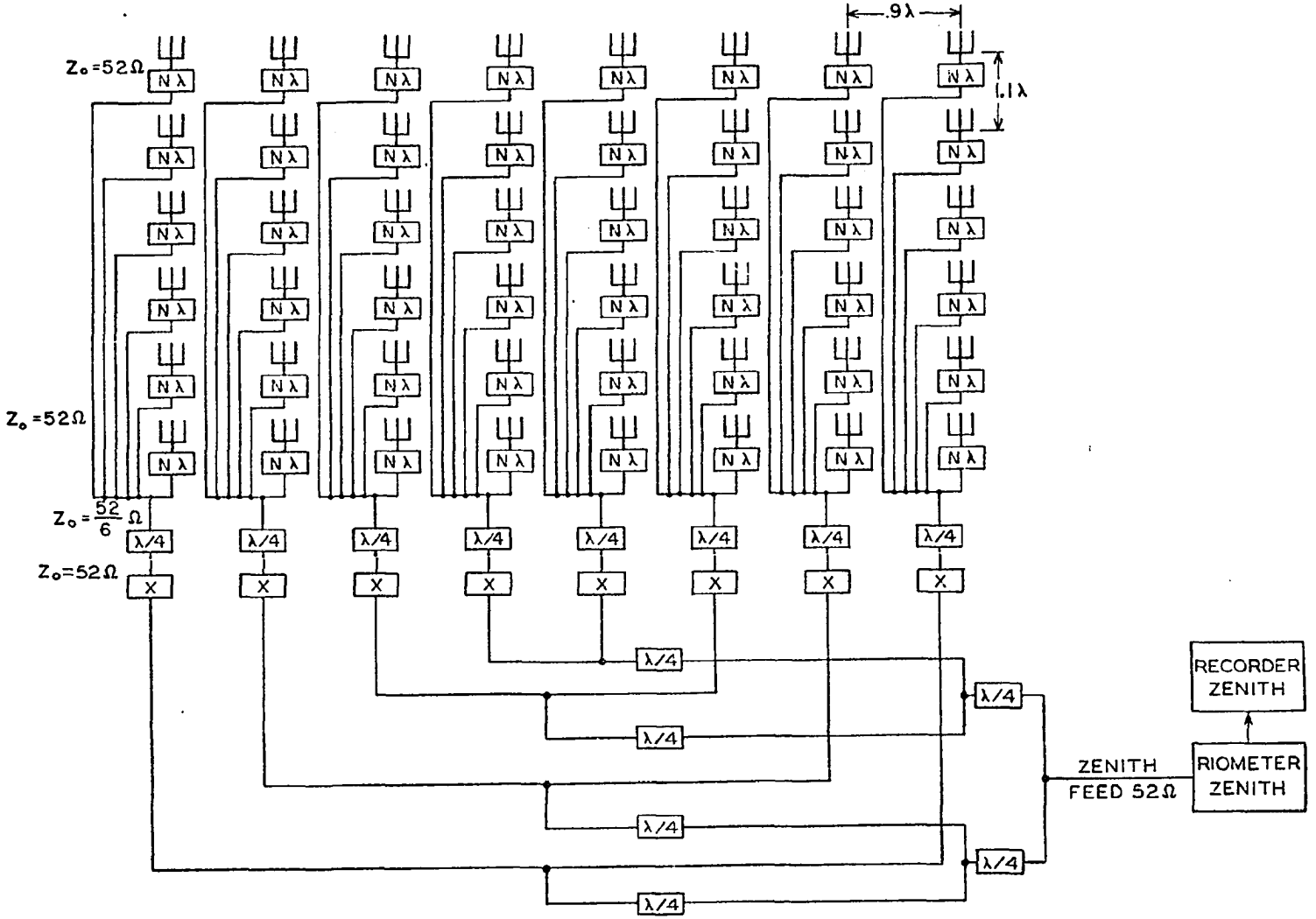

Figure (2.2) Schematic diagram of 6 x 8 Yagi array with cable phasing adjusted for zenithal position of main lobe.

2.4 Emission Lines Monitored

Auroral emission lines or bands at 4059A, 4278A, 4861A, 5294A, and 5577A were monitored during the two observing seasons discussed in this study; the basic excitation processes are outlined below.

The 4278A emission is a First Negative band of nitrogen excited directly by the bombardment of energetic electrons. Similarly, excitation of atomic oxygen at auroral heights produces a prominent emission line at 5577A. Both of these emissions are characteristic of the auroral spectrum and the intensity of either can, on occasion, reach 1000kR.

The H_β emission at 4861A is excited by precipitated protons; the intensity rarely exceeds 1 kilorayleigh. The (2-0) transition of the First Negative system of O_2^+ with band head near 5295A is a faint emission whose absolute intensity has not been accurately measured. However, Shemansky (1966) has theoretically derived an intensity of 6.8kR for this emission during an IBC III type-B aurora. An enhancement of the O_2^+ First Negative group during type-B red aurora has been reported by Shemansky and Vallance Jones (1968) as well as others.

A second emission band, also thought to be associated with type-B aurora, is the (0-3) transition of the Second Positive system of nitrogen at 4059A (see Figure 2.3). The origin of the Second Positive system is not well known, and several processes have been postulated: Gadsen (1961) suggested an ion-exchange process

$$N_2^+ (X^2\Sigma) + O^- \rightarrow N_2(C^3\pi) + O(^1D)$$

where the First Positive band system arises from electron impact

Figure (2.3) Spectrogram of the near-ultraviolet region obtained with a 0.8A spectral slit width on 24/25 May 1955 (after Vallance-Jones, 1965).

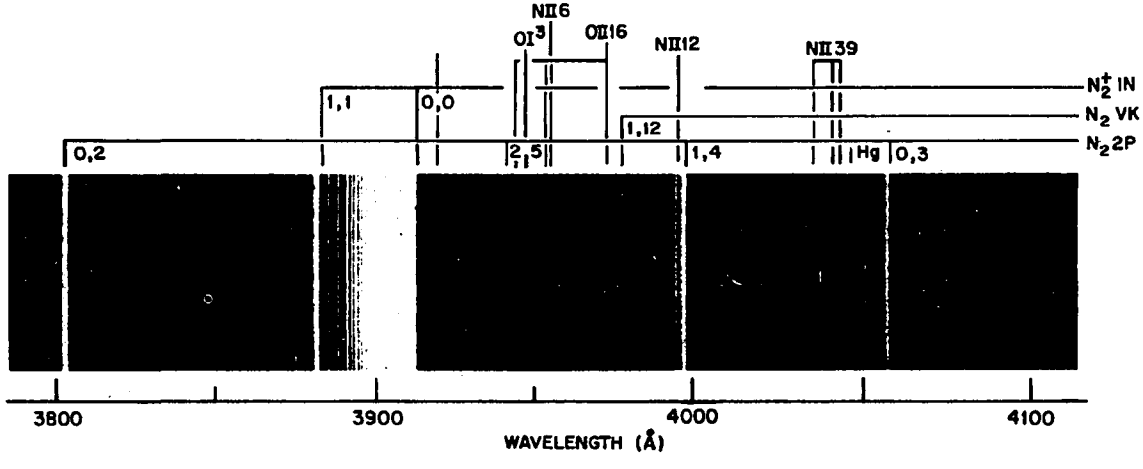

(Malville, 1959):

$$N_2 + e \rightarrow N_2^+ + e + e$$

$$e + O_2 \rightarrow O_2^-$$

$$N_2^+(X^2\Sigma) + O_2^-(\pi) \rightarrow N_2(B^3\pi) + O_2(^3\Sigma)$$

However, Eftestøl and Omholt (1965) have criticized Gadsen's process, pointing out that such processes must build up gradually in order to establish a significant positive and negative ion density. Shemansky (1966) suggests that the most likely excitation process is electron impact with the N_2 molecule in the electronic ground state. This process proceeds

$$N_2\ (X^1\Sigma) + e \rightarrow N_2(C^3\pi) + e$$

Low (1966) suggested that X-rays may account for nitrogen excitation, particularly in the lower region of the aurora. Broadfoot (1963) has pointed out that the (0-3) transition is surrounded by strong emissions and seems to be sitting on a considerable background.

Among spectroscopists, considerable controversy exists relative to the enhancement of the First Positive system in type-B aurora. Hunten (1955) reported that the red color of type-B was due to O_2^+ 1NG and N_2 1PG in "about equal proportions". Evans and Vallance Jones (1965) observed a 22-55% increase in the ratio N_2 1PG/3914A during type-B aurora. They suggest the process

$$N_2(a^1\pi) + e \rightarrow N_2(B^3\pi) + e$$

which would "become more effective with decreasing height and therefore lead to the enhancement of type-B aurora." On the other hand, a careful study of type-B aurora performed by Shemansky and Vallance Jones (1968)

at Saskatoon led to the conclusion that the N_2 IPG was not enhanced in type-B aurora.

Type-B red aurora is characterized by a purplish red lower border (Størmer, 1955). Due to the active nature of this type of aurora, very few accurate height measurements have been made. Harang and Bauer (1932) reported a lower border height of less than 70 km while Currie (1955) has reported a measurement of 74 $\pm$ 3 km. Since normal auroras occur in the height range 100-130 km, the occurrence of aurora at 70-80 km would suggest that such aurora might be more closely correlated with auroral radio-wave absorption. The existence of such a relationship will be examined in this thesis.

2.5 Data Processing Technique

The Esterline-Angus chart recordings, on which the original signals from the riometer and photometer were recorded, were scaled using the OSCAR scaling device. The OSCAR transferred the data to computer cards for input to the University IBM 360/40. During the periods of activity selected for study, the data were scaled at 2.5 minute intervals (season I) or 1 minute intervals (season II).

A computer program was developed to provide the following output: (1) absolute magnitude of absorption in decibels; (2) absolute photometer intensities in kilorayleighs; (3) the ratios A/I, $A/\sqrt{I}$, 4278/5577, 4059/4278; (4) the mean of recorded values for each sensor for each hour; (5) the standard deviation for each sensor for each hour; (6) the correlation coefficient for the relation A/I; (7) the correlation coefficient for the relation $A/\sqrt{I}$;

(8) a least squares linear and power-law fit between each photometer output and the absorption for each hour; (9) data storage on magnetic tape; (10) graphical output when the standard deviation of the absorption exceeded 0.4 db or if the standard deviation of the 4278A intensity for the previous hour exceeded 1.2kR. The last option insured graphical output only during periods of disturbance.

A second computer program was developed to analyze the magnetic tape recorded during the analysis phase of the project. The outputs from this program were as follows: (1) for a given UT hour and emission line, the mean and standard deviation of the ratio $A/\sqrt{I}$; (2) for the total data sample and each emission line, the correlation coefficient based on the assumptions $A \propto I$ and $A \propto \sqrt{I}$; (3) the linear and power-law least-squares fit between absorption and luminosity. The program also allowed for certain conditions to be imposed on the data and results derived therefrom.

2.6 The Quiet-Day Curve

Due to frequent variations in the quiet-day level, resulting from changes in the resonant frequency of the antenna array, no single quiet-day curve was utilized throughout the study. Instead, the month of October 1966 was used as a reference level and a quiet-day curve derived by one of two methods from that level. The first method was to determine the level of the nearest quiet day and to adjust the reference quiet-day curve accordingly. The second method involved determining the average absorption of the first hour of the night under study. If the average absorption deviated more than $\pm$ .25db

from the reference quiet-day level, then the whole reference level was corrected (by adding or subtracting a small value of noise current) until the average absorption fell within these limits. Normally the first hour of the night corresponded to some hour between 03^h and 05^h UT, the time at which the least amount of absorption occurs at College (Hook, 1968). This latter method was incorporated in the computer program and required only a few seconds of execution time.

2.7 Derivation of the Ratio $A/\sqrt{I}$

A parameter which will be used extensively throughout this study to indicate change (hardening or softening) in the spectrum of precipitated electrons is the ratio $A(db)/\sqrt{I(kR)}$. Application of this ratio is based on the premise that equilibrium is rapidly established in the auroral ionosphere. To express this assumption quantitatively, the term representing the rate of change of electron density in the ionospheric continuity equation is set equal to zero:

$$dN_e/dt = 0 = q/(1+\lambda) - \alpha N_e^2$$

which becomes upon rearrangement

$$N_e = \sqrt{q/(1+\lambda)\alpha} = \sqrt{q/\alpha_{eff}}$$

where q = electron production

λ = negative-ion to electron ratio

α = recombination coefficient

$(1+\lambda)\alpha$ = effective recombination coefficient

N_e = electron density.

Next, consider the effect of enhanced ionization upon the passage of a radiowave through the ionosphere; the electric field of

the radiowave will impart a sinusoidal motion to the electrons and ions in the region under consideration. Such ordered motion, superimposed on the thermal velocities (random motion) of these particles, will be reradiated in toto unless the particles undergo collisions. With each collision, some of the energy imparted to the electron or ion by the radiowave will be lost and less energy re-radiated. In the D-region, much of the energy imparted to the electrons will be lost as a result of dense ionization and the collisions between the resulting electrons and neutral particles; thus the radiowave signal will be attenuated due to energy absorbed from it in passing through this region. From this simple physical description it can be seen that radiowave absorption is proportional to the free electron density and the collision frequency in the ionosphere.

At auroral heights, excitation of visual emission results from the impact of an energetic electron with a molecule. The intensity, I, of the visual emission is proportional to the integral with respect to height of the electron production rate, q. Now, using the expression derived from the continuity equation for equilibrium and recalling that absorption is proportional to electron density we find:

$$A \propto N_e = \sqrt{q/\alpha_{eff}} \propto \sqrt{I}$$

or $$A/\sqrt{I} = c$$

where the constant c is a function of the electron flux parameters (see Ospiv et al., 1968).

Electrons capable of ionizing atmospheric constituents in the D-region (50-90km) must have energies greater than about 30kev (Rees,

1964) while less energetic (1-10kev) are involved in the excitation of auroral emissions (McIlwain, 1960). Thus it can be stated with some certainty that the variations of the ratio $A/\sqrt{I}$ reflect changes in the spectrum of electrons precipitated into the auroral ionosphere.

This derivation and the first investigation of the behavior of the ratio $A/\sqrt{I}$ was made by Johansen (1965). Ospiv et al. (1968) developed the derivation in somewhat greater detail and showed that the ratio is less sensitive to the form of the assumed spectrum than to the choice of the recombination coefficient.

CHAPTER 3

STATISTICAL RESULTS

3.1 Diurnal Variation of Auroral Spectrum

In Chapter 2 it was shown that the ratio $A(db)/\sqrt{I(kR)}$ can be used to infer variations in the spectrum of electrons precipitated into the auroral ionosphere. The diurnal variation of the spectrum was obtained by deriving the mean value of the ratio $A/\sqrt{I}$ for each UT hour and each of the three emission lines monitored during season II. These results are illustrated in Figure 3.1(b), 3.1(c), and 3.1(d).

There is no essential difference between the diurnal variation for the ratio $A/\sqrt{I}_{5577}$ and that for $A/\sqrt{I}_{4278}$: a broad minimum, or softening of the spectrum, occurs between approximately 07^h and 12^h UT ($21\text{-}02^h$ LT); the ratio gradually increases (spectrum becomes harder) toward dawn and is also higher at twilight. On the other hand, the diurnal variation of the ratio $A/\sqrt{I}_{4059}$ does not exhibit a minimum, but increases gradually from dusk to dawn. It does imply, however, that the ratio of 4278A intensity to 4059A intensity is much less during aurora which occurs immediately after twilight than during aurora which occurs at other times during the night. The average absorption was derived for each UT hour and is shown in Figure 3.1(a); this result is not intended to be representative of the diurnal variation of absorption at College, since only periods of disturbance were analyzed.

The results presented in Figure 3.1(b) can be compared with Figure 3.2 in which the diurnal variation of the ratio $A/\sqrt{I}_{5577}$ obtained

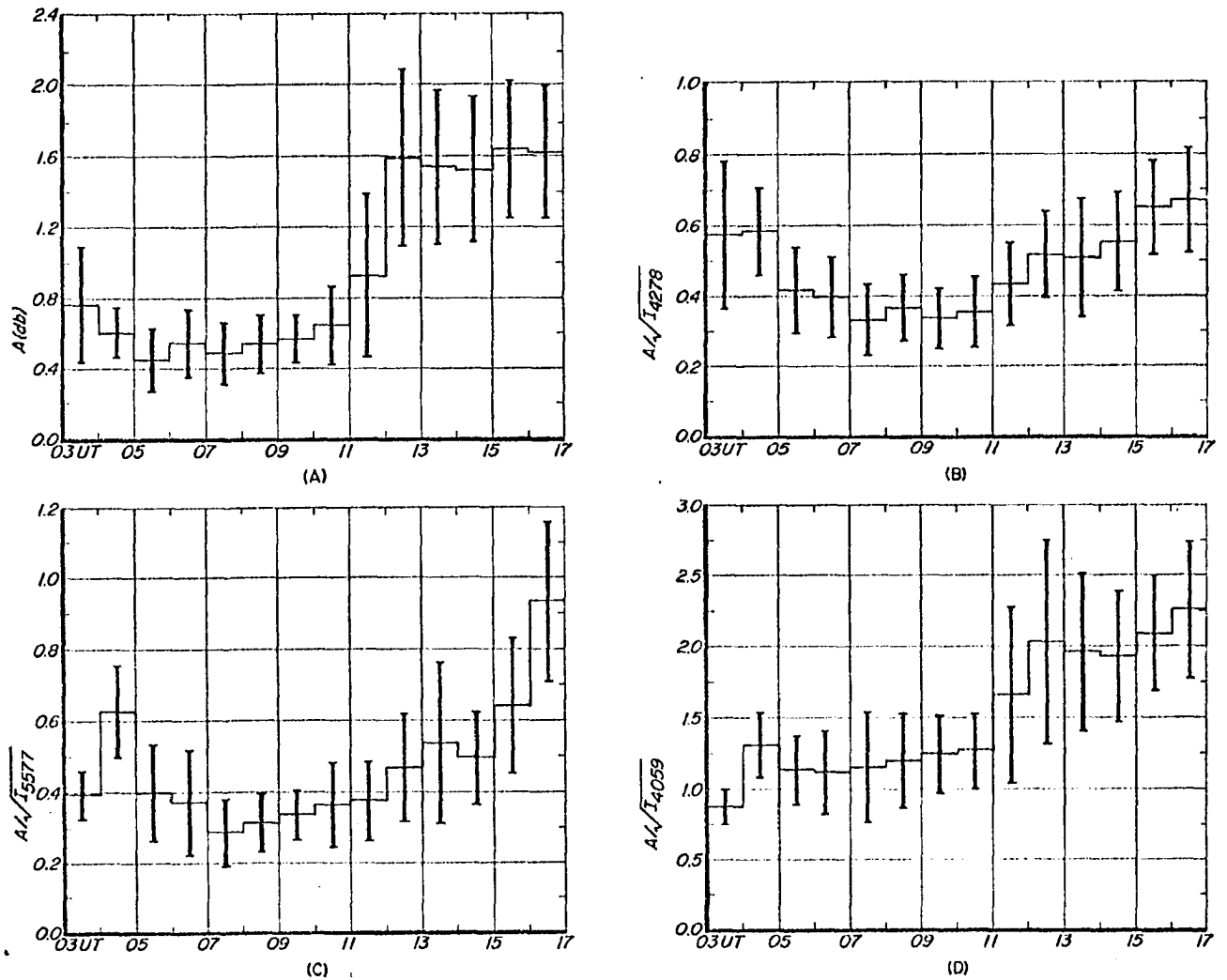

Figure (3.1) Histograms showing the average variation of: (a) absorption; (b) the ratio $A/\sqrt{I_{4278}}$; (c) the ratio $A/\sqrt{I_{5577}}$, and; (d) the ratio $A/\sqrt{I_{4059}}$. This diagram is for data gathered during the 1966-67 winter at College.

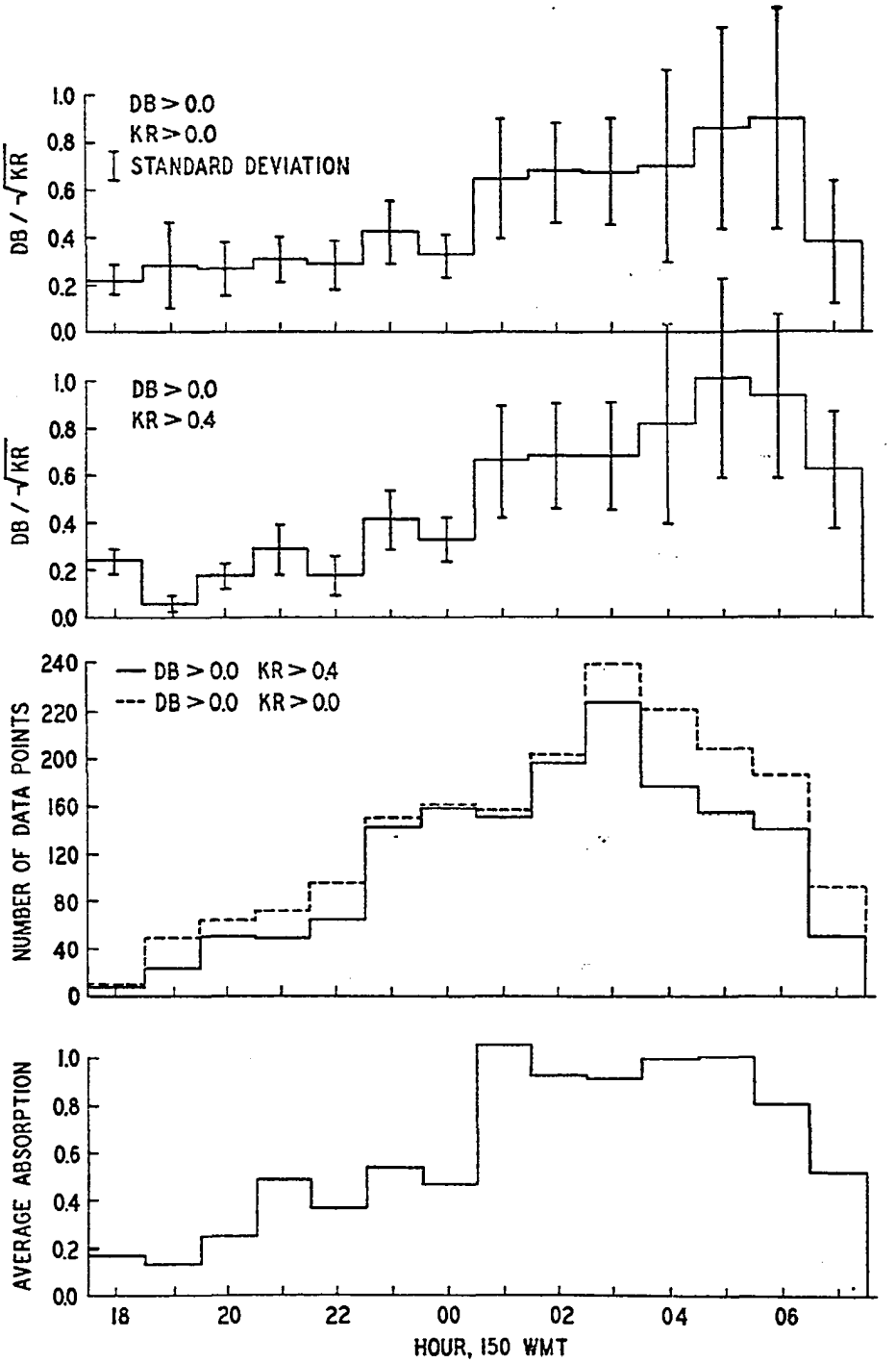

Figure (3.2) Histograms showing the average variation of the ratio $A/\sqrt{I_{5577}}$ and the absorption in the 6° North direction. The number of data points is also shown. This histogram is for data obtained during the 1965-66 winter at College (after Berkey, 1968).

during season I is illustrated. Although the gradual hardening of the spectrum toward dawn is evident in this diagram, there is no evidence of a softening of the spectrum before midnight as found during season II. However, this discrepancy may be attributed to the larger amount of data available for analysis during season II; less than 2,000 values were used in deriving Figure 3.2, while more than 10,000 were used to derive Figure 3.1(b). Also, the data extended farther into the dusk and dawn periods.

3.2 Derivation of Empirical Relations

Derived previously in this work was a relation between absorption and the square root of auroral luminosity; it was demonstrated that the ratio $A(db)/\sqrt{I(kR)}$ should be a constant, the value of which is a function of the spectral parameters of the precipitated electron flux. Using the large collection of data arising from this study and taking advantage of the rapid computation time of the computer, it was possible to test the validity of this derivation. To make this test the coefficients c_o and c_1 of the equation

$$A(db) = c_o I(kR)^{c_1} \qquad (1)$$

were derived by the method of least squares. If the quasi-equilibrium assumption invoked in deriving the relation $A(db)/\sqrt{I(kR)} = c$ is valid, then the value of the coefficient c_1 should be 0.5.

Next, the coefficients of the equation

$$A(db) = c_2 + c_3\sqrt{I(kR)} \qquad (2)$$

were computed, again by the method of least squares. The coefficient c_2 represents the experimental error inherent in the measurement of absorption (usually $\pm$ 0.2db).

Table III sets forth the numerical values of the coefficients c_o, c_1, c_2, and c_3 derived in the manner outlined above. It is important to note the constraints imposed upon the data in obtaining these values; in some cases an attempt was made to eliminate near zero values by varying the lower limit of the data values.

The entire data sample, consisting of 15,880 simultaneous measurements of 4278A luminosity and absorption, was used in deriving the coefficients c_o and c_1 of the expression given in equation (1). The result may be expressed:

$$A(db) = 0.295(I_{4278})^{0.486}$$

where I is in kilorayleighs. Once again using all available data points, the same coefficients for the 5577A data set were derived:

$$A(db) = 0.303(I_{5577})^{0.314}$$

The implication of this result is that the quasi-equilibrium assumption invoked in the derivation of the dependence of absorption on luminosity is more valid for 4278A data than for 5577A.

Deriving the same coefficients for the 4059A band emission, a larger value of the coefficient c_1 was found:

$$A(db) = 1.40(I_{4059})^{0.754}$$

At 4059A, the night-sky background level was large; as an attempt to eliminate such values from the data sample, only those measurements of 4059A intensity which exceeded 250 rayleighs were used to derive c_o and c_1:

$$A(db) = 3.52(I_{4059})^{1.62}$$

TABLE III

λ	c_o	c_1	c_2	c_3	r_1	r_2	n	A(dB)	I(kR)
4059	1.40	.754	- .941	3.473	.172	.451	8895		>0.
"	2.01	.741	-1.138	4.177	.195	.518	6900	> .2	
"	2.20	.715	-1.138	4.370	.203	.538	6000	> .3	
"	3.37	1.15	-2.716	7.070	.163	.554	2700	> .2	> .2
"	4.56	1.51	-4.471	9.865	.153	.583	1200	> .2	> .25
"	1.95	1.05	-2.403	6.137	.137	.482	3504		> .2
"	3.52	1.62	-4.836	10.093	.118	.518	1308		> .25
4278	.295	.486			.463	.614	15880		>0.
"	.458	.376			.437	.594	12813	> .2	
"	.276	.538			.449	.608	15204		> .4
"	.446	.393	- .018	.473	.406	.572	12469	> .2	> .4
"	.526	.366			.438	.604	11111	> .3	
"	.396	.496			.391	.567	10962	> .2	>1.
"	.496	.439			.397	.577	9721	> .3	>1.
"	.348	.519			.459	.630	18552	+ .2	+ .4
"	.627	.327			.467	.618	17795	+ .2	- .4
"	.521	.268			.460	.586	17125	- .2	- .4
5577	.303	.314	.223	.227	.202	.324	11312	>0.	>0.
"	.497	.207	.371	.219	.186	.305	8641	> .2	>0.
"	.578	.202	.439	.226	.187	.312	7469	> .3	
"	.500	.198	.430	.190	.132	.237	7517	> .2	>1.
"	.578	.205	.486	.208	.143	.257	6471	> .3	>1.
"	.307	.323	.195	.249	.211	.330	10607	> .2	> .4
"	3.00	-.065	3.094	-.146	-.045	-.138	445	>2.	>4.
"	4.18	-.091	4.006	-.191	-.018	-.130	44	>9.	>3.
"	.290	.359	.157	.229	.110	.251	3563	<4.	<2.

Statistical Parameters Derived for the Relationship between Auroral Absorption and Luminosity at Three Wavelengths

Examining the relationship between absorption and luminosity predicted by the quasi-equilibrium assumption, the coefficients c_2 and c_3 of equation (2) were derived. Only one set of coefficients was derived for the 4278A data sample for which A > 0.2db and I > 0.4kR:

$$A(db) = -0.018 + 0.473\sqrt{I}_{4278} \quad (kR)$$

The corresponding relationship found for the 5577A data set is:

$$A(db) = 0.223 + 0.227\sqrt{I}_{5577} \quad (kR)$$

As before, the coefficients derived for the 4059A data depart significantly from the values for either 4278A or 5577A:

$$A(db) = -4.84 + 10.09\sqrt{I}_{4059} \quad (kR)$$

or $$A(db) = -4.84 + 0.316\sqrt{I}_{4059} \quad (R)$$

The night-sky background level at 4059A usually exceeded 150 rayleighs, so that this value may be considered as a lower limit to the measurements. Similarly, the background levels at 4278A and 5577A were on the order of 400 rayleighs.

3.3 Correlation Between Recorded Parameters

In determining the correlation between absorption and luminosity, correlation coefficients were derived using the formula:

$$r = \frac{\Sigma XY - (\Sigma X)(\Sigma Y)/n}{\sqrt{[\Sigma X^2 - (\Sigma X)^2/n]}\ \sqrt{[\Sigma Y^2 - (\Sigma Y)^2/n]}}$$

In discussing correlation, it is useful to take into consideration its meaning; Sterling and Pollack (1968) present a rather lucid description of the use of correlation: "Correlation does not mean causation; correlation implies two concepts: the quantity X becomes a predictor of Y to the extent that variations in X are paralleled by variations

in Y. The covariation is measured by the sum of the cross products $\Sigma(X-\bar{X})\ (Y-\bar{Y})$ which is called covariance. This number will tend to be large when fluctuations of X and Y coincide. Secondly, correlation defines the pragmatic 'usefullness' of a predictor. The degree of correlation helps us decide whether it is or is not worthwhile to use a specific predictor."

Correlation coefficients were derived assuming both a linear and square root dependence of luminosity on absorption; the relative magnitude of the correlation between absorption and each emission line is stressed. The correlation coefficients discussed below are all significant at the 1 percent level.

For the entire data sample at 4278A the following correlations were derived:

$r_1 = 0.46$ (1 for linear dependence)

$r_2 = 0.61$ (2 for square-root dependence)

Derived from the data set containing 5577A measurements were the values:

$r_1 = 0.20$

$r_2 = 0.32$

Finally, utilizing the 4059A data, the correlation coefficients were:

$r_1 = 0.17$ $\qquad$ $r_2 = 0.45$ (all data)

$r_1 = 0.12$ $\qquad$ $r_2 = 0.52$ ($I_{4059} > 250R$)

Based on the premise that the 4059A datawere obtained during only active auroral conditions and may therefore represent a significantly unique sample of aurora, the correlation coefficients for the 4278 data taken at the same time were derived:

$r_1 = 0.49$

$r_2 = 0.63$

With reference to the correlation coefficients derived for the 4278A and 5577A data samples, it can be inferred that the assumption of a linear dependence of luminosity on absorption is only slightly inferior to the assumption of a square root dependence. This result is true for a limited amount of data, such as considered above, as well as for the total data set which contains an order of magnitude more data. However, the correlation analysis does support the earlier conclusion that the 4278A emission is more closely related to auroral absorption than is the 5577A emission.

The correlation coefficients derived for the 4059A data imply that the square root dependence of luminosity on absorption is significantly better than a linear dependence. However, the magnitude of r_2 was less than the corresponding value for the 4278A data implying that auroral luminosity at 4059A is a slightly poorer predictor of absorption than is 4278A luminosity.

During season I correlation coefficients were derived between absorption and 5577A luminosity; the magnitude of the correlation coefficients was of the same order as derived in season II.

Also during season I, the correlation of absorption between the 6° north and 6° south directions was investigated; coefficients of 0.96 (A > 0.0db), 0.90 (A > 0.5db), and 0.87 (A > 1.0db) were derived (see Figure 3.3). A correlation coefficient of 0.77 was derived for correlation of 5577A luminosity in the 6° north and 6° south directions.

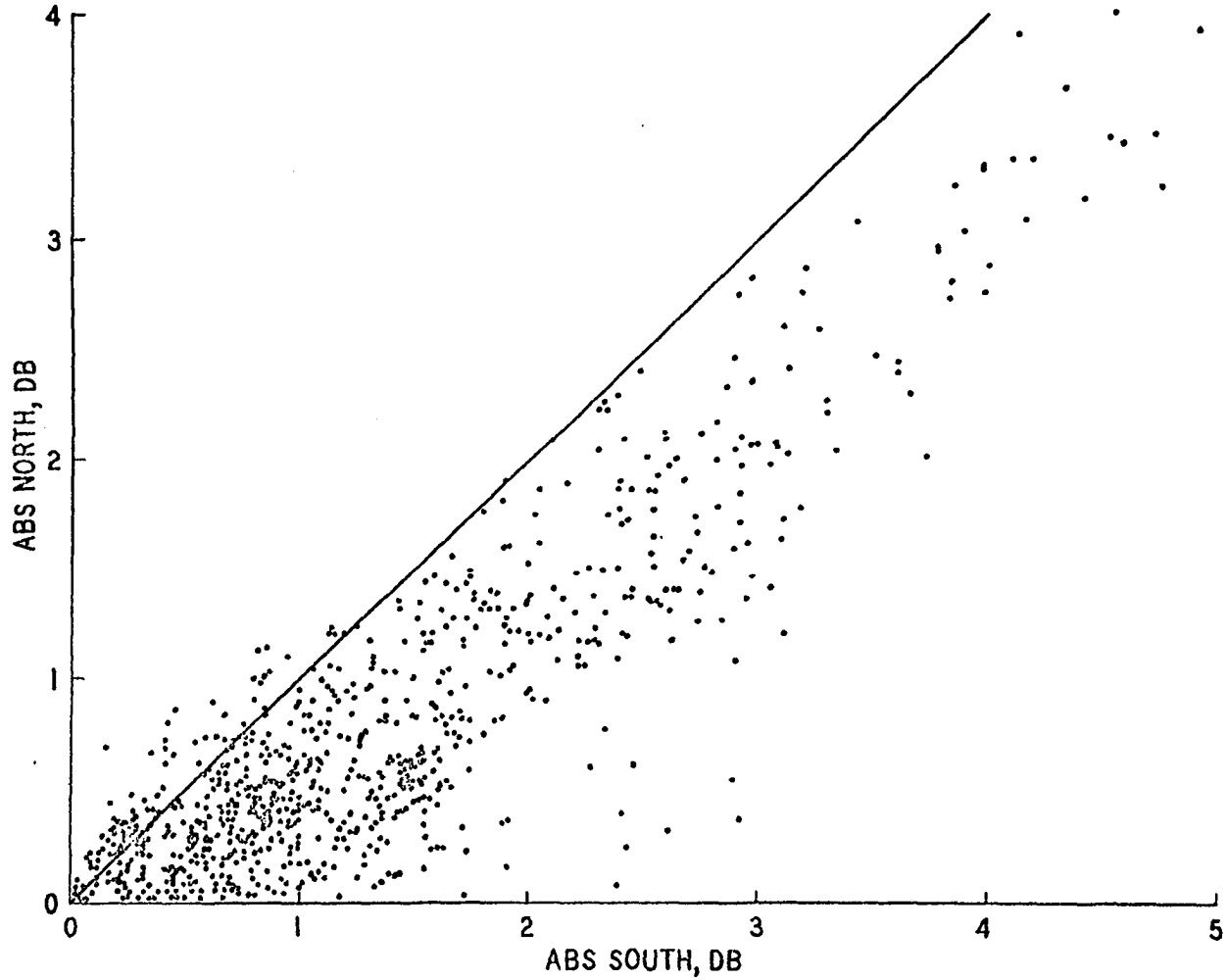

Figure (3.3) Scatter plot of absorption in 6° North orientation plotted versus absorption in 6° South orientation (after Berkey, 1968).

Correlating the narrow beam absorption events with the same events measured with the standard Yagi antenna, a value of 0.83 was found. These correlation coefficients are also listed in Table IV.

3.4 The Spatial Extent of Auroral Absorption

Using autocorrelation functions, Graf (1960) made computations of the structural extent of an absorbing region as a function of the correlation of absorption between two adjacent directions. Although the major lobe of his array was of greater angular dimensions in the east-west plane than the array used in this study (see Table I), to a first approximation his results can be applied here. From Figure 3.4 (Graf's Figure 6) it is possible to infer a spatial extent of the absorbing region from previously derived knowledge of the correlation coefficient. In the first instance, in which all available data were correlated (A > 0.0db), the spatial extent of the absorbing region can be inferred to exceed 80 kilometers; next, considering only those values of absorption which exceeded 0.5db, the spatial extent (in the north-south plane) exceeds approximately 60 kilometers. Restricting the data event even further (A > 1.0db), a spatial extent of only 48 kilometers can be assumed. It can therefore be concluded that as the magnitude of the absorption increases, the spatial volume in which it occurs decreases. This result is consistent with observation; intense absorption is frequently associated with bright, narrow auroral forms. However, this is not to imply that the spatial dimensions of the absorbing region and the

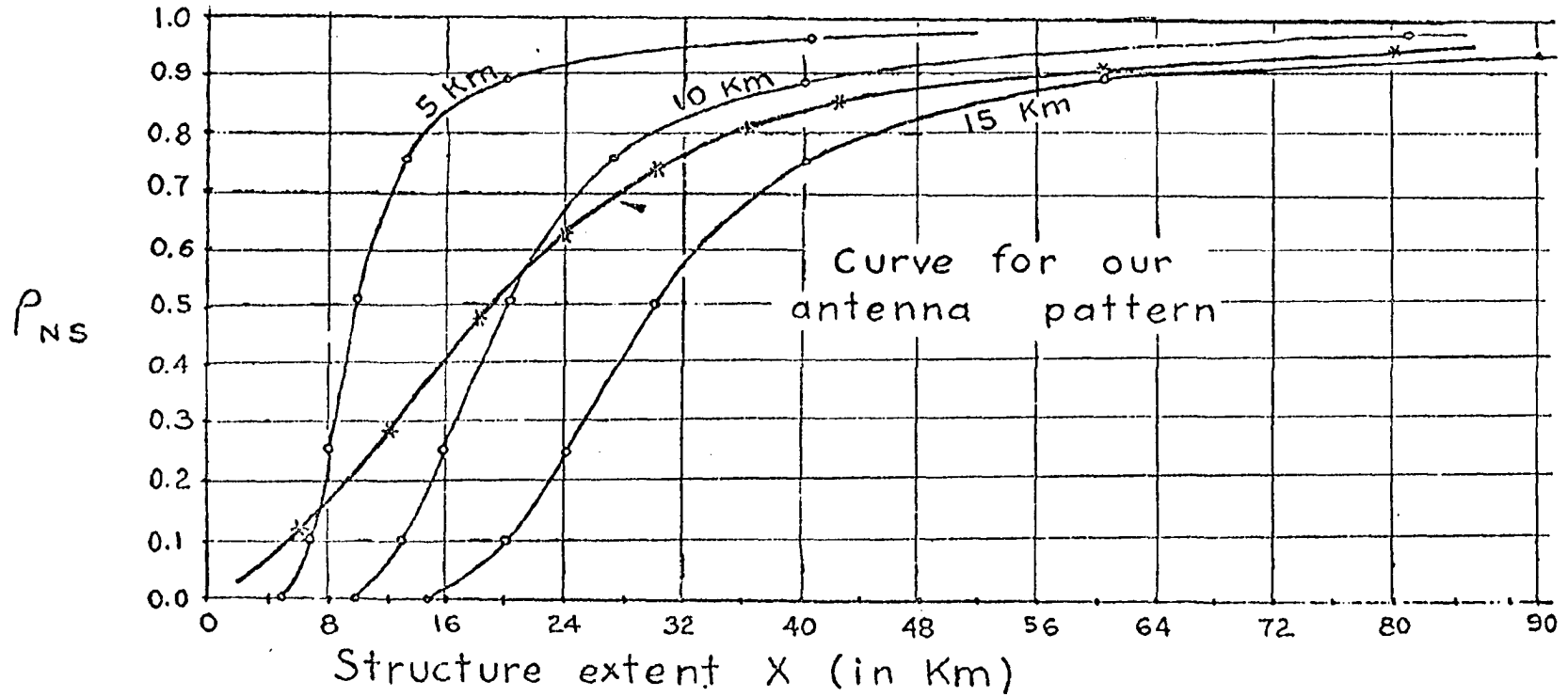

The (*)'s show the curve for our antenna pattern. The (o)'s show values which a very much narrower beam (say 1 Km wide), displaced 5, 10, and 15 Km, would have given.

Figure (3.4) Structural extent of the absorbing region as a function of correlation for an array with a beamwidth of 6.5° (after Graf, 1960).

TABLE IV

Type of Correlation	Criteria For Correlation A(db)	I(kR)	Correlation Coefficient (r_2)		Number of Data Points (n)	
6° north versus 6° south absorption	>0.0		0.96		1476	
6° north versus 6° south absorption	>0.5		0.90		879	
6° north versus 6° south absorption	>1.0		0.87		472	
6° north versus widebeam (70°x70°) absorption	>0.5		0.83		422	
6° north versus 6° south luminosity		>0.0	0.77		2203	
			North	South	North	South
db versus $(kR)^{1/2}$	>0.0	>0.0	0.31	0.46	1812	2133
db versus $(kR)^{1/2}$	>1.5	<4.0	-0.02	0.11	178	280
db versus $(kR)^{1/2}$	>1.5	>4.0	0.16	0.19	62	222
db versus $(kR)^{1/2}$	<1.5	>4.0	0.35	0.26	183	248

Correlation Coefficients for Auroral Absorption Measurements
In two Directions and for the Correlation of Absorption and 5577 Luminosity (after Berkey, 1968).

luminous aurora are the same; applying Graf's analysis to the correlation of 5577A luminosity in the 6° north and 6° south directions, a spatial extent or coherence of only 32 kilometers is predicted. Therefore, based on this analysis, it can be concluded that the spatial dimensions of the absorbing region exceed those of the luminous aurora.

3.5 Observations of 4861A and 5294A

Observations of the H_β emission at 4861A were made only during season I and reported by Berkey (1968). No correlation studies were undertaken, and the conclusion that the H_β was not well correlated with auroral absorption was based on an inspection of the data. Figure 3.5 exemplifies the complete lack of H_β emission during pulsating aurora such as observed in the morning sector.

Although the 5294A band emission was monitored throughout season II, the data were not utilized for the correlation analysis due to the lack of sensitivity of the photometer system. A general impression obtained from observations during intense aurora was that it varied in proportion to the 4059A luminosity.

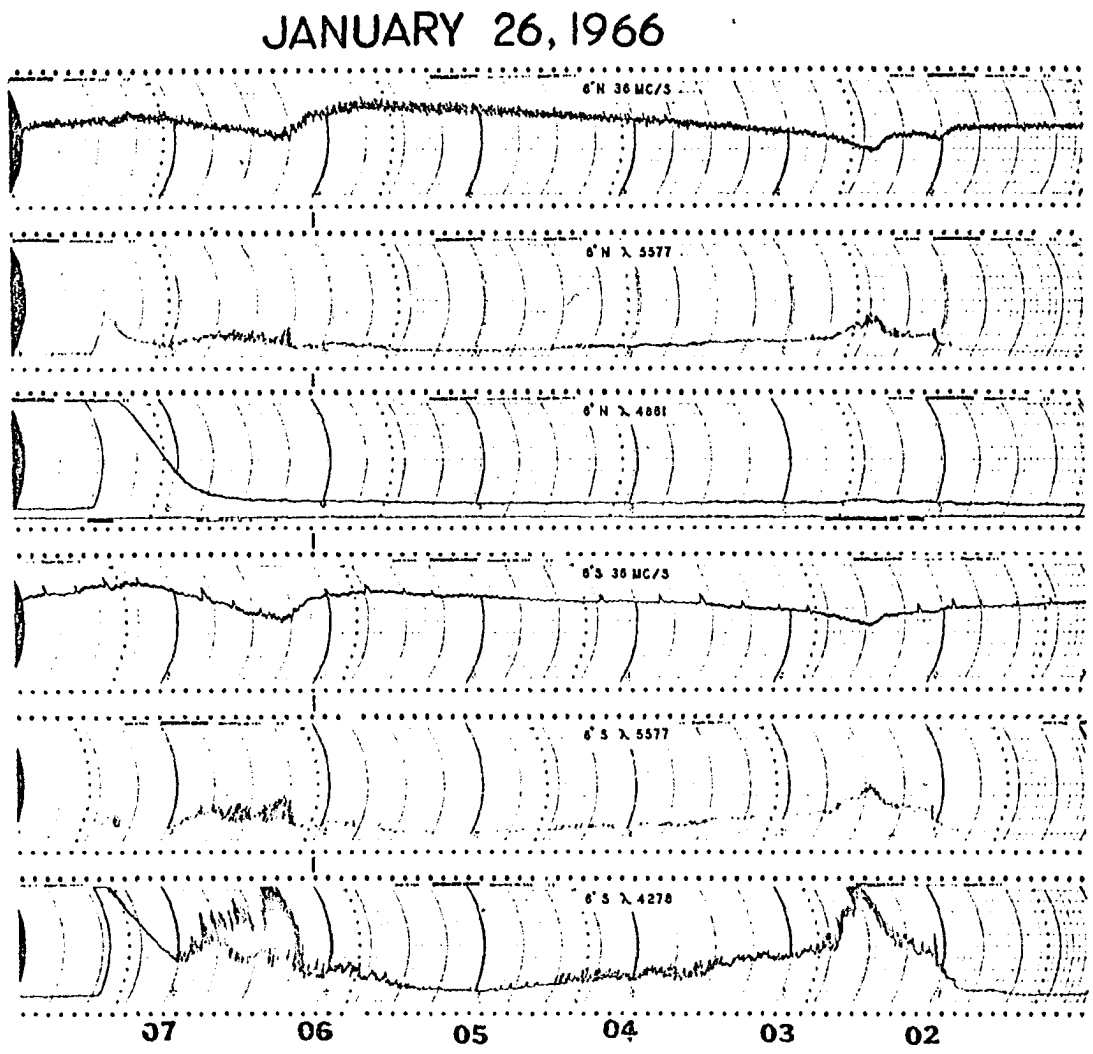

Figure (3.5) Original recordings for the morning of January 26, 1966. Note that no enhancement of 4861 A (H_β) occurs during the pulsating aurora at 0230 LT and 0630 LT (after Berkey, 1968)

CHAPTER 4

THE RELATION OF AURORAL ABSORPTION AND LUMINOSITY DURING THE SUBSTORM

4.1 Introduction

A classification of auroral absorption events according to their variation with time has been made by a number of authors (Ansari, 1963; Berkey and Parthasarathy, 1964; Eather and Jacka, 1966; Akasofu, 1968). Where Akasofu has defined E-type absorption as a brief impulsive evening event and N-type as the "heavy absorption with a sharp onset in the mid-night and early morning hours," other authors have not differentiated between these events and classified both types as SAI (sudden absorption increase) (Ansari, 1963), type-F (Berkey and Parthasarathy, 1964) or SIA (sudden ionospheric absorption (Eather and Jacka, 1966). The less impulsive absorption events, which increase at a slower rate and occur primarily in the morning hours, have been termed SVIA (slowly varying intense absorption) by Ansari (1963) and type-S by Berkey and Parthasarathy (1964). Akasofu has termed such absorption M-type events. A third classification (type-P) was made by Berkey and Parthasarathy (1964) which defined quasi-periodic absorption events with periods up to several hundred seconds.

Akasofu (1968) pictured the daily variation of E, N and M type absorption at a typical auroral zone station (such as College) as a function of magnetic activity. He inferred an increase in the frequency of occurrence and magnitude of E- and M- type absorption events with magnetic activity.

In this chapter, several examples of substorm and non-substorm associated absorption events will be examined. Most of these events

can be classified according to the schemes described previously, although such will not be the purpose of this discussion. Instead, selected events from each of several time sectors will be used to illustrate the relation of absorption to auroral luminosity during the substorm. Events representative of all levels of magnetic activity have been selected for this purpose.

A definition of the time sectors used in this discussion is given in Table V; the approximate local geomagnetic time interval corresponding to the local time sector is also given.

Table V

Definition of Time Sectors

Sector	Local (150°WMT) Time	Local Magnetic Time
Dusk	1600 - 2030	1430 - 1900
Evening	2030 - 2230	1900 - 2100
Midnight	2230 - 0130	2100 - 2400
Early Morning	0130 - 0330	2400 - 0200
Dawn	0330 - 0800	0200 - 0630
Morning	0800 - 1030	0630 - 0900
Noon	1030 - 1330	0900 - 1200
Afternoon	1330 - 1600	1200 - 1430

4.2 Dusk Sector Events

The dusk sector is generally a period of minimal auroral activity as the auroral oval lies 5° - 7° poleward of College during this time. It is also the period during which the diurnal variation of auroral absorption at College is a minimum. However, Montbriand (1969) observed patchy forms in the dusk sector which he identified with intense absorption. In the following section, three examples of dusk sector patchy forms will be examined.

4.2.1 The events of January 18, January 20, and February 4, 1968.

Although the quantitative relationship between absorption and luminosity was not derived for these events, they were considered to be of enough significance to merit discussion. In addition, due to the similarities between these events, the ensuing discussion will pertain to all three.

There was no evidence of substorm activity at College during the periods of interest, however; each of the events was preceeded by the occurence of a substorm at Kiruna and followed by substorm activity at College near midnight.

Figure 4.1 illustrates these events using the 36 MHz riometer trace, the 4278 A photometer output, and a record showing the variation dI_{4278}/dt. The 4278A photometer output was available only during the February 4 event. The periods of interest are the time during and just following twilight, after the photometers had turned on. It will be noted that pulsations of the 4278A emission occurred during these times and that the riometer showed intense absorption during the pulsating aurora. The normal 4278A photometer trace for February 4 shows the magnitude of the type of pulsations which occurred in the evening twilight; the character of these pulsations is markedly different from the pulsations observed in the morning sector.

All-sky camera data were available only during the February 4 event; the camera was not operating while the events of January 18 and January 20 were in progress. Using cinematic projection it was possible to discern very weak arc segments drifting equatorward. They appeared to be similar in nature to the dusk sector patches documented by Montbriand (1969).

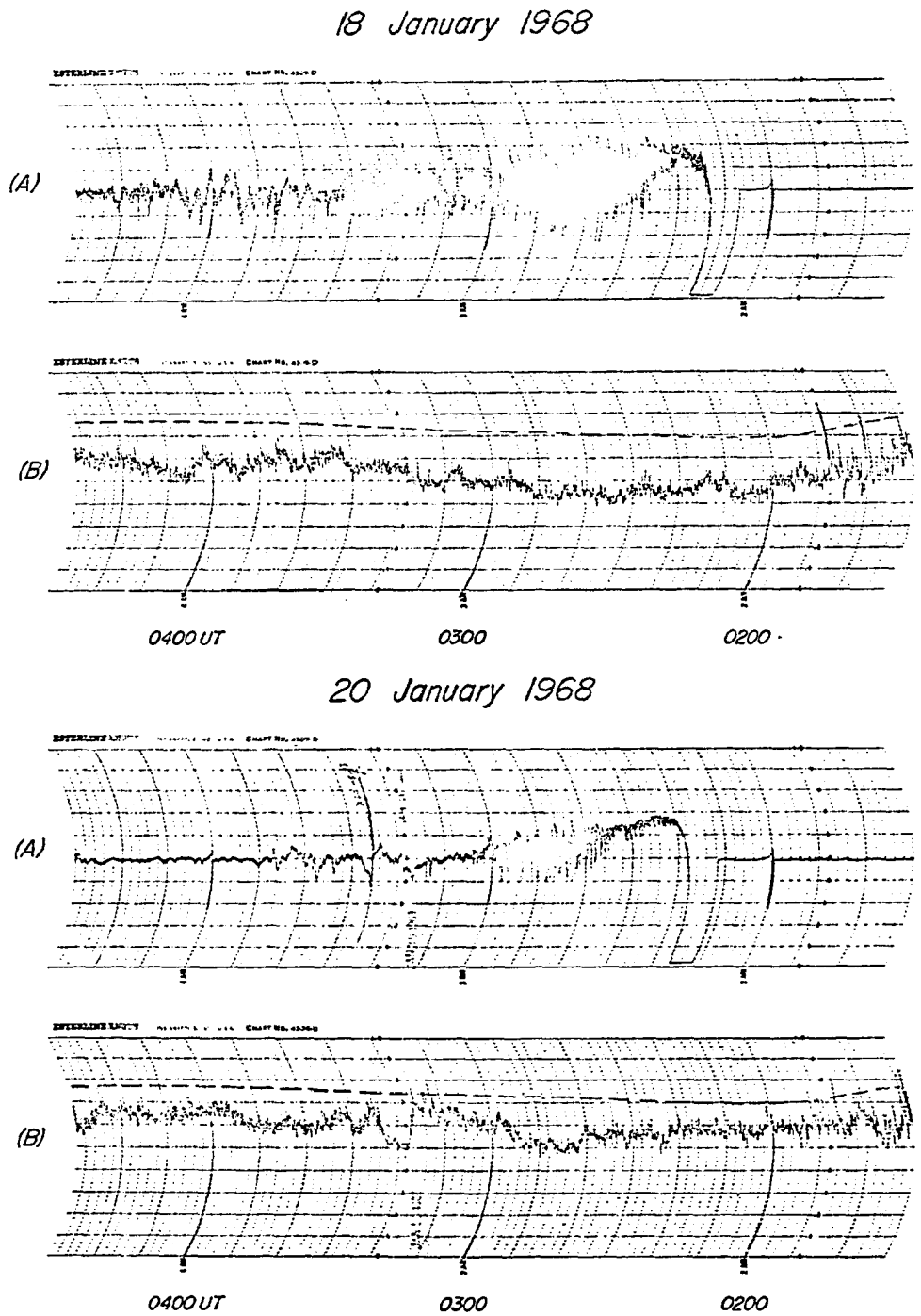

Figure (4.1a) Reproduction of the original records of January 18 and January 20, 1968. The upper trace (A) is a record of the short period fluctuations of 4278A (dI/dt). The 36 MHz riometer record is shown in (B). Note the increased absorption at times of 4278A fluctuations.

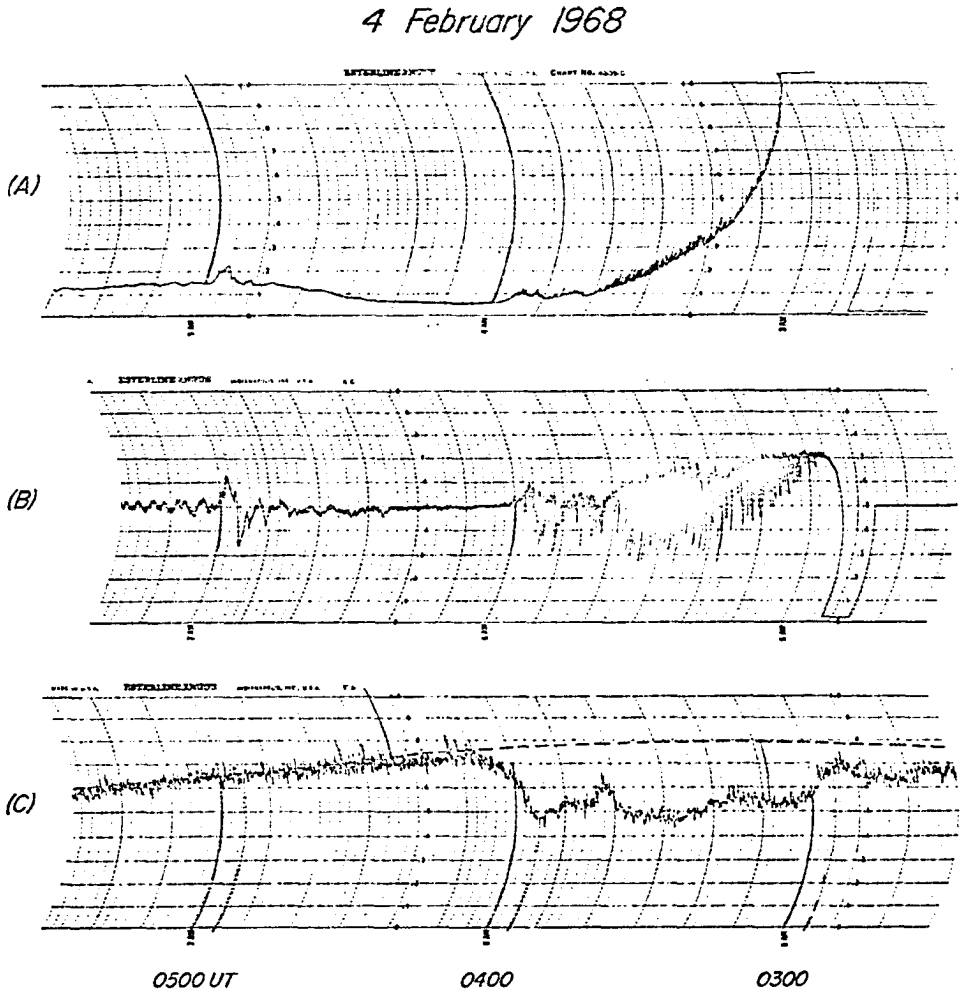

Figure (4.1b) Reproduction of the original records for February 4, 1968. In this figure the upper trace (A) is the normal 4278A photometer record. Trace (B) shows the short period fluctuation recording, and (C) is the 36 MHz riometer record.

From such observations, it can be concluded that absorption occuring in the late afternoon (or dusk sector) and not correlated with substorm activity is associated with dusk sector patches. That these patches pulsate is demonstrated by the observations reported here. The association of such patches with intense absorption as suggested by Montbriand (1969) is further strengthened. It is suggested that this type of event is associated with prior substorm activity in the midnight sector; it is not unlikely that the pulsating aurora is merely an eastward extension of the pulsating aurora seen in the morning sector. The same is true of the absorption; in Part II of this thesis the eastward drift of absorption will be documented and discussed in some detail.

4.2.2 The event of February 11, 1967

On February 11, 1967 a substorm onset was signalled by a positive change of the H-component at College beginning at approximately 0530 UT. The positive impulse reached a maximum (ΔH = 150γ) several minutes later at 0545 UT; this coincided in time with an absorption event which reached a maximum of 1.2 db at 0546 UT. The variations of absorption and 4278 A luminosity are depicted in Figure 4.2. Note that the increase in auroral luminosity was almost negligible; this is further exemplified by the all-sky camera photographs of Figure 4.3 which show a faint arc, only slightly brighter than the Milky Way, extending through the zenith between 0544 and 0548 UT.

Positive excursions of the H-component continued until 10^hUT; between 0740 and 0800 UT an event similar to the 0545 UT event occurred, however the onset was less well defined and the magnitude was somewhat less.

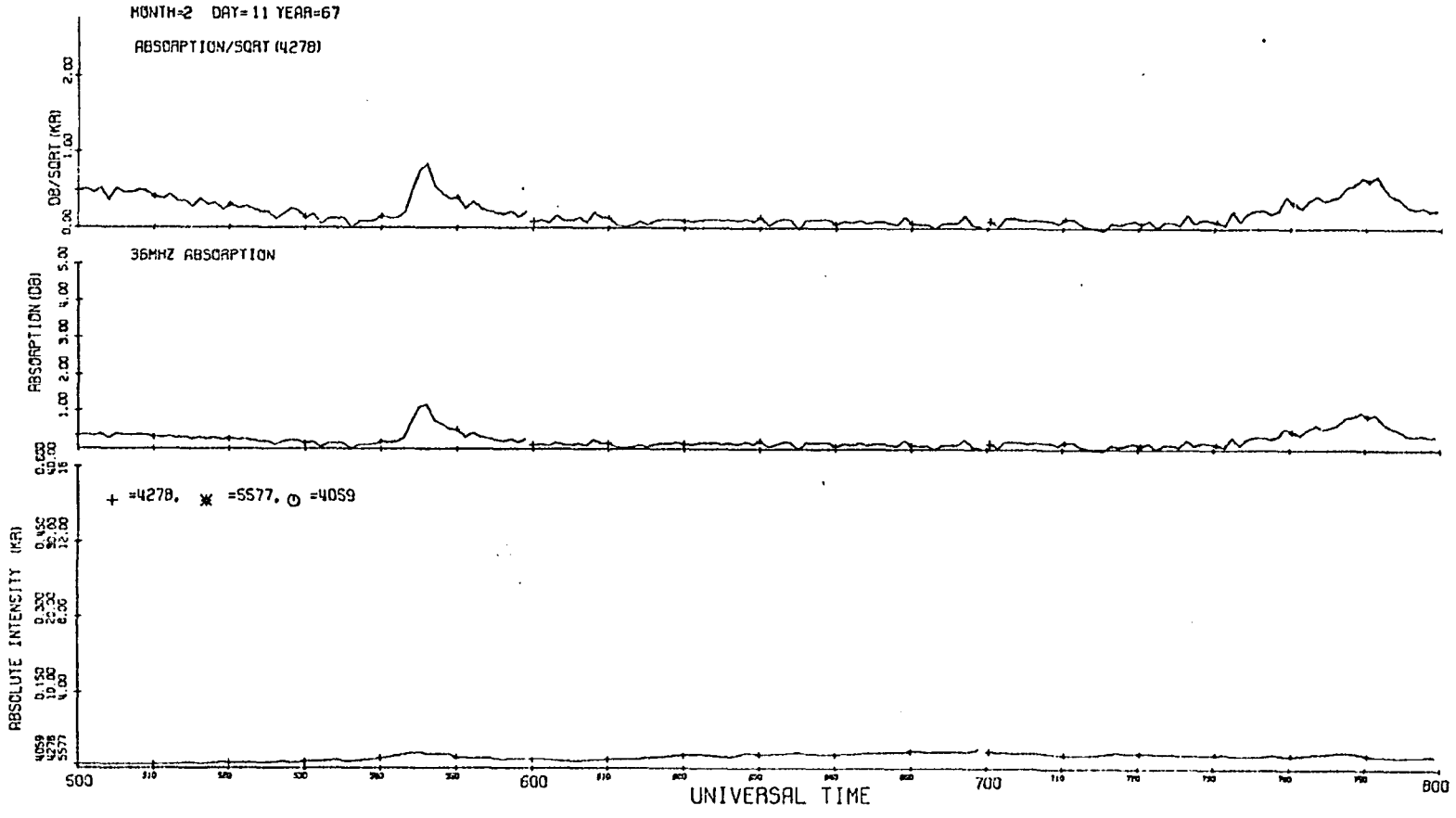

Figure (4.2) In this diagram and the similar diagrams which follow, the data have been reduced at one minute intervals; in the lower portion of the figure, the auroral intensity (in kilorayleighs) has been plotted for 4278A, 5577A, or 4059A, using different symbols for each wavelength. In the center trace the absorption in decibels at 36 MHz is plotted, and the upper row represents the ratio $A/\sqrt{I_{4278}}$ Symbols have been plotted at 10 minute intervals on each graph. This data is for the dusk-sector event of February 11, 1967.

Figure (4.3) All-sky camera photographs for the interval 0540 to 0549 UT on February 11, 1967.

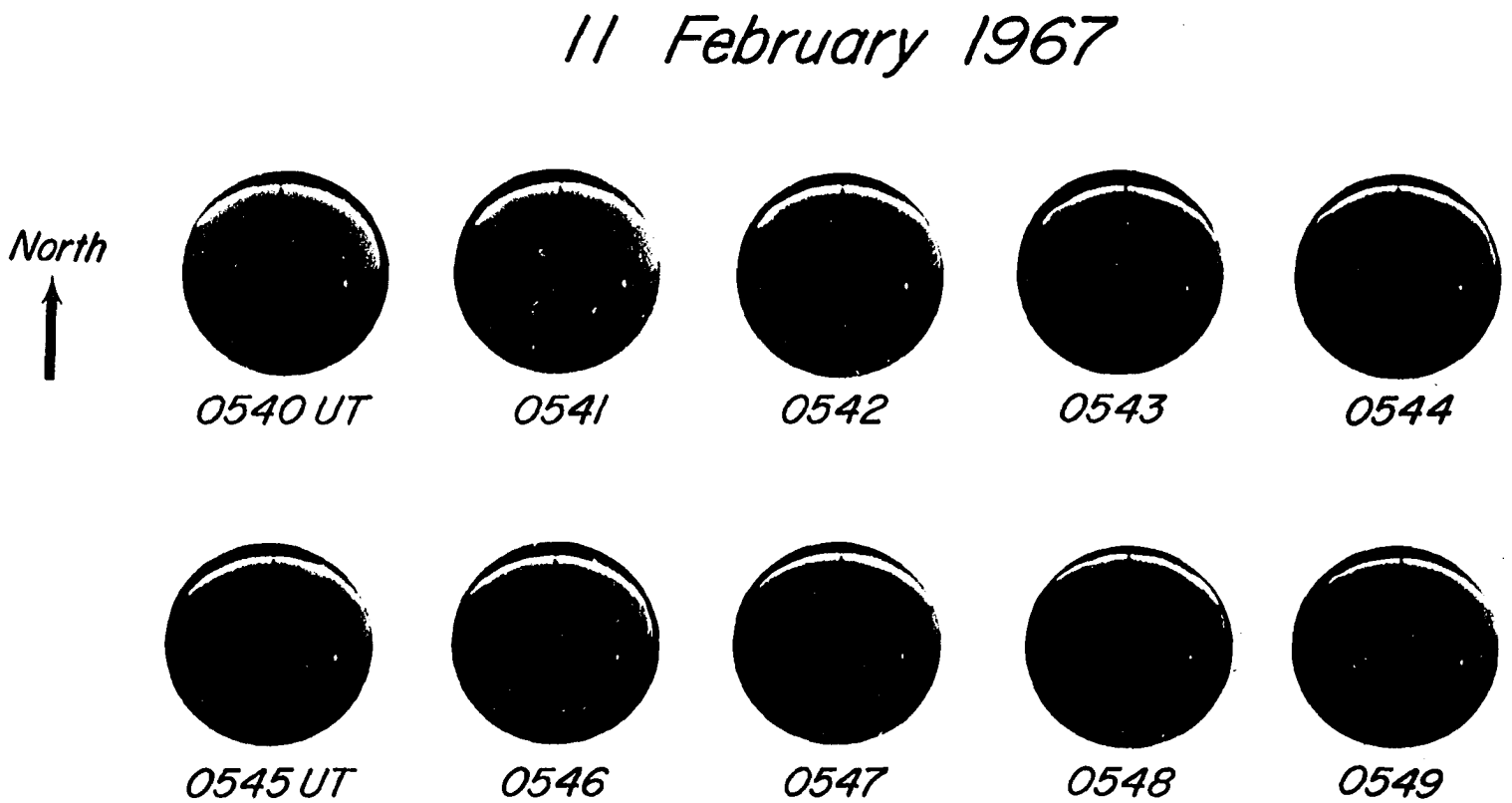

4.2.3 The event of October 6, 1966

The substorm which occurred between about 0630 and 0730 UT on October 6, 1966 also produced a positive bay in the H-component at College. An absorption event lasting nearly 30 minutes began at 0638 UT (see Figure 4.4), reaching maxima of 2 db at 0640 UT and again near 0700 UT. The maxima coincided in time with the largest positive excursions ($\Delta H \cong 250\gamma$). Once again, no appreciable increase of 4278A or 5577A luminosity was observed.

During both of these events, the ratio $A/\sqrt{I}$ was large, inferring a hard electron spectrum. Furthermore, the association with substorm activity and the absence of pulsating aurora suggests that these events are different in nature than those discussed in section 4.2.1. It can be concluded that during substorms which cause a positive deflection of the H-component, intense absorption accompanied by only a negligible increase in auroral luminosity can occur. It is also suggested that during such events, intense absorption also occurs within the auroral oval associated with the propagation of the westward travelling surge (WTS).

4.3 The Evening Sector

In the evening sector, College is situated 2 - 3° equatorward of the auroral oval except during very intense substorms ($K_p > 5$) when the oval expands to include College. During the auroral substorm, any one of several auroral types may be observed: the westward travelling surge, the westward drifting loop (WDL), or a poleward expansion. The absorption events which occur in the evening sector are characterized

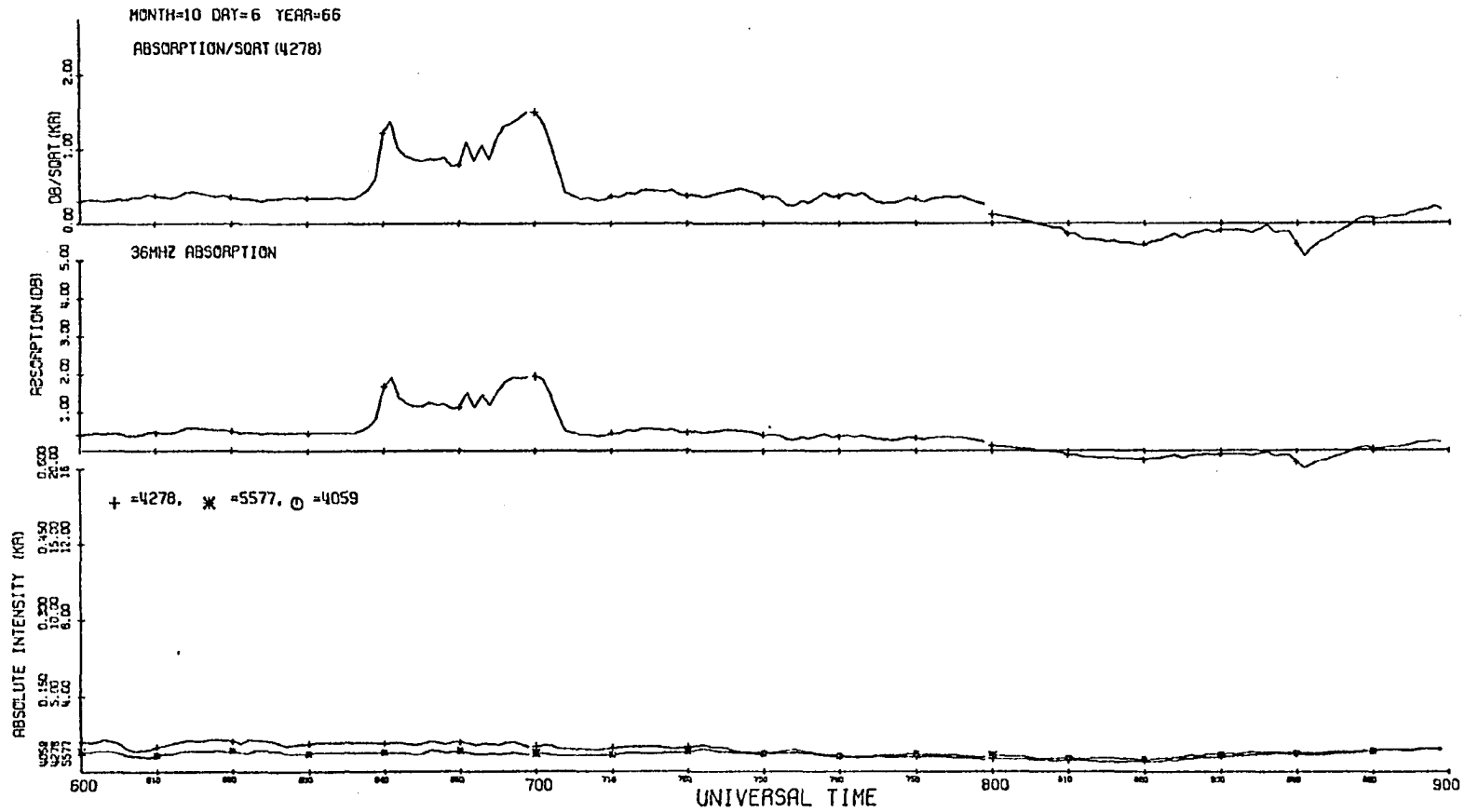

Figure (4.4) Data for the dusk-sector event of October 6, 1966.

by a rapid onset and a rapid recovery and are usually of short duration.

4.3.1 The events of January 14, 1967

No definite onset time could be ascribed to the activity which occurred on January 14, 1967 although the College K-index for the 03 - 06^h UT interval was 6. Small (50 - 150γ) fluctuations were recorded in the H-component between 05 and 06^h UT.

At 0505 UT, a rayed arc extended through the zenith at College, the brightest part of the arc being to the west of College, near Kotzebue (see Figure 4.5). Between 0509 and 0510 UT a surge propagated eastward along the arc followed by equatorward displacement of the arc of approximately 30°. As seen from Figure 4.6, the absorption reached approximately 1.3 db during this time while 11 kR of 4278A luminosity was observed.

Several minutes later, at 0522 UT a westward drifting loop could be seen near the horizon east of College (see Figure 4.5). The loop passed through the zenith at 0524 UT at which time the 4278A, 5577A, and 4059A photometers registered a sharp increase in luminosity (26 kR at 4278A). Maximum absorption ($\sim$1 db) and maximum luminosity at 4059A were reached a minute later at 0525 UT. At 0527 UT a rayed arc formed the poleward boundary of the aurora as seen from College. A small negative bay occurred in the College H-component during this event.

At approximately 0605 UT a sudden positive increase was recorded in the College H-component which coincided with a westward travelling surge which propagated across the sky to the north of College (see Figure 4.5). At 0610 UT the equatorward boundary of this surge moved

Figure (4.5) All-sky camera photographs for the intervals 0505 to 0531, 0604 to 0615 UT on January 14, 1967.

14 January 1967

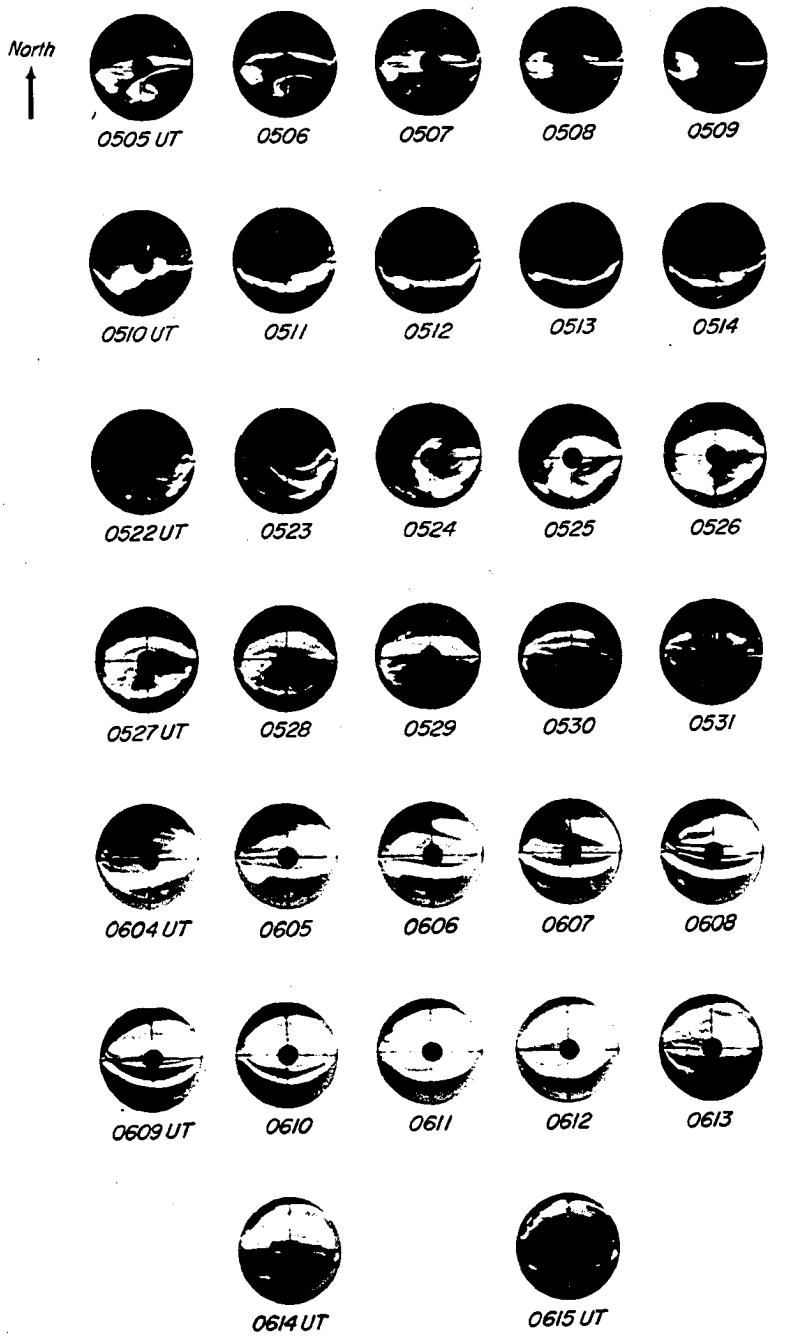

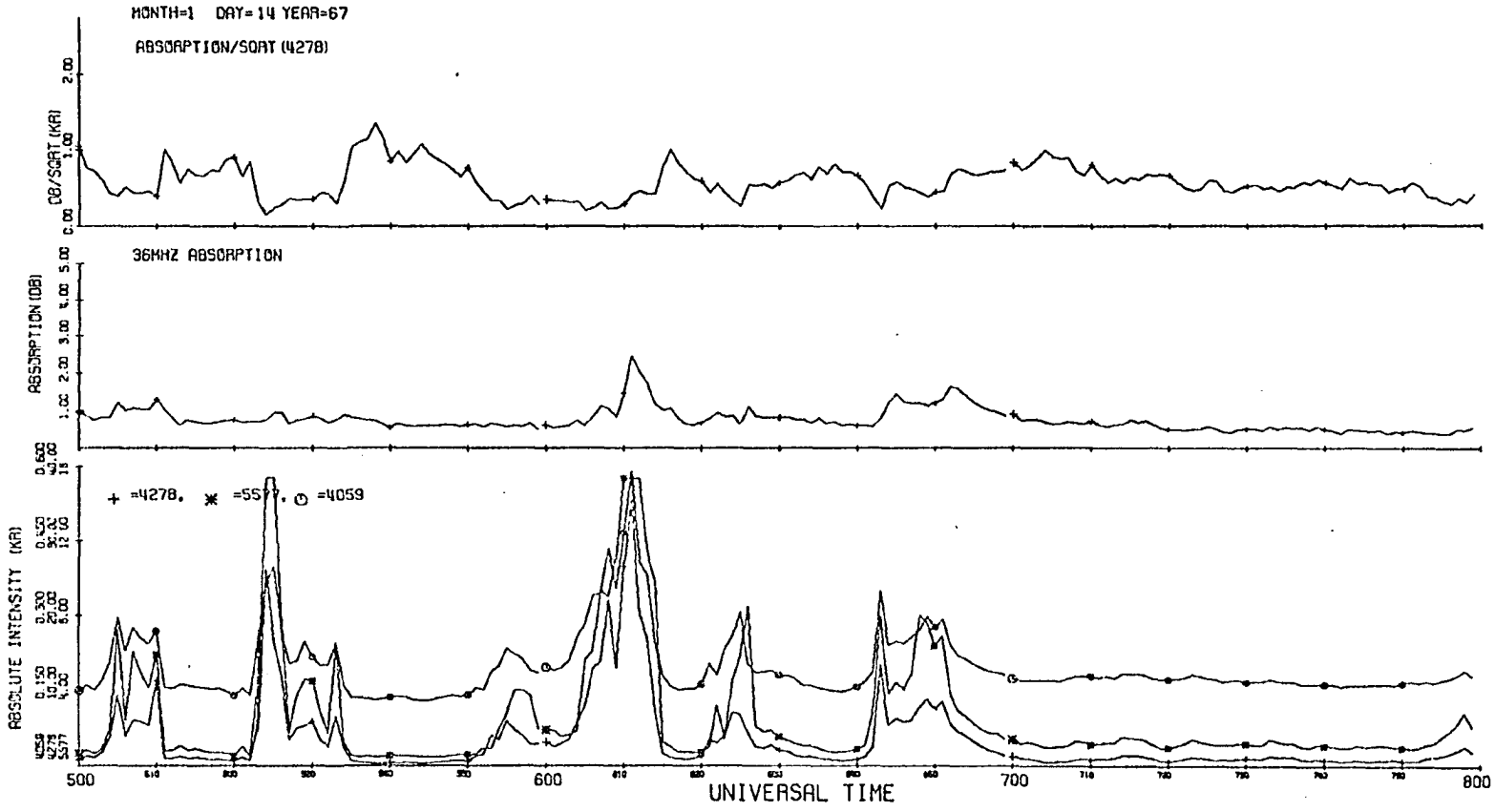

Figure (4.6) Data for the evening-sector events of January 14, 1967.

into the zenith at College causing a sudden increase in absorption and luminosity. The absorption increased from 0.87 db to 2.5 db and 4278A intensity reached 35 kR at 0611 UT. During each of these events the ratio A/I 4278 indicated a softening of the electron spectrum.

The nature of the auroral events recorded between 05^h and 07^h UT on this date appears to be typical of those periods when College lies just equatorward of the auroral oval. Auroral luminosity tends to occur at discrete intervals between which there is no other auroral activity. A similar event, associated with a WDL, was discussed by Berkey (1968).

4.3.2 The event of October 16, 1966

On October 16, 1966 substorm activity began at approximately 07^h UT. The maximum amplitude of the negative bay which lasted until 0830 UT was approximately 1300 gamma (K_{col} = 7). Several rapid onset absorption events occurred during the transit of Cassiopeia A through the antenna pattern; this caused large amplitude scintillations which tended to mask the absorption events (see Figure 4.7). Close examination of the original records indicates that an absorption event occurred coincident with the increase of luminosity observed at 0717 UT.

Although no all-sky camera data were available for this event, it is assumed that the spike-like increases of absorption were associated with the propagation of the WTS through the College zenith. The enhancement of the 4059A emission supports this assumption.

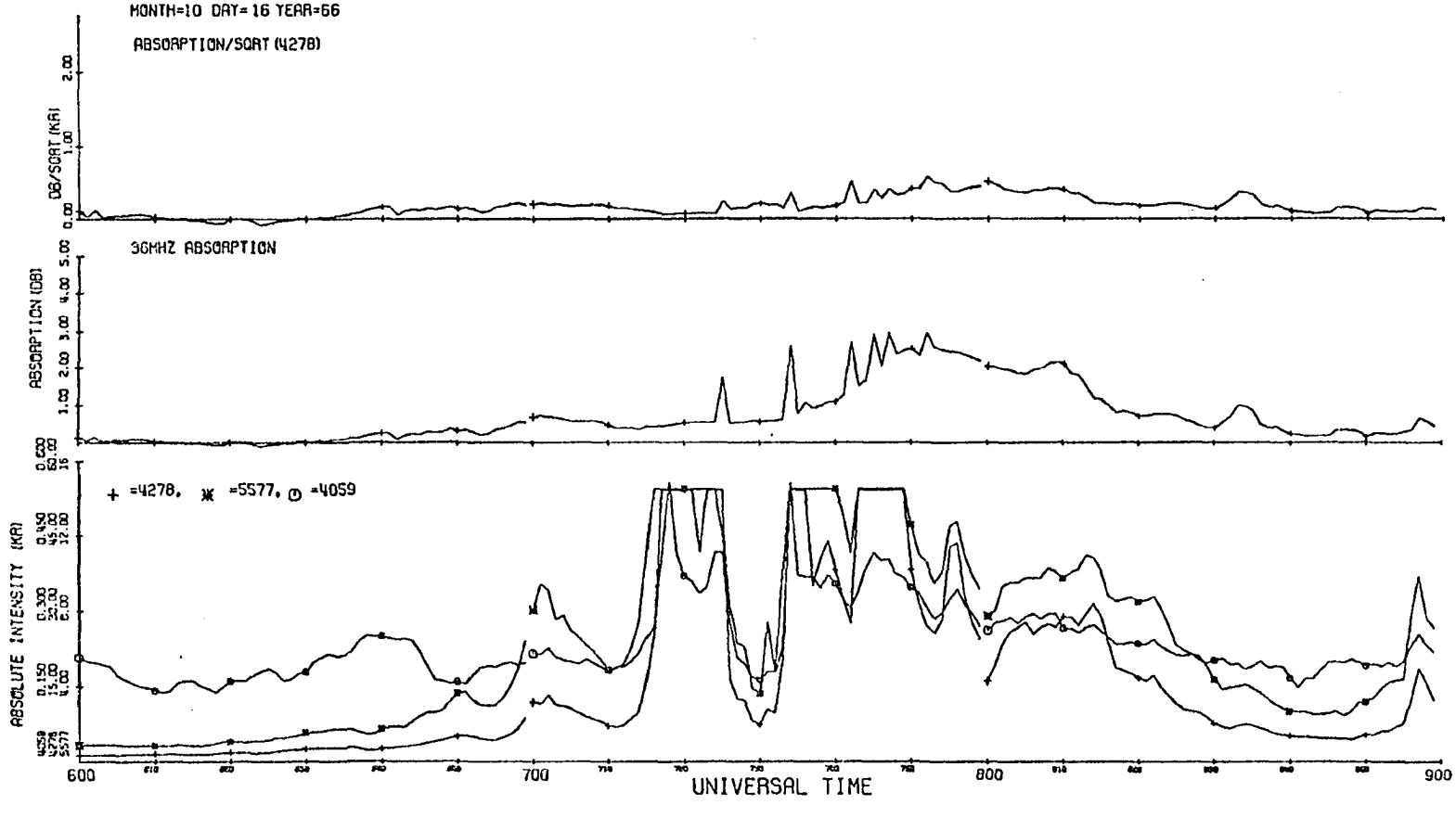

Figure (4.7) Data for the evening sector event of October 16, 1966.

4.3.3 The Event of January 8, 1967

At approximately 0630 UT on January 8, 1967 sudden onsets were recorded in the magnetometer, riometer, and photometer records (see Figure 4.8). The magnitude of the H-component negative bay was about 900 gamma and signalled the onset of a polar magnetic substorm which lasted until 07^h UT. A sudden increase in absorption was recorded almost simultaneously at Fort Yukon, indicating that the event may have been associated with the poleward expansion of the auroral substorm. No all-sky camera data were useable during this event.

4.4 Midnight Sector Events

In the midnight sector, College exists within a transition zone, moving from outside to inside the auroral oval. The maximum in auroral occurrence is reached during this period and poleward expansions and westward travelling surges are typically observed auroral features. In the riometer records, sharp onset absorption events frequently occur.

4.4.1 The Event of December 13, 1967

On December 13, 1966 a substorm onset occurred at approximately 1000 UT as evidenced by a negative bay onset at College. Prior to the substorm onset rayed auroral structures filled much of the sky. At 0957 UT a poleward expansion began and by 1005 UT diffuse aurora filled the whole sky (see Figure 4.9). Auroral intensities increased beyond 10 kR, but the increase in radiowave absorption was only 0.7 db (see Figure 4.10). This event provides an example of a relatively weak substorm occurrence ($\Delta H = 225\gamma$) while College was located within the auroral oval.

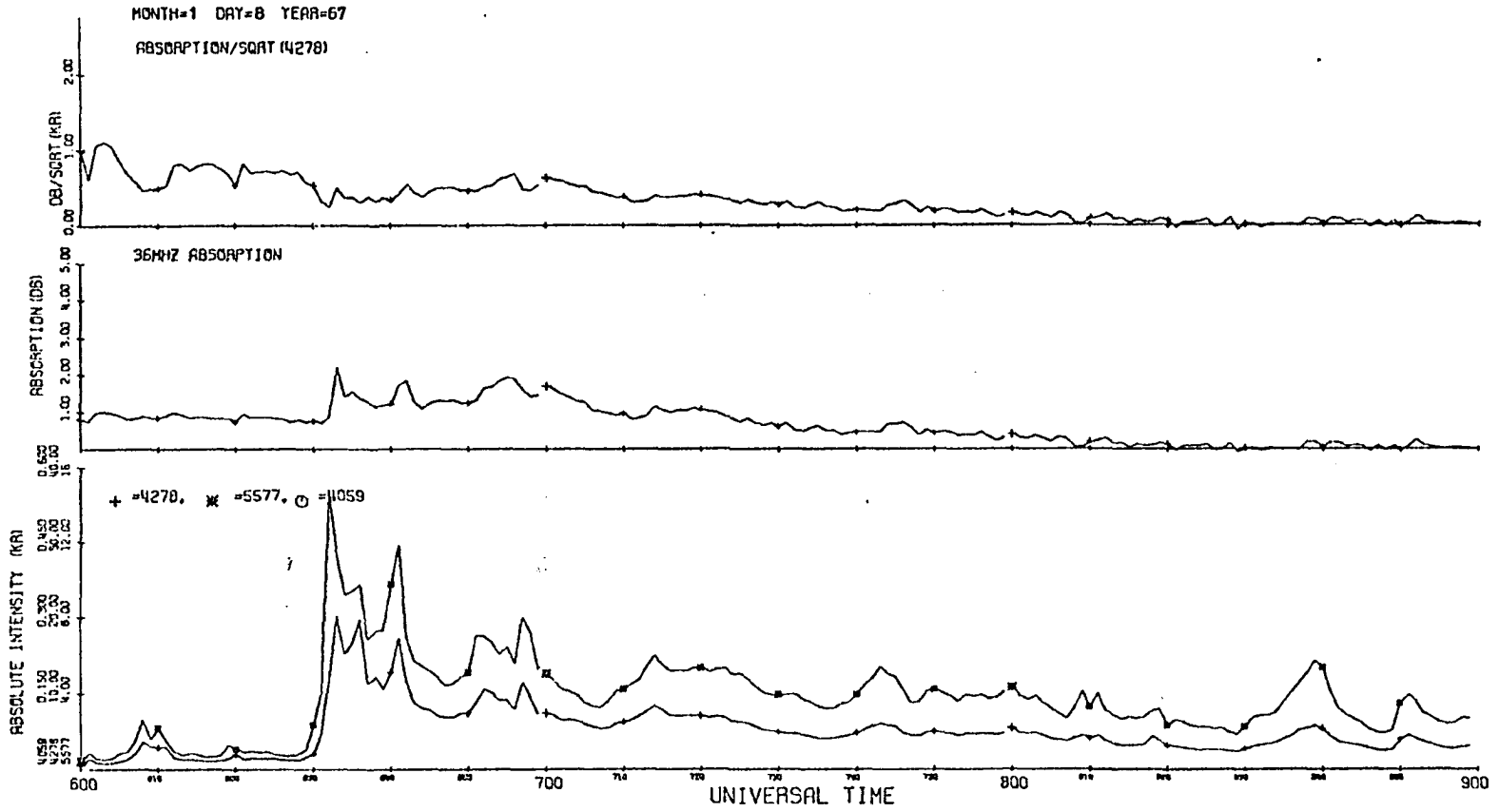

Figure (4.8) Data for the evening-sector event of January 8, 1967.

Figure (4.9) All-sky camera photographs for the interval 0948 to 1002 UT on December 13, 1966.

13 December 1966

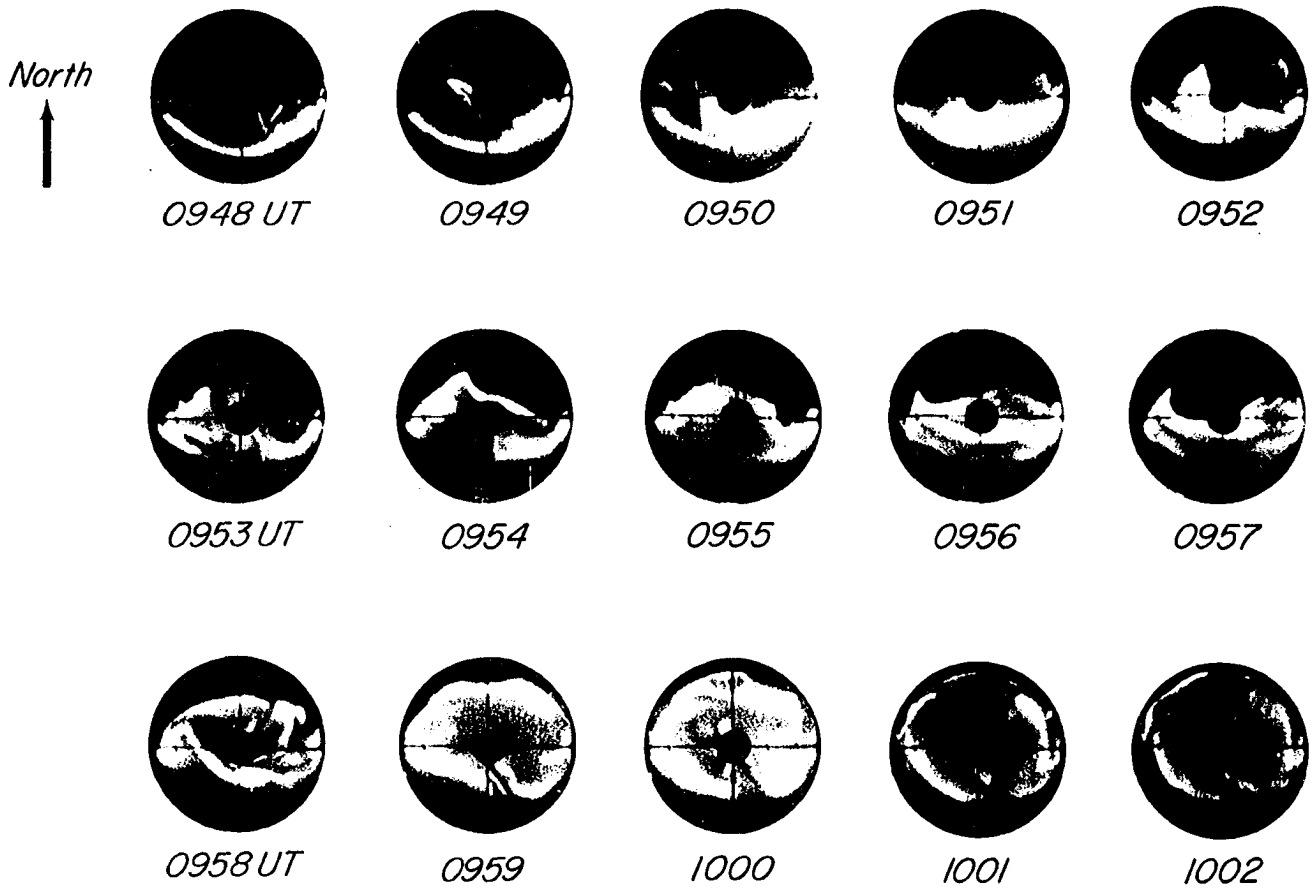

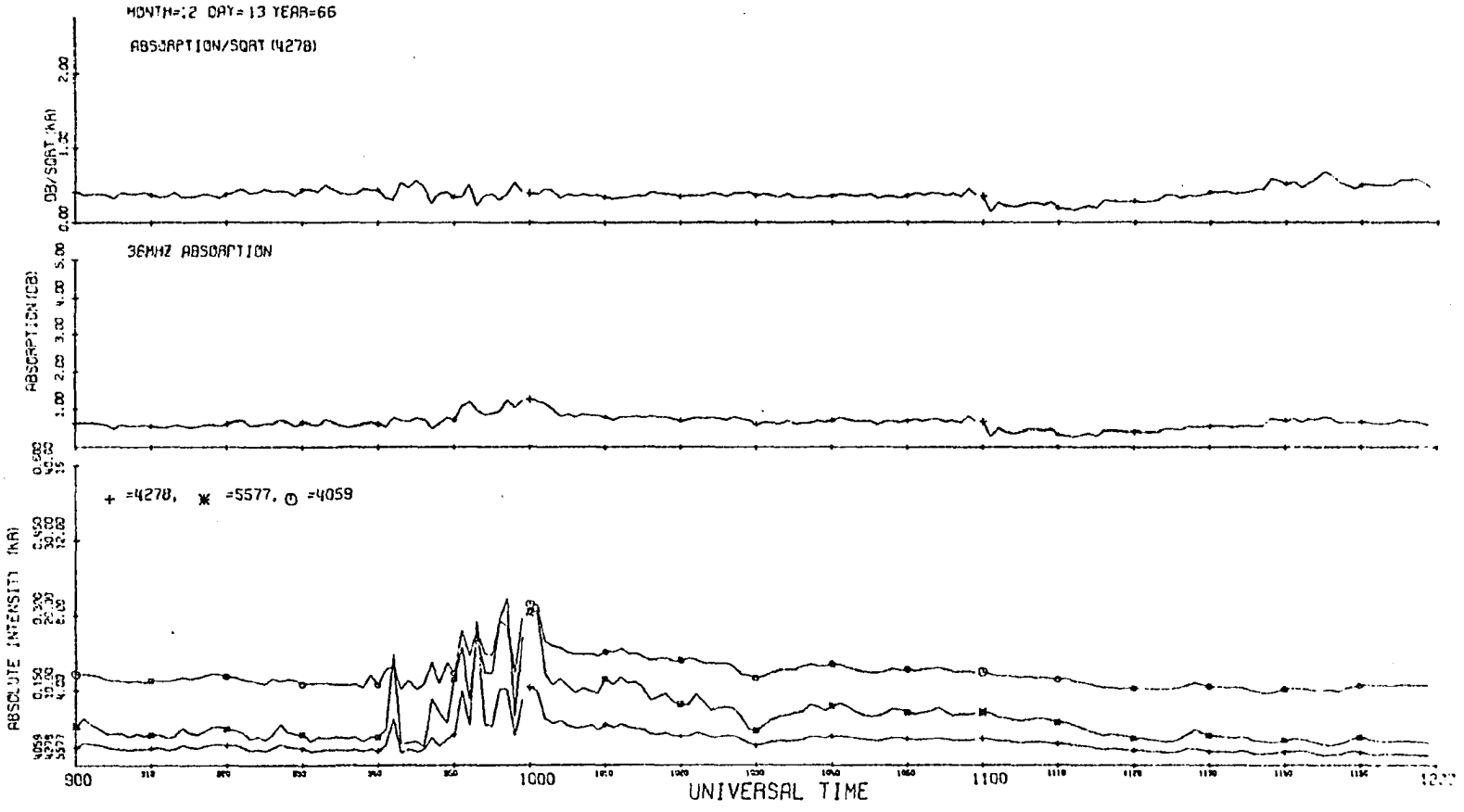

Figure (4.10) Data for the midnight-sector event of December 13, 1966.

4.4.2 The Event of December 5, 1966

On December 5, 1966 a particularly interesting event occurred between 0840 and 0850 UT, apparently associated with a substorm occurrence which caused a large positive increase in the College H-component. Although this event has been described in the literature (Beach et al., 1968), the auroral absorption and luminosity have not been discussed in detail. As illustrated by the all-sky camera photographs in Figure 4.11 the aurora moved equatorward into the zenith at College (∿0820 UT), became activated (∿0840 UT) and then moved poleward (∿0850) UT). In Figure 4.12 the corresponding photometer and riometer variations are depicted. Prior to 0839 UT no absorption was recorded, although the photometers registered an increase in luminosity beginning at 0820 UT when auroral forms moved into the zenith. At 0837 UT the auroral luminosity increased several fold, and numerous times over the next 13 minutes the recording range of all three photometers was exceeded. At 4278A more than 30 kR was recorded, and the 4059A photometer registered in excess of 600 Rayleighs. Maximum absorption was reached at 0845 UT (2.7 db) and again at 0849 UT (2.8 db), both times correlating with a maximum in luminosity. Although the luminosity decreased abruptly at 0850 UT from 34 kR to 7 kR (4278A), the absorption magnitude remained at 2.6 db decreasing to 0.3 db at 0851 UT. The correlation coefficient between luminosity and absorption for the period 08-09^{h} UT was in the range 0.60 - 0.79 for all photometers. The ratio $A/\sqrt{I}_{4278}$ exceeded a value of 0.5 only at 0850 UT when the auroral luminosity decayed.

Cresswell (1968) observed that the aurora was flickering during the period of time discussed above. According to Beach et al. (1968)

Figure (4.11) All-sky camera photographs for the December 5, 1966 event. The right sides of four of the photographs were printed darker in order to show details of the auroral structure at times of most intense aurora (after Beach et al, 1968).

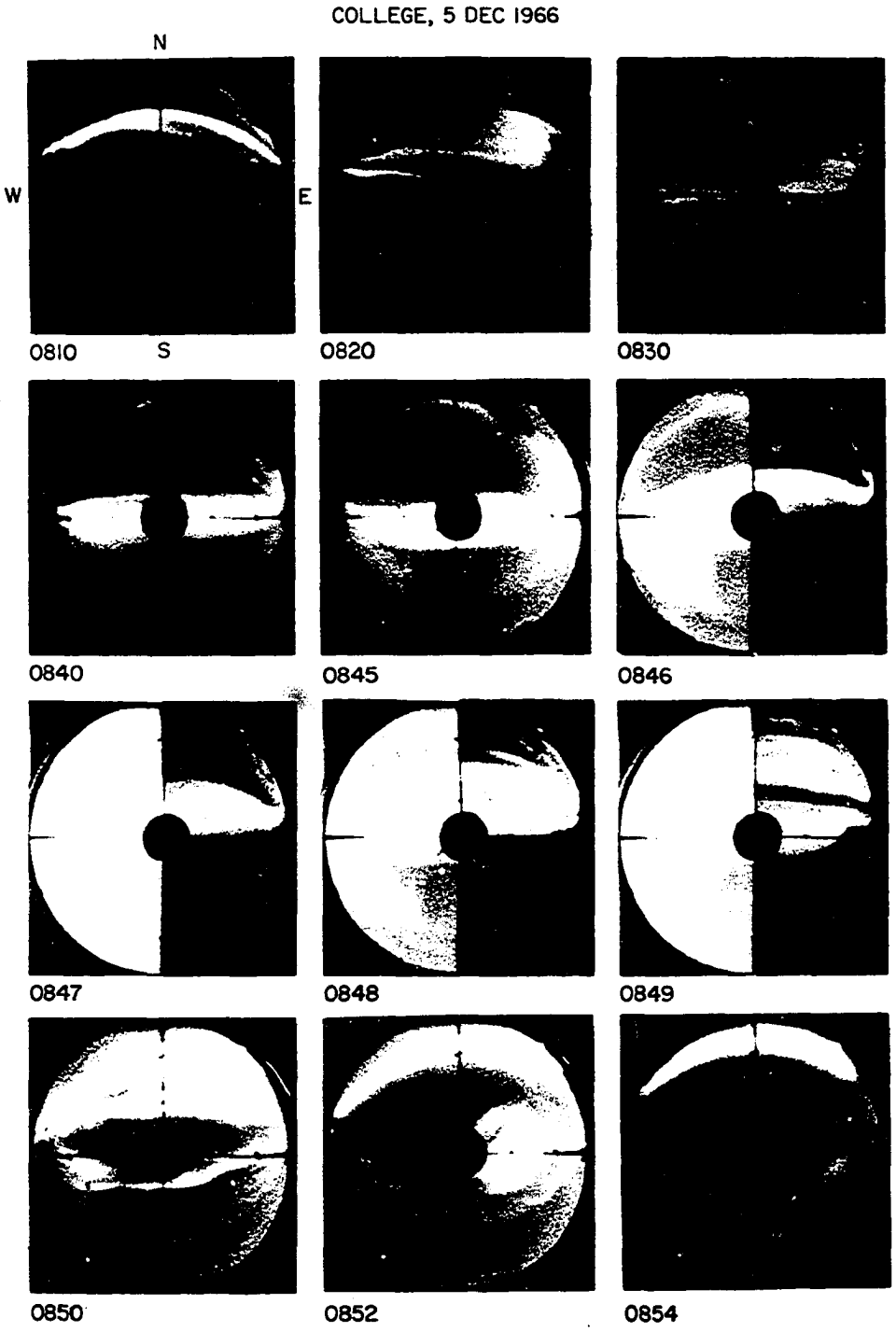

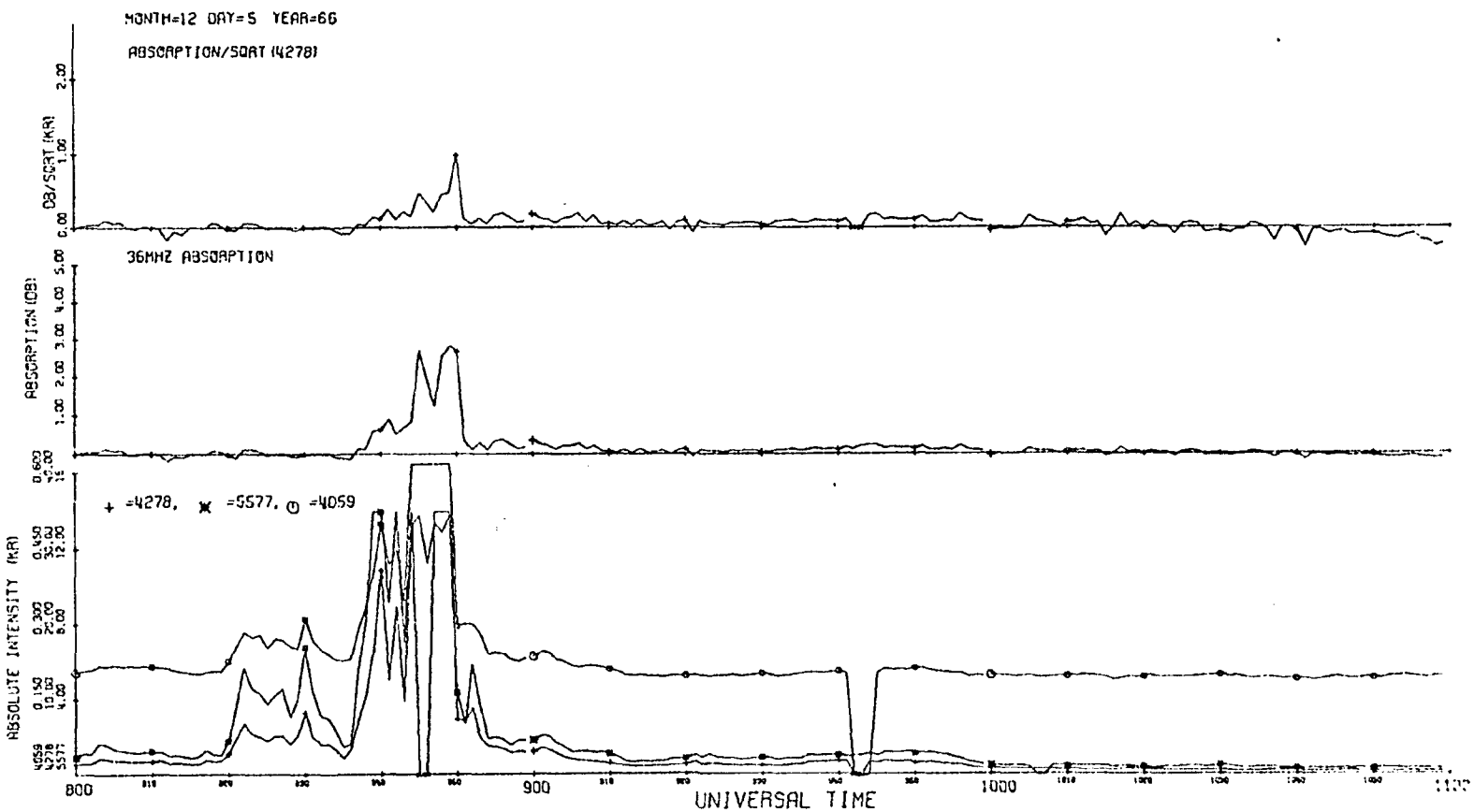

Figure (4.12) Data for the midnight-sector event of December 5, 1966.

"flickering auroras occur only just before and during breakup; the frequency (of flickering) is relatively fixed at 10±3 Hz; the intensity is high...; the flickering features are mainly in the form of interconnected spots of diameter 1-5 km; and high speed (>5km/sec) horizontal motions are observed during the flickering: the motion involves either the flickering elements or nearby filamentary structures." In an attempt to express the flickering quantitatively, Cresswell (1968) defined a flickering "index" with which he derived a histogram on which the 36 MHz was also plotted. From this histogram, Cresswell (1968) concluded that "the precipitation of large fluxes of energetic electrons was associated with the precipitation of highly time-structured fluxes of auroral energy electrons." Cresswell (1968) noted that the arc containing the flickering elements aligned itself through the zenith at 0845 UT, coincident with the maximum in absorption and just prior to a sharp positive spike of 400γ amplitude in the H-component. No flickering was observed after 0850 UT.

Using the image orthicon television observations made during this event, Beach et al. (1968) were able to deduce the spatial extent of an individual flickering patch. Their calculated dimensions were 7.5 by 10 km; since the patch was not rectangular (see Figure 2 of Beach et al.), it may be assumed that the total area was less than 75 km^2, say 55 km^2. The projected area subtended at 80 km height by the major lobe of the array used in this study is approximately 75 km^2. Thus a patch of 55 km^2 area would fill approximately 75 percent of the field of view; it can further be shown that the effect of a uniform absorbing

layer covering 75 percent of the field of view of the array would result in approximately 2.8 db of absorption, similar to that recorded during the flickering aurora.

The observation discussed here associated increased radio wave absorption with pulsing patches contained in an arc and termed 'flickering aurora.' A close spatial coherence of the emission and absorption mechanisms is inferred from measurements of the size of a typical pulsing patch. This inference can be used either to support Cresswell's conclusion that both the high (>30 kev) and low energy electrons were highly time structured, or to conclude that the flickering was occurring in the same height regime as was the absorption.

4.5 Early Morning and Dawn Sectors

Because of the similarity of activity which is observed after midnight, the early morning and dawn sector events will not be differentiated. For all but the weakest substorms, College lies within the boundaries of the auroral oval until approximately dawn. During this period of time characteristic auroral features are pulsating patches and arcs, Ω - bands, and during intense storms, flaming aurora. The auroral absorption is found to increase at a slower rate than during, say, the midnight sector but is often of a greater intensity and duration.

4.5.1 The Event of March 6, 1971

On March 6, 1967 a slowly increasing negative bay was associated with a substorm which began at approximately 12^h UT. The amplitude of the negative bay was largest ($\Delta H = 150\gamma$) at 1400 UT and by 1500 UT had

recovered to a quiet-day level. However, between 1337 and 1347 UT a positive increase of the H-component occurred which coincided with the eastward propagation of an Ω - band approximately halfway between College and Fort Yukon (see Figure 4.13). At the same time, patchy aurora appeared in the zenith at College. Note that while the absorption began to increase at 1327 UT (see Figure 4.14), no marked increase in 4278A luminosity occurred until 1337 UT when the positive impulse in the H-component was recorded. At 1344 UT maximum absorption (2.1 db) was recorded; three minutes earlier, a maximum of 5 kR was observed at 4278A.

4.5.2 The Event of January 9, 1967

An event recorded on January 9, 1967 near 15^h UT exemplified the disintegration of an arc into eastward drifting patches. A substorm onset occurred near 1430 UT with the amplitude of the associated negative bay reaching ∿510γ at 1504 UT. At 1441 UT a faint arc extended through the zenith (see Figure 4.15) and at 1443 UT the first indications of a surge propagating eastward along the arc could be detected. At 1446 UT the surge passed through the zenith causing the 4278A intensity to increase to 26 kR while creating only a small increase in the absorption (see Figure 4.16). However, about two minutes later the absorption began to increase, reaching 2.8 db at 1456 UT. At this time the 4278A intensity was 7.6 kR, but the aurora consisted of eastward drifting patches.

Figure (4.13) All-sky camera photographs for the interval 1330-1345 on March 6, 1967.

6 March 1967

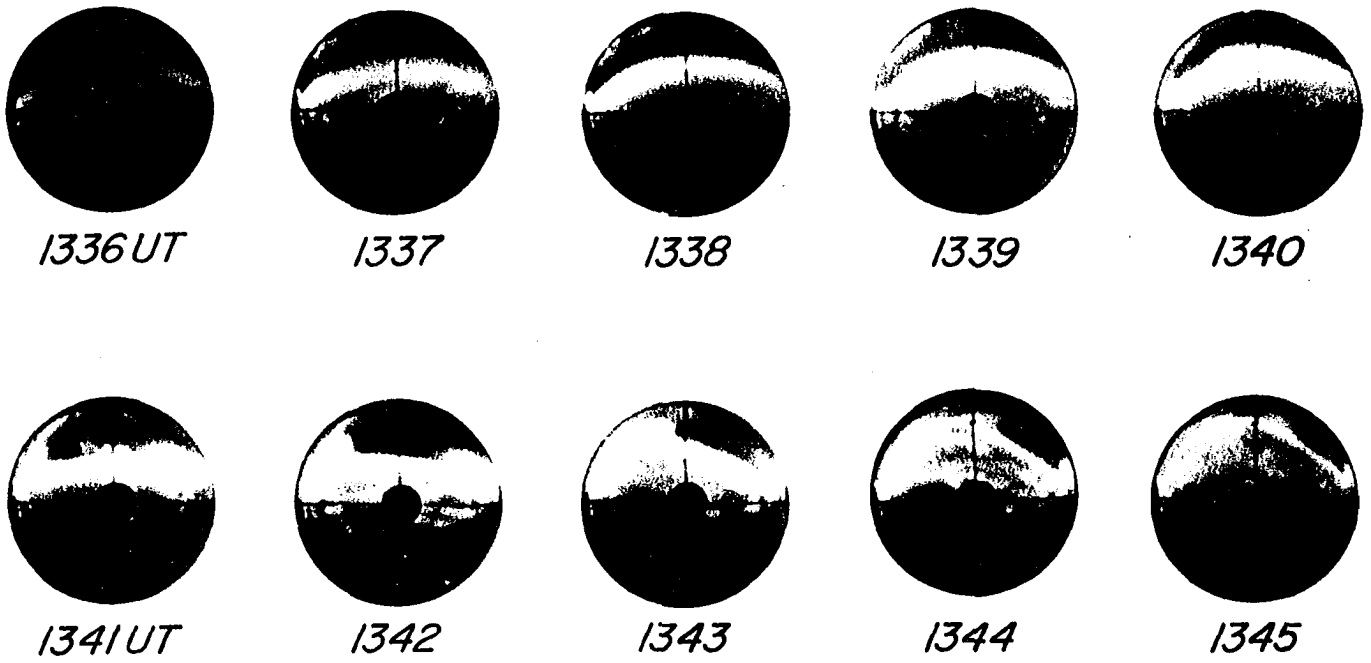

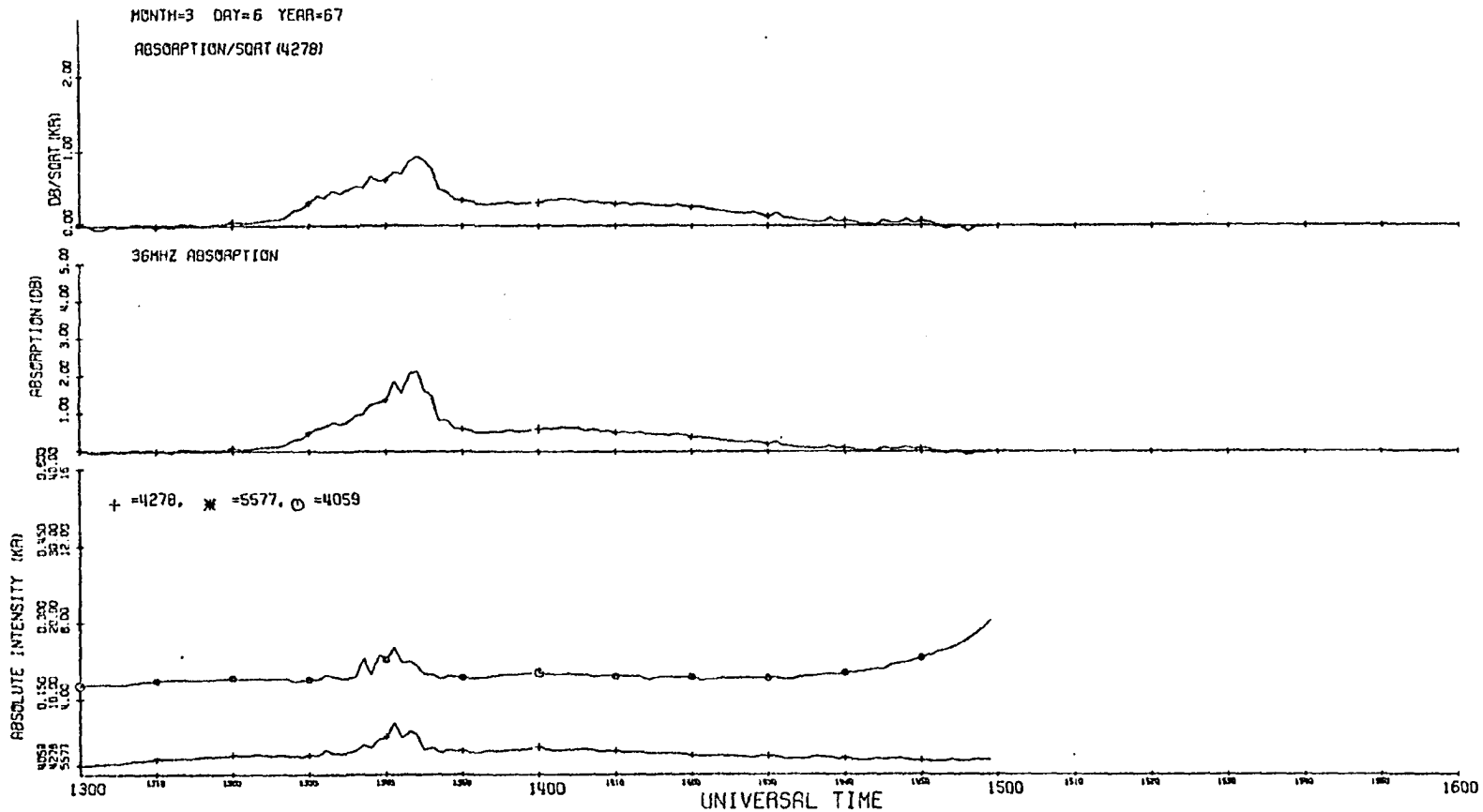

Figure (4.14) Data for the morning-sector event of March 6, 1967.

Figure (4.15) All-sky camera photographs for the interval 1441 to 1504 on January 9, 1967.

9 January 1967

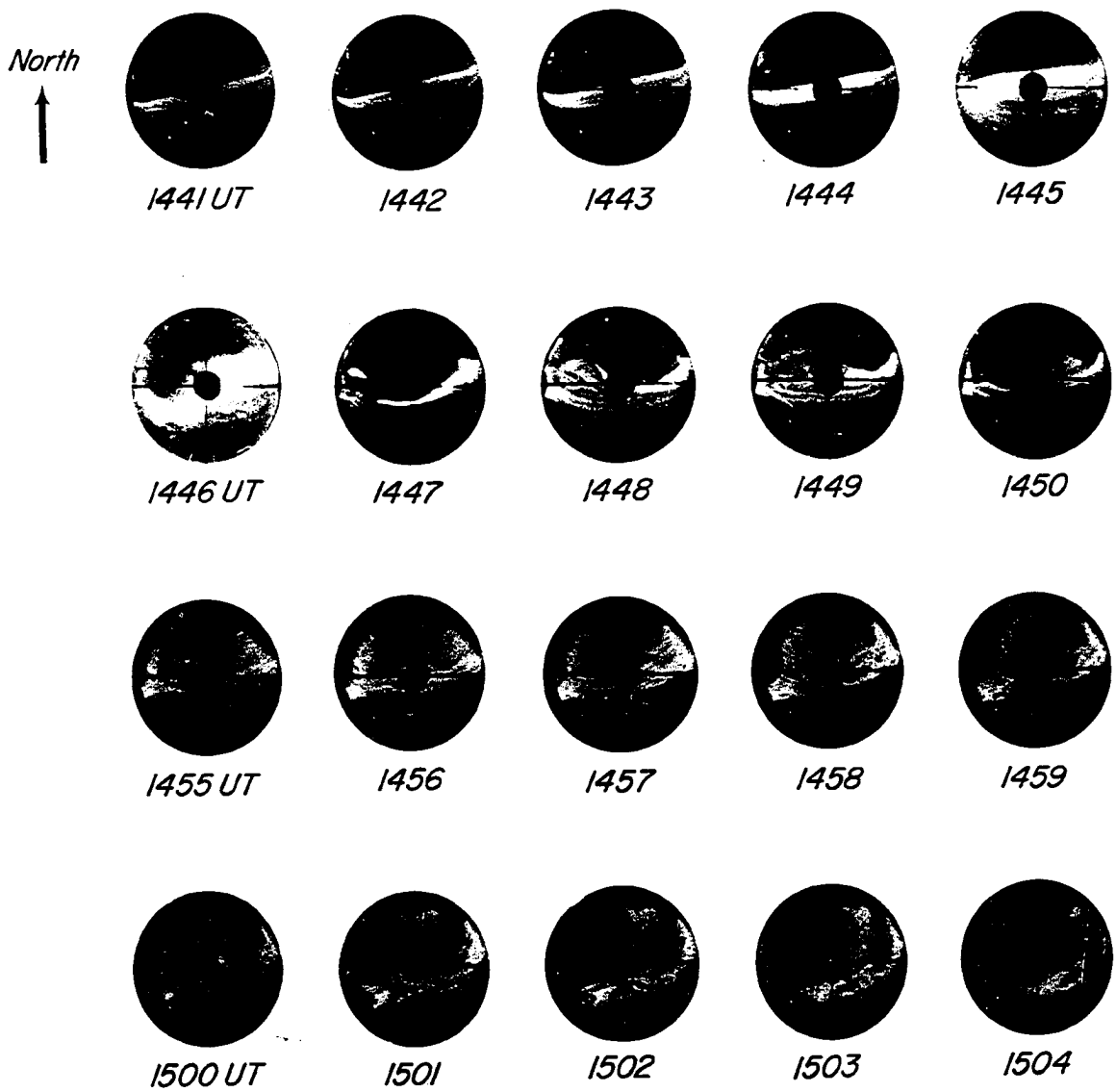

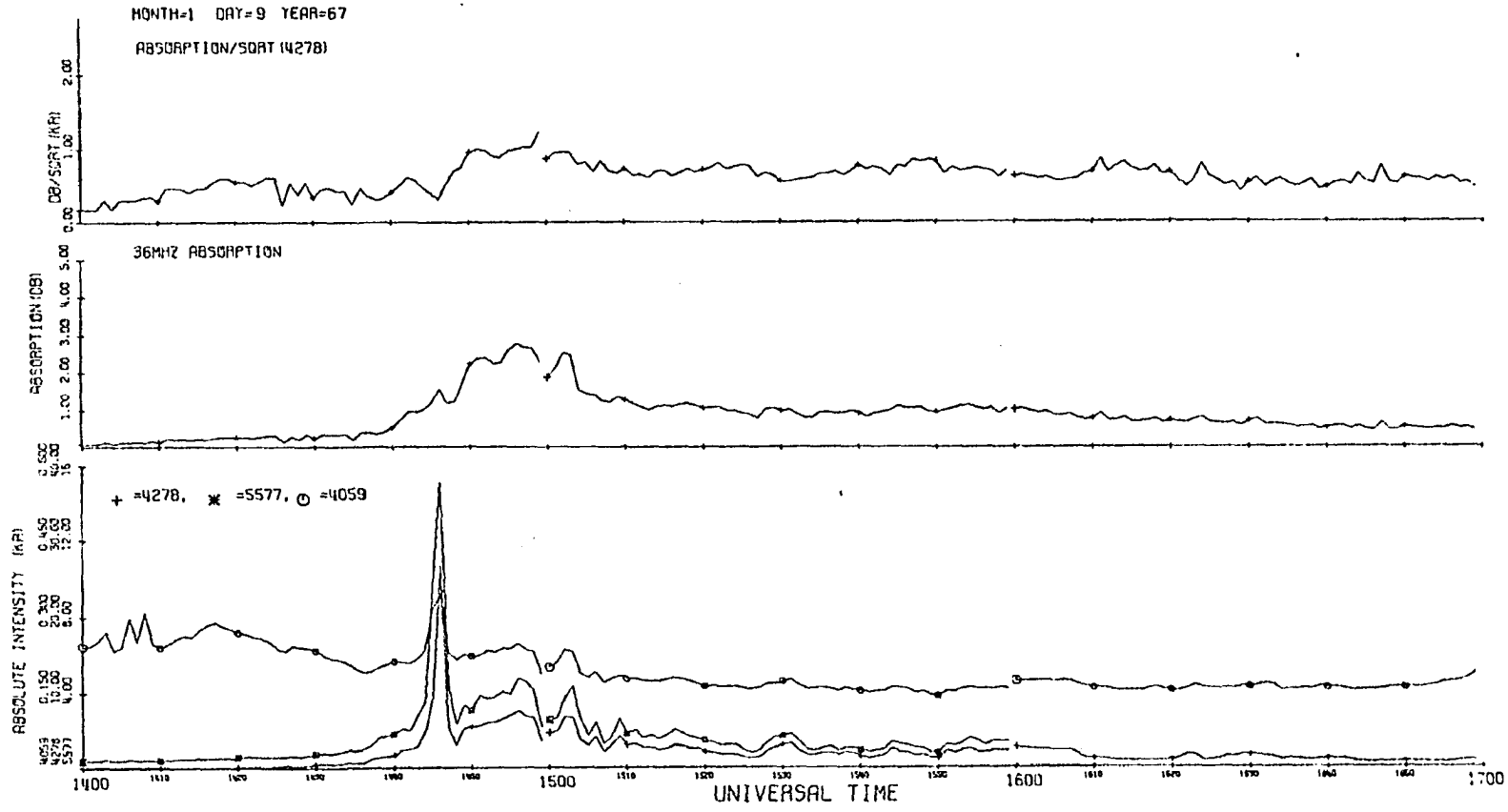

Figure (4.16) Data for the morning-sector event of January 9, 1967.

4.5.3 The Event of January 11, 1967

In the previous example, the negative bay associated with the substorm had a gradual onset. Furthermore, College was located well to the east of the midnight sector. In this example, College is situated closer to the midnight sector and the onset of the polar magnetic substorm is more abrupt.

At 1252 UT on January 11, 1967 the onset of a substorm was signalled by a sudden decrease of the H-component on the order of 670γ; at approximately the same time, the absorption began to increase, reaching 2.2 db at 1255 UT (see Figure 4.17). The increase in absorption was coincident with the movement of an arc into the zenith (see Figure 4.18), the intensity of which was about 4 kR at 4278A. At 1307 UT a further decrease of the H-component was accompanied by the disintegration of the arc into patches and an increase in absorption; the onset of pulsating aurora began a few minutes later. The absorption maximized at 1318 UT with a magnitude of 2.8 db. Note the increase of 4059A luminosity relative to that at 4278A between 1316 and 1333 UT; this increase occurs several minutes after the maximum in absorption was reached.

From the all-sky camera data it appears as though College is located near the poleward boundary of the region in which pulsating, patchy aurora occurs during this substorm. This suggests that the auroral oval may have expanded equatorward during this substorm.

4.5.4 The Event of December 21, 1966

Although the substorm onset was first evidenced by a sudden decrease in the H-component at 1512 UT on December 21, no appreciable

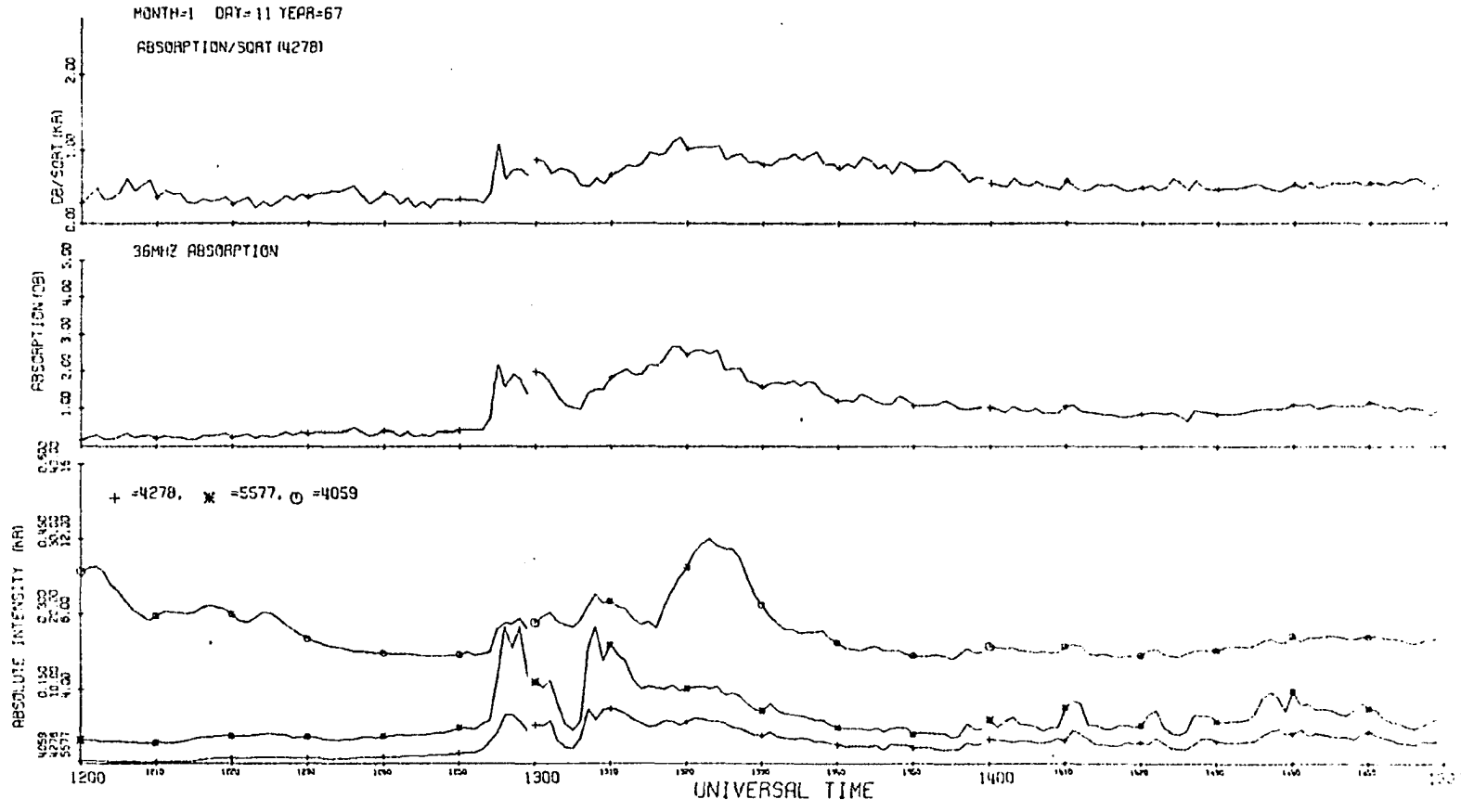

Figure (4.17) Data for the morning sector evening of January 11, 1967.

Figure (4.18) All-sky camera photographs for the intervals 1254 to 1308 and 1317 to 1330 UT on January 11, 1967.

11 January 1967

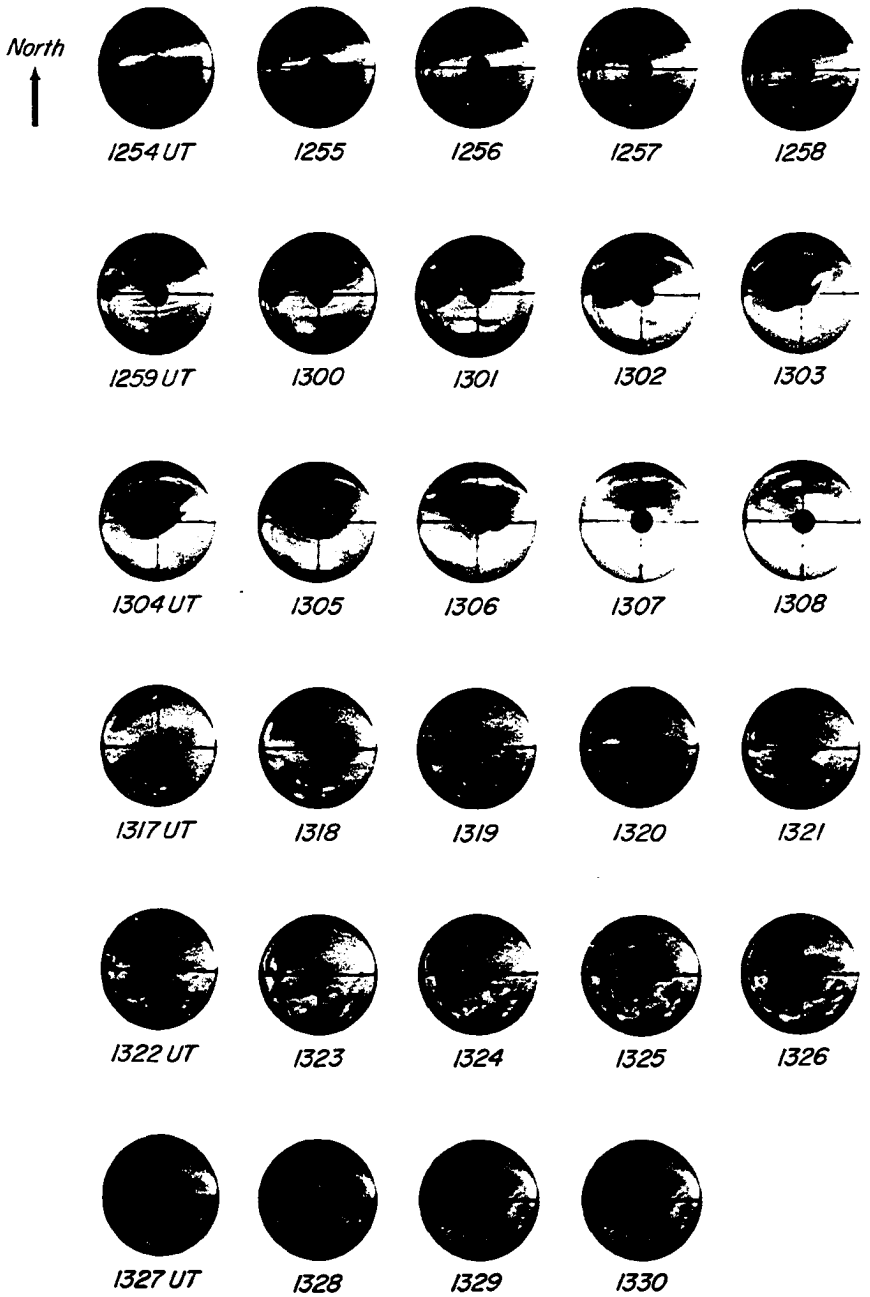

increase in absorption occurred until about 1520 UT (see Figure 4.19). Maximum absorption (2.0 db) was reached at 1528 UT; auroral luminosity did not exceed 4 kR (at 4278A) at any time during this event. Again, note an increase in 4059A luminosity relative to 4278A shortly after the absorption maximum.

This substorm was considerably less intense than the two discussed previously as evidenced by the less than 200 amplitude of the H-component negative bay. The patchy aurora which occurred during this event arose from the disintegration of an arc poleward of College (See Figure 4.20). Small amplitude pulsations accompanied the patchy aurora.

4.5.5 The Events of October 6, October 16, December 14, 1966, January 7, and January 8, 1967.

Substorms occurring in the morning sector on October 6, October 16, December 14, 1966 and January 7, 1967 were all associated with intense magnetic pertubations ($\Delta H \geq 900\gamma$) during which the College K - index reached a value of 7.

On October 6, there appeared to occur a succession of substorms commencing at about 09^h UT. The absorption increased sharply at 1025 UT and exceeded 1 db throughout the rest of the night. The most intense absorption occurred at 1318 UT (5.6 db) and 1331 UT (6.3 db); maximum 4278A luminosity occurred at 0909 UT (14 kR). Note that the ratio $A/\sqrt{I}_{4278}$ exceeded a value of 2 after 1230 UT (see Figure 4.21).

Substorms occurred at 07^h UT, near 11^h UT and near 13^h on October 16 with the most intense substorm beginning at approximately 1230 UT. Again the absorption exceeded 3 db, reaching 3.1 db at 1303 UT and

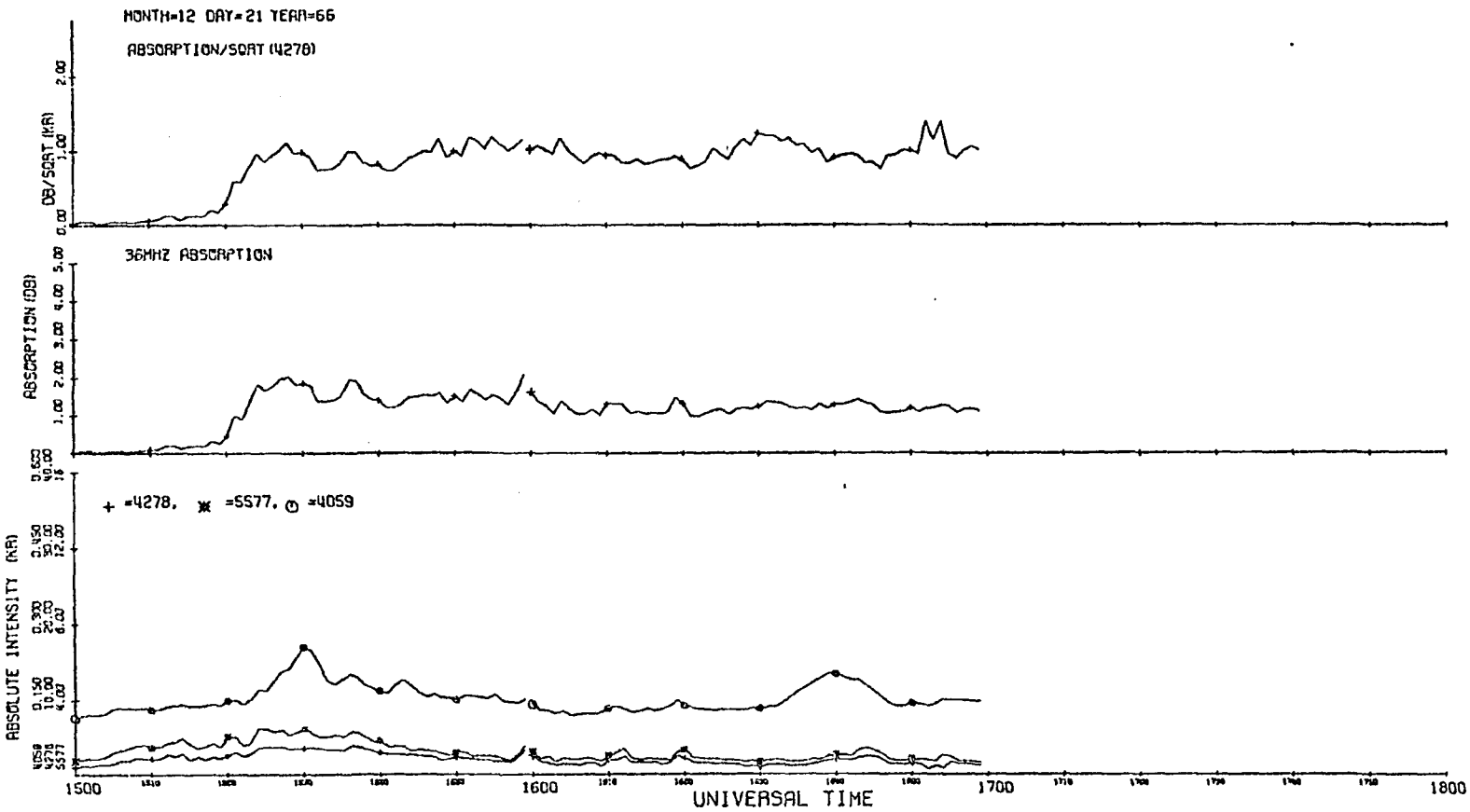

Figure (4.19) Data for the morning sector event of December 21, 1966.

Figure (4.20) All-sky camera photographs for the interval 1514 to 1538 UT on December 21, 1966.

21 December 1966

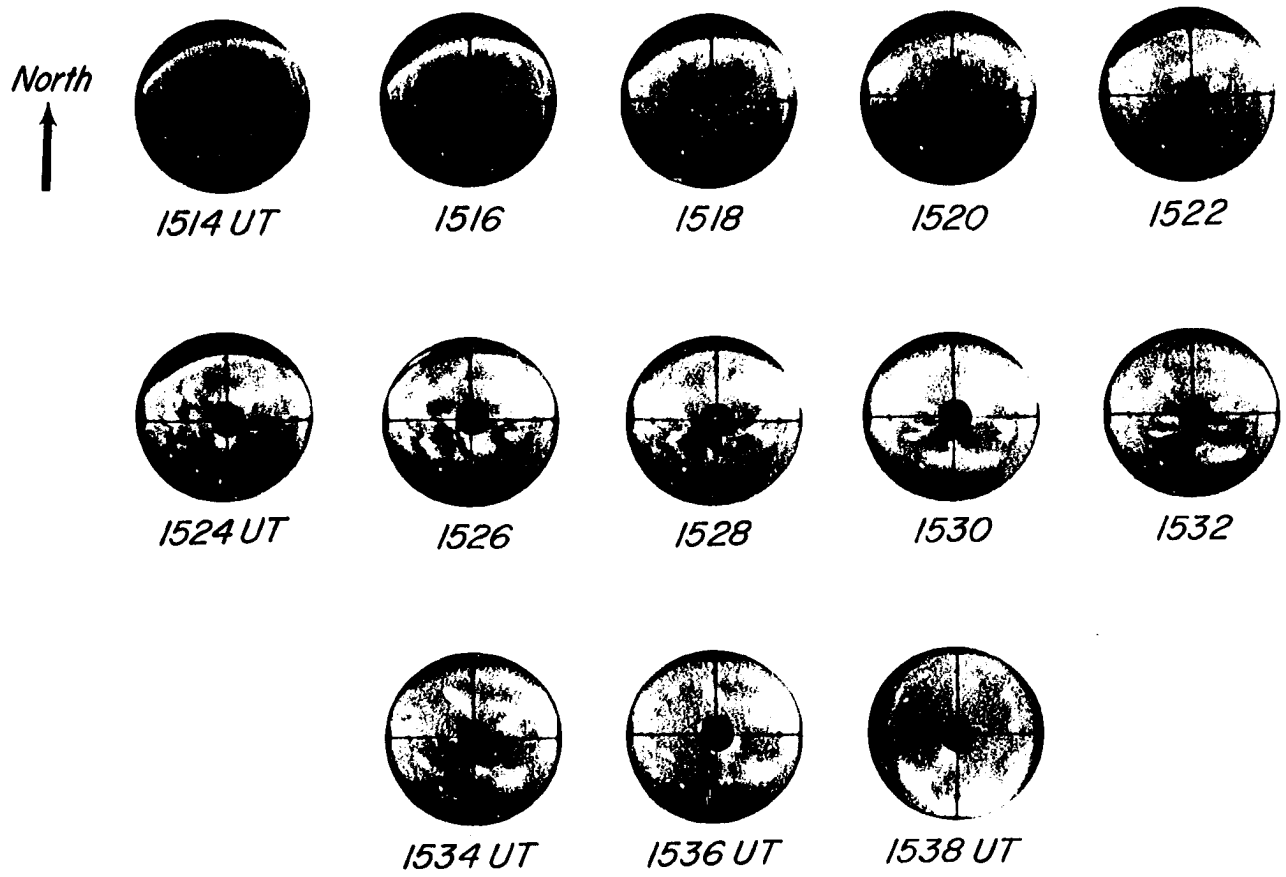

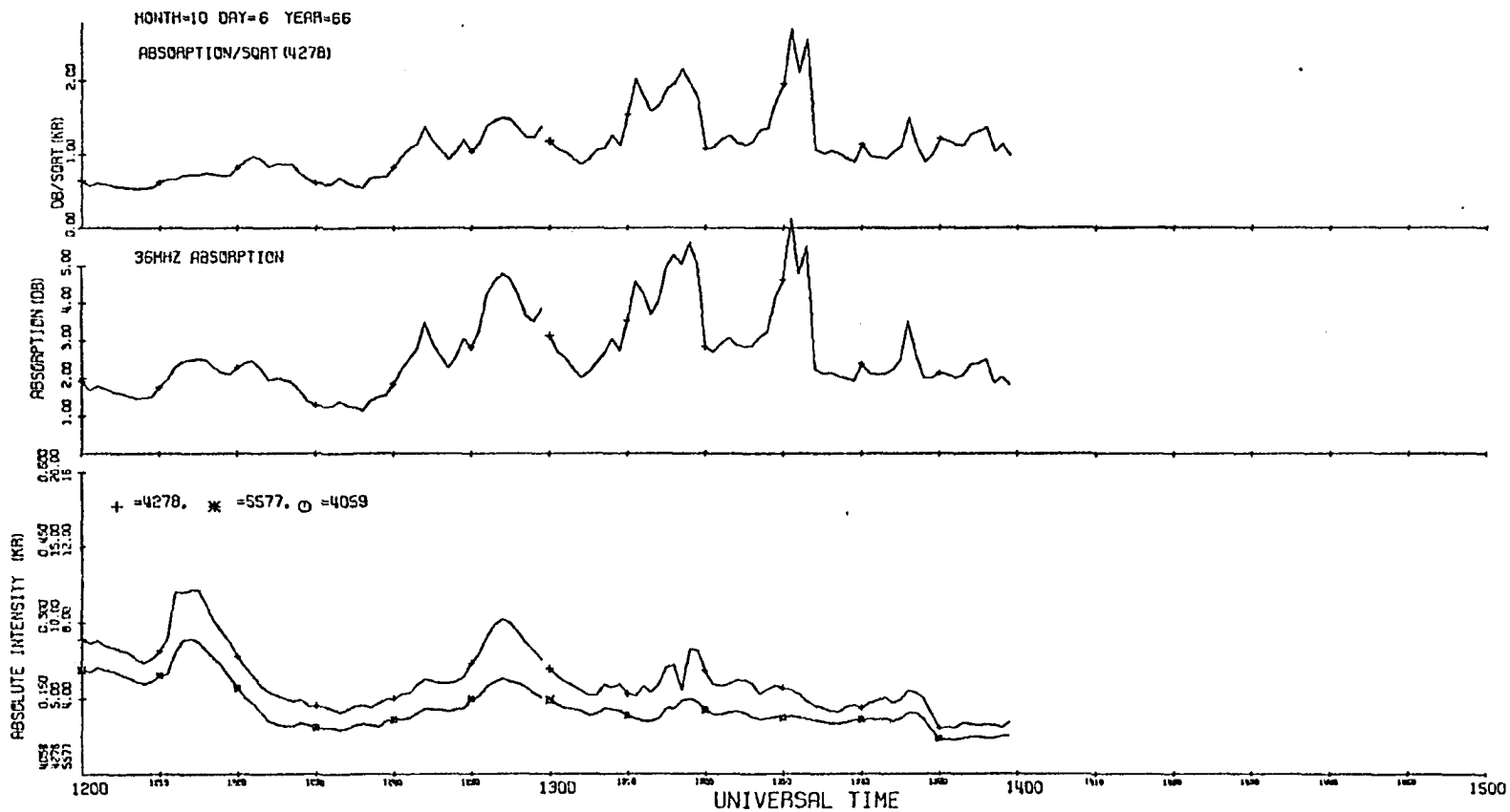

Figure (4.21) Data for the morning sector event of October 6, 1966.

3.6 db at 1337 UT (see Figure 4.22). However, the 4278A intensity exceeded 50 kR during both of these times and the ratio $A/\sqrt{I}_{4278}$ indicated a soft spectrum. No all sky camera datawere available for either this substorm or the substorms of October 6.

A single substorm was observed on December 14, 1966 beginning at approximately 1345 UT. The absorption had a gradual onset at nearly the same time, reaching maximum at 1408 UT and 3.0 db at 1522 UT and 1529 UT. Pulsations were superimposed on the 4278A variations; the absorption maximum at 1408 UT was associated with pulsating aurora. Maximum luminosity occurred at 1519 UT and the electron spectra was soft relative to the October 6 event (see Figure 4.23).

The polar magnetic substorm which began shortly before 13^h UT on January 7, 1967 was very similar to the substorms described previously, having a maximum negative deflection in the H-component at 1320 UT. Disturbed conditions persisted until 17^h UT. The absorption which occurred during this time was highly structured as can be seen in Figure 4.24; the associated 4278A and 5577A luminosity variations were similarly structured and the correlation of absorption and 4278A luminosity exceeded 0.9 between 13^h and 14^h UT. The following table details the activity which occurred between 13^h and 17^h UT:

Hourly Averages of Activity During the Substorm of January 7, 1967

	13-14^{h}UT	14-15^{h}UT	15-16^{h}UT	16-17^{h}UT
Average absorption	1.76 db	2.43 db	2.74 db	2.49 db
Average 4278A Intensity	8.09 kR	10.75 kR	12.06 kR	8.33 kR
Correlation coefficients				
r_1	0.92	0.68	0.60	0.80
r_2	0.91	0.68	0.57	0.81
Average value ratio $A/\sqrt{I}$	0.59	0.74	0.80	0.86

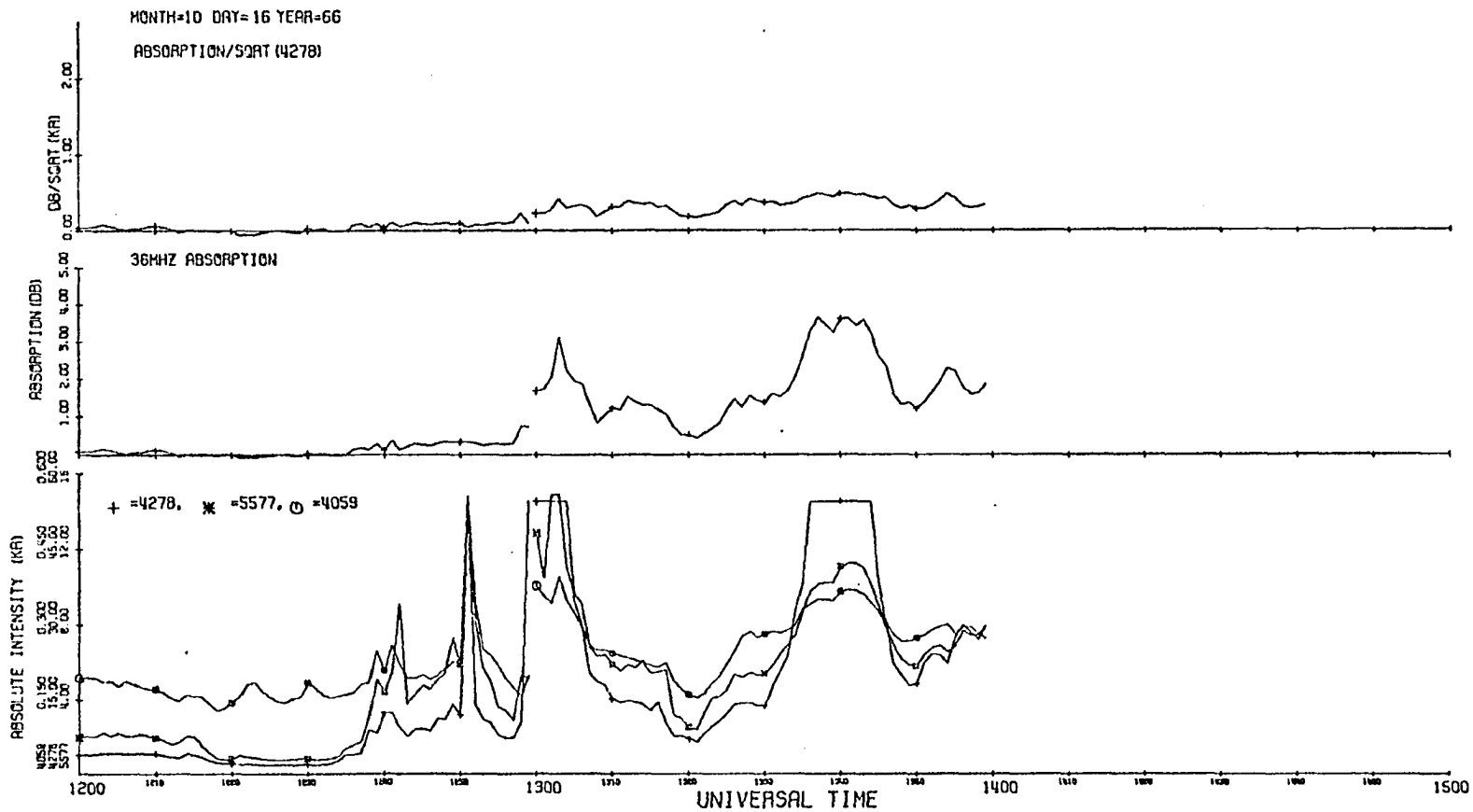

Figure (4.22) Data for the morning sector event of October 16, 1966.

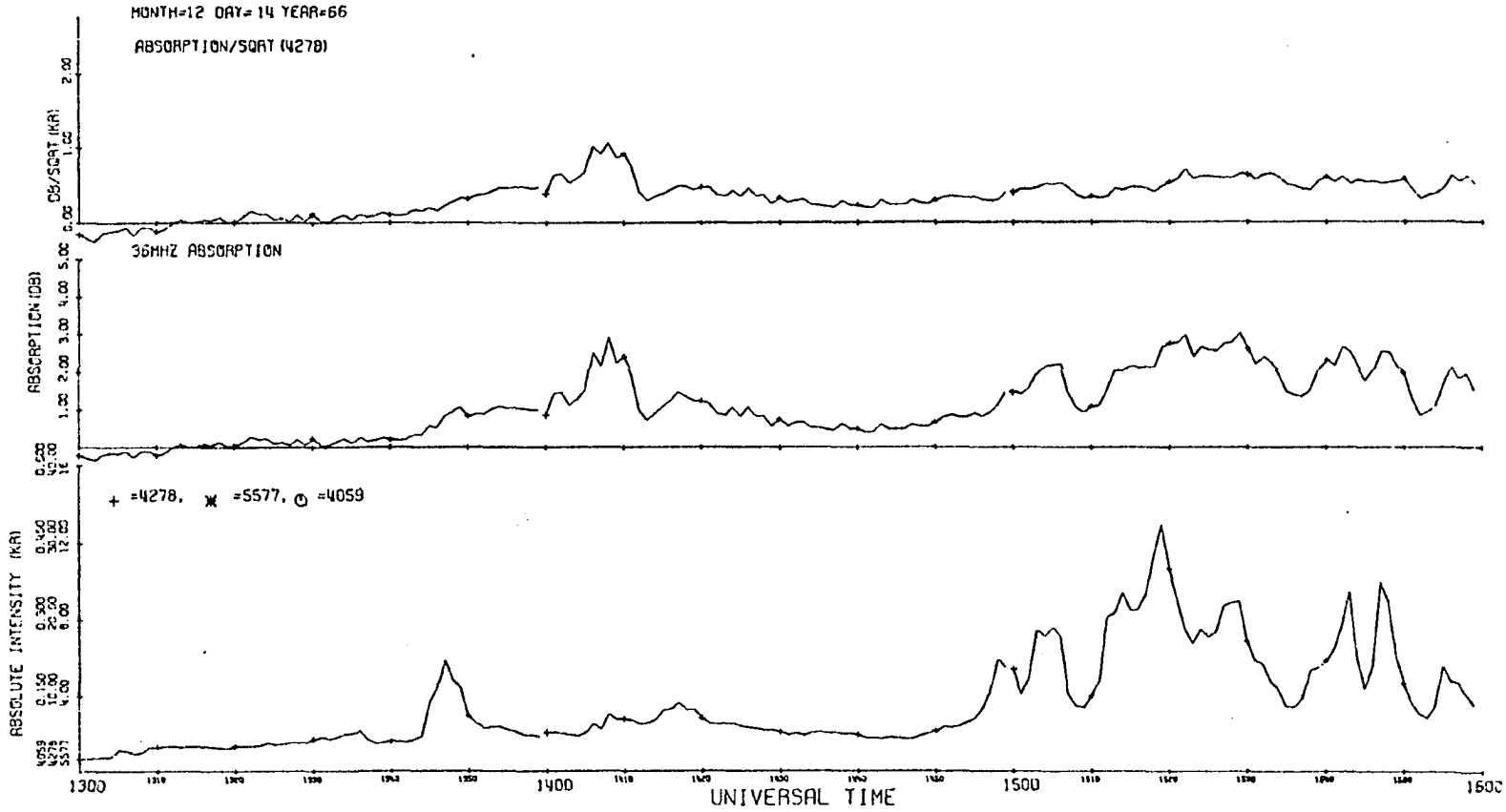

Figure (4.23) Data for the morning sector event of December 14 1966.

Figure (4.24) All-sky camera photographs for the intervals 1304 to 1324 UT and 1444 to 1520 UT on January 7, 1967.

7 January 1967

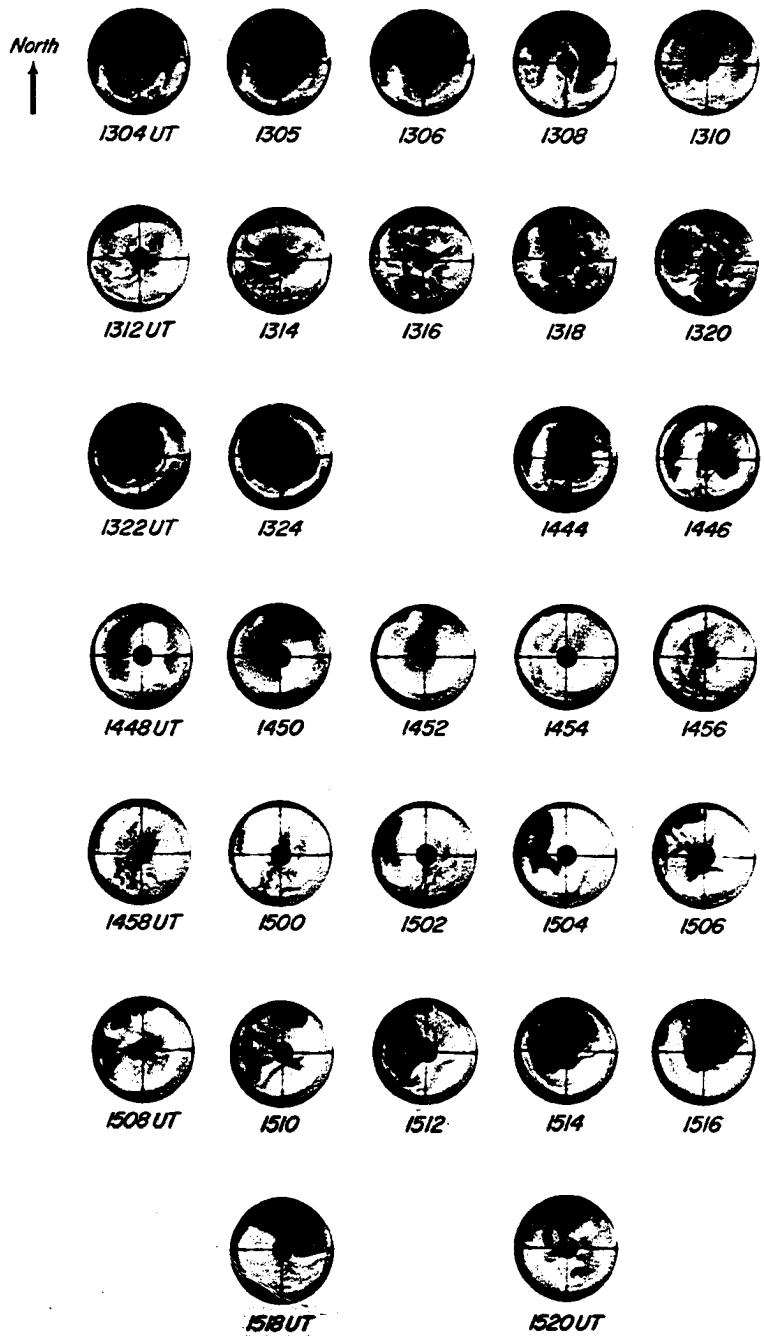

A sequence of all-sky camera photographs is shown in Figure 4.25 to illustrate the chaotic behavior of the aurora during this interval. Large patches of auroral luminosity can be seen to move from west to east through the zenith in the sequence beginning at 1304 UT and again at 1444 UT. No detailed correlation with individual forms was attempted as the individual patches were pulsating.

Two intense substorms, during which the College K-index reached 7, began at 0630 UT and again at 1007 UT on January 8, 1967. By 12^h UT substorm activity at College had subsided, although the all-sky camera showed patchy aurora to occur between 1230 and 1500 UT. Between 1420 and 1430 UT, a large patch whose intensity was about 10 kR, moved eastward through the zenith (see Figure 4.26). Although this patch was only slightly less intense than those which were observed on January 7, the associated increase in absorption was about 0.5 db (see Figure 4.27). There were, however, no pulsations superimposed on the 4278A variations.

At 0630 and 1006 UT increased fluxes of 50-150 kev electrons were observed at synchronous orbit by ATS 1 (6.6 R_e, 150°W) (Lezniak and Winckler, 1970). There were no further increases in the 50-150 kev electron counting rate after 11^h UT; this suggests that there were no substorm occurrences west of College. Had there been a substorm, ATS 1 would have recorded an increase in electron flux before the patches were observed at College.

The significance of this example lies in the fact that only a small increase of absorption was associated with this patch, in contrast with the previous examples. However, there are two primary differences between this event and, say, the preceeding night:

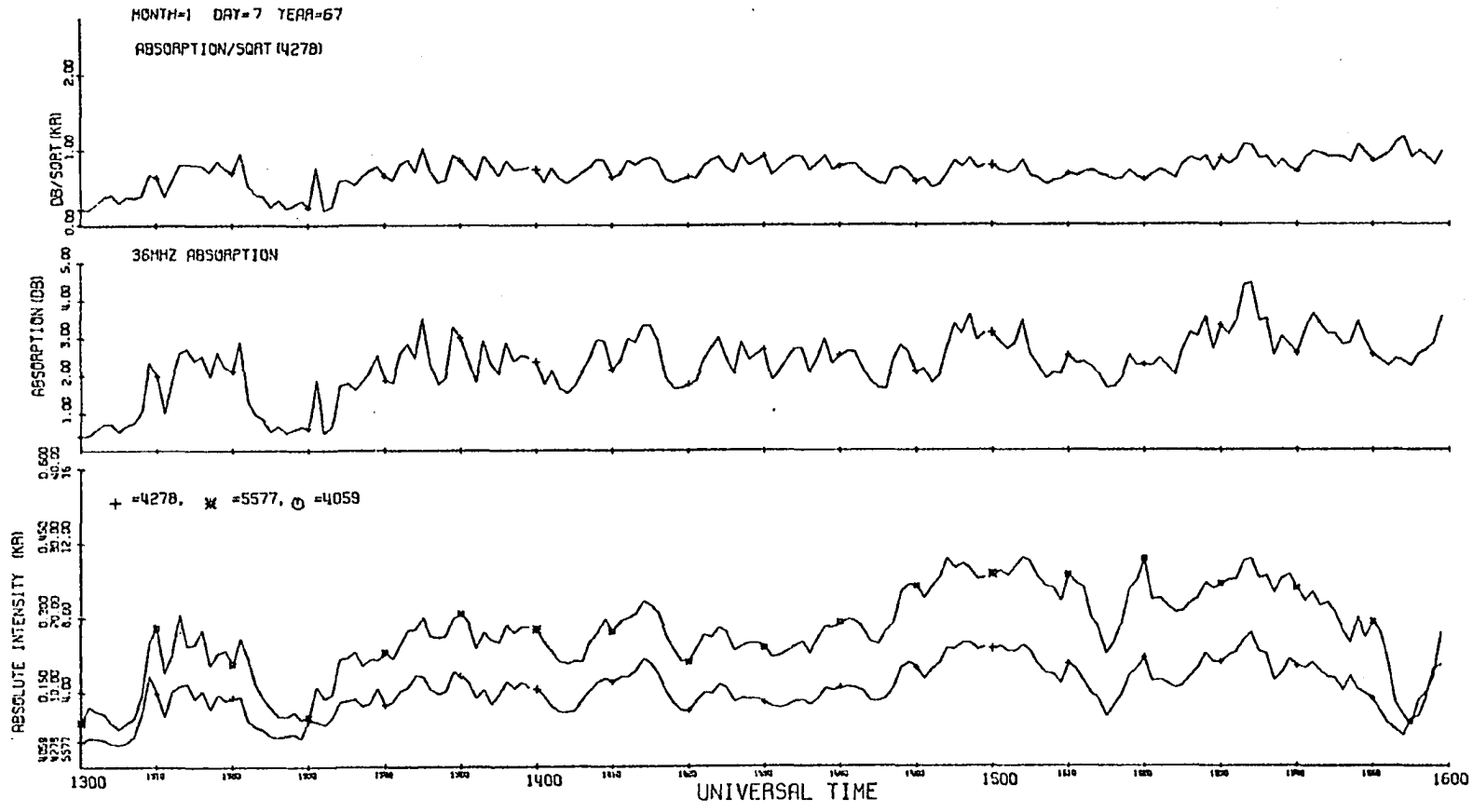

Figure (4.25) Data for the morning sector event of January 7, 1967.

Figure (4.26) All-sky camera photographs for the interval 1420 to 1434 UT on January 8, 1967.

8 January 1967

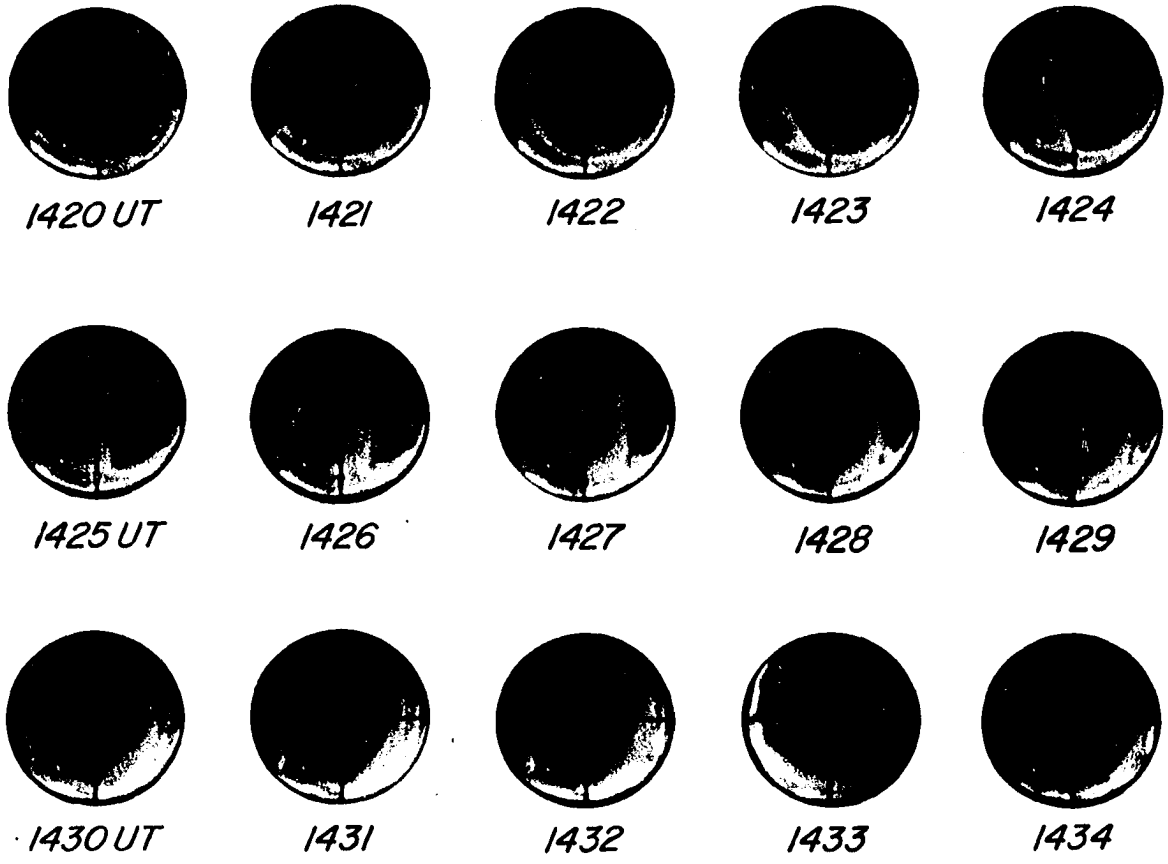

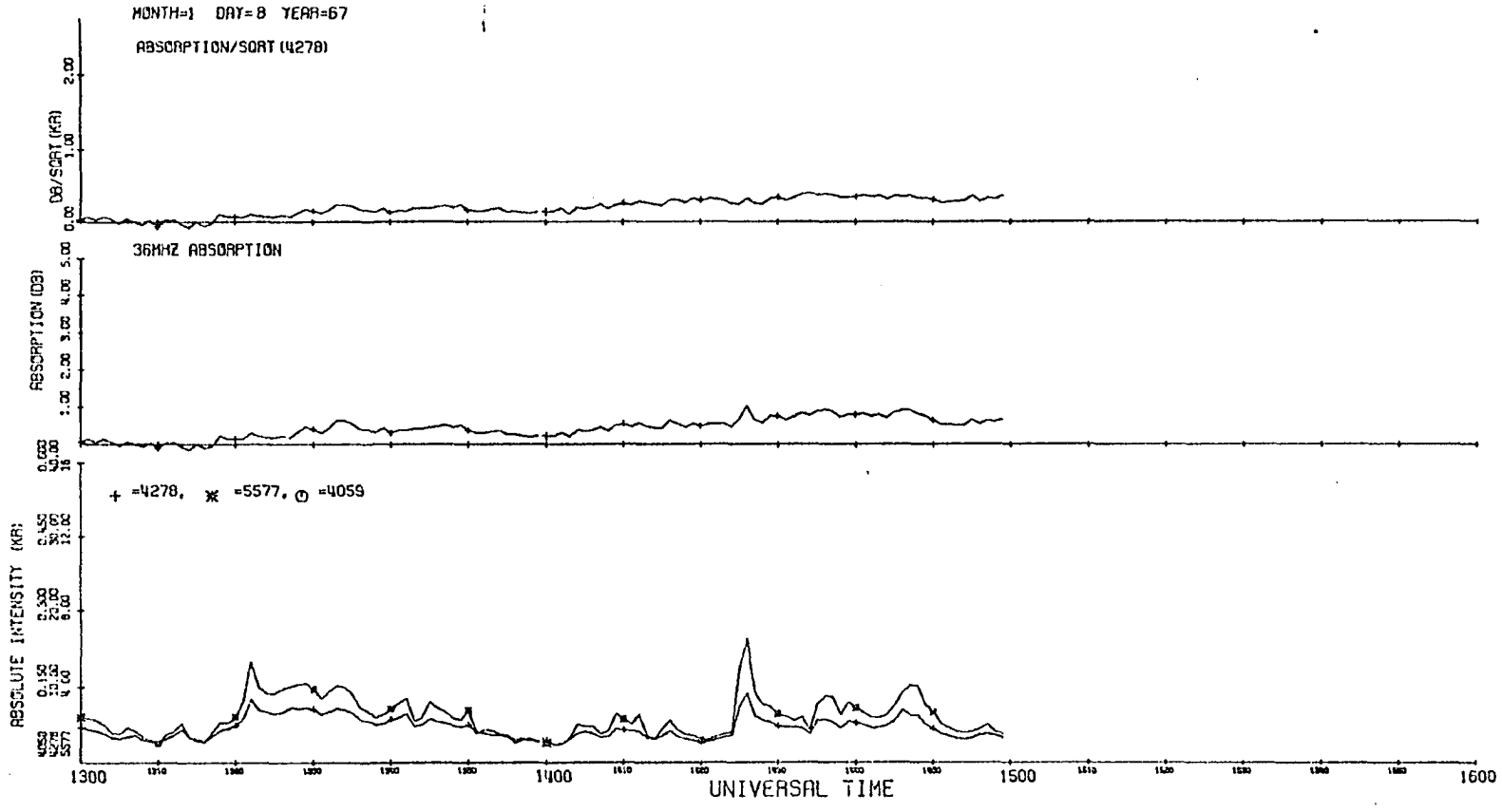

Figure (4.27) Data for the morning sector event of January 8, 1967.

(1) no polar magnetic substorm in progress at the time, and; (2) the absence of pulsating aurora.

4.5.6 The Event of February 16, 1967

On February 16, 1967 a particularly intense disturbance occurred between approximately 11^h and 14^h UT. A negative bay onset was recorded at 1130 UT; the amplitude of the H-component decrease was about 2300 gamma. The local K-index during the period 09^h to 15^h UT attained a value of 8. Beginning at 1130 UT a spectacular display of flaming aurora was observed and is described by Cresswell (1969). Chamberlin (1961) has defined flaming aurora as "waves of light (which) move rapidly upward, one after the other, from the base of the aurora toward the magnetic zenith." This definition accurately characterizes the aurora seen on February 16, 1967.

In the interval from 1130 UT to 1135 UT, the absorption increased dramatically from 0.2 db to 7.5 db (see Figure 4.28), the latter value being the largest absorption magnitude recorded during the course of the experiment. It is also of interest to note that the broadbeam 30 MHz riometer recorded nearly 14 db of absorption at the same time. At 4278A, the auroral luminosity increased from 2.2 kR to some value in excess of 40 kR, the level at which the recorder was limited. Similarly, the 4059A photometer was off scale at a level of 780 Rayleighs. The value of the ratio $A/\sqrt{I}_{4278}$ increased from 0.3 at 1130 UT to a value of 1.14 at 1134 UT, shortly before the 4278A photometer reached its saturation level. It is interesting to note that between 11^h and 12^h UT the correlation coefficient between absorption and the square root of luminosity was 0.97 for both 4278A and 4059A.

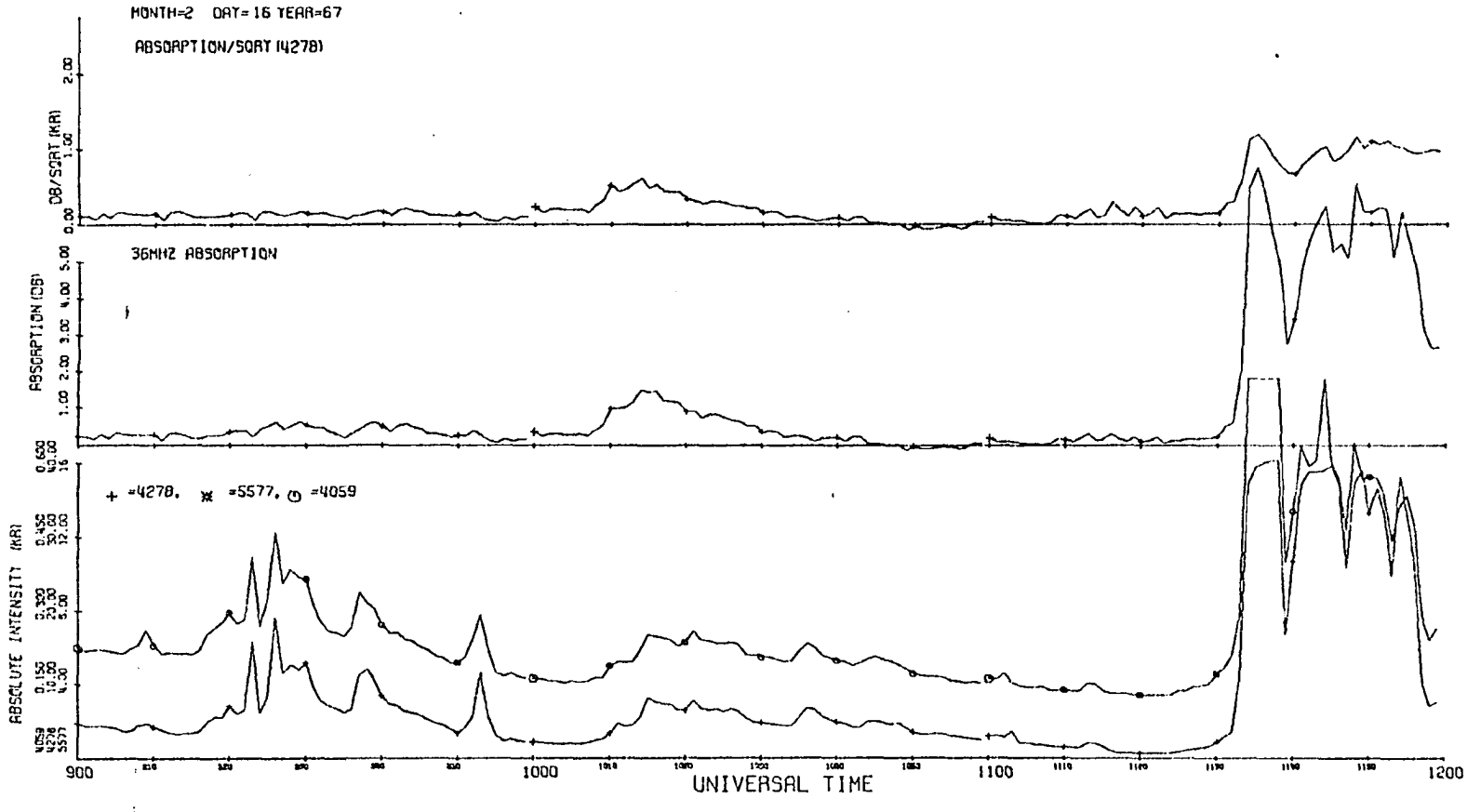

Figure (4.28) Data for the morning sector event of February 16, 1967.

The sequence of all-sky camera photographs in Figure 4.29 illustrates the auroral movements near the time of substorm onset. That the auroral oval had expanded equatorward can be inferred from this sequence. At 1125 UT a bright arc could be seen on the southern horizon; over the next nine minutes it moved poleward, passing through the zenith at College between 1133 and 1134 UT. After this time individual forms were not distinguishable, although a TV system in operation at Ester Dome recorded details of the flaming aurora (Cresswell, 1969).

4.5.7 The Event of December 8, 1967

The discussion of morning sector events will be closed with the description of an unusual event with periodic structure which occurred during a substorm on December 8, 1967.

Periodic variations in the range from 2-10 minutes are occasionally recorded in the cosmic noise absorption records at College (Parthasarathy and Hessler, 1963) as well as at other locations in the auroral zone (see Hargreaves, 1969). Such variations usually occur during magnetically disturbed periods and are observed at College most frequently around 1600 UT (Berkey and Parthasarathy, 1964). A striking example of such a periodic variation was observed at approximately 14^h UT on December 8, 1967. The sinusoidal structure was also evident in the Paxson (63.5°N CGM) riometer records, but not at Fort Yukon (67.1°N CGM) nor at Anchorage (60.8°N CGM). The narrow latitudinal confinement is consistent with the observations of the spatial structure of such events by Barcus and Rosenberg (1965).

On December 8, 1967 the onset of a substorm occurred at approximately 1308 UT when a 300 gamma negative bay was registered; substorm activity

Figure (4.29) All-sky camera photographs for the interval 1127 to 1143 UT on February 16, 1967.

16 February 1967

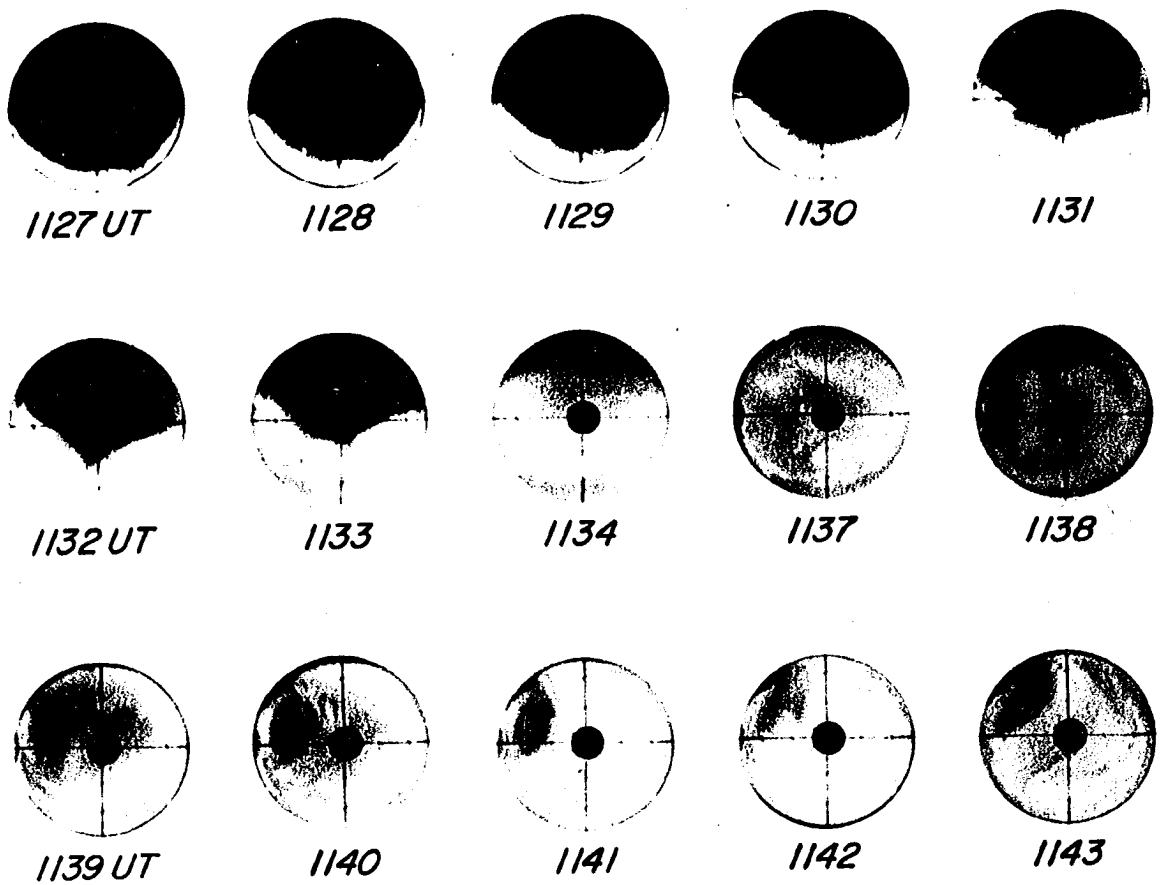

persisted until 16^h UT. The absorption also began to increase at 1308 coincident with the onset of pulsations in the 4278A emission. In Figure 4.30 the original records have been reproduced; both the 30 MHz and 36 MHz (narrow beam) records have been inverted so that absorption increases toward the top of the page. The width of the 30 MHz trace emphasizes the factor by which the original data was multiplied. The temporal coherence between the 36MHz riometer data and the 4278A record is particularly noteworthy; the rise and decay times are coincident to within the inherent recording error (estimated at ± 15 seconds). High-frequency pulsations are superimposed on the larger variations in the 4278A intensity.

In many of the examples discussed previously, patches of auroral luminosity, typical of those observed in the morning sector, could be followed from frame-to-frame in the all-sky camera data as they drifted eastward. Such was not the case during this event; while large patches of luminosity were visible (Figure 4.31), there was no coherency between frames. Instead, patches with a large angular extent (> 10°), which went "on and off" at times corresponding to increased absorption and luminosity, appeared in the zenith. No patches appeared in the zenith during times of absorption minimum. These patches disappeared about 1415 UT, however patches were observed at Fort Yukon between 1417 and 1630 UT.

The ratio $A(db)/\sqrt{I}_{4278}$ was calculated for times corresponding approximately to the maxima and minima phases of the event. Only relative values of the 4278A luminosity were used for this calculation. As seen in Table VI, the ratio varies by factor of approximately 2 between the times of minimum and maximum during the event. It should be noted

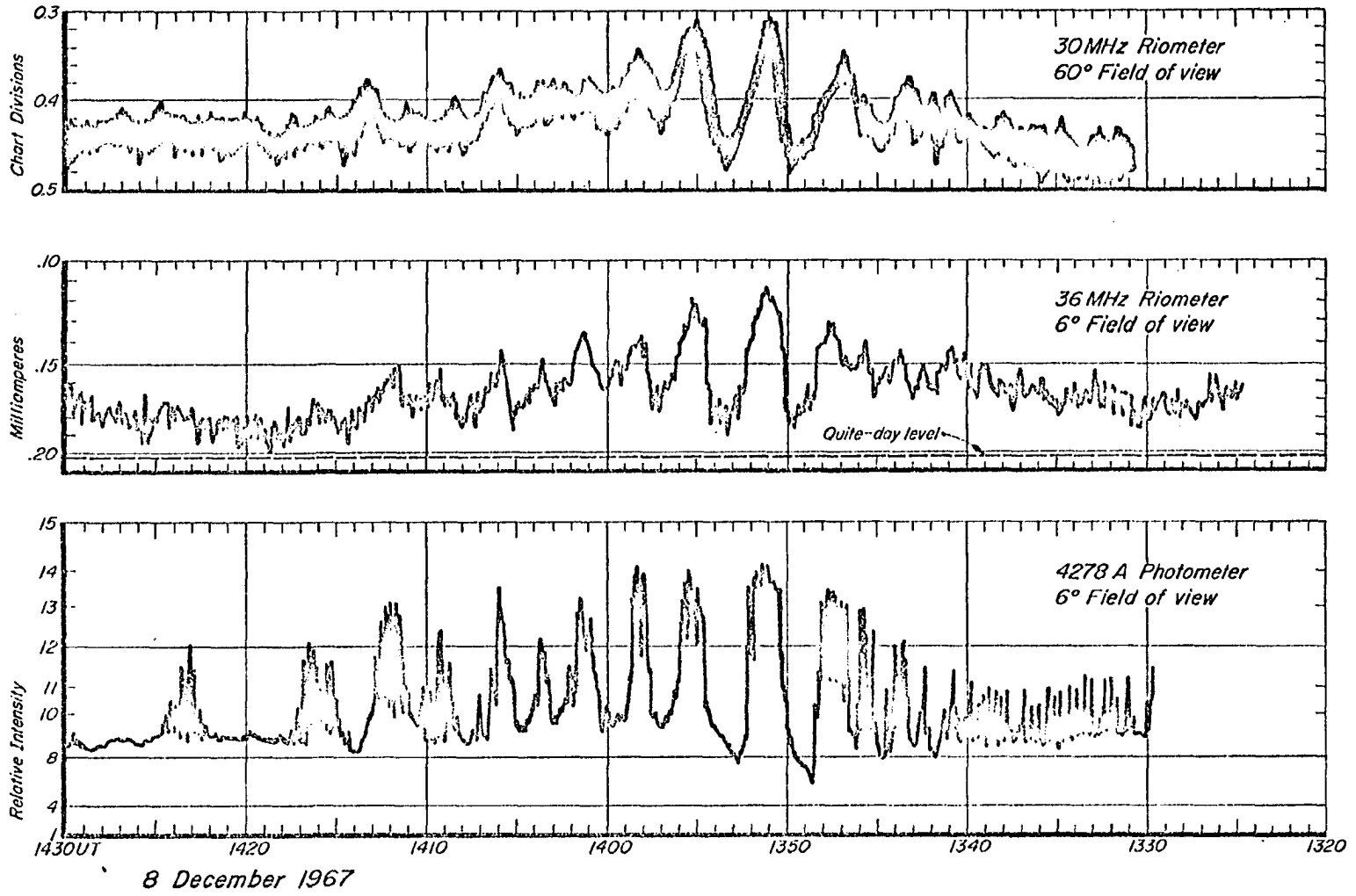

Figure (4.30) Representation of the original 30 MHz riometer (top), 36 MHz riometer (middle), and 4278A photometer (bottom) recordings during a quasi-periodic absorption on December 8, 1967. The riometer records have been inverted so that absorption increases toward the top of the page.

8 December 1967

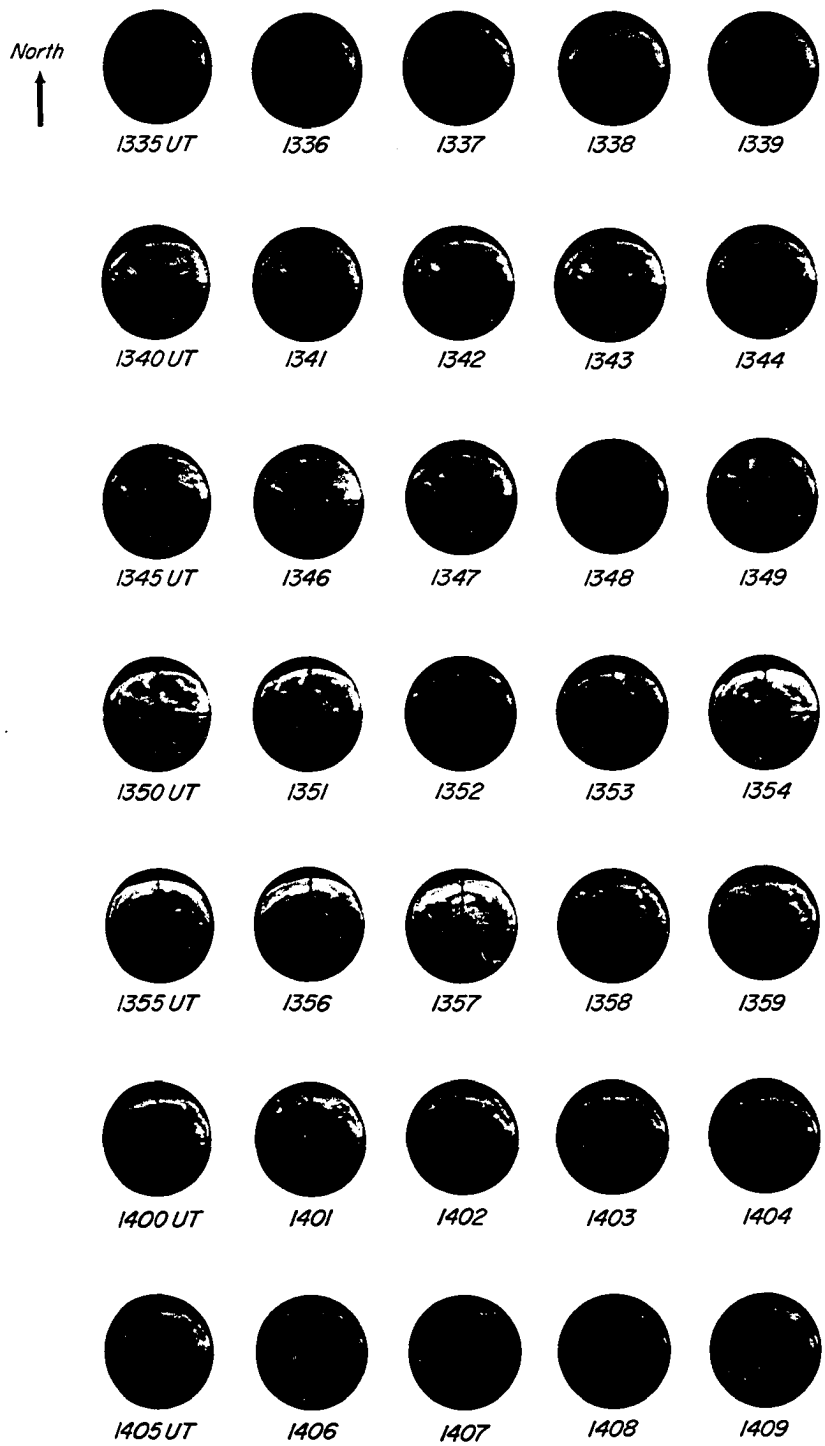

Figure (4.31) All-sky camera photographs for the interval 1335 to 1409 UT on December 8, 1967.

that during the times of minimum, no pulsations were observed although the luminosity during such periods exceeded the pre-disturbance night-sky background level. Presumably the luminesence during these periods could be attributed to the auroral veil (Montbriand, 1969). It therefore can be concluded that pulsating aurora is characterized by a much harder spectral indice than is the diffuse or veil type aurora. Furthermore, the high degree of temporal correlation observed here lends support to the inference that pulsating auroras occur at a much lower height than do other forms of aurora (Moore, 1971).

Table VI

Variation of the Ratio $A/\sqrt{I}_{4278}$ on December 8, 1967

TIME UT	ABSORPTION db	RELATIVE INTENSITY	RATIO $A/\sqrt{I}$
1345	.79	8	.28
1345:30	1.46	9.5	.47
1346:30	1.03	19.1	.34
1347:30	1.90	13.1	.52
1349	.68	6.7	.27
1350:30	2.61	14.0	.70
1353	.68	8.0	.24
1355	2.25	13.8	.60
1357	.79	9.5	.25
1358	1.61	13.8	.43
1400	.89	9.5	.29
1401	1.61	13.0	.45
1402:30	.79	9.7	.25
1403:30	1.31	12.2	.38
1405	.68	9.5	.22
1405:30	1.46	13.3	.40
1408	.53	8.6	.18

Of the eleven events discussed in this section, ten were associated with substorms; during these ten substorm events, the absorption reached a maximum of at least 2 db, while a maximum of 1 db was recorded during the eleventh (non-substorm) event. During the largest substorms ($\Delta H \geq 900\gamma$) the absorption ranged from at least 3 db to more than 7 db.

The examples given here demostrate the correlation of intense absorption with pulsating aurora. This is exemplified most clearly by the January 9, 1967 event when absorption maximized after the onset of pulsating aurora. During the January 8, 1967 event when a non-pulsating patch moved through the zenith, the increase in absorption was only a small fraction of that normally observed during pulsating aurora.

At least three different morphological types of aurora were discussed: (1) flaming aurora; (2) patchy aurora, and; (3) Ω - band aurora. All were associated with intense absorption; flaming aurora was associated with the largest event (> 7 db) recorded.

The increase in the ratio $A/\sqrt{I}$ in the morning sector infers that a hard spectrum is characteristic of the events discussed above. In all of these events, the ratio $A/\sqrt{I}$ increased relative to its value near midnight. The event of December 8. 1967 vividly illustrates the hardness of the precipitated electron spectrum during pulsating aurora, in contrast with the softer spectrum characteristic of the auroral veil.

4.6 Statistical analysis of substorm events

The College magnetograms were used to determine the existence of a substorm during the nights for which riometer and photometer data were both available. Furthermore, the duration of a positive or negative bay event in the H-component was used as an indicator of the length of the substorm. The College K-indices for these same substorms were used to further subdivide the data for the purpose of deriving a statistical result pertaining to the type of spectrum which occurred at different levels of K_{col} during a substorm. The statistical parameters which were

discussed in the preceeding chapter were derived for values of the College K-index between 3 and 8. For non-substorm associated events, the same parameters were derived and are listed in the row labeled NSE.

TABLE VII

Statistical Parameters Derived for the Relationship Between Absorption and 4278A Luminosity for Substorm Events As a Function of the College K-Index.

K_{col}	A(db) Mean	/√4278 Standard deviation	r_1	r_2	c_0	c_1	c_2	c_3	n
3	0.56	0.31	0.11	0.23	0.63	0.07	0.39	0.26	160
4	0.54	0.38	0.23	0.43	0.40	0.56	-0.08	0.59	1139
5	0.51	0.28	0.19	0.40	0.43	0.50	0.08	0.48	1234
6	0.57	0.28	0.05	0.19	0.82	0.22	0.99	0.17	795
7	0.48	0.26	0.27	0.49	0.38	0.54	0.26	0.40	856
8	0.72	0.22	0.42	0.82	0.50	0.61	-0.95	0.96	185
NSE	0.43	0.24	0.23	0.37	0.46	0.23	0.27	0.25	8100

Since the K index is derived from the maximum deflection of the H-component during a 3 hour interval, another index which could be used for ordering the data was sought. An hourly indicator of magnetic activity in the form of telluric current amplitudes (mv/km) was readily available; these values were published quaterly in the High Latitude Geophysical Data series (Hessler, 1966). According to Hessler (1966) the telluric amplitude scalings are highly correlated with the magnetic index A. Since the maximum amplitude of the telluric current fluctuations was approximately 1050 mv/km, 8 intervals with a range of 150 mv/km were defined. The same data analyzed previously were again processed, and the results are displayed in Table VIII. The last row (labeled Σ) represents the derivation for the whole data set; these values should be compared with the NSE row in the previous table.

TABLE VIII

Statistical Parameters Derived for the Relationship Between Absorption and 4278A Luminosity for Substorm Events As a Function of Telluric Current Magnitudes.

INDEX	A(ab) MEAN	$/\sqrt{I}_{4278}$ STANDARD DEVIATION	r_1	r_2	c_0	c_1	c_2	c_3	n
1	0.50	0.30	-0.23	-0.45	0.57	-0.22	0.84	-0.22	99
2	0.55	0.32	0.15	0.38	0.42	0.58	-0.04	0.58	823
3	0.46	0.25	0.16	0.38	0.41	0.47	0.05	0.43	918
4	0.53	0.27	0.27	0.59	0.32	0.71	-0.57	0.79	562
5	0.48	0.34	-0.07	-0.13	1.23	-0.25	1.41	-0.15	318
6	0.53	0.28	0.17	0.39	0.42	0.55	0.21	0.45	590
7	0.51	0.23	0.16	0.30	0.93	0.17	0.90	0.21	298
8	0.65	0.35	0.28	0.48	0.67	0.42	0.52	0.48	822
Σ	0.53	0.31	0.37	0.56	0.44	0.51	0.04	0.52	4430

The results of the foregoing analysis indicate that there is virtually no dependence of the ratio $A/\sqrt{I}$ on magnetic activity; except for periods of intense disturbance (index = 8), the ratio was in the range 0.52 ± 0.06. During intense magnetic disturbance, the value of the ratio was significantly larger.

It is interesting to compare the mean value of the ratio for substorm and non-substorm events (NSE); the mean for substorm events was about 20 percent larger. The same trend exists for the other parameters; substorm events show a higher correlation between absorption and luminosity. The quantitative relation $A = c_0 I^{c_1}$ infers a nearly square-root dependence, while NSE reveal an approximately cube root dependence.

CHAPTER 5

SUMMARY AND CONCLUSIONS

The purpose of this chapter is to summarize the results derived in the previous two chapters, emphasizing those results which are new, and comparing these results with comparable measurements reported in the literature.

5.1 Diurnal variations

Using the diurnal variations of the ratios $A/\sqrt{I}_{4278}$ and $A/\sqrt{I}_{5577}$ to infer changes in the spectrum of precipitated electrons, the softest spectrum was observed over the four hours preceeding local magnetic midnight (approximately 1130 UT at College). This result is consistent with the observations of Brewersdorff et al. (1966) who used the ratio of balloon-borne X-ray detectors with different energy thresholds to infer spectral changes (see Figure 5.1) and with the Injun 3 satellite measurements of Fritz (1966), who reported that the energy spectrum between 10 and 40 kev is much softer during the evening hours than at any other time during local night. On the other hand, Johansen (1965) observed a hardening between 19^h and 24^h UT while Gustafsson (1969) inferred a hardening between 15^h and 05^h UT; both of these results were based on the variation of the ratio $A/\sqrt{I}_{5577}$.

According to Hartz and Brice (1967), who derived an idealized pattern of auroral particle precipitation as a function of geomagnetic time (see Figure 5.2), the pre-midnight hours are dominated by intense fluxes of soft ($E \leq 10$ kev) precipitation. They show that hard precipitation occurs at all local times near 65°, maximizing in the late morning hours. Taking into consideration that the observations discussed here correspond to periods of activity during which $K_p > 4$, the

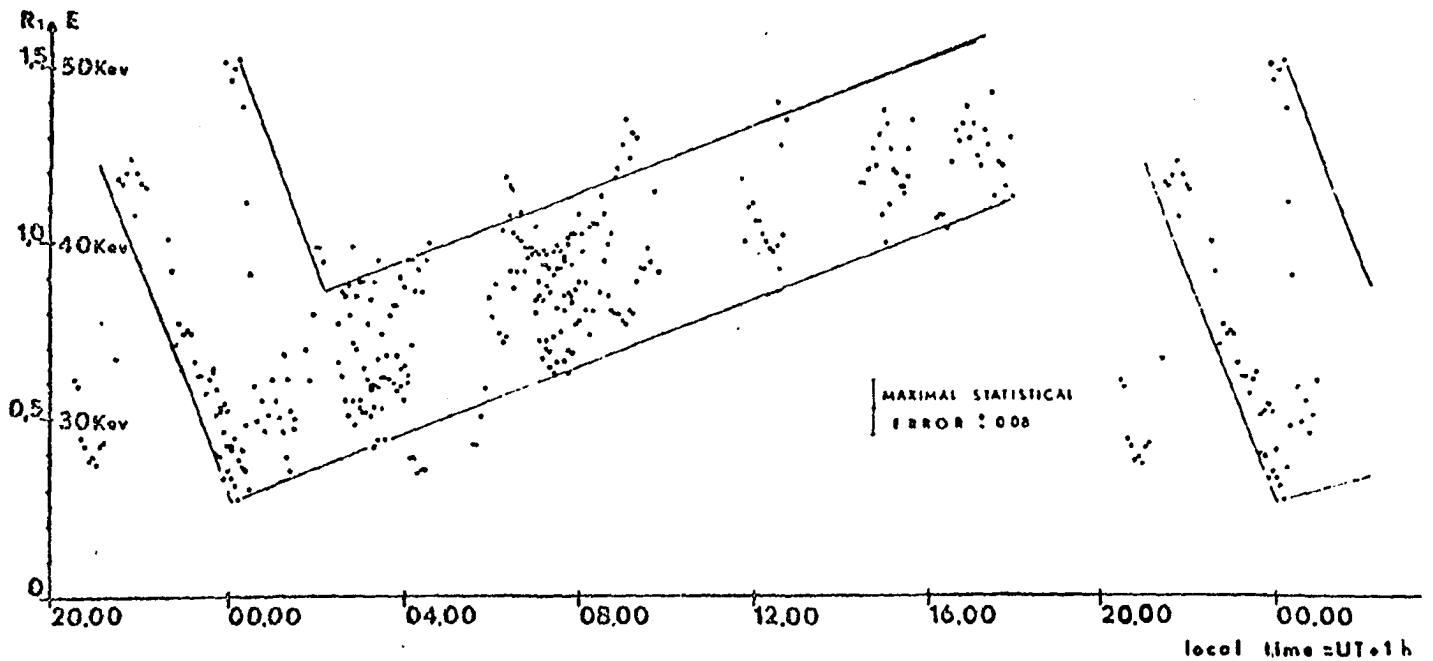

Figure (5.1) The ratio R_1 (counting rate) for all flights with standard detectors at Kiruna plotted versus local time (after Brewersdorff et al, 1966).

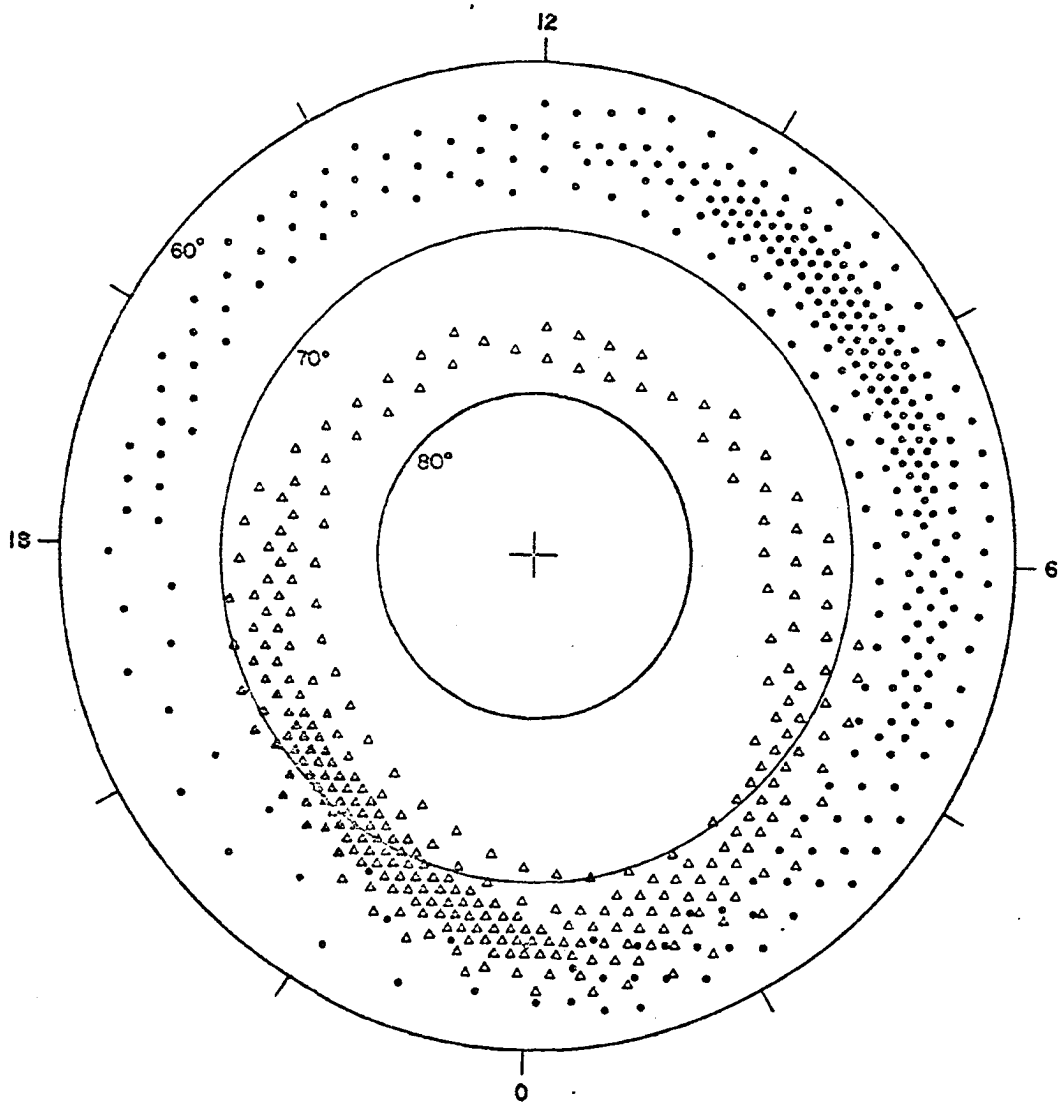

Figure (5.2) Precipitation pattern of electrons. The density of the symbols denotes the average density in latitude and time of two types of precipitation. The triangles represent the softer discrete precipitation and the dots represent the harder diffuse precipitation (after Hartz and Brice, 1967).

diurnal variation of the electron spectrum observed in this study supports the idealized representation of Hartz and Brice.

No particular significance is attached to the diurnal variation of the ratio $A/\sqrt{I}_{4059}$ because of the uncertainities surrounding the excitation mechanism of the Second Positive (Nitrogen) band. However, a comparison of the diurnal variation can be made with that of 4278A; from this comparison it can be concluded that the ratio 4278A/4059A is not constant. This would imply that the excitation mechanism for the (0-3) transition is other than direct electron excitation.

The diurnal variation of auroral absorption agrees well with other investigations (Hook, 1968) in that an evening minimum and a morning maximum occur. The step-like increase in the diurnal variation near 12^h UT coincides in time with the occurence of pulsating aurora in the morning sector.

5.2 Statistical results

The values of the coefficients derived for the least squares fit to the relation $A(db) = c_o[I(kR)]^{c_1}$ infer that for the 4278A emission line the assumption of quasi-equilibrium in the auroral ionosphere is quite valid. The equation derived in Chapter 2 can be re-expressed for absorption at 30 MHz by multiplying by a factor of 1.4:

$$A_{30}(db) = 0.41\ [I_{4278}(kR)]^{0.49}$$

This relation should be useful for obtaining a first-order estimate of absorption, knowing the corresponding auroral intensity at 4278 A or vice-versa.

On the assumption that equilibrium is rapidly established in the auroral ionosphere, the coefficients of the relation

$$A(db) = c_2 + c_3\sqrt{I}(kR)$$

were derived. Substituting values of 4278A intensity into the two equations shows that the latter equation predicts a larger absorption magnitude than does the power-law representation; the predicted absorption is larger by a factor of approximately 1.6. No attempt will be made to account for this factor except to comment that the coefficients for these two equations were derived under different criteria imposed on near zero values of absorption and luminosity.

The significant feature of this technique of data analysis is the verification of the assumptions made in using the ratio $A/\sqrt{I}_{4278}$ as an indicator of changes in the spectrum of precipitated electrons. The results derived from the least-squares analysis indicate that on the average absorption varies proportionately to the square root of 4278A luminosity, confirming the assumption of quasi-equilibrium upon which the derivation of the ratio $A/\sqrt{I}$ is based. The result is consistent with the production mechanism for the N_2^+ emissions, that of direct electron excitation.

The same analysis showed that absorption is proportional approximately to the cube root of auroral luminosity at 5577A and varies almost linearly with changes in 4059A intensity. These results infer that direct electron excitation is not the primary mechanism by which either

of these emissions are excited. In the case of 5577A, this result tends to confirm the results of Romick and Belon (1967) who suggested that dissociative recombination of O_2^+ is the dominant mechanism for excitation.

The range of the coefficient c_1 derived from the analysis of 4059A data was 0.75 to 1.6, implying that absorption varies almost linearly with 4059A luminosity variations. This observation lends support to the suggestion of Gadsen (1961), who proposed an ion-exchange process for the excitation of Second Positive emissions. The result also implies that no contamination of the data by the 3914A emission exists since a square-root dependence would be anticipated if such were the case.

5.3 Correlation analysis

Correlation coefficients were derived for each emission and for each constraint imposed on the data; two assumptions were made, that of a linear (r_1) and square-root (r_2) dependence of absorption on luminosity.

The correlation between absorption and $\sqrt{I}_{5577}$ was nearly the same as derived for the data set collected during 1965-66 (season I). It is interesting to note that Eather and Jacka (1966) found a correlation of 0.31 for SVIA events; they also measured the 5577A emission.

The significant result of this analysis is the larger value of the correlation coefficient for the 4278A emission. The coefficients r_2 varied from 0.57 to 0.63 for 4278A, while the same correlation varied between 0.24 and 0.33 for 5577A. No comparable measurements for the 4278A emission have been reported in the literature.

The correlation coefficients r_2 derived from the 4059A data set had nearly the same values (0.45 to 0.58) as the corresponding values for

4278A; however, the coefficients r_1 were much less than the same values derived for 4278A or 5577A. The ratio of the correlation coefficients r_2/r_1 was approximately 3 for the 4059A data set; approximately 1.4 for the 4278A data, and; about 1.5 for 5577A variations.

It can therefore be concluded that more than half the variation of absorption can be attributed to changes in 4278A luminosity, assuming a square-root dependence. Next, making the assumption of a linear dependence, slightly less than half the variation of absorption can be accounted for by changes in 4278A luminosity. For the 5577A data, only a third of the variation of absorption can be accounted for with a square-root dependence, while only 1/5 is attributable to a linear dependence. Finally, for the variation of absorption and 4059A luminosity, about half of the variance can be attributed to a square-root dependence and less than 1/6 to a linear dependence. The latter result conflicts with the earlier finding which showed that a linear dependence is predicted by the least-squares analysis.

5.4 The spatial extent of auroral absorption

Using the autocorrelation analysis of Graf (1960), it was demonstrated that as absorption increases in magnitude, the spatial coherence between two adjacent absorbing regions decreases. From the correlation of absorption events larger than 1 db in magnitude, a spatial coherence of less than 48 kilometers (in the N-S plane) was found. This can be interpreted as meaning that the spatial extent of the absorbing region is less than 48 km when A > 1.0 db. Application of the same analysis to the 5577A luminosity measurements made during the winter of 1965-66 inferred a spatial coherence of only 32 km. Graf (1960) derived a somewhat larger

spatial extent for the absorbing region as a result of the high degree of correlation he found between his two antenna beams; he inferred that the absorbing region exceeded 80 km. From a statistical standpoint, the result of this analysis implies that during aurora, the latitudinal extent of the ionosphere in which absorption occurs is larger than the corresponding region in which visual auroral emissions are observed.

5.5 Auroral Absorption and Luminosity Variations during the Substorm

Using all-sky camera data, Montbriand (1969) established the existence of dusk sector patchy aurora; however, his conclusion that such aurora is associated with intense absorption was based on only one example for which coincident riometer data was available. From the three events illustrated here, it is concluded that dusk sector patches pulsate as do patches which occur in the morning sector. Furthermore, it is suggested that such events are associated with substorms which have occurred near the midnight meridian and therefore represent the limit of eastward drift of the substorm. These examples lend additional support to Montbriand's conclusion relative to the association with intense absorption. The almost negligible amount of 4278A luminosity would suggest that the ratio $A/\sqrt{I}_{4278}$ would be larger than for events which occur in the morning sector, as suggested by Montbriand.

Absorption which occurs in the evening sector is associated with the westward propagation of the auroral substorm. In the early evening hours, equatorward of the oval, yet associated in time with the westward travelling surge (WTS), are increases of auroral absorption which are accompanied by almost negligible increases of auroral luminosity. These

events are associated with positive increases in the H-component and presumably occur when $K_p > 4$.

Westward drifting loops (WDL) are observed near the western extremity of the WTS; this phase of the auroral substorm is characterized by strong (20 kR) auroral emissions and little to no associated absorption. Small negative deflections of the H-component are observed at this time.

Intense absorption accompanies the WTS if the surge is characterized by type-B red aurora; the absorption is typically of short duration, with a rapid onset and a rapid recovery time. The intensity of both the absorption and luminosity can be quite large. A sharp negative deflection of the H-component accompanies the increased absorption and luminosity.

The events occurring in the midnight sector have been extensively discussed (Ansari, 1964; Eather and Jacka, 1966; Berkey and Parthasarathy 1964); no new results were derived from this study. However, the study confirmed the earlier observations of intense absorption and luminosity accompanying the poleward advancing bulge.

The morning sector is characterized by pulsating aurora and intense (> 2 db) absorption. In general, the increases of absorption are longer in duration than those observed at other local times. In contrast, the auroral luminosity rarely exceeds a few kilorayleighs, the exceptions being those rare occasions on which flaming auroras occur. Negative bays in the H-component typically accompany the absorption in the morning sector. Since, at this time, the origin of the substorm lies to the west of College, the rate of decrease of the H-component is generally less than observed during the midnight sector.

A quasi-periodic absorption event (called type-P by Berkey and Parthasarathy, 1964) was shown to be associated with patchy, pulsating

aurora. This is the first event to be so documented. The observation suggests that all such events are characterized by discrete patches of precipitation with highly time structured fluxes.

5.6 Substorm statistical results

The correlation of absorption and 4278A luminosity was investigated for substorm events. Using the statistical parameters discussed in Chapter 2, it was shown that there was no systematic dependence of either the correlation coefficients or the least-squares fit coefficients on the level of magnetic activity during the substorm with the exception of the most disturbed ($K_{col} = 8$) periods. At such times, the correlation between absorption and luminosity increases and the ratio $A/\sqrt{I}$ is significantly larger. It was shown that, during the substorm, the absorption is proportional to the square root of 4278A variations, while during events not associated with the substorm a fourth root dependence is predicted. Similarly, the correlation between absorption and luminosity is significantly smaller during non-substorm associated events.

5.7 Suggestions for further work

A number of technical improvements could be made to the existing experimental apparatus if further use of the narrow beamwidth technique is to be made.

(1) The mainlobe beamwidth and sidelobe distribution has only been computed theoretically; the pattern should be measured in the geomagnetic east-west and north-south planes using an airborne transmitter.

(2) The sidelobe amplitude should be reduced by tapering the current distribution across the array. This can easily be accomplished for the

pattern in the north-south plane by adding appropriate lengths of coaxial cable. Appendix A gives a table of values for the attenuation necessary to produce a given sidelobe level.

(3) Digital techniques should be introduced into the recording and processing of the raw data; digital format data allow for more expedient data processing.

The most promising area for further research with the narrow beam array is that of determining the spatial coherence of absorbing regions. Development of an auto-correlation function for the 6 x 8 array is suggested; application of the methods developed by Graf (1960) could then be applied. The correlation of absorption between several different directions along the meridian plane would yield more extensive information concerning the dimensions of auroral absorption. The derivation of correlation coefficients for different types of aurora is suggested, as well as the derivation of correlation of auroral luminosity in the same directions.

If further investigation of the ratio $A/\sqrt{I}$ is to be carried out, it is suggested that more emphasis be placed on substorm activity for which $K_p < 4$.

PART II

A SYNOPTIC STUDY OF THE GEOGRAPHICAL DISTRIBUTION OF AURORAL ABSORPTION DURING FIVE SUBSTORMS OF THE IQSY

CHAPTER 6

MEASUREMENTS OF AURORAL ABSORPTION ON A GLOBAL SCALE

6.1 Introduction

When applied to the study of the morphology of auroral particle precipitation, the riometer (see Chapter I) possesses important advantages over other types of instrumentation. In contrast with photographic or photometric techniques, the riometer is not affected by weather or limited to night-time operation. Nor is application of the riometer technique restricted to moderately disturbed conditions as is the case with ionospheric sounders. Although the spatial response of the riometer is a less flexible parameter than it is for optical measurements, it is controllable to a certain degree. Finally, it should be noted at the outset of this study that the D-layer ionization which causes the absorption of radiowaves occurs over a rather ill-defined height regime between about 50 and 90 kilometers. However, it can be safely assumed that such ionization results from the precipitation of primary electrons with energies in excess of 30 kev. The contributions of proton precipitation and Bremsstrahlung X-ray ionization are considered to be negligible during auroras.

Historically, application of the cosmic noise technique to high latitude radiowave absorption studies dates to 1954 when Little and his co-workers first applied the technique at College (Little, 1954). It was, however, not until about 1964 that there was dense enough coverage by riometers within the auroral regions to allow inter-comparison of various features of auroral absorption between stations. Investigating a type of absorption event (type-F) known to be associated with the

auroral breakup, Berkey and Parthasarathy (1964) found a better correlation between stations separated by 13° in longitude than between stations separated by 2° of latitude. However, utilization of the type-F event as a reference broke down when correlation over greater spans of longitude was attempted (Berkey and Parthasarathy, 1964 - unpublished results). It was subsequently demonstrated that absorption increases at a lesser rate east of the midnight sector, and what was observed as a sudden-onset (type-F) event in the midnight sector becomes a slowly increasing absorption (bay) event in the morning sector, (see also Parthasarathy & Reid, 1967).

6.2 The Auroral Substorm

It was also in 1964 that Akasofu introduced the concept of the auroral substorm (Akasofu, 1964). Using all-sky camera data, he showed that the aurora undergoes a pattern which can repeat itself several times during the course of a night; each repetition of this pattern was termed a substorm. Akasofu defined an expansive and recovery phase within the substorm process; during the expansive phase, the poleward expanding bulge, the westward travelling surge, eastward drifting patches and the Ω-band are the characteristic features. To an observer in synchronous orbit on the meridian of the substorm origin, the westward travelling surge would be seen propagatin westward along the auroral oval; the Ω-band moving eastward near the poleward boundary of the oval, patches moving in the same direction, but near the equatorward boundary; and, generally poleward motion along the meridian of observation. The expansive phase, which can last up to 30 minutes, is followed by the recovery phase, the onset of which is defined by equatorward motion of the most poleward

auroral arcs within the poleward bulge. During the recovery phase, the bulge which formed during the poleward expansion contracts, eventually to reach a configuration consisting of quiet arcs such as existed prior to the onset of the substorm. Near the dusk and dawn meridians, the propagation of the westward travelling surge and also of eastward drifting patches may be observed until the end of the substorm. These motions are represented diagrammically in Figure 6.1.

6.3 The Auroral Oval

Coupled with the substorm concept is the use of the auroral oval as a coordinate within which the substorm process occurs. Feldstein (1963) and Akasofu (1968) have found from photographic observations that auroras occur within an oval shaped belt; this belt is found at a higher geomagnetic latitude on the day side than at night. Feldstein and Starkov (1967) have shown that the width of the belt is dependent on the level of geomagnetic activity (see Figure 6.2). Whalen (1970) has produced a nomograph with which the position of the auroral oval can be projected onto the Northern Hemisphere for any time of day.

6.4 Measurements of the Longitudinal Distribution of Auroral Absorption

Application of the substorm concept to many of the other manifestations of the effects of auroral particle precipitation in the ionosphere has brought order to otherwise complex phenomena (see Akasofu, 1968). Such is the case with observations of radiowave absorption. Discussed in the first part of this thesis were the observations of auroral absorption made at College during substorms; the variety of such observations does not lend themselves to interpretation on a global basis, with

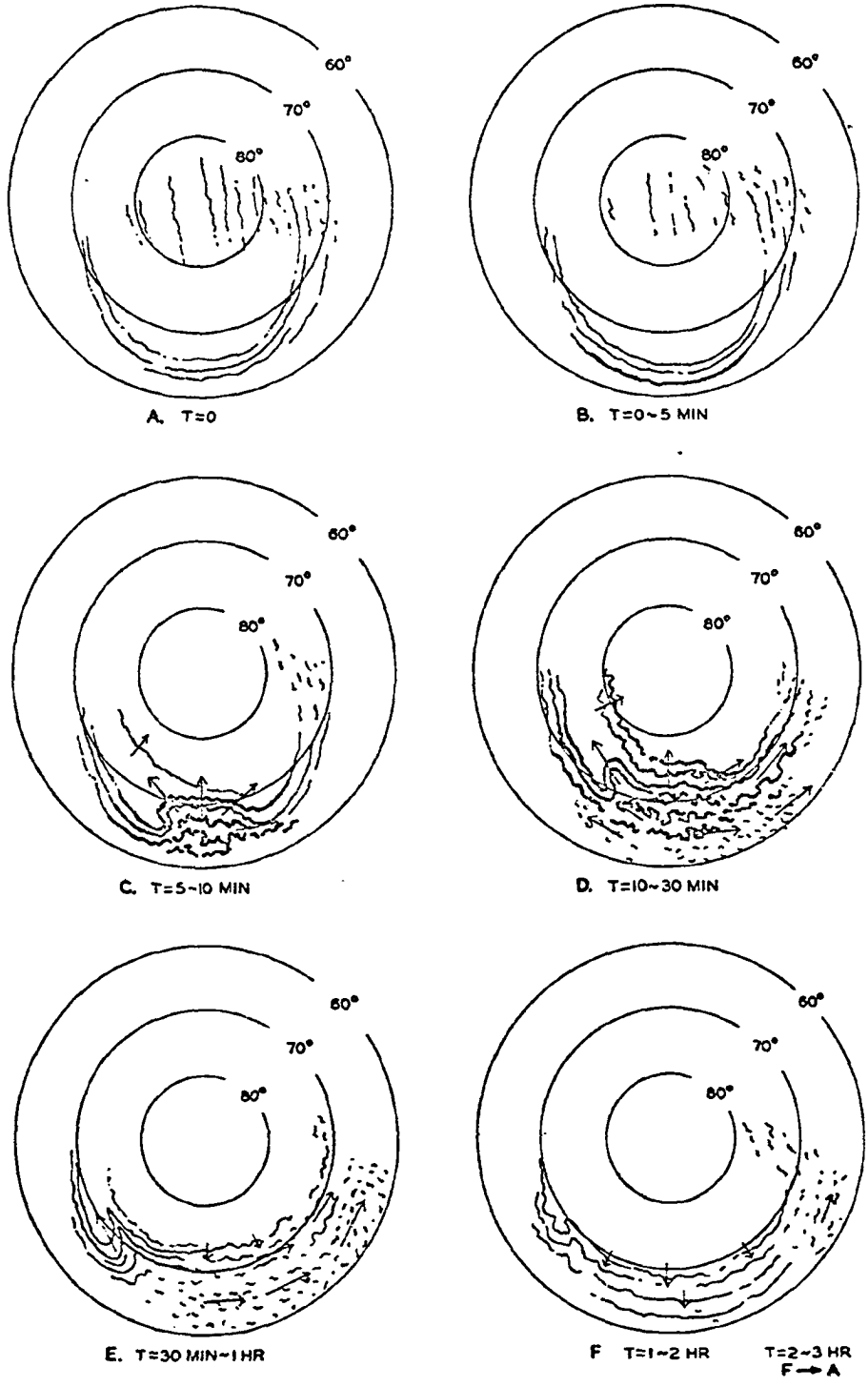

Figure (6.1) Schematic diagram to show the development of the auroral substorm (after Akasofu, 1964).

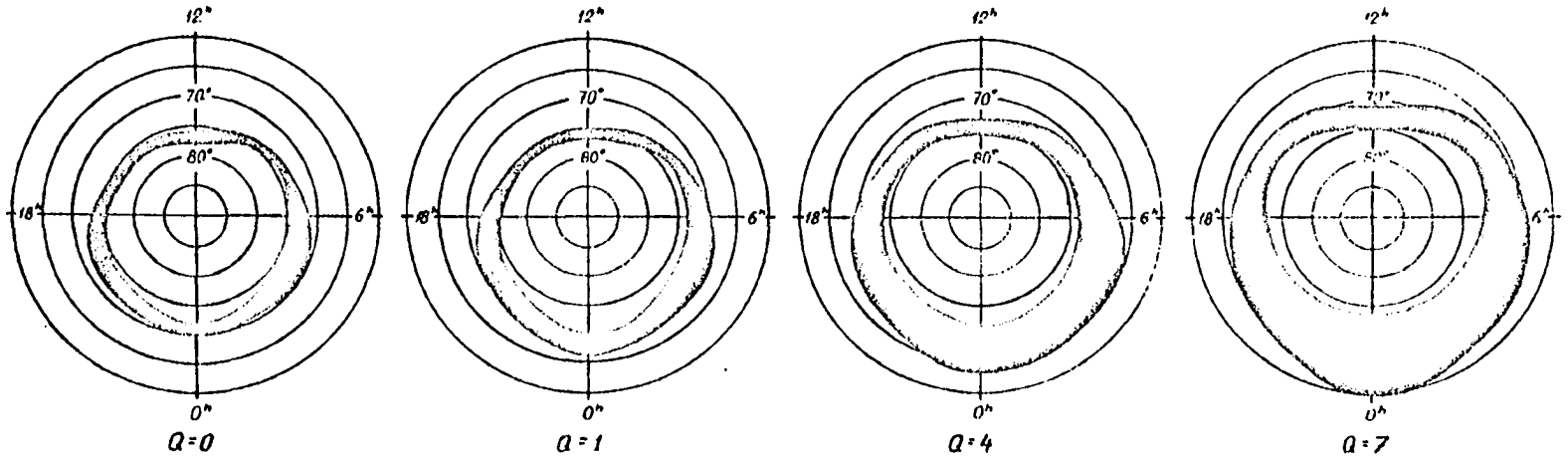

FIG. 5. AN AURORAL BELT AT DIFFERENT DEGREES OF GEOMAGNETIC ACTIVITY.

Figure (6.2) The auroral belt at different degrees of geomagnetic activity (after Starkov and Feldstein, 1967).

the exception of statistical or event analyses. It is therefore important to study data from stations separated by several hours in local time. However, as mentioned previously, a common factor is necessary upon which to base the analysis; the substorm concept provides such a factor.

Studies of auroral absorption at stations widely separated in longitude have been carried out by a number of investigators, notably Hargreaves (1967, 1968, 1970) Driatsky (1969, 1970) and Jelly (1970). These studies and others have been summarized in Table IX.

Hargreaves (1967) studied absorption events at three stations separated by 80° of longitude and situated between L-values of 5.6 and 6.9. Analyzing the time of onset or maximum of an event, he derived both eastward and westward movements; for events originating near local midnight, he found a drift rate of 4° of longitude per minute (2.8 km/sec). A second analysis, based on event reports from Reyjavik and Great Whale, showed a lower rate of movement, 1.3°/min. In this instance the movements were also both eastward and westward.

Hargreaves (1968) also studied events from 3 locations between L=4 and L=14 in the Southern Hemisphere. He combined these results with those of his previous analysis to derive a global pattern (see Figure 5.3). The global pattern shows a westward velocity of 0.2 R_e/min and 0.5 R_e/min in the eastward direction. The salient features of this model are: (1) the minimum in occurrence and magnitude near 15^h magnetic time; (2) the maximum in absorption at a longitude reached after 30 minutes, and; (3) the greater eastward drift velocity.

Dubatovko et al (1968) correlated absorption bays occurring at College and Loparskaya. They found a systematic time lag between the events at each station which they interpreted as being the result of

TABLE IX
SUMMARY OF LONGITUDINAL DRIFT MOTIONS

Investigator	Eastward motion Velocity	Eastward motion Duration	Westward motion Velocity	Westward motion Duration	Type of Analysis	Stations	L-value
Hargreaves (1967)	4°/min	06-16^h UT	4°/min	18-04^h UT	Event onset	College	5.5
						Great Whale	6.9
	1.3°/min		1.3°/min		Event "reports"	Reyjavik	6.2
Hargreaves (1968)	<0.5R_e/min	00-14^{h}MLT	>0.2R_e/min	15-24^h MLT	Event onset	Eights	4.0
						Byrd	7.2
						South Pole	14.0
Dubatovko et al. (1968)	3.1-3.7°/min		none derived		Bay onsets	College	5.5
						Loparskaya	5.4
Jelly (1970)	2.3°/min (estimate)		none derived		"Substorm" events	College	5.5
						Kiruna	5.4
						Dixson Island	6.9
						Cape Jones	6.2
Driatsky (1970)	4.5°/min	22-06^h (60°EMT)	2.5°/min	10-18^h (60°EMT)	Bay onsets	College	5.5
						Amderma	5.4
						Tixie Bay	5.6
Driatsky et al. (1970)	1.5-2.5°/min	21-14^{h}LT	1-1.5°/min	14-21^{h}LT	Bay maxima	Siberian	
	3-6°/min		1.5-3°/min		Bay onset		
Hargreaves (1970)	37 km/min	02-11^{h}LT	9 km/min	15-02^{h}LT	Absorption "features"	Great Whale	7.0

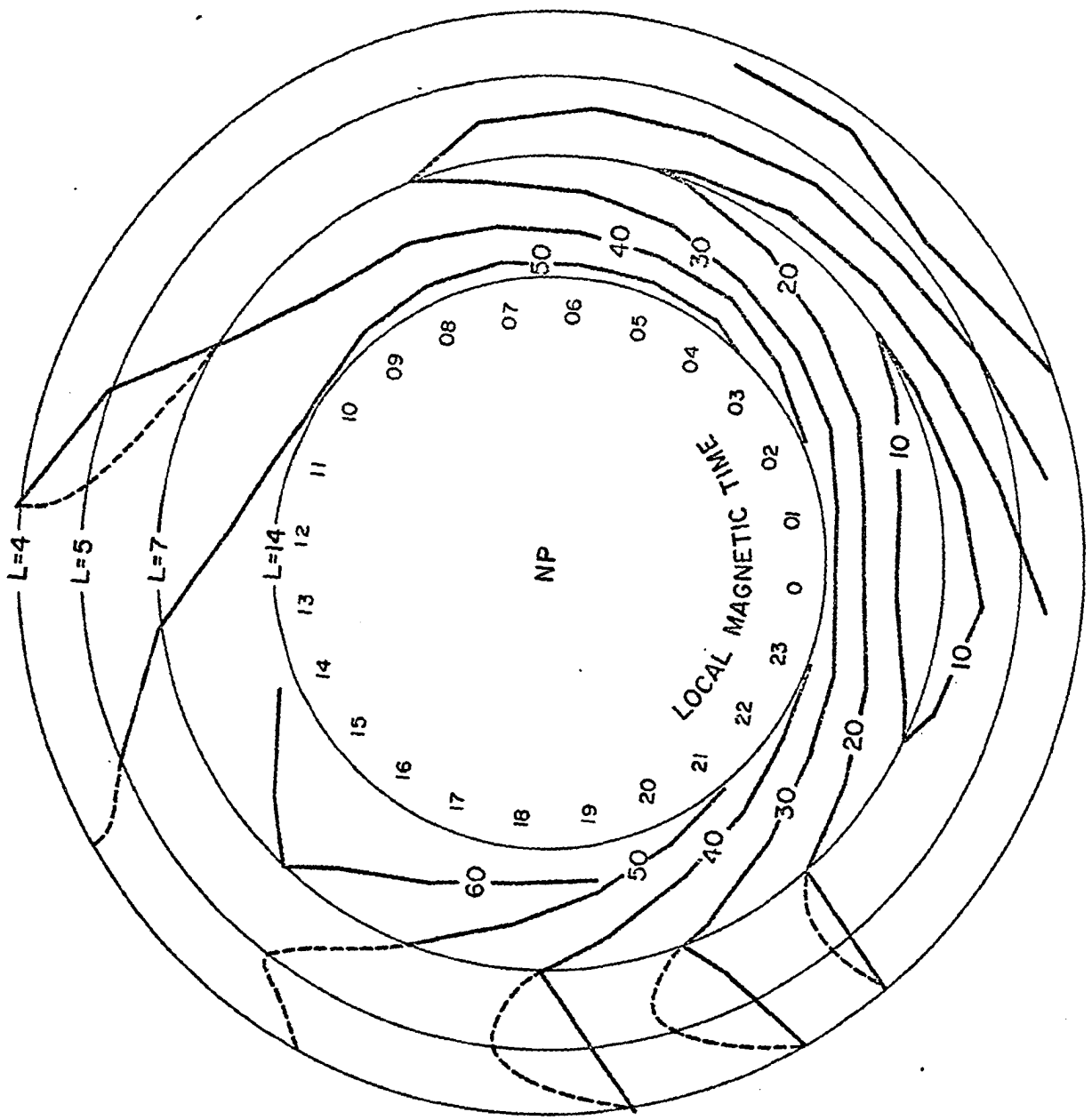

Figure (6.3) Progression of absorption onsets drawn at 10 minute intervals (Hargreaves, 1967 ala' Wilson, 1970).

150 kev electrons drifting from the vicinity of the midnight meridian.

Driatsky (1969) used data from Amderma, College, and Tixie Bay to investigate longitudinal motions. Over the time interval 22^h to 06^h 60° EMT, an eastward drift of 4.5°/min was observed, while for the westward drift, a rate of 2.5°/min was derived for the interval 10^h to 18^h 60° EMT.

Using substorm events, defined as abrupt absorption increases, as a reference, Jelly (1970) analyzed longitudinal motions at 4 stations separated by 50° to 110° of longitude. Although no drift rate was given, a rate of approximately 2.3°/min (50-90 km/min) can be derived from her results. Two maxima in the longitudinal distribution of absorption were observed, one just before midnight and a second in the morning hours.

Driatsky et al. (1970) derived a model for the longitudinal drift of auroral absorption based on riometer data from Soviet stations located near L=5.5. They concluded that absorption begins in the evening sector around 21^h LT and spreads eastward between 21^h and 14^h LT and westward from 14^h to 21^h LT. They derived drift rates for both the event onset and the event maximum. They observed a higher velocity for the event onset; 3° - 6°/min for eastward drifts and 1.5° - 3°/min for westward drifts. They observed a maximum eastward velocity at 03^h LT for both bay onsets and maxima. Investigating the latitudinal distribution of bay events, they concluded that absorption spreads both poleward and equatorward from about L=5.7. The rate of expansion was a function of latitude, varying from 0.2°/min to 0.5°/min.

Investigating the movement of auroral events over a distance of 250 km, Hargreaves (1970) derived median velocities in both the eastward and westward directions. These velocities are considerably smaller than derived previously (37 km/min eastward, 9km/min westward); the

eastward movement predominates between 07^h and 16^h UT (02 - 11^h LT) and the westward between 20^h and 07^h UT (15^h-02^h LT).

6.4.1 The Ionospheric Substorm

Akasofu (1968) inferred the development in time of the ionospheric substorm (see Figure 6.4); this development was based on: (1) the auroral substorm; (2) statistical studies of auroral absorption, and; (3) absorption measurements by ionosondes. This model differs from the studies of the longitudinal distribution of absorption outlined above in the following respects: (1) association of intense absorption with the westward travelling surge and within the auroral oval; (2) identification of the eastward drift motion along both the auroral oval and the auroral zone in the noon sector, and; (3) the confinement of absorption to a narrow region at the onset of the substorm.

6.5 Satellite Measurements

Using ATS-1 satellite measurements of trapped electrons with energies in the range 50-150 kev, Rosen (1969) studied the correlation of increased electron fluxes at geostationary orbit with precipitation events at a chain of riometer stations in Alaska. He found that 85% of the ATS-1 flux increases were correlated with increased radiowave absorption (± 15 minutes), while 92% of the observed absorption (precipitation) events were associated with flux increases at ATS-1. He also found a greater percentage of flux increases associated with precipitation events in the dawn-noon sector than in the evening-midnight sector.

Examining the latitudinal distribution of precipitation events,

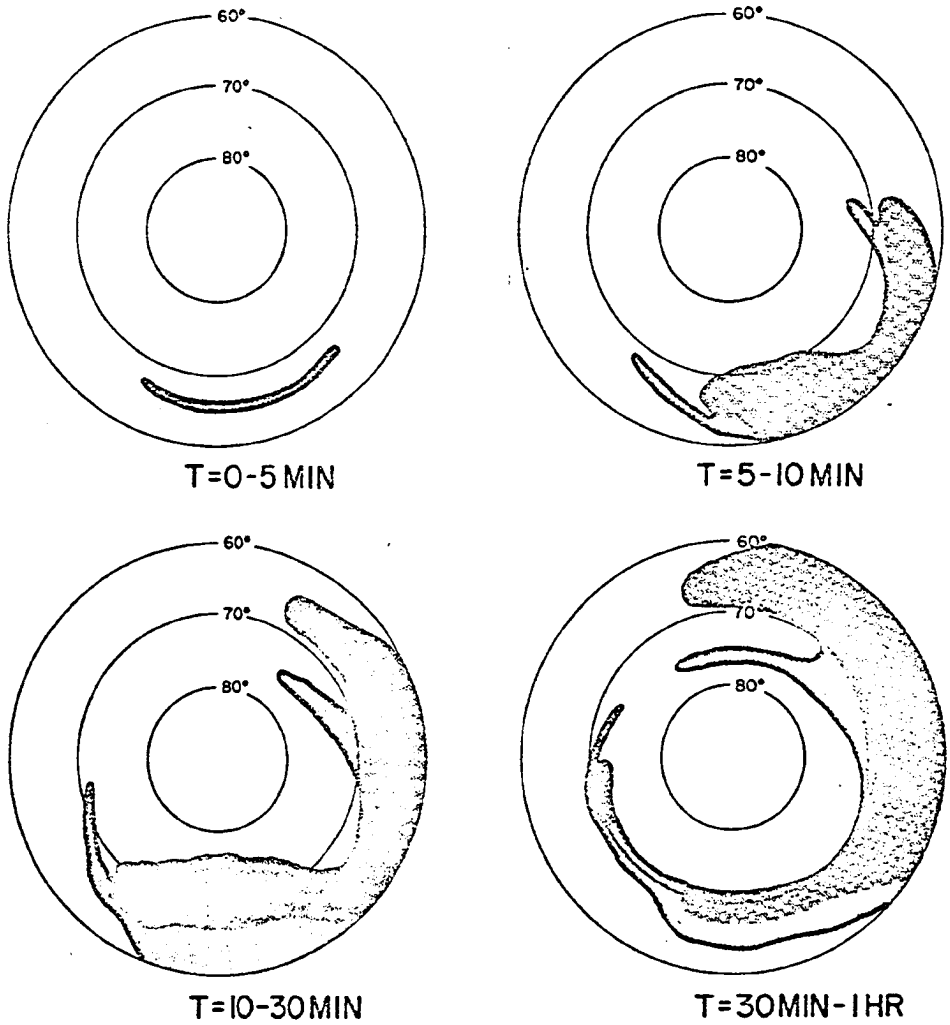

Figure (6.4) Development of the ionospheric substorm (after Akasofu, 1968).

Rosen observed that such events were observed first at high latitude stations at all local times other than midnight. He suggested that this observation supports his proposed model, that of a dribbling cloud of electrons, because of the inverse dependence of particle drift period on L. His model is based on the gradient drift of trapped electrons, assuming that the initial longitude of the precipitation region is where most of the electrons are accelerated.

6.6 Purpose of Synoptic Study

While the studies discussed previously have contributed extensively to a knowledge of the morphology of auroral absorption, an exact picture of the temporal development over the polar regions during a substorm has not been derived. The areas of greatest uncertainty can be summarized as follows:

(1) What is the distribution in longitude and latitude of absorption at the time of onset of substorm?

(2) How does this distribution change as a function of substorm time?

(3) Is the auroral oval or the auroral zone a better coordinate with which to describe the absorption substorm?

(4) At what rate does the region in which auroral absorption occurs expand and upon what parameters does this expansion depend?

(5) What is the relation of expansion velocities to processes which are known to occur in the magnetosphere?

(6) Can the eastward expansion be explained by the gradient and curvature drift of energetic electrons injected in the midnight sector?

(7) How is the auroral absorption substorm related to the polar magnetic and auroral substorms?

(8) Can all auroral absorption events be explained in terms of the absorption substorm?

In the following chapters, an attempt will be made to answer some of the questions posed above. In particular, in Chapter 8 five substorms of the IQSY (1964-65) period will be examined in detail. This analysis should provide a basis for anwering (1) - (4) and (7). The drift period of energetic electrons will be computed and compared with the observational measurements in Chapter 9; and a model of the auroral absorption substorm will be derived.

CHAPTER 7

REDUCTION AND PRESENTATION OF DATA

7.1 The ESRO Working Group on Auroral Absorption Substorms

In March 1969, during an ESRO Colloquium held in Kiruna, Sweden, a Working Group on Auroral Absorption Substorms was formed (Ortner and Moore, 1969). It was agreed by the Group to exchange data for the IQSY period (1964-65) and for the IYAS (1969), then in progress. Professor Hultqvist of the Kiruna Geophysical Observatory was chosen as the Coordinator of the study, whose task it was to select 30 substorm events for investigation. Several criteria were imposed on the selection of the events: (1) that the record be undisturbed for the previous hour; (2) that the event have an abrupt onset with a rate of increase of absorption of at least 1db per minute; (3) that the duration be in excess of 30 minutes; (4) that the maximum amplitude exceed 1db for more than five minutes; (5) that the onset occur between 18^h and 06^h LT. The 30 events were to be distributed among the Working Group participants whose task it was to reduce the data in the form of contour maps. It was further agreed that at least one joint paper be co-authored by all the participating members before proceeding individually with the analysis. The purpose of the joint paper is to present collectively the results of the synoptic maps derived by each group.

7.2 Technique of Data Reduction

As outlined above, the cooperative study called for the analysis of the absorption substorm data in the form of contour maps, produced

for every 15 minute interval during the substorm. A set of programs developed by IBM for the System/360 (Gussow et al., 1968) was adapted for this purpose. The STAMPEDE (Surface Techniques, Annotation, and Mapping Programs for Exploration, Development, and Engineering) programs are designed to make numerical and analytical approximations to a set of three coordinate values defining any surface and for preparing a display of surface geometry in the form of plotted contour maps. Utilization of this technique has the advantage of eliminating 'human bias' in the construction of the contour map. Also advantageous is the use of a numerical method in approximating the surface and deriving the contours.

The first step in approximating the surface is to superimpose a square grid system on the input x,y,z data and to interpolate missing values onto the grid. Note that x and y define the location on the surface of a point whose magnitude is represented by z. Also note that the grid interval is chosen so that a grid square contains, on the average, one input point. Following the superimposition of a grid system over the input data, a value is calculated for each mesh point (grid intersections) within the grid system. For grid squares containing data points, mesh-point values are established at each corner. This is accomplished mathematically by passing a plane surface, which is determined from the surrounding data points by taking a weighted least-squares fit, through the data point.

After evaluating all the mesh-point values for grid squares containing data points, the remaining mesh points are evaluated using

those values previously determined in a manner analogous to that outlined above. The technique builds up tiers of mesh-point values around each established mesh point until the grid system has been completely evaluated. For a detailed description of the technique the reader is referred to Gussow et al. (1968).

It is important to note that if a z value occurs near the boundary of the surface being approximated, no mesh points will be derived for the grid square containing this point if they lie outside the boundary. And, if the distribution of data points around the edges of the surface is irregular many of the mesh points near the boundary will be derived by extrapolation.

After all of the mesh-points within the mapped area have been evaluated, they serve as input to the CONTOUR program. For each grid square the contouring is accomplished using the equation:

$$z = z_o + (z_3 - z_0)x + (z_1 - z_0)y + (z_0 + z_2 - z_1 - z_3)xy$$

where z_0, z_1, z_2, and z_3 are the mesh values at the corners of a grid square and x,y are the coordinates of the data point z. According to Gussow et al. (1968) "this equation has the advantage of being linear along the edges of the grid square (and therefore a contour line is continuous from one grid square to another), without being linear over the area of the square." The program allows the annotation of contour lines or data points and enables one to emphasize certain contour lines; special emphasis can be made by drawing a heavy (double) contour line.

In the version of STAMPEDE used in this study, the contour interval was chosen as 0.5db, and the grid interval was 0.25 inches (except for the August 2, 1965 substorm where the contour interval is 0.25db). Every integer contour line is annotated and drawn as a heavy line. The location of each observation point is annotated on this grid using a coding system (see Table X). As a foreground to the contour map, the continental outlines have been plotted in corrected geomagnetic coordinates by a computer program developed by J. Dryden (private communication).

7.3 Coordinate Systems

It becomes obvious, after searching the literature, that no universally accepted geomagnetic coordinate system has been adopted for use in describing auroral phenomena. As a result, a number of systems were investigated and compared before a choice of coordinate system was made. A brief description of each of the systems considered follows.

7.3.1 The centered dipole coordinate system

The centered dipole system of geomagnetic coordinates is the system most frequently utilized in the description of auroral phenomena. An analytical transformation between geographic and geomagnetic coordinates can easily be made using the formulae (Chamberlain, 1961):

$$\sin\lambda_m = \sin\lambda_p \sin\lambda + \cos\lambda_p \cos\lambda \cos(\phi - \phi_p)$$

$$\sin\phi_m = \cos\lambda \sin(\phi - \phi_p)/\cos\lambda_m$$

where ϕ is longitude and λ is latitude and where λ_p, ϕ_p represent

Table X

A Comparison of Different Coordinate Systems for 46 Observatories In the Northern Hemisphere

Station	Station ID	Geographic Coordinates		Geomagnetic (Centered Dipole) Coordinates		1965 "Corrected" Geomagnetic Coordinates		1970 "Corrected" Geomagnetic Coordinates		Eccentric Dipole Coordinates		Invariant Geomagnetic Coordinates		L Value
		Lat.	Long.	Lat.	Long.	Lat.	Long.	Lat.	Long.	Lat.	Long.	Lat.	Long.	
Thule	41	76.55	291.17	88.05	1.16	86.0	37.8	85.97	33.14	84.61	198.02	85.7	39.8	177.85
Resolute Bay	12	74.70	265.10	82.96	289.18	84.3	306.0	84.14	304.32	83.32	311.44	84.1	310.7	94.63
Godhaven	42	69.30	306.50	79.96	32.04	77.7	43.6	77.68	41.71	76.24	225.49	77.25	46.1	20.53
Frobisher Bay	13	63.80	291.40	75.30	0.52	74.9	14.7	75.15	11.86	72.31	359.16	74.9	16.7	14.73
Heiss Island	28	80.62	58.05	71.07	155.50	74.6	144.3	74.32	143.15	72.34	244.64	74.6	146.8	14.18
Isfjord	22	78.06	13.63	74.58	126.92	74.6	113.9	74.99	113.48	73.94	106.45	74.9	116.75	14.73
Longyearbyen	43	78.20	15.70	74.36	130.94	74.5	115.2	74.90	114.98	73.81	105.01	74.75	117.95	14.45
NP-13 (Aug.65)	39	80.25	159.30	70.62	202.40	74.3	207.4	74.40	207.19	73.83	188.69	74.15	210.15	13.40
NP-13 (Nov.65)	35	80.50	149.70	70.18	200.10	74.2	200.8	74.27	201.45	73.26	183.15	74.05	204.40	13.24
NP-13 (Oct.64)	38	77.27	181.58	69.27	219.48	72.9	224.4	72.91	224.69	73.69	207.95	72.9	227.65	11.56
NP-13 (Mar.65)	37	77.93	167.32	69.25	209.38	72.6	215.4	72.57	215.65	72.57	197.54	72.3	218.8	10.81
NP-13 (Jan.65)	36	77.27	169.63	68.62	213.77	72.0	217.5	72.04	217.98	72.24	200.13	71.85	221.0	10.30
Cape Chelyuskin	29	77.80	104.30	66.30	176.50	71.3	173.9	71.64	174.20	68.48	159.81	71.18	177.46	9.61
Cape Zhelania	30	77.00	68.60	67.90	156.90	71.1	147.5	71.48	147.39	68.27	221.62	71.1	151.4	9.53
Inuvik	48	68.35	226.20	70.41	264.63	71.1	268.4	71.08	267.71	72.64	264.14	71.1	272.25	9.53
Churchill	14	58.80	265.80	68.70	322.70	70.3	325.9	70.26	325.85	67.55	322.84	69.9	331.15	8.47
Bar I	2	69.60	219.80	70.20	256.90	70.2	261.3	70.88	260.75	72.79	255.17	70.85	265.55	9.29
Barrow	1	71.60	203.60	68.86	240.95	69.7	247.0	69.92	246.49	71.99	235.88	69.9	250.65	8.47
Great Whale River	15	55.28	282.17	66.59	347.29	68.2	353.8	67.97	353.68	64.26	344.74	67.55	358.95	6.86
Dixson Island	31	73.50	80.40	62.98	161.44	67.9	154.7	68.27	154.53	64.28	144.50	67.75	158.2	6.97
Cape Jones	16	54.01	280.99	65.26	345.87	67.2	350.1	66.79	351.62	63.02	343.14	66.4	356.85	6.24
Fort Yukon	3	66.57	214.75	66.63	256.84	67.1	260.7	66.99	260.14	69.16	253.85	66.9	264.7	6.50
Reyjavik	21	64.10	338.20	70.16	70.82	66.5	71.2	66.76	69.38	66.96	56.72	66.35	72.7	6.21
Andoya	44	69.30	16.10	67.30	113.94	66.1	103.1	66.61	102.45	65.90	95.87	66.45	105.55	6.26
Tromso	23	69.70	19.00	67.14	116.80	66.0	105.2	66.78	104.84	65.87	98.53	66.55	108.1	6.31
Tixie Bay	32	71.60	128.90	60.45	191.35	65.6	195.2	65.84	195.40	63.05	177.80	65.1	198.5	5.64
College	4	64.87	212.20	64.62	256.51	64.9	260.3	64.84	259.68	67.14	252.98	64.75	264.3	5.49
Kotzebue	6	66.90	197.50	63.71	242.16	64.4	247.5	64.32	247.16	66.67	236.36	64.1	251.4	5.24
Kiruna	24	67.80	20.40	65.27	115.60	64.3	104.3	64.77	104.23	63.92	97.97	64.6	106.9	5.43
Loparskaya	45	68.25	33.08	63.47	125.78	64.0	115.5	64.42	113.87	62.73	108.13	64.25	117.0	5.29
Amderma	33	69.77	61.68	61.00	147.70	63.9	137.5	65.09	137.26	61.47	130.26	64.65	140.75	5.45
Moosonee	17	51.50	279.33	62.68	344.08	63.8	348.7	64.40	348.81	60.56	340.97	64.05	354.2	5.22
Healy	5	64.00	211.00	63.63	256.58	63.7	260.2	63.78	259.54	66.11	252.57	63.45	264.2	5.00
Paxson	7	63.04	214.50	63.45	260.47	63.5	263.6	63.48	262.93	65.75	257.11	63.35	267.6	4.97
Sodankyla	27	67.40	26.60	63.79	120.00	63.4	108.9	63.93	108.46	62.73	102.58	63.65	111.45	5.07
Norilsk	46	69.43	88.09	58.40	164.80	63.4	159.5	64.60	160.08	59.93	159.09	63.65	163.5	5.07
Appatity	40	67.55	33.30	62.80	125.28	63.09	114.0	63.73	113.54	62.03	107.92	63.5	116.75	5.02
Prince Albert	18	53.20	254.30	61.69	310.98	62.2	311.2	62.86	311.12	61.26	308.43	62.55	316.45	4.70
Talkeetna	8	62.30	209.90	61.88	257.00	61.9	260.9	61.88	258.40	64.29	252.90	61.75	264.4	4.46
Salekhard	34	66.50	66.70	57.01	148.50	61.8	140.4	62.07	140.17	57.86	132.76	61.35	143.65	4.35
Lycksele	25	64.70	18.80	62.77	111.03	61.2	101.4	61.79	100.77	61.25	94.35	61.7	103.65	4.45
Sheep Mountain	9	61.82	212.50	61.95	259.77	61.0	262.9	61.92	262.22	64.25	256.01	61.75	267.15	4.46
Anchorage	10	61.20	210.15	60.93	258.17	60.8	261.3	60.83	260.74	63.26	254.03	60.65	265.55	4.16
Baie St. Paul	47	47.38	289.45	58.87	357.97	60.6	4.4	60.14	4.07	56.31	353.06	59.85	9.40	3.96
Wildwood	11	60.56	208.75	60.07	257.42	59.7	260.6	59.91	260.04	62.41	253.06	59.7	264.85	3.93
Val D'or	19	48.00	282.20	59.32	348.32	59.3	352.7	61.00	353.09	57.09	344.39	60.55	358.45	4.14
Ottawa	20	45.40	284.10	56.80	351.52	58.9	355.4	58.52	355.68	54.51	346.56	58.15	361.15	3.59
Uppsala	26	58.85	17.92	58.51	106.23	56.4	98.0	55.93	96.96	55.86	84.14	55.75	99.5	3.16

127

the coordinates of the geomagnetic pole. The centered dipole coordinates of the stations used in this study are given in Table X.

7.3.2 Corrected geomagnetic coordinates (1965)

This system of geomagnetic coordinates is based on a correction applied to the centered dipole representation of the geomagnetic field. Hultqvist (1958) used the first five terms of the spherical harmonic expansion of the magnetic potential rather than just the dipole term, to represent the geomagnetic field. Hakura (1965) applied the results of Hultqvist to derive what he termed corrected geomagnetic coordinates (CGM). In deriving the coordinate transformation, he used the equations:

$$\alpha = \frac{\sqrt{A^2(Q) + P^2(Q)}}{a} \cdot \frac{180}{\pi}$$

$$a = 6371.2 \text{ kilometers}$$

$$\sin\xi = \frac{P(Q)}{\sqrt{A^2(Q) + P^2(Q)}}$$

$$\cos\xi = \frac{A(Q)}{\sqrt{A^2(Q) + P^2(Q)}}$$

$$\theta_c = \frac{180}{\pi} \cos^{-1}(\cos\theta\cos\alpha + \sin\theta\sin\alpha\cos\xi)$$

$$\Delta\Lambda = -\frac{180}{\pi} \sin^{-1}(\sin\alpha\sin\xi/\sin\theta_c)$$

$$\phi_c = 90^\circ - \phi_c$$

$$\Lambda_c = \Delta\Lambda + \Lambda$$

where (ϕ_c, θ_c) are the corrected geomagnetic coordinates; A(Q), P(Q) are components of the displacement of the 'real' field line along and perpendicular to the meridian of the dipole field line; and Λ is the dipole longitude.

Hakura (1965) presented tables of corrected geomagnetic coordinates as a function of geographic coordinates for two degree intervals in latitude and five degree intervals in longitude. An interpolation formula was given to find the corrected coordinates for any point in the higher latitude regions. He also calculated the corrected coordinates for a large number of principal geophysical observatories. Mayuad (1960) has drawn polar maps in centered dipole geomagnetic coordinates over which he has superimposed the corrected geomagnetic system.

The corrected geomagnetic coordinates for the stations used in this study are tabulated in Table X. Note that major differences between the two systems occur near 130°E and 340°E geographic longitude; for example, in the centered dipole system the latitude of Tixie Bay is 60.4° while in the CGM system the latitude is 65.6°N. Similarly, the latitude of Reyjavik changes from 70.2° in the centered dipole system to 66.5° in the corrected geomagnetic system.

7.3.3 Corrected geomagnetic coordinates (1970)

Gustafsson (1970) has updated Hakura's (1965) computation of the corrected geomagnetic coordinate system. He utilized the Goddard Space Flight Center field 12/66 for epoch 1965 and added two terms to the spherical harmonic expansion used by Hultqvist (1958) in his derivation. In the manner of Hakura, Gustafsson also tabulated the geomagnetic coordinates as a function of geographic latitude and longitude. Figure 7.1 represents a polar geographic grid with the corrected geomagnetic system superimposed thereon.

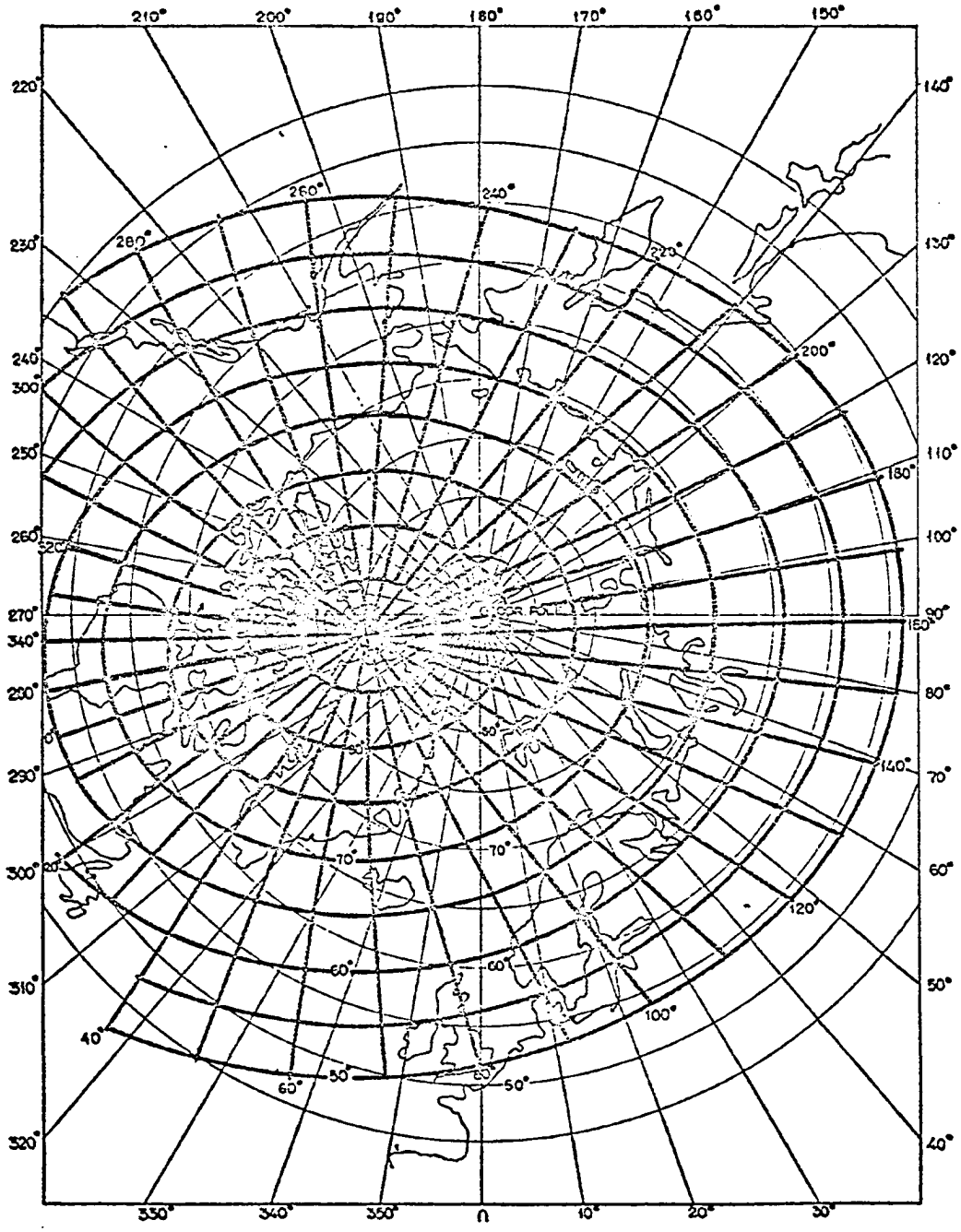

Figure (7.1) A polar projection in geographic coordinates with the corrected geomagnetic coordinate system superimposed (after Gustafsson, 1970).

For purposes of comparison, the CGM coordinates were calculated for the 48 stations of Table X. The tabular values of Gustafsson were used to derive a map projection which is used in the following data presentation. These values were also stored on magnetic tape and used in conjunction with a computer program (CORRGM) for calculating the CGM coordinates of any station (J. Dryden, private communication).

7.3.4 The eccentric dipole coordinate system

Cole (1963) derived equations for the transformation of geographic coordinates into eccentric dipole coordinates by means of the equations:

$$\cot\theta' = \frac{l_3(\sin\theta\cos\phi-X) + m_3(\sin\theta\sin\phi-Y) + n_3(\cos\theta-Z)}{\left[[l_1(\sin\theta\cos\phi-X) + m_1(\sin\theta\sin\phi-Y) + n_1(\cos\theta-Z)]^2 + [l_2(\sin\theta\cos\phi-X) + m_2(\sin\theta\sin\phi-Y) + n_2(\cos\theta-Z]^2\right]^{1/2}}$$

$$\tan\phi' = \frac{l_2(\sin\theta\cos\phi-X) + m_2(\sin\theta\sin\phi-Y) + n_2(\cos\theta-Z)}{[l_1(\sin\theta\cos\phi-X) + m_1(\sin\theta\sin\phi-Y) + n_1(\cos\theta-Z)]}$$

where θ is the geographic co-latitude and ϕ is geographic longitude. The transformation constants are defined as:

$l_1 = -0.5146$	$m_1 = -0.8481$	$n_1 = -0.262$
$l_2 = 0.8543$	$m_2 = -0.4947$	$n_2 = -0.1596$
$l_3 = 0.0728$	$m_3 = -0.1894$	$n_3 = 0.9791$
$X = -0.0577$	$Y = 0.0320$	$Z = 0.0184$

According to Chapman and Bartels (1940) "in the Northern Zone (25°-65°N) the approximation (to the geomagnetic field) furnished by the eccentric dipole is even a little inferior to that furnished by the centered dipole." This is borne out in Table X where the eccentric

dipole coordinates are compared with other coordinate systems. The discrepancy appears to be greatest in the Alaskan sector where the eccentric coordinates yield latitude values some two degrees greater than other coordinate systems.

7.3.5 The invariant geomagnetic coordinate system

Evans et al. (1969) have calculated a system of invariant magnetic coordinates for six different altitudes. They used a computer program to trace out field lines in space as a function of geographic coordinates of points on the field line. They present tables of geographical latitude and longitude at six altitudes for 5° intervals of invariant geomagnetic latitude and 10° intervals of invariant geomagnetic longitude. The invariant geomagnetic coordinates for each station and the corresponding L-value are listed in Table X.

Note that this coordinate system corresponds quite closely to the corrected geomagnetic coordinate system described previously. Although minor differences in latitude can be noted, the principal difference is an approximately 3° shift in longitude brought about by the definition of the 0° meridian in the invariant system.

The McIlwain L-values were derived from the invariant magnetic latitude of each station using the equation

$$L = 1/(\cos\theta)2$$

where θ is the invariant magnetic latitude. The values of invariant magnetic latitude and longitude were derived from the tables given by Evans et al. (1969) using an interpolation algorithm. This algorithm

(see Appendix B) determined the invariant coordinates through an interpolation of the geographic coordinates. The computations were performed on an InterData model-4 computer.

7.4 Choice of Coordinate System

For the purposes of the study undertaken here, the corrected geomagnetic coordinate system was selected in which to display the synoptic motions of the absorption substorm. A determining factor in the choice of coordinate systems was the degree of difficulty involved in transforming from geographic to geomagnetic coordinates. The tables provided for this purpose by Evans et al. (1969) were found to be exceedingly cumbersome to use, in contrast with the corresponding tables of Hakura (1965) or Gustafsson (1970).

CHAPTER 8

A SYNOPTIC STUDY OF FIVE SUBSTORMS DURING THE IQSY

8.1 Introduction

In the following analysis, the contour plotting technique described in the previous chapter is used to illustrate the development of the absorption substorm. For this analysis, data were obtained from more than two dozen observatories at auroral latitudes in the Northern Hemisphere. The density of these observatories is such that the predominant motion to be considered herein is the longitudinal motion. In general the latitudinal motion and extent of the contours will not be considered relevant. A coding system has been used to identify the observatories; these observatories are listed in Table X.

8.2 The Substorm of November 7, 1965

The polar substorm, which began shortly before 10^h UT on this date, was of moderate size; the planetary magnetic index K_p attained a value of 3+ during the interval 09^h to 12^h UT. However, the onset of the polar magnetic substorm was quite intense: negative excursions of the H-component were observed between 0957 and 1000 UT at Cape Wellen, Barrow, College, and Sitka. At College and Barrow, the amplitude of the negative-bay was in excess of 750 γ (see Fig. 8.1). Positive increases of the H-component were noted at Dixson Island, Cape Chelyuskin and Heiss Island (all located in the afternoon sector) between 10 and 11^h UT. No significant activity was recorded at observatories located in the late morning or noon sectors.

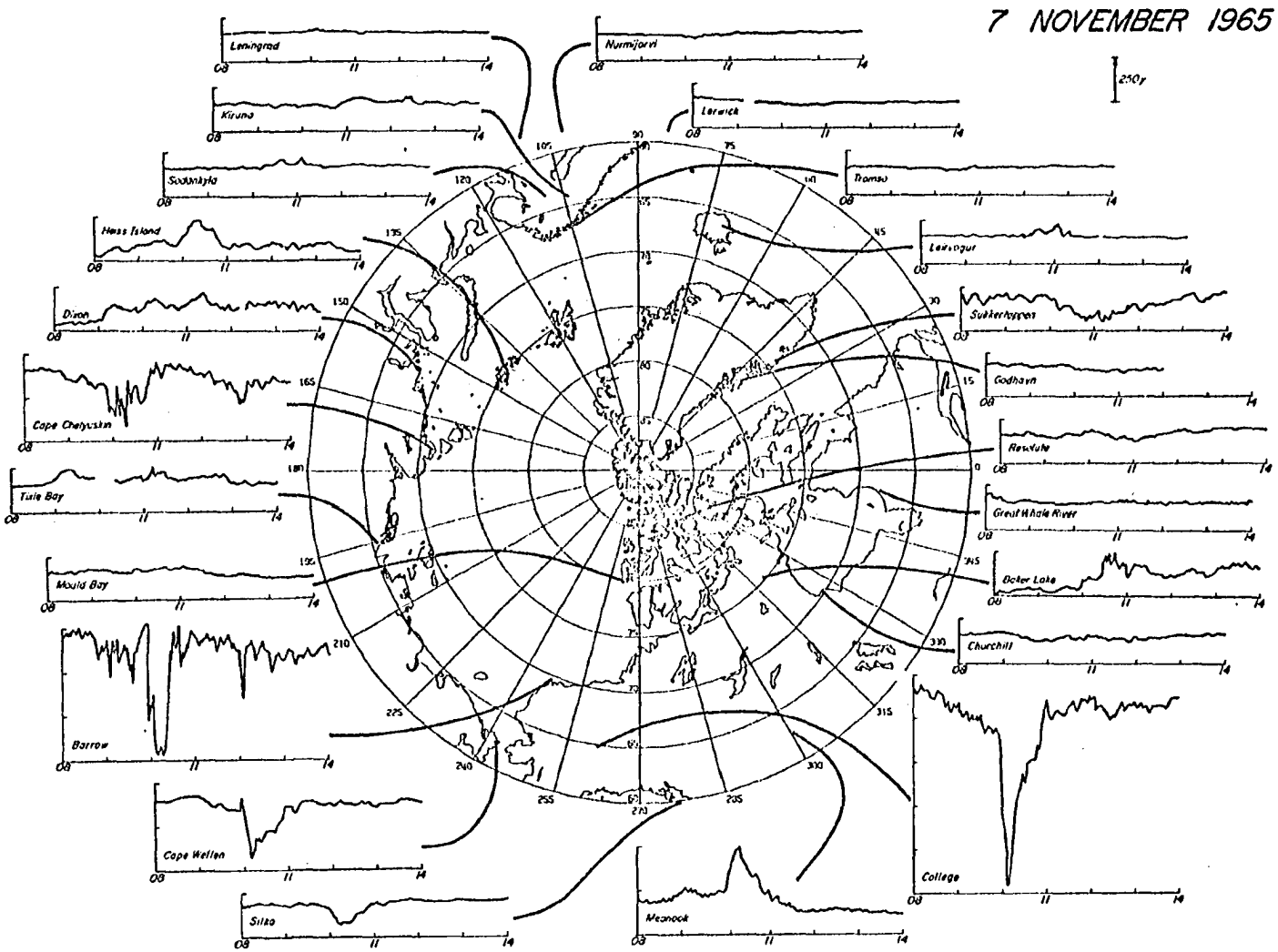

Figure (8.1) A collection of magnetic records (H or X component) from magnetic observatories in the Northern Hemisphere on November 7, 1965.

The auroral absorption substorm began at ∿ 0955 UT when a sudden increase in absorption was registered almost simultaneously at Bar I, Fort Yukon, College, Healy, and Kotzebue. The precipitation region expanded rapidly; absorption onsets occurred at Prince Albert (62.2°N, 311.2°E) at 1003 UT and North Pole-13 (74.2°N, 200.8°E) at 1006 UT. Thus, within 10 minutes of the substorm onset, precipitation was recorded over 110 degrees of longitude and 12 degrees of latitude. At Talkeetna (61.9°N), the only Alaskan station where overcast conditions did not prevail, equatorward motions were observed by the all-sky camera from 0956-0957 UT.

Prior to the onset of the substorm (0950 UT) no significant absorption is observed within the auroral region (see Figure 8.2). There were, however, small precursor events recorded at Fort Yukon and College around 0900 UT. The substorm appeared to develop from a source region centered near Fort Yukon (67.1°N) where the absorption magnitude was greatest (6.9 db, see Figure 8.3). The absorbing region grew rapidly (Figure 8.4) and by 1010 UT extended from NP-13 to Moosonee (63.8°N, 348.7°E) (see Figure 8.5). At this time regions in which the absorption exceeds 2 db were located at 74° latitude over NP-13 (4.3 db), at 67°N in the Alaskan sector and at 63°N over eastern Canada. At 1020 UT (Figure 8.6) the magnitude of the absorption had decreased in the evening sector, but remained constant over eastern Canada. The continuing eastward drift can be inferred from the extent of the 1 db contour beyond Iceland (point 21). Approximately 40 minutes after the onset of the substorm (1035 UT) the absorption had drifted nearly to

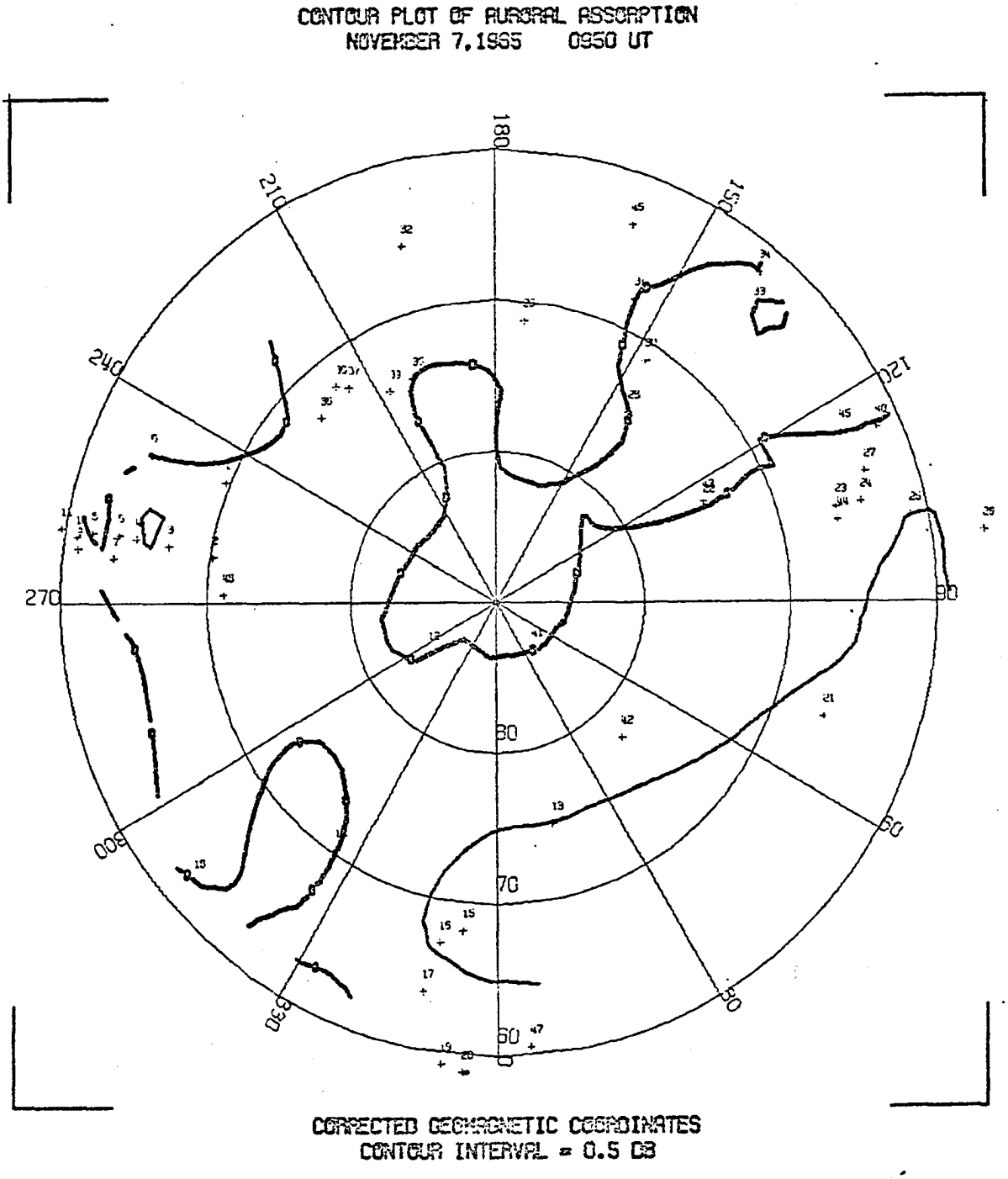

Figure (8.2) In this diagram and the similar diagrams which follow, contours of auroral absorption over the Northern Hemisphere have been constructed for selected intervals of time. The numbered points on the map denote observatories from which data may have been available. These observatories are identified in Table X. The plastic overlay with continental outlines can be used for reference. This figure contains data for 0950 UT on November 7, 1965.

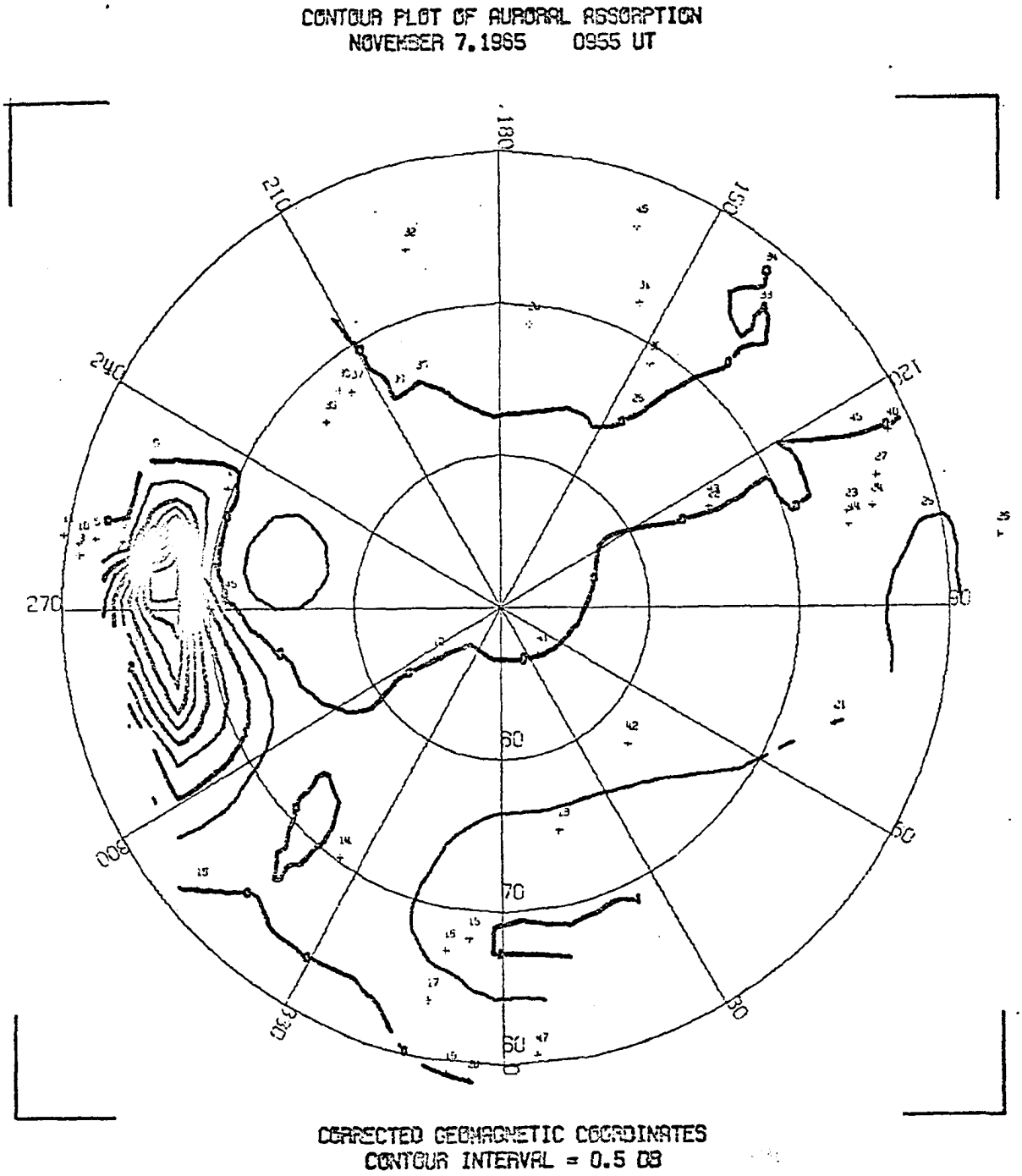

Figure (8.3) Contour map for 0955 UT on November 7, 1965.

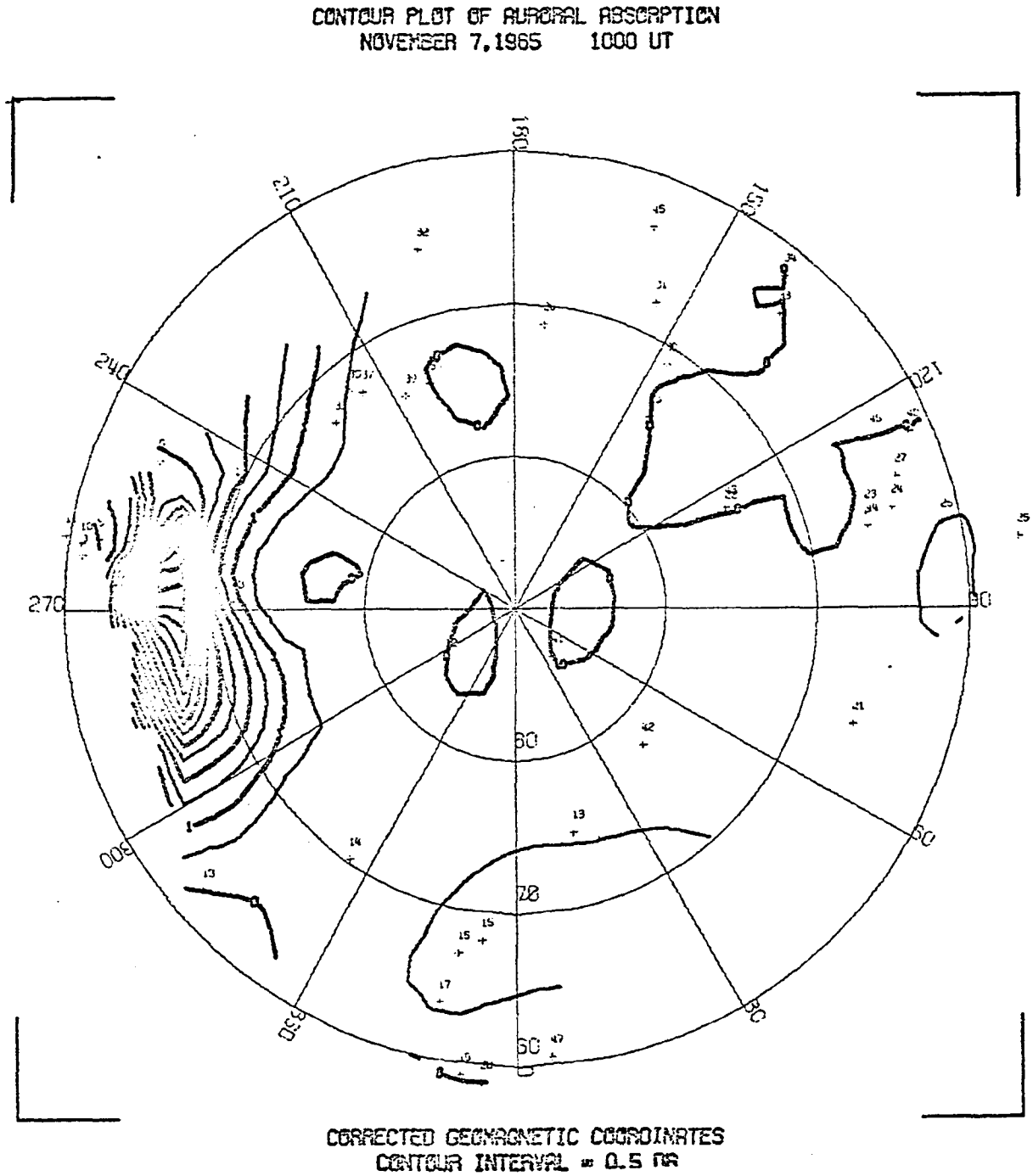

Figure (8.4) Contour map for 1000 UT on November 7, 1965.

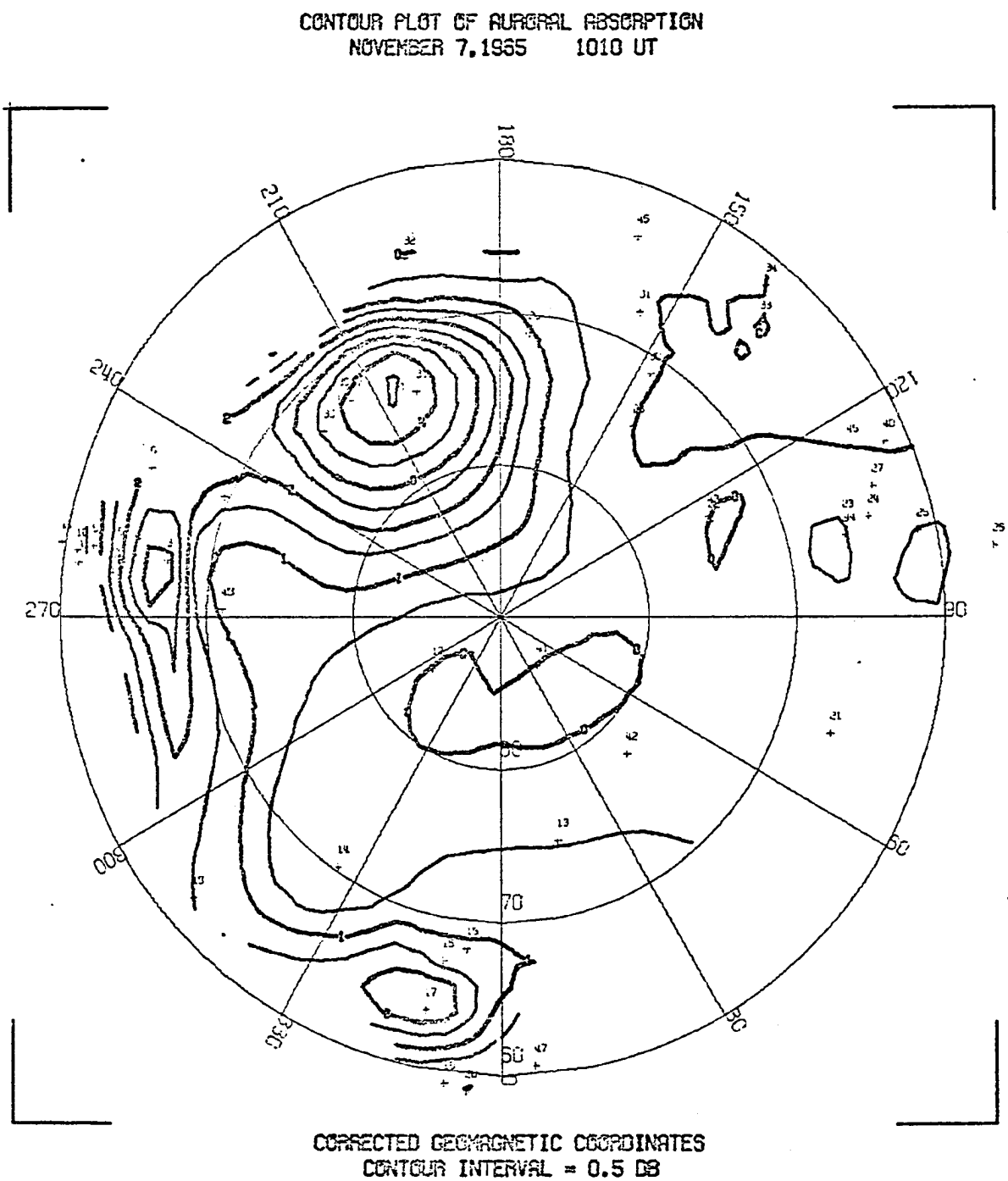

Figure (8.5) Contour map for 1010 UT on November 7, 1965.

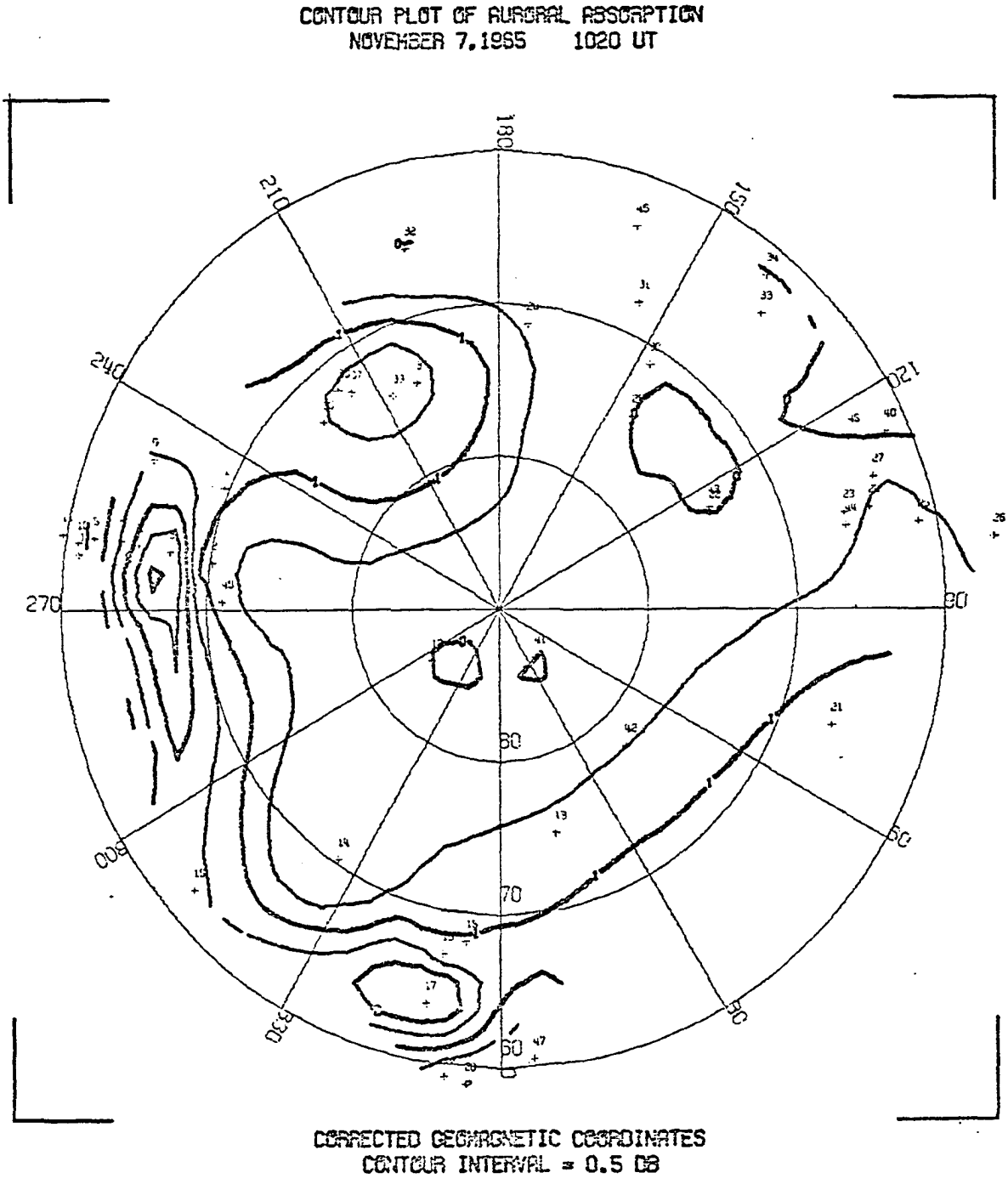

Figure (8.6) Contour map for 1020 UT on November 7, 1965.

the noon meridian; the magnitude of absorption had increased beyond 2 db in Iceland, and had decreased slightly in Alaska (see Figure 8.7). Ten minutes later at 1045 UT (Figure 8.9) more than 1 db of absorption had been recorded at Tromsø and in excess of 3 db at Reyjavik, Iceland. At 1055 UT (Figure 8.9) maxima were still centered near Reyjavik and Tromsø at which time additional maxima occurred near Amderma and NP-13. By 1125 UT only a small amount of absorption ($\leq$ 0.7 db) was observed in Alaska; the greatest amount was recorded at Reyjavik (2.3 db) (see Figure 8.10) while 1.2 db was recorded at Amderma (63.9°N, 137.5°E) nearly 240 degrees east of the meridian at which the substorm was first observed. At 1150 UT (Figure 8.11), the most intense region of absorption was centered near Reyjavik (66.5°N, 71.2°E), now located near the noon meridian.

During this substorm, absorption was observed as far equatorward as Uppsala (54.4°N), which was located in the noon sector, and poleward as far as NP-13 (74.2°N), which was located in the evening sector. No absorption was recorded at high latitude stations such as Thule, Resolute Bay, Heiss Island or Isfjord. The magnitude of absorption did not exceed 0.5 db at Anchorage (60.8°N) in the midnight sector, at Ottawa (58.9°N) in the morning sector, or at Salekhard (61.8°N) and Uppsala in the noon sector.

It is inferred that the absorption observed at NP-13 during this event was associated with the westward traveling auroral surge (Akasofu et al., 1965, 1966). Morphologically, the event is of the type usually

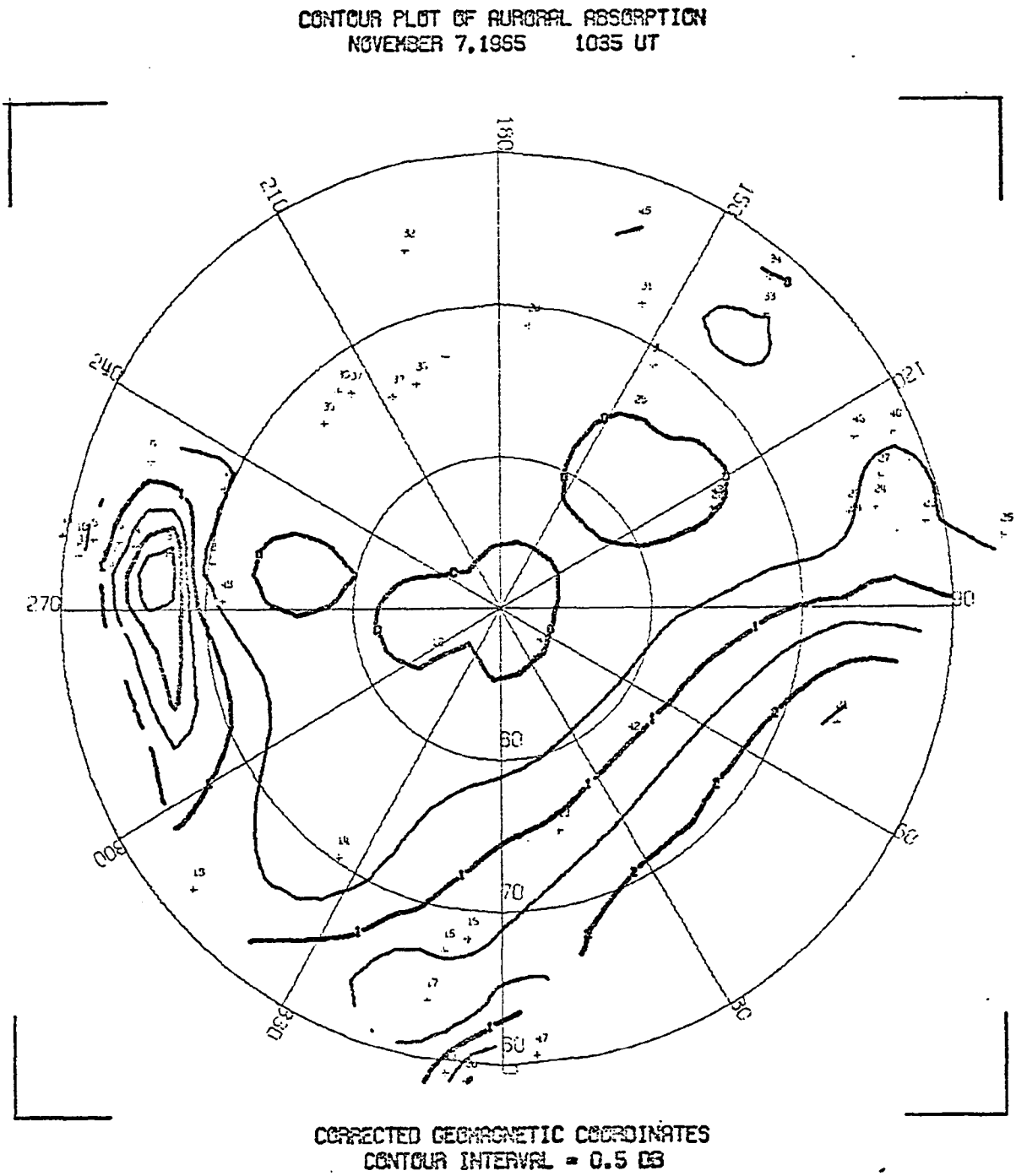

Figure (8.7) Contour map for 1035 UT on November 7, 1965.

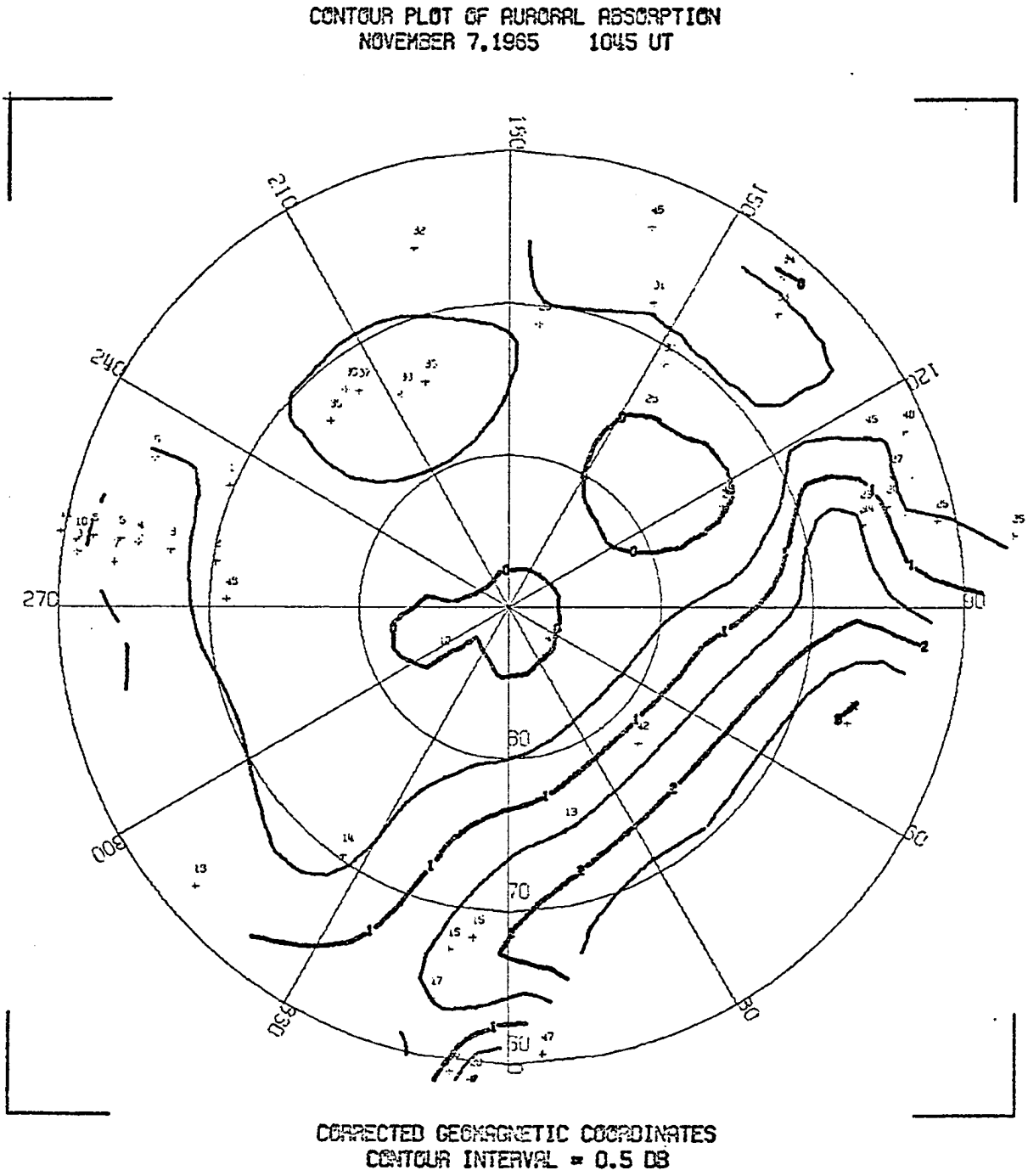

Figure (8.8) Contour map for 1045 UT on November 7, 1965.

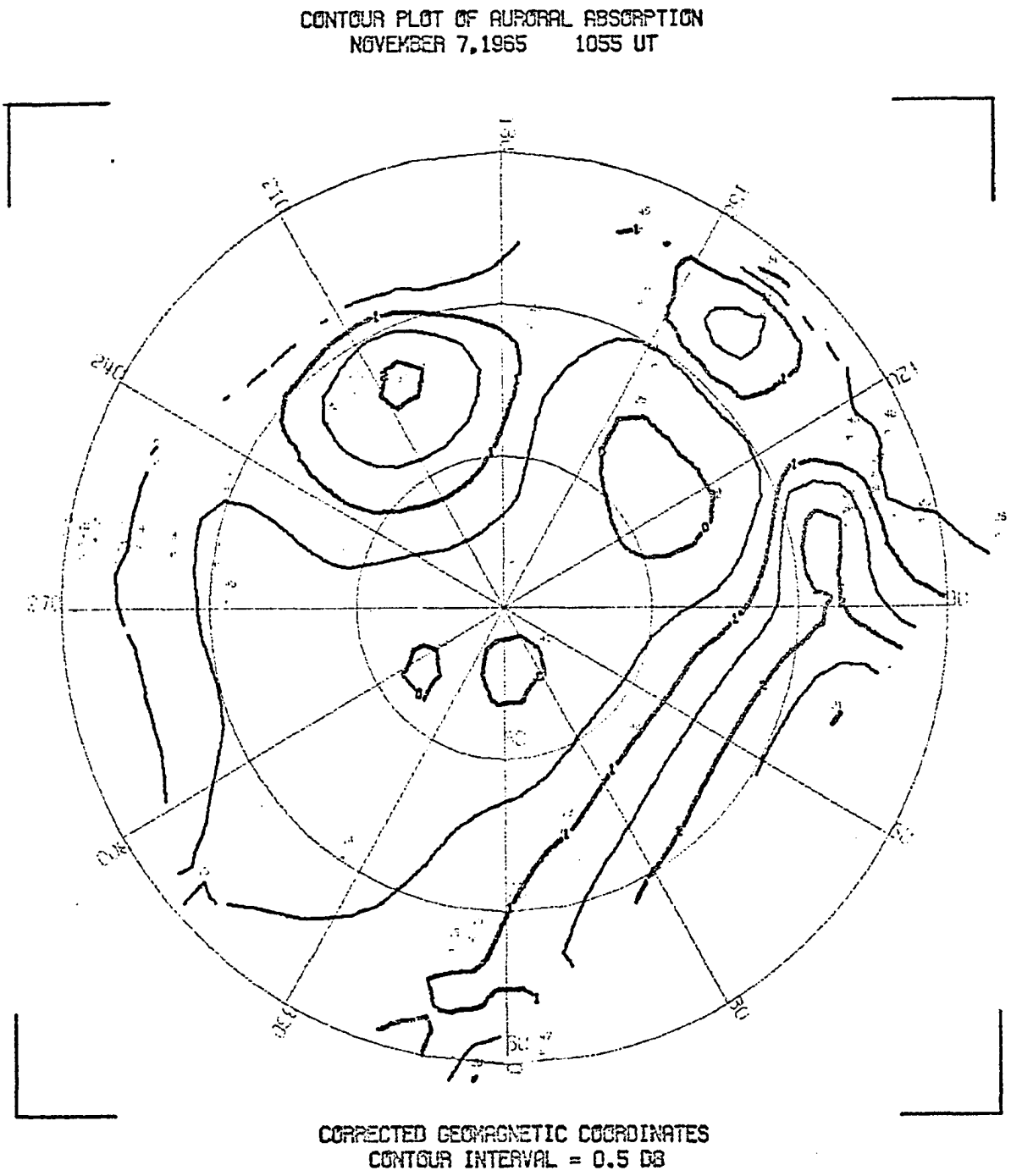

Figure (8.9) Contour map for 1055 UT on November 7, 1965.

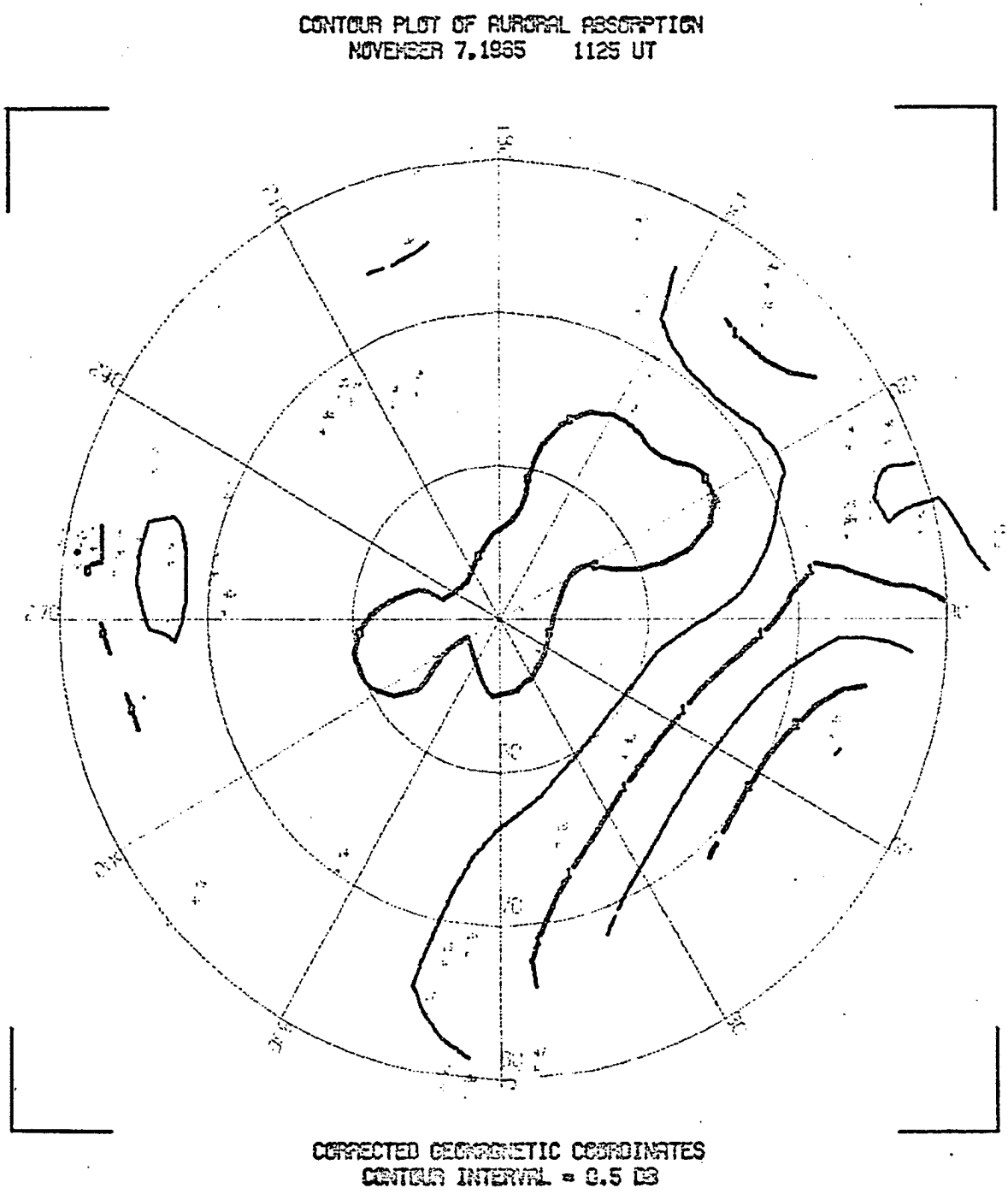

Figure (8.10) Contour map for 1125 UT on November 7, 1965.

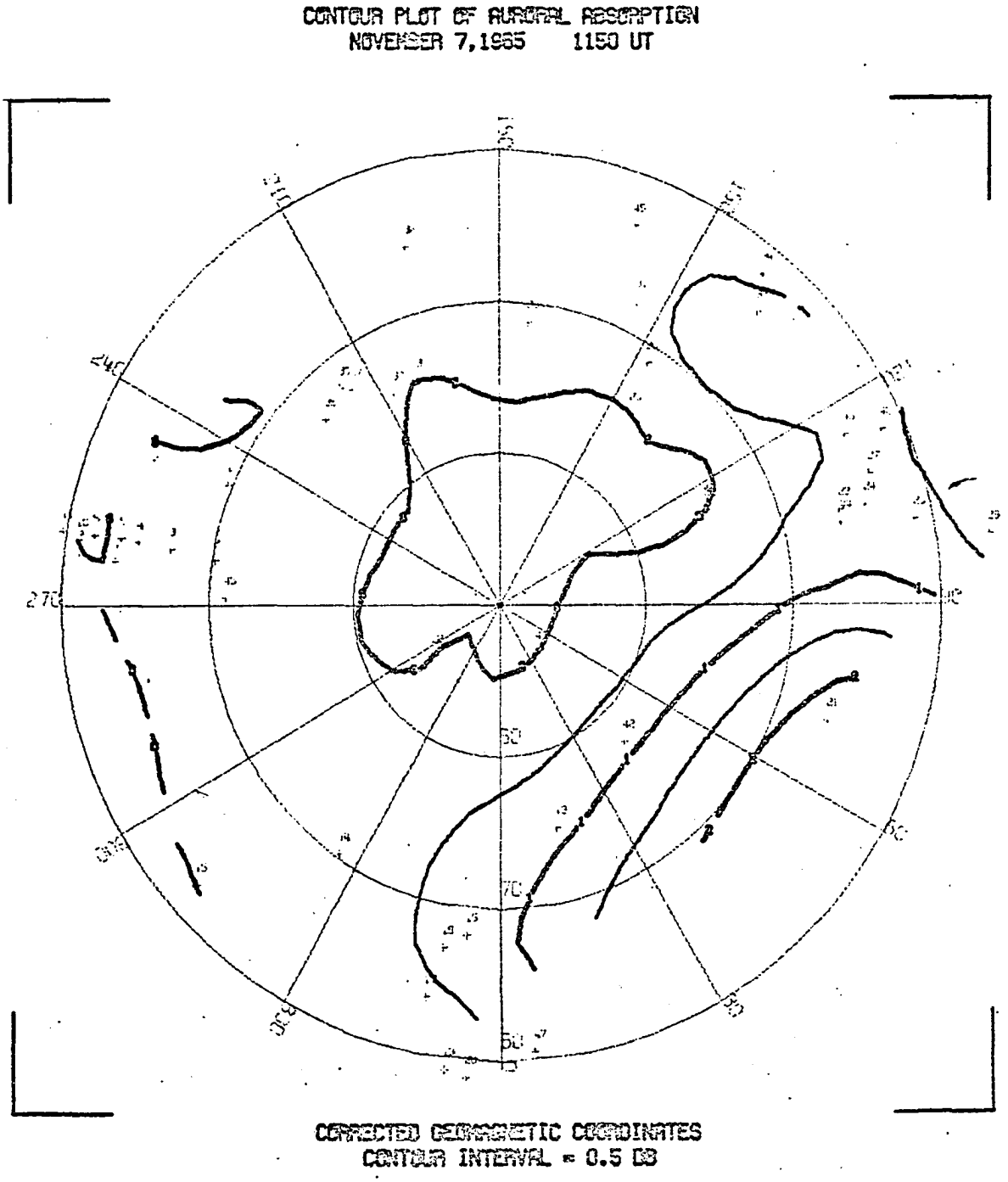

Figure (8.11) Contour map for 1150 UT on November 7, 1965.

observed during the passage of an intense surge. Furthermore, NP-13 was located within the auroral oval at the time of the substorm, whereas at Tixie Bay (65.6°N, 195.2°E), located nearly on the same meridian as NP-13, but near the center of the auroral zone, no absorption > 0.5 db was recorded. Farther to the west, but slightly lower in latitude (than NP-13) positive bays in the H-component were recorded at Cape Chelyuskin and Dixson Island. According to Akasofu (1968), this is evidence that a surge propagated along the auroral oval poleward of the station. At Heiss (144.3°E) and Isfjord (113.9°E), both situated within the auroral oval in the afternoon sector, no absorption was recorded. However, the WTS propagated at least as far west as the 19^h meridian. This suggests that: (1) the surge "died out" before reaching the noon meridian, or (2) that the surge and absorption were contained in an extremely narrow latitude range.

Beyond the 06^h meridian, toward the noon sector, the absorption occurred well equatorward of the auroral oval, more nearly within the auroral zone. Absorption exceeding 1 db was recorded at Reyjavik, Tromsø, and Amderma, all typical auroral zone stations.

8.3 The Substorm of October 9, 1964

During the polar substorm which began near 08^h UT the Kp index reached 4+ during the interval $06-09^h$, decreasing to 3 between $09-12^h$ UT. At Meanook (62.6°N, 300.8°E), the polar magnetic substorm was first recorded at 0758 UT when a negative bay event of 600 γ amplitude was recorded (see Figure 8.12). Negative bays were observed throughout the evening sector at College, Sitka, Barrow, NP-13, and Cape Wellen

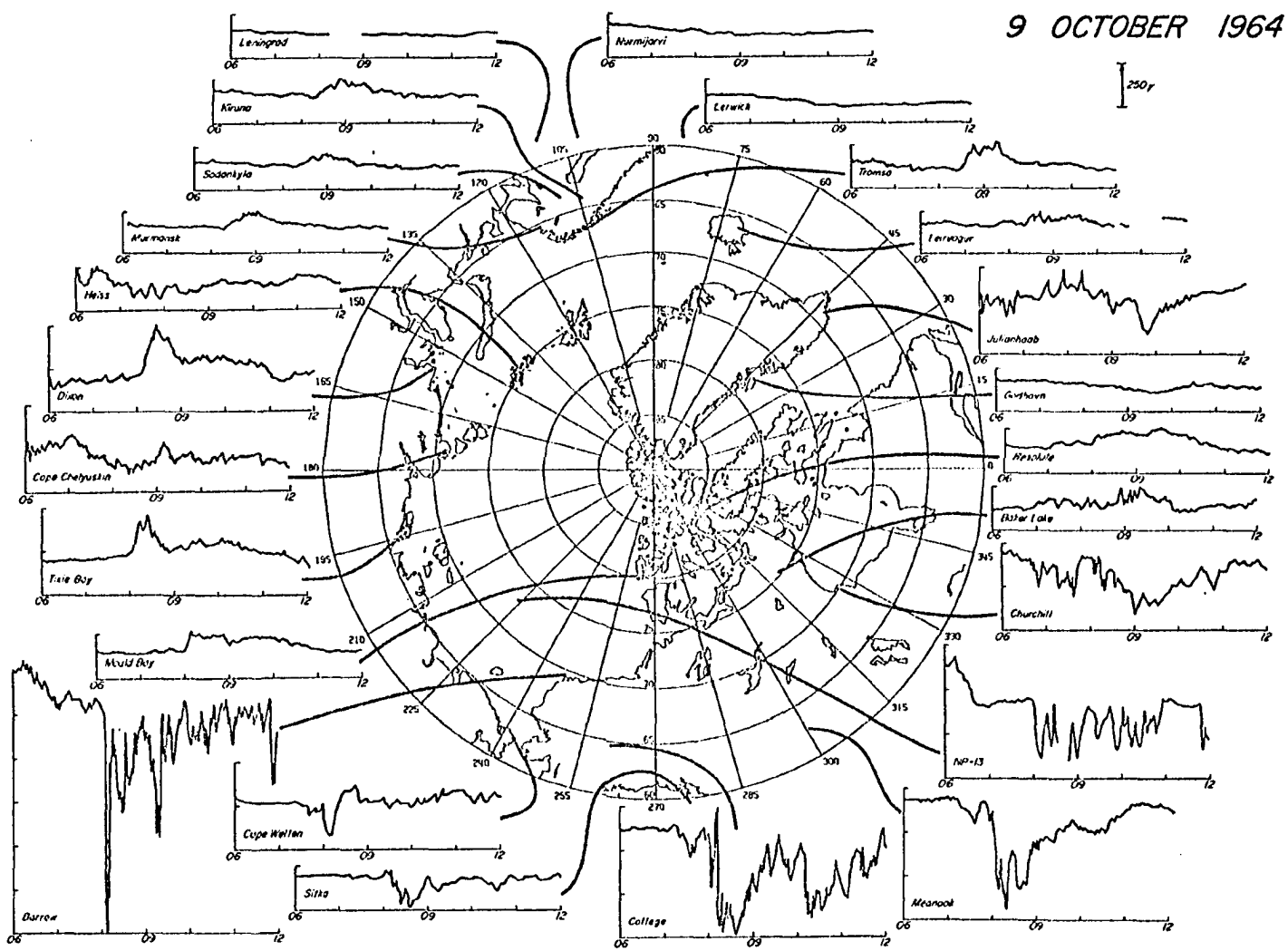

Figure (8.12) A collection of magnetic records (H or X component) from magnetic observatories in the Northern Hemisphere for October 9, 1964.

and at Churchill in the morning sector. At Barrow, a sharp negative deflection of 1350 γ occurred at 0806 UT while simultaneously a 500 γ positive deflection was seen at College. At the same time, a positive deflection of 125 γ (in the H-component) was recorded at Mould Bay (80.6°N, 263.5°E). Positive bays (ΔH = 250-300 γ) were observed in the afternoon sector at Dixson, Chelyuskin, and Tixie. No significant activity was observed in the noon sector except at Tromsø and Murmansk where small positive bays were seen at 0830 UT.

The onset of the auroral absorption substorm was not well defined; maximum absorption occurred almost simultaneously at Point Barrow and Prince Albert, separated by nearly 65° in longitude. At Fort Yukon, a large absorption increase occurred at 0804 UT; again, what might be considered precursor events were observed at both Fort Yukon and College between 0730 and 0815 UT. The onset of this substorm is assumed to have occurred 15-30° east of the College meridian (260°E).

At 0755 UT (Figure 8.13) absorption appeared to be centered near Fort Yukon and Moosonee; little change occurred over the next 5 minutes as the same pattern existed at 0800 UT (Figure 8.14). Between 0805 and 0810 UT the magnitude of absorption increased at Moosonee (Figures 8.15 and 8.16) and by 0815 UT (Figure 8.17) the precipitation had expanded to cover Canada, Alaska, and the western part of Siberia. Note the intense absorption at Prince Albert, Fort Yukon, and Moosonee. At the same time, more than 2 db was recorded at Tixie Bay, nearly 100 degrees west of the midnight meridian. A decrease in the absorption magnitude could be seen at

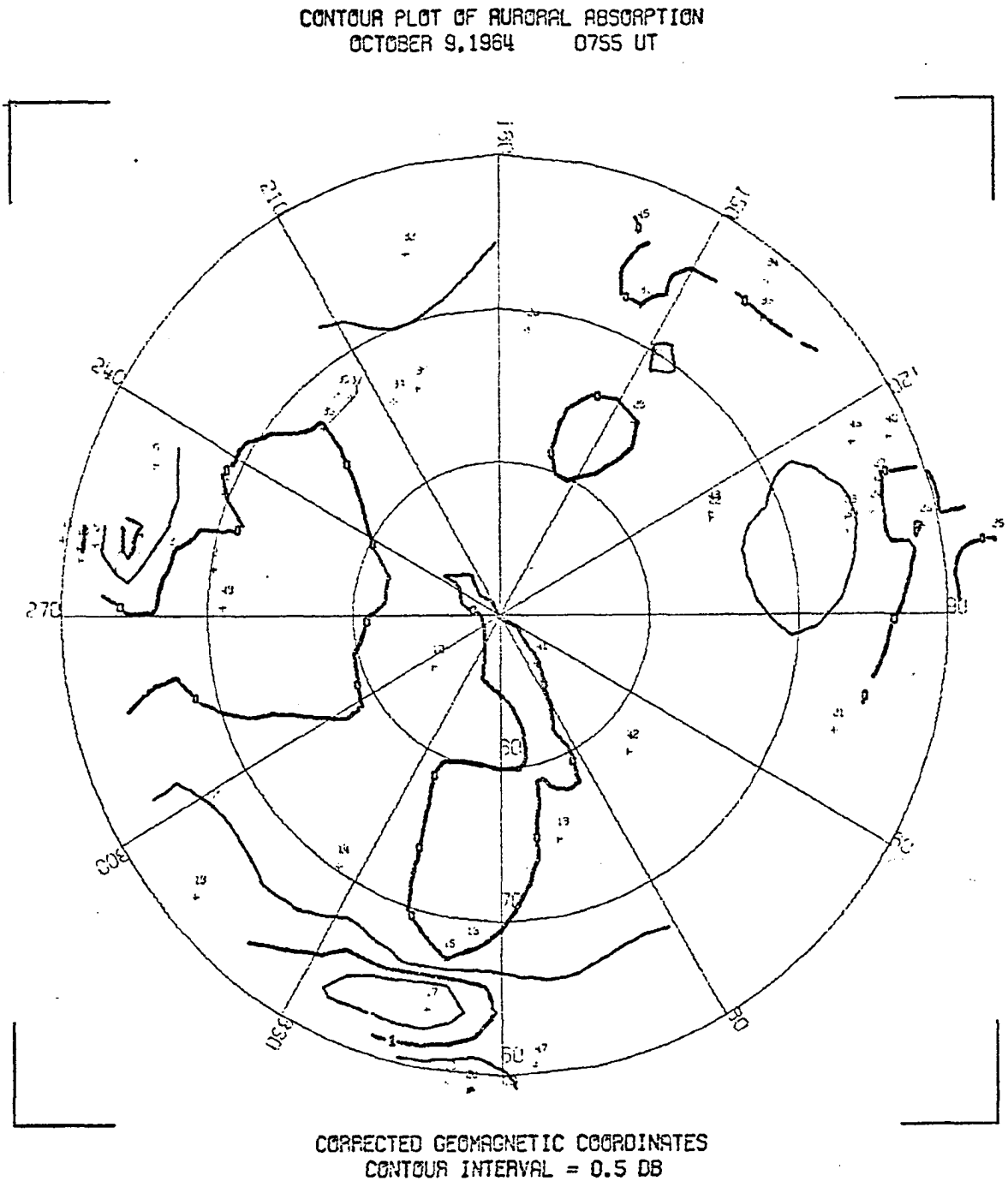

Figure (8.13) Contour map for 0755 UT on October 9, 1964.

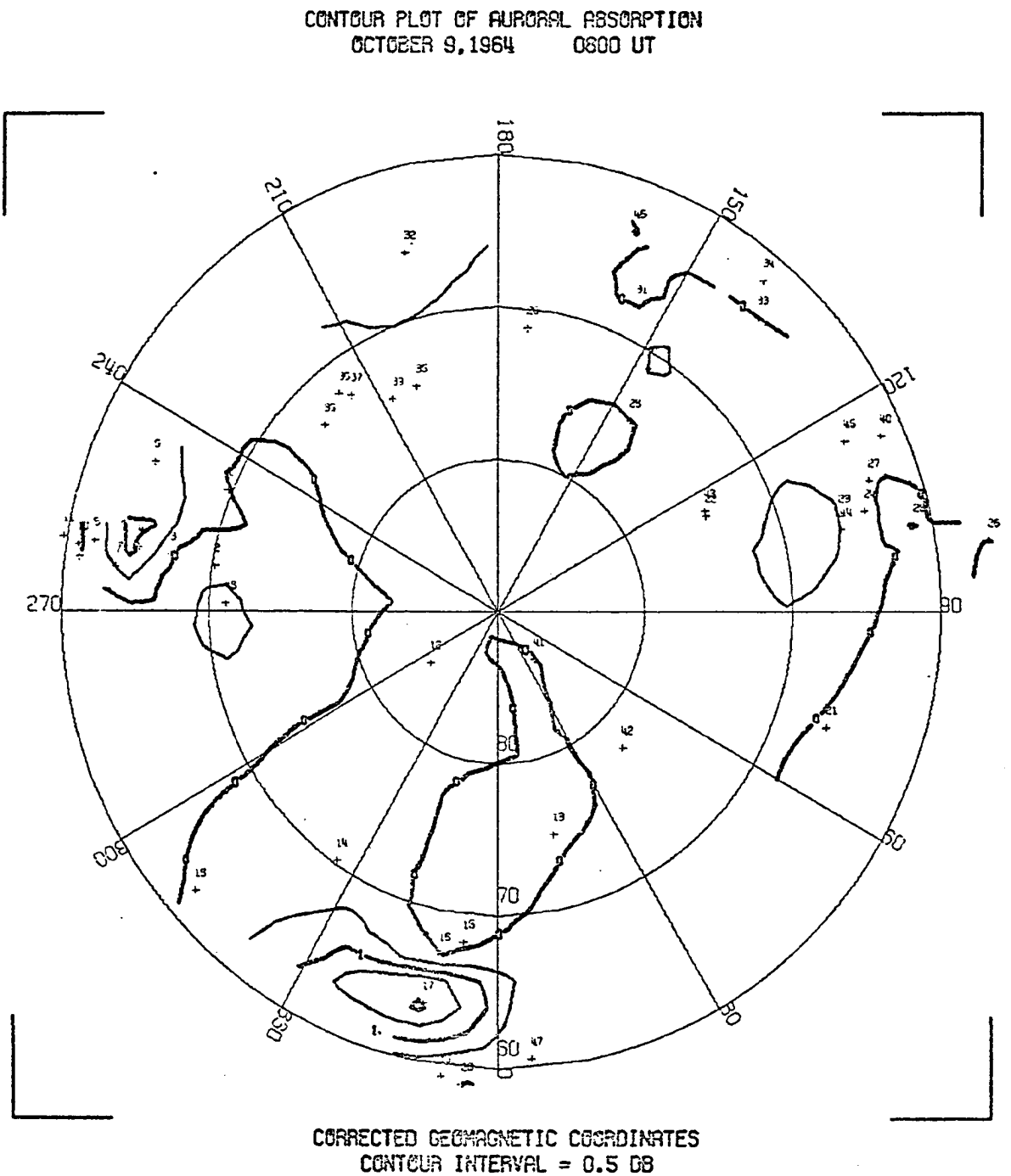

Figure (8.14) Contour map for 0800 UT on October 9, 1964.

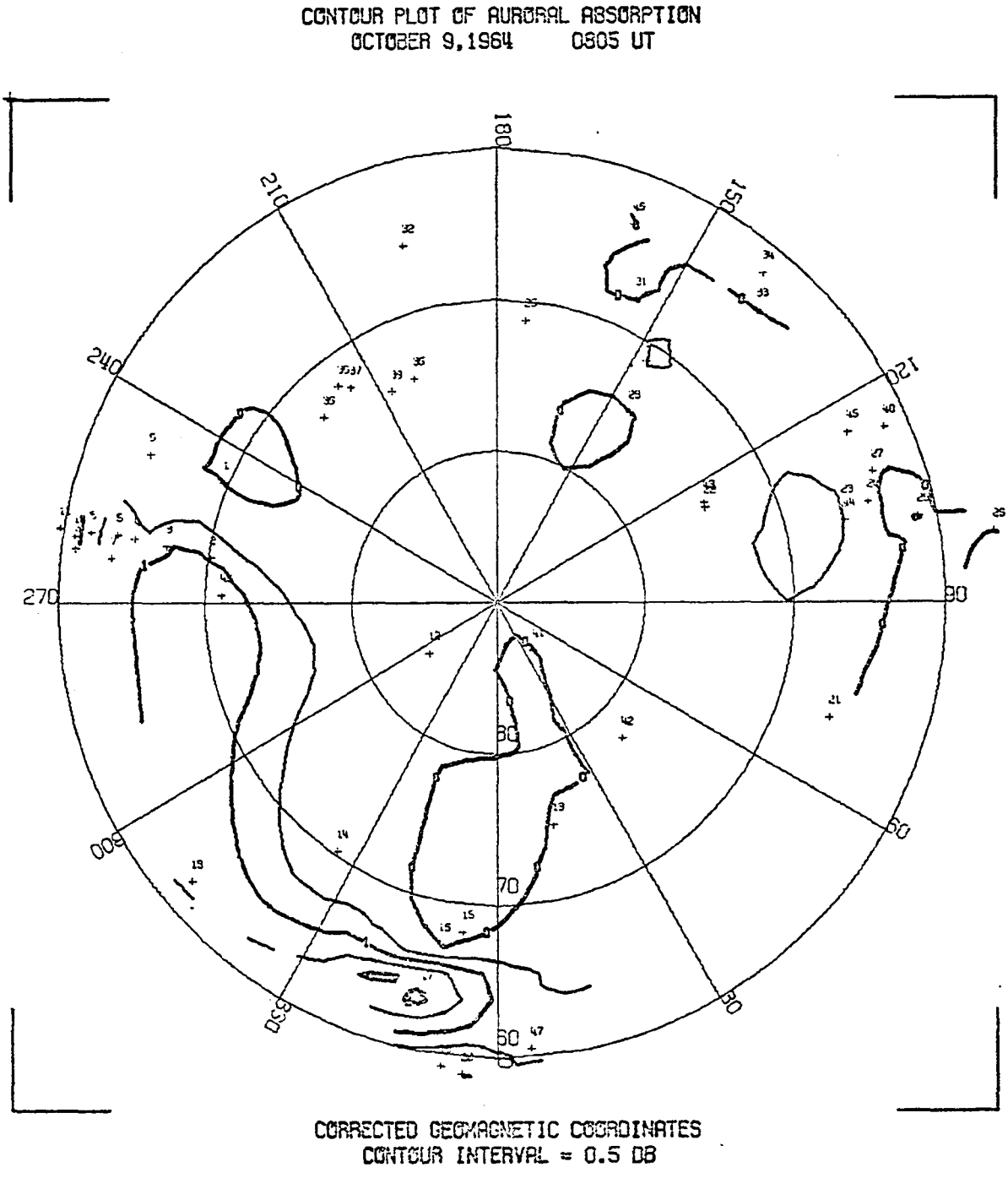

Figure (8.15) Contour map for 0805 UT on October 9, 1964.

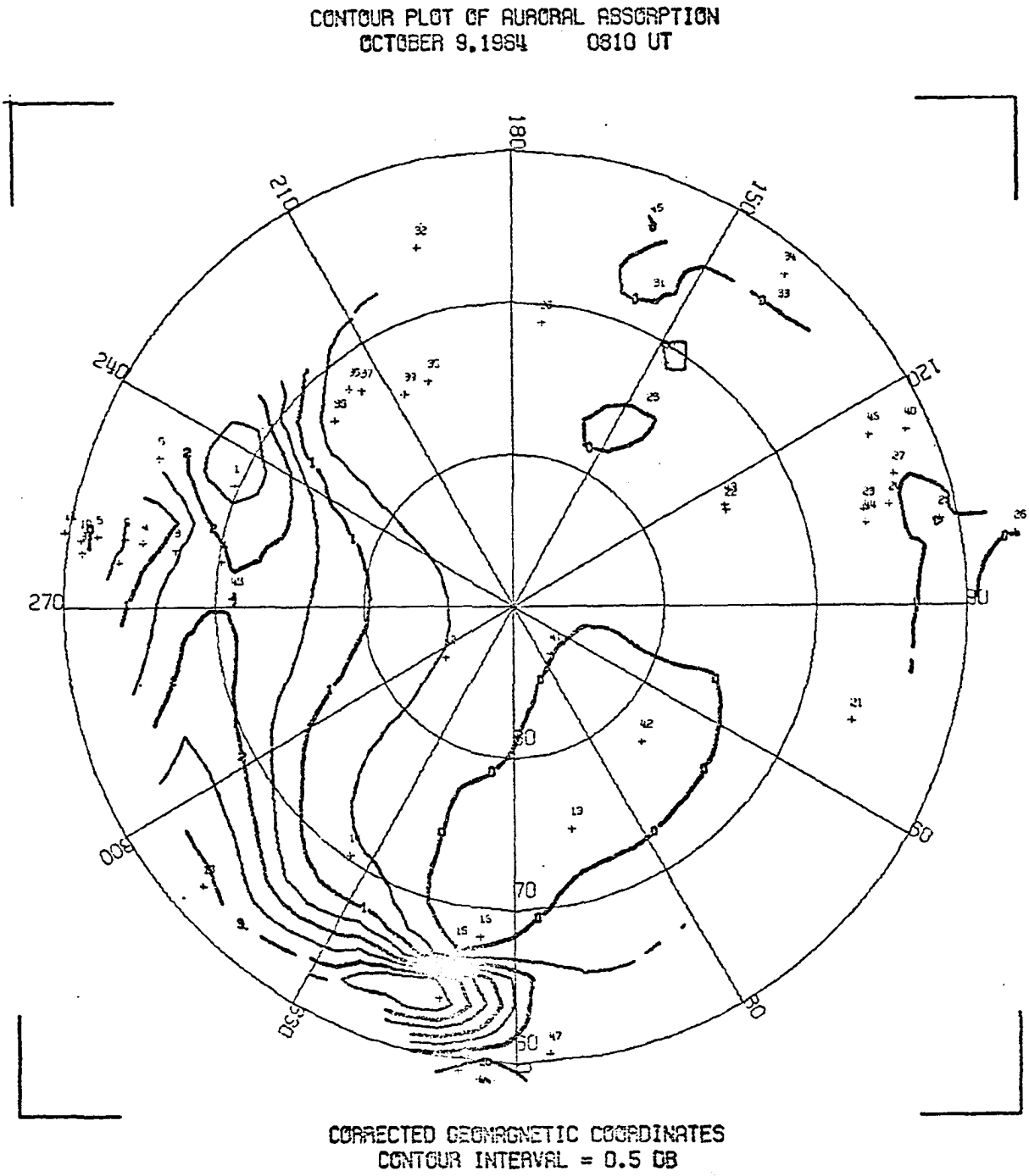

Figure (8.16) Contour map for 0810 UT on October 9, 1964.

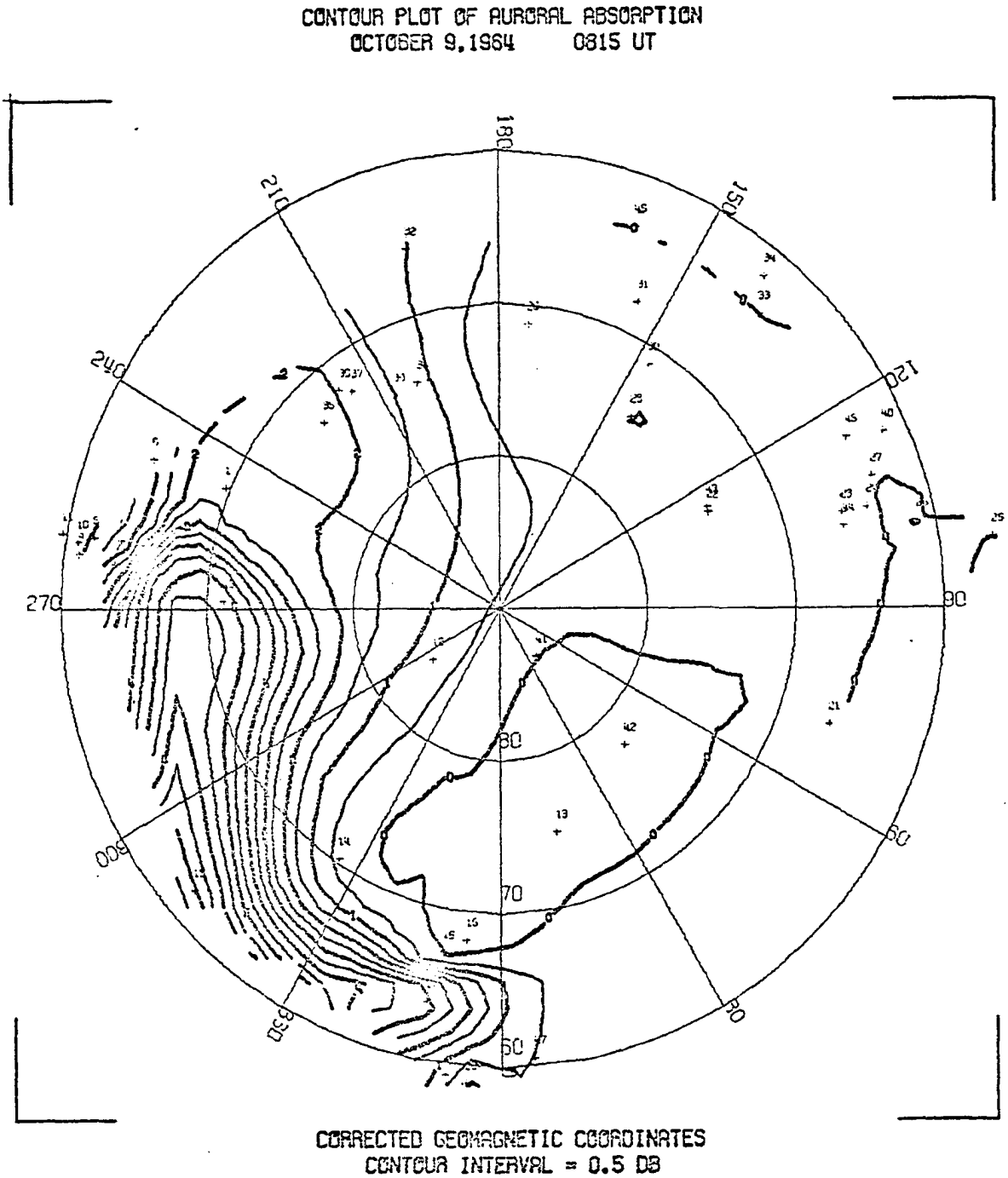

Figure (8.17) Contour map for 0815 UT on October 9, 1964.

0820 UT (Figure 8.18); five minutes later at 0825 UT (see Figure 8.19) the intense region of absorption previously centered over Prince Albert had drifted to Fort Yukon and Moosonee. Note that absorption was recorded at Val D'or (59.3°N) and Ottawa (58.4) in the morning sector, and at Anchorage (60.8°N) in the evening sector. By 0900 UT (Figure 8.20) a region in which the absorption exceeds 2 db extended from Barrow in the evening sector to Tromsø, Kiruna and Amderma in the noon sector. At Dixson Island (67.9°N, 154.7°E) maximum absorption of approximately 1 db was seen; at Cape Chelyuskin, situated at a somewhat higher latitude (71.3°), no absorption greater than 0.3 db was recorded at any time during the substorm.

Figure 8.21 illustrates the substorm development at 0905 UT; in the European sector, the absorption appeared to be growing in intensity while in the Alaskan and Canadian sectors it was decreasing. This is seen more clearly at 0920 UT (Figure 8.22) at which time more than 4 db of absorption was recorded at Tromsø, Kiruna, and Sodanklya. It should be noted that these stations are situated near the noon meridian and well equatorward of the oval. The absorption persisted near Kiruna and Tromsø until 10^h (see Figure 8.23) at 0935 UT and Figure 8.24 at 0950 UT). At 1010 UT, 3.4 db existed at Kiruna and Tromsø while 2.7 db was recorded at College and Healy, more than 150° to the east (see Figure 8.25). It is suggested that the absorption recorded in the Alaskan meridian at 1010 UT may have resulted from the gradient drift of electrons from the midnight meridian, past the noon meridian and back to the midnight sector.

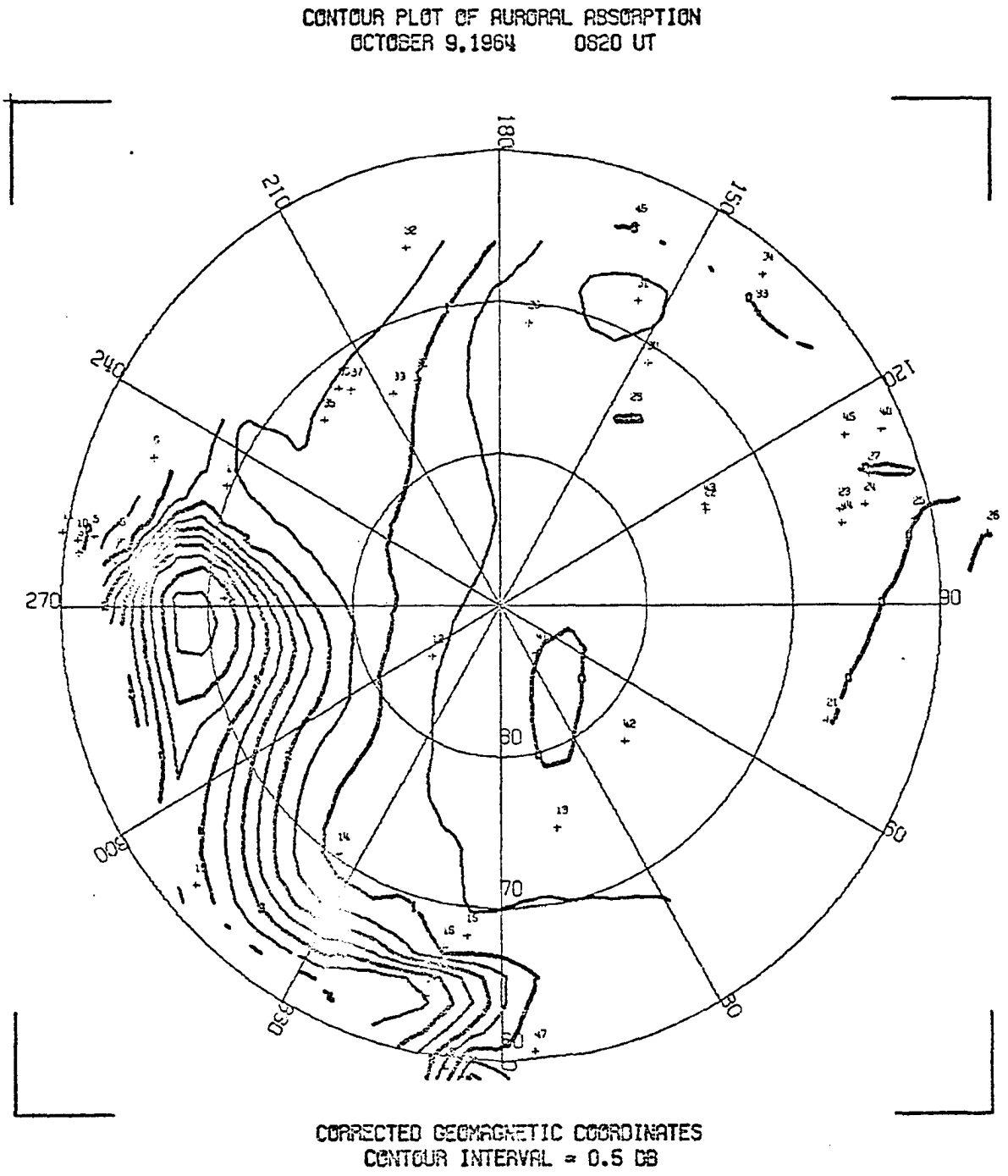

Figure (8.18) Contour map for 0820 UT on October 9, 1964.

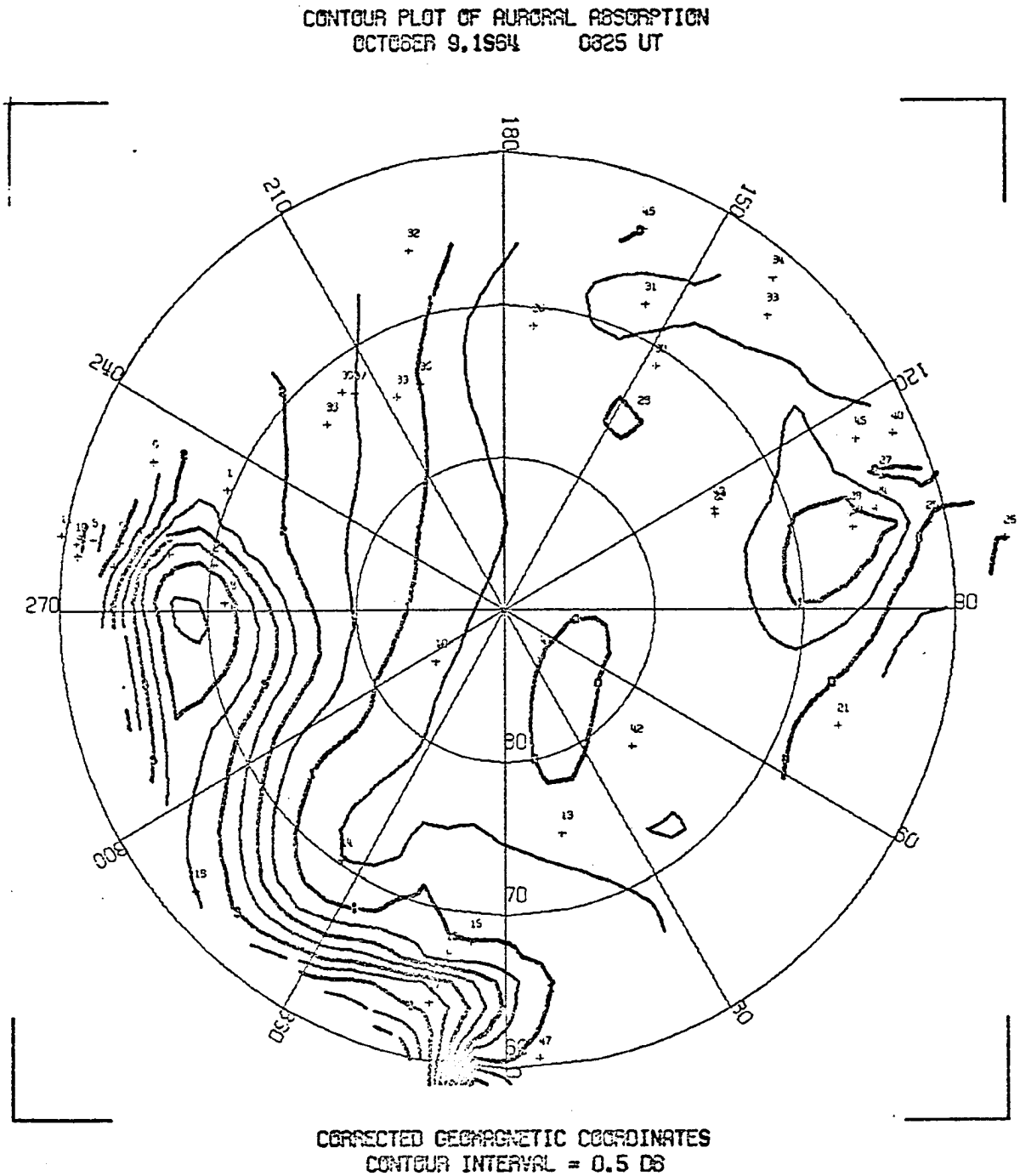

Figure (8.19) Contour map for 0825 UT on October 9, 1964.

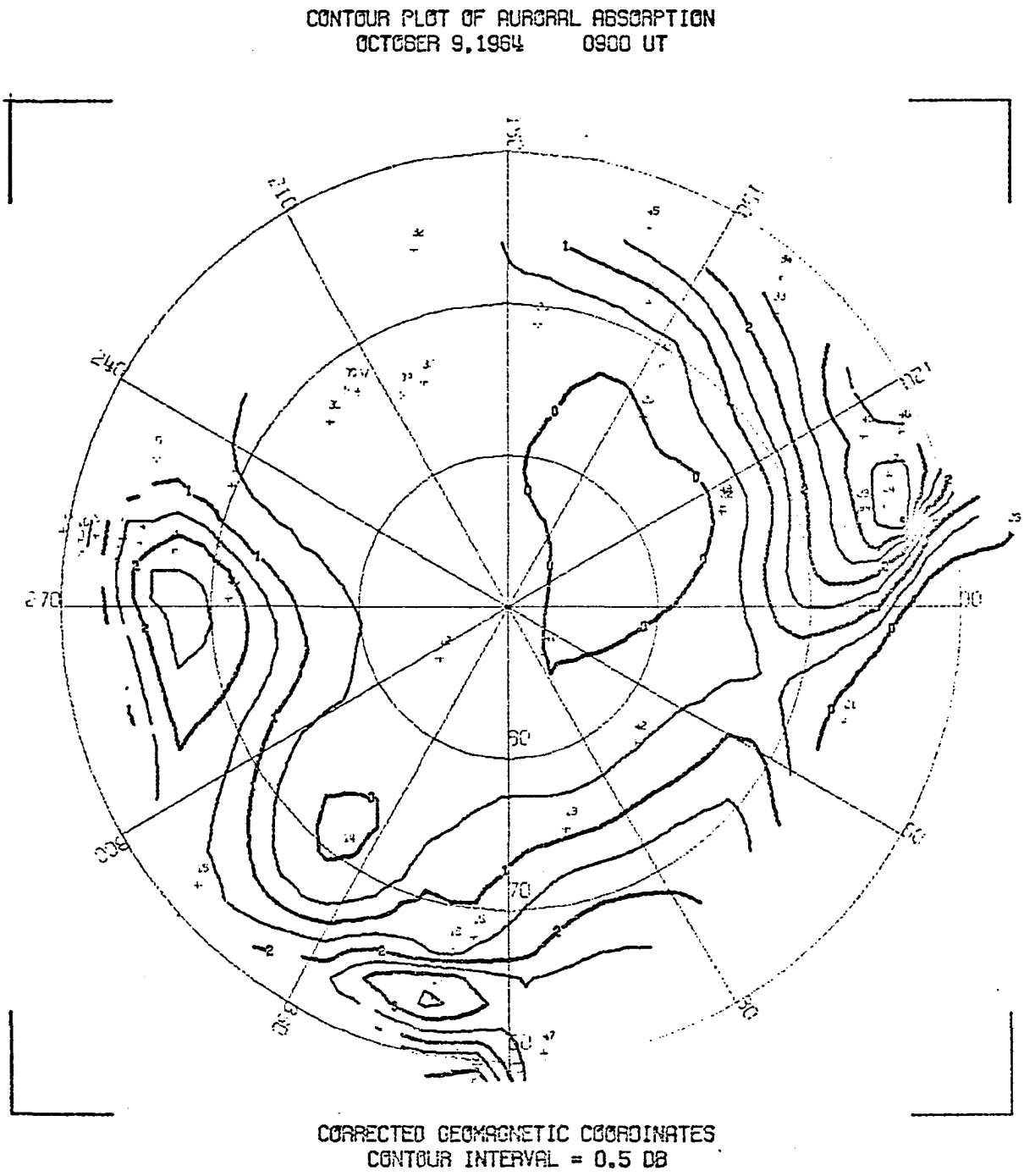

Figure (8.20) Contour map for 0900 UT on October 9, 1964.

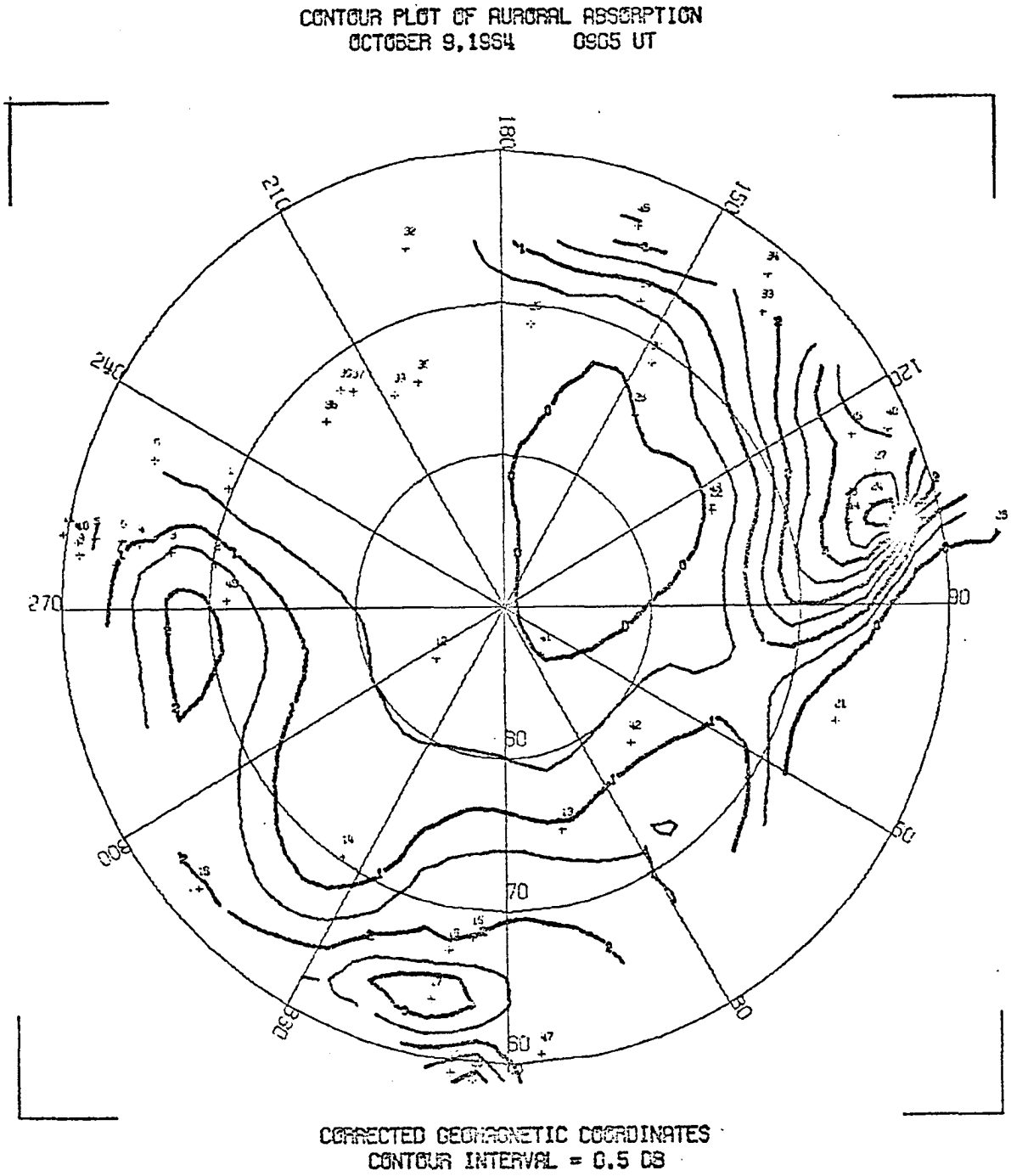

Figure (8.21) Contour map for 0905 UT on October 9, 1964.

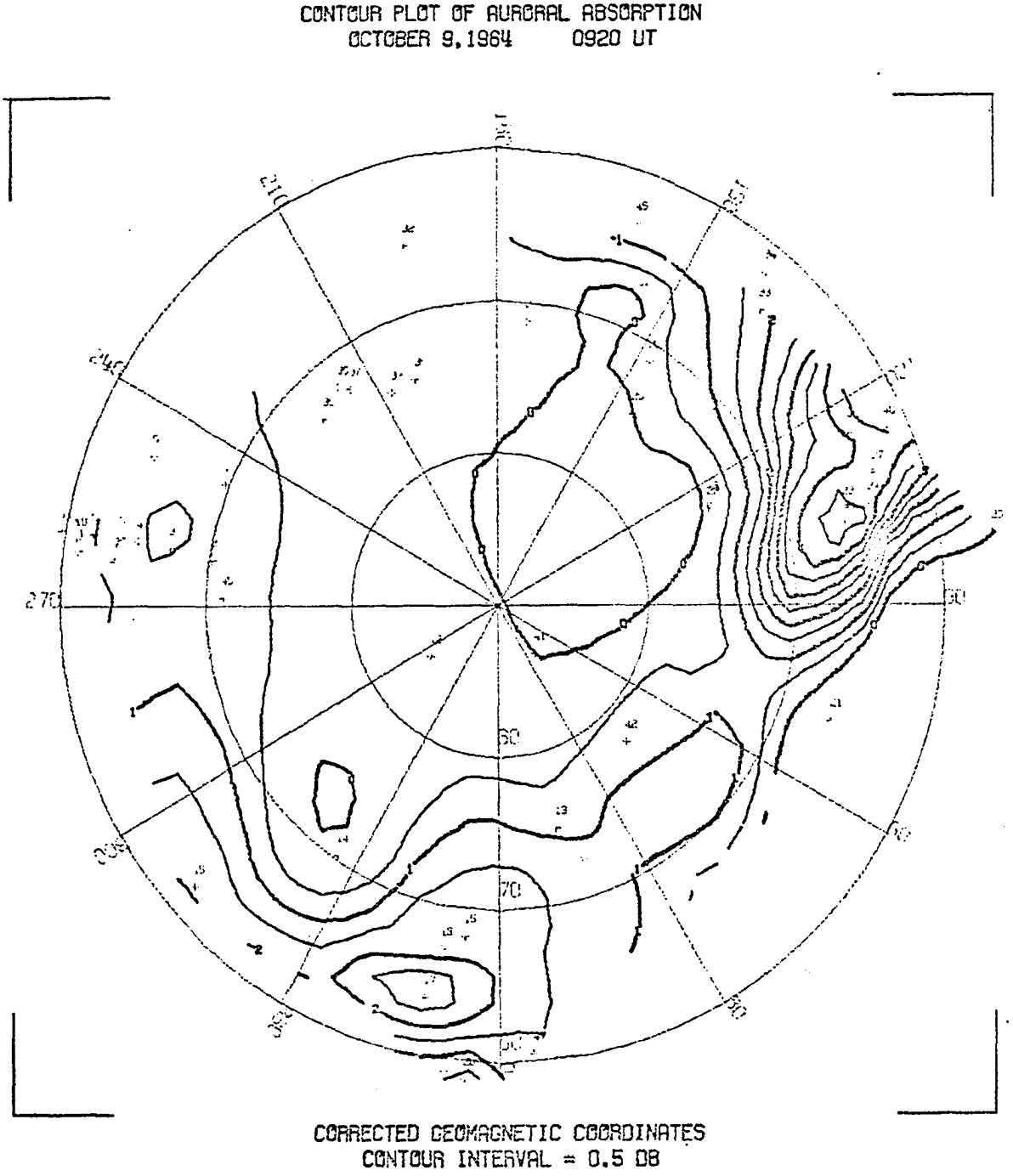

Figure (8.22) Contour map for 0920 UT on October 9, 1964.

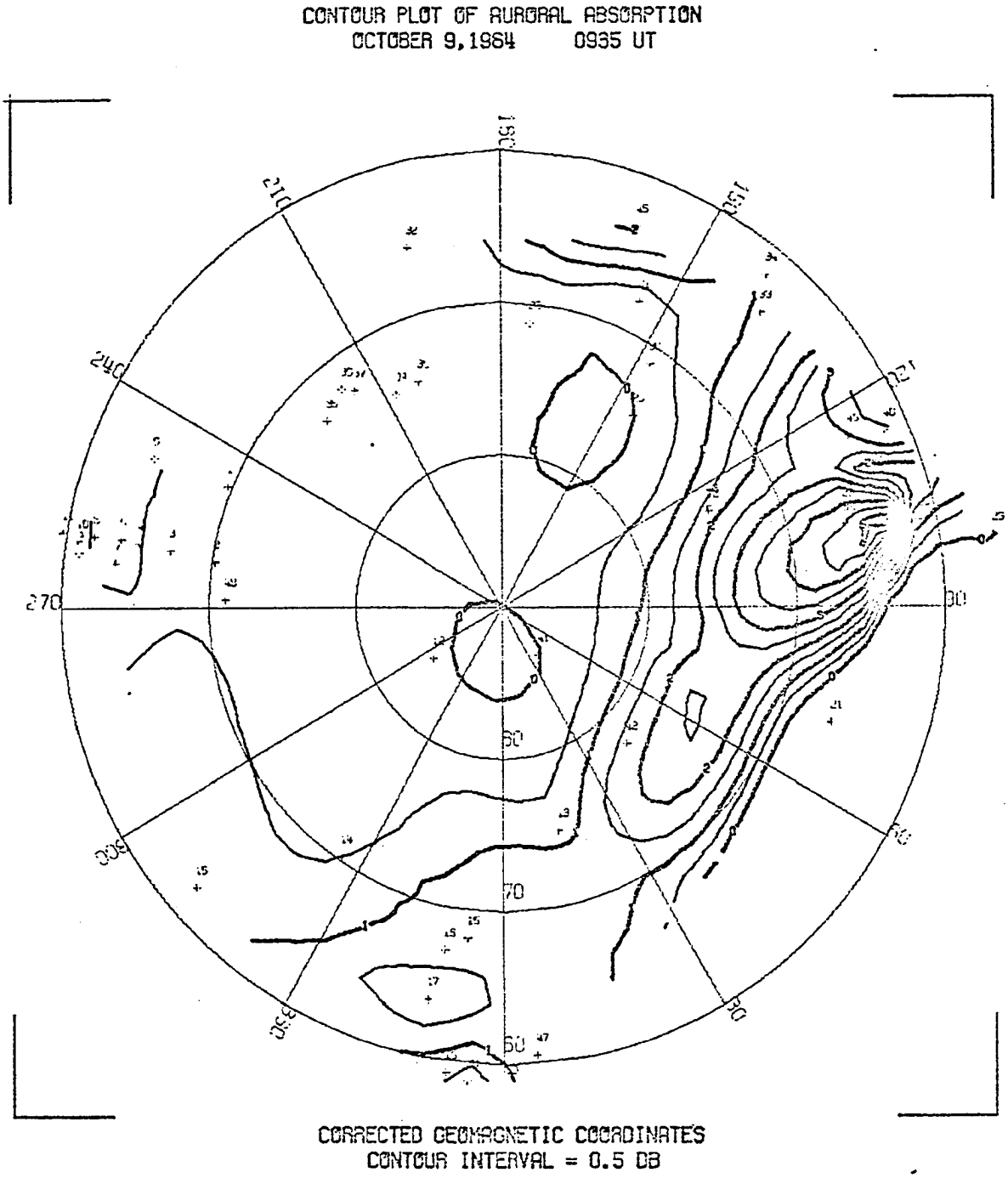

Figure (8.23) Contour map for 0935 UT on October 9, 1964.

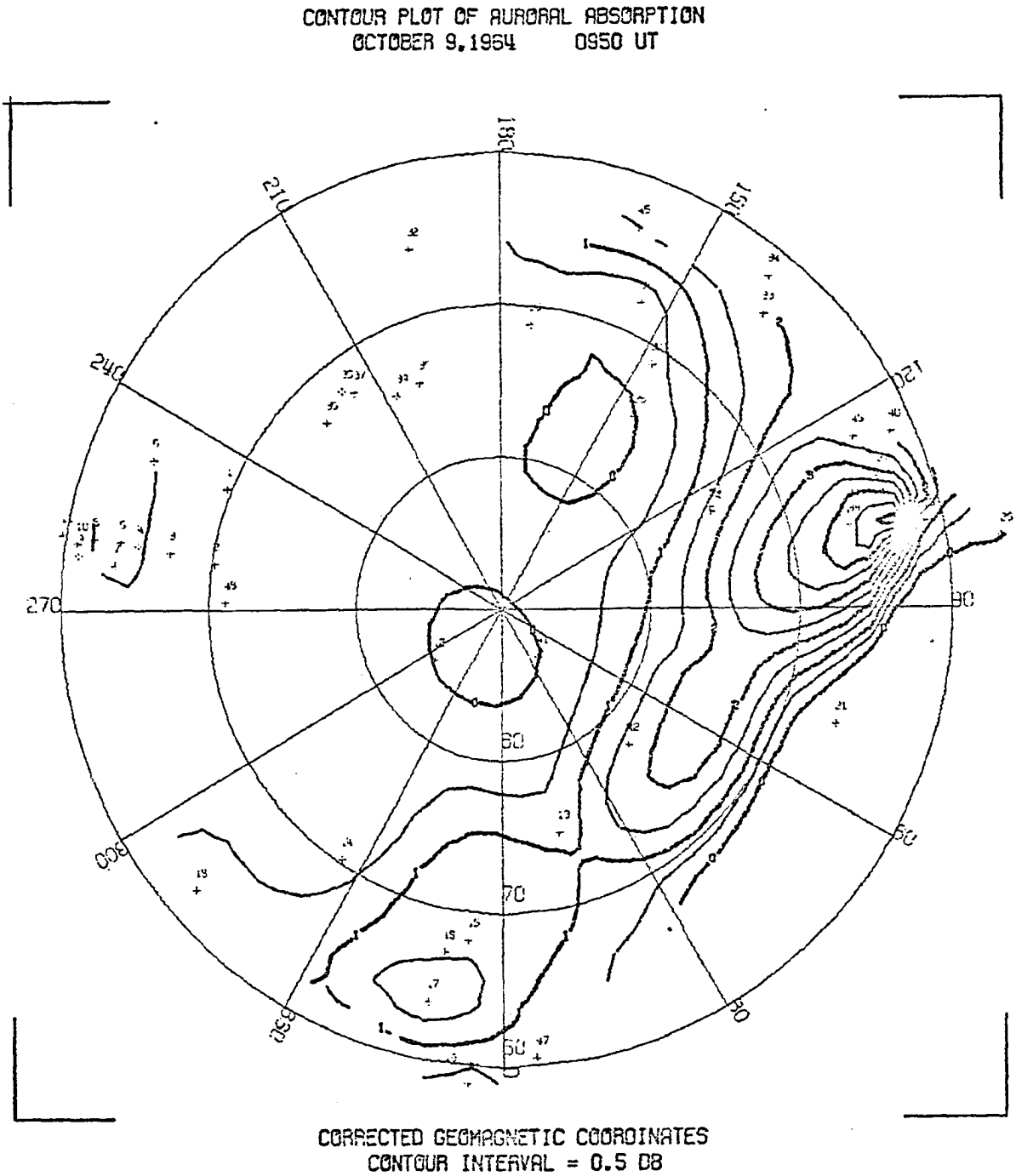

Figure (8.24) Contour map for 0950 UT on October 9, 1964.

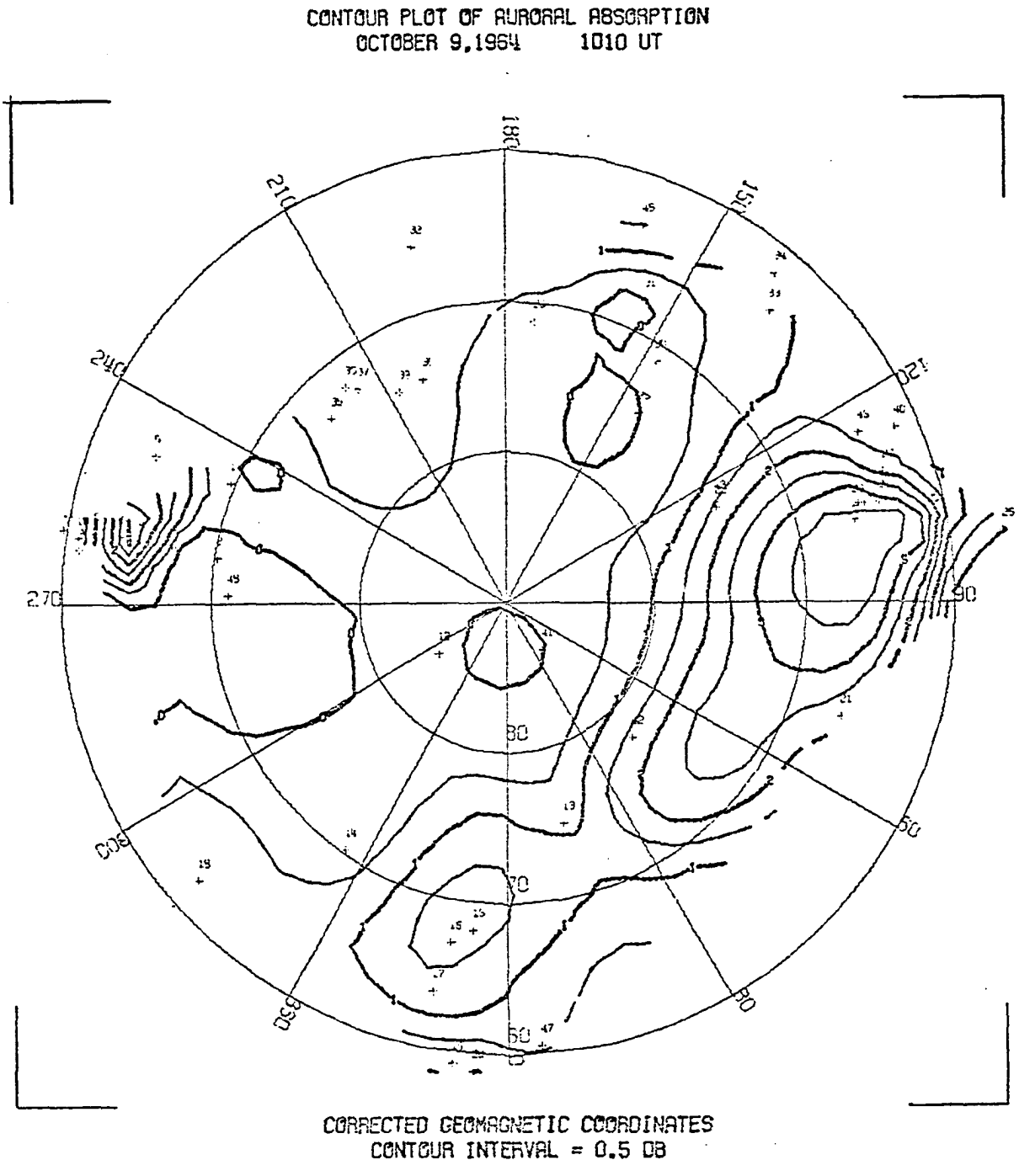

Figure (8.25) Contour map for 1010 UT on October 9, 1964.

Although the absorption seen at 1010 UT persisted until 1020 UT (Figure 8.26), the magnitude had decreased. At 1035 UT (Figure 8.27) 2.6 db was recorded at Prince Albert, 50° east of the College meridian. Although the event seen at College and Healy at 1010 UT could be interpreted as the onset of a second substorm, there is no evidence of a poleward expansion in the Fort Yukon riometer record. Note also that the time delay between maximum absorption at College and Prince Albert was considerably longer than it was for the November 7 event (25 minutes versus 10-15 minutes).

A significant feature of this substorm is the absorption associated with the westward traveling surge; associated absorption events were observed at Fort Yukon at 0803 UT, Point Barrow at 0807 UT and at NP-13 at 0817 UT. The westward expansion of the absorbing region is well defined on the maps in Figures 8.16, 8.17, and 8.18 covering the period 0810-0820 UT; at 0810 UT 2.5 db of absorption was observed at Point Barrow; at 0815 UT >2 db was recorded at NP-13. At 0820 UT, maximum absorption of 1.75 db occurred at Tixie Bay. Except for Tixie each of these stations is located within the auroral oval at 08^h UT. At College only a small event was observed; at this time College lies just equatorward of the auroral oval and it is assumed that the westward traveling surge propagated along the oval and therefore poleward of College. It should also be noted that no absorption was observed at Kotzebue (64.4°N, 247.5°E) which also lies outside the auroral oval. The fact that a negative bay was recorded in the H-component of the College magnetogram between 08^h and 12^h UT is attributed to the larger "field of view" of

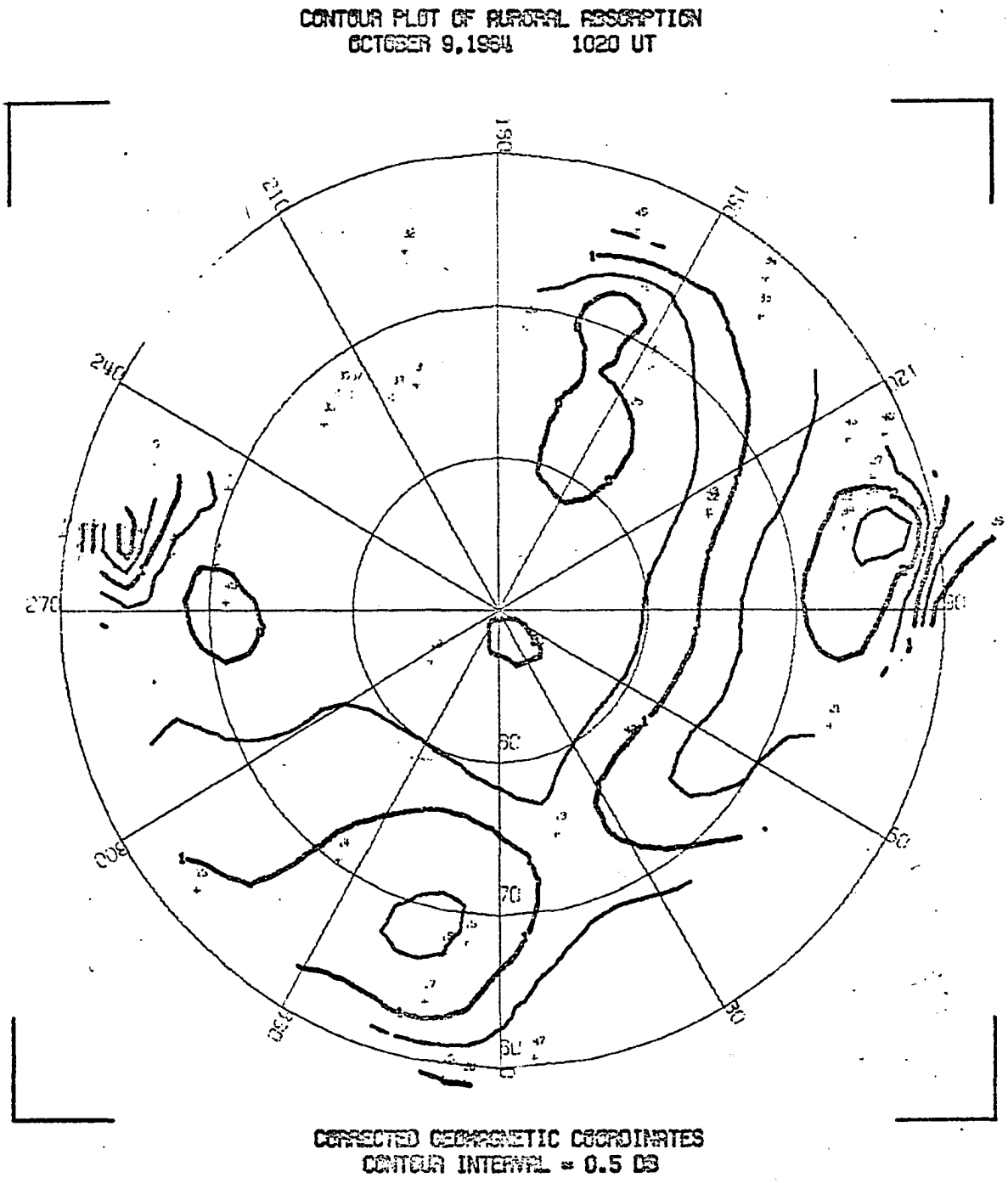

Figure (8.26) Contour map for 1020 UT on October 9, 1964.

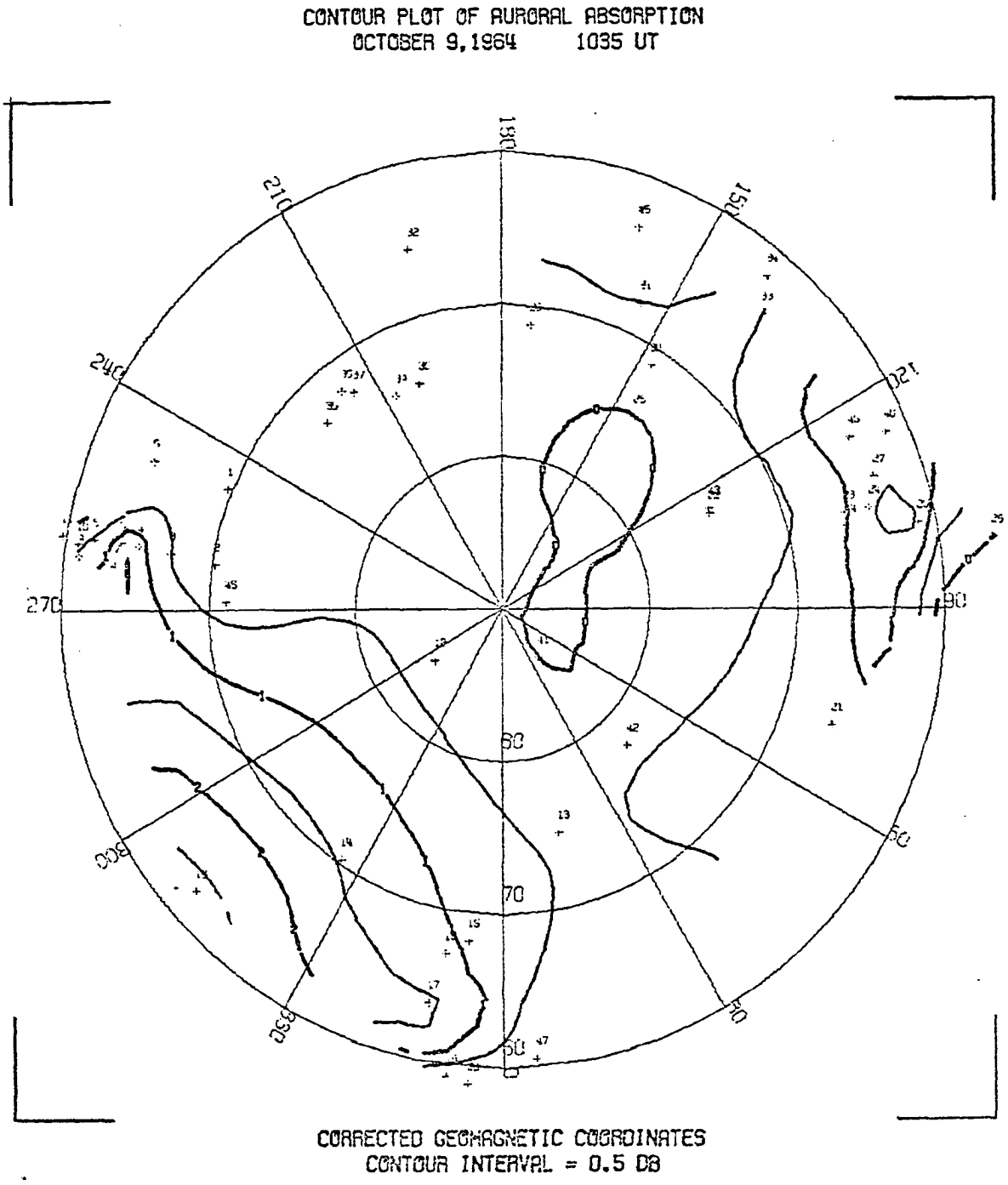

Figure (8.27) Contour map for 1035 UT on October 9, 1964.

the magnetometer. In fact, a positive excursion of the H-component, superimposed on the negative bay, was observed at approximately the same time the surge was assumed to have propagated over Fort Yukon.

During the period of the substorm, absorption was recorded at Isfjord, located within the auroral oval at 08^h UT, but since the absorption began at approximately 05^h UT it is assumed not to be associated with the substorm. No absorption was observed at Heiss Island (74.6°N, 144.3°E) farther to the east, also within the auroral oval. At lower latitudes, absorption was recorded at Ottawa (58.9°N) in the morning sector, at Anchorage (60.8°N) in the evening sector and at Lycksele (61.2°N) in the noon sector. At Uppsala (56.4°N), also located near the noon meridian, no absorption was noted.

Approximately 25 minutes after the onset of the substorm, the absorbing region had drifted eastward to the European sector; the increasing eastward drift of the absorbing region was evidenced by absorption onsets at Amderma (0820) and Norilsk (0825). In the same sector, but at a somehwat higher latitude at Cape Zhelania (71.1°N, 147.5°E), no absorption which could be attributed to the substorm was observed. At Tixie Bay (65.6°N, 195.2°E), absorption was observed prior to 08^h UT with maximum absorption occurring at approximately 0820 UT. The maximum absorption coincides in time with the expansion of the precipitation region along the auroral oval to the Tixie Bay longitude; it should also be noted that the region of most intense absorption on the dayside (06^h-18^h) was located at the noon meridian. Another interesting feature of this substorm is that absorption was recorded prior to the

onset at Isfjord and Cape Zhelania. Both of these stations are located north of 70° corrected geomagnetic latitude.

8.4 The Substorm of March 26, 1965

The level of activity associated with the polar substorm which commenced at approximately 08^h UT on March 26, 1965 was very similar to that of the substorm of October 9, 1964; the Kp index between 06^h and 09^h UT was 4- and during the interval $09-12^h$ UT, 2+. The onset of the polar magnetic substorm was first observed at Meanook where a negative (~225γ) bay was observed at 0750 UT. At College and Sitka, positive bays were observed commencing at 0754 UT. At Churchill, Great Whale River, and Baker Lake, negative excursions of the H-component were observed from 0811 to 0820 UT. At Barrow and NP-13, located in the evening sector, negative bay onsets occurred at 0754 and 0822 UT, respectively, with maxima observed at 0821 and 0830 UT. In the late afternoon and noon sectors, no significant activity was noted (see Figure 8.28).

All-sky camera datawere available only from Bar-1, although no riometer was operating there at the time. At 0803 UT, corresponding in time to the increase in absorption at Fort Yukon, a WTS was initially observed. The film was saturated during the next several minutes, until the WTS had propagated out of the field of view.

As in the previous example, the onset of the auroral absorption substorm was not well defined at any of the 30 stations used in this analysis. Significant (>1db) absorption was first noted at Prince Albert at 0757 UT and at Fort Yukon at 0803 UT; it is assumed that the

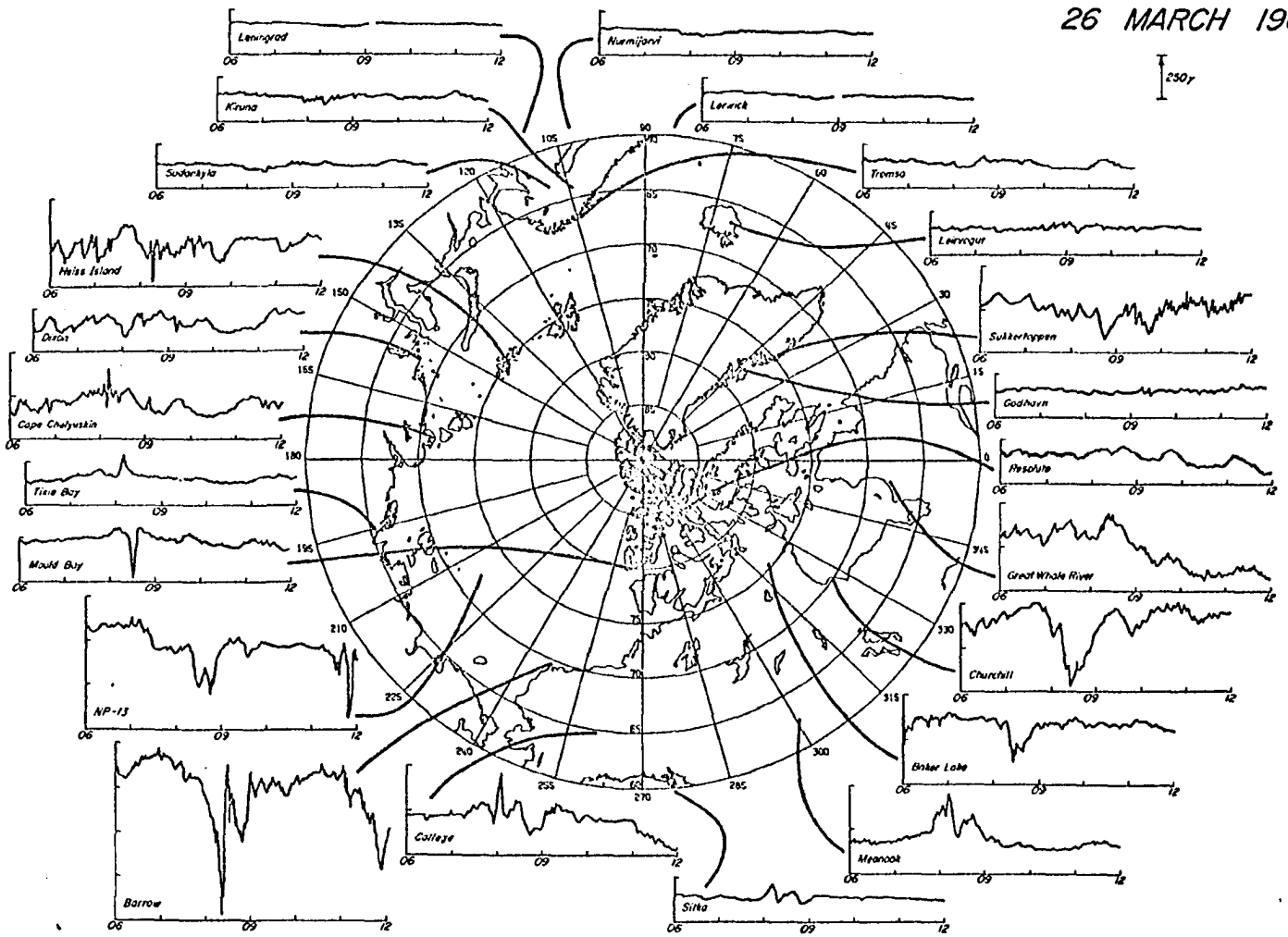

Figure (8.28) A collection of magnetic records (H or X component) from magnetic observatories in the Northern Hemisphere on March 26, 1965.

absorption substorm originated near the midnight meridian (i.e. east of College) between 0750 and 0755 UT. At 0755 UT (Figure 8.29) no absorption greater than 0.5 db was observed anywhere over the polar regions; by 0805 UT (Figure 8.30) the absorbing region extended to Cape Jones in the morning sector and to Fort Yukon and College in the evening sector. Five minutes later at 0810 UT (Figure 8.31) the magnitude had decreased in the Alaska sector and increased somewhat in the Canadian sector. Due to a lack of observatories east of the Canadian chain, the eastward drift could not be readily followed. At 0815 UT (Figure 8.32) the intensity of the substorm began to increase again, as evidenced by increased absorption over Canada and Alaska; at 0820 UT absorption exceeding 2 db was recorded at both Tromsø and Point Barrow (Figure 8.33). Absorption in the Canadian sector was greater than 1 db only at Moosonee. At 0830 UT (Figure 8.34) absorption was recorded at Amderma (2.0 db) and appeared to be growing in intensity at Tromsø. In the Canadian sector, more than 1 db was observed at Cape Jones, Prince Albert, Moosonee, and Great Whale River while less than 0.5 db was seen in the Alaskan sector. While it is not well defined on the map, an absorption onset was observed at NP-13 (72.6°N, 215.4°E) at this time. Approximately 30 minutes after the onset of the substorm (0850 UT), absorption was recorded at Norilsk (63.4°N, 159.5°E) in central Siberia (see Figure 8.35). Absorption on the order of 1 db was observed in Canada and Alaska while at the same time the magnitude of absorption was increasing in the noon sector. By 0900 UT (Figure 8.36) the intensity of the absorption had decreased over Alaska

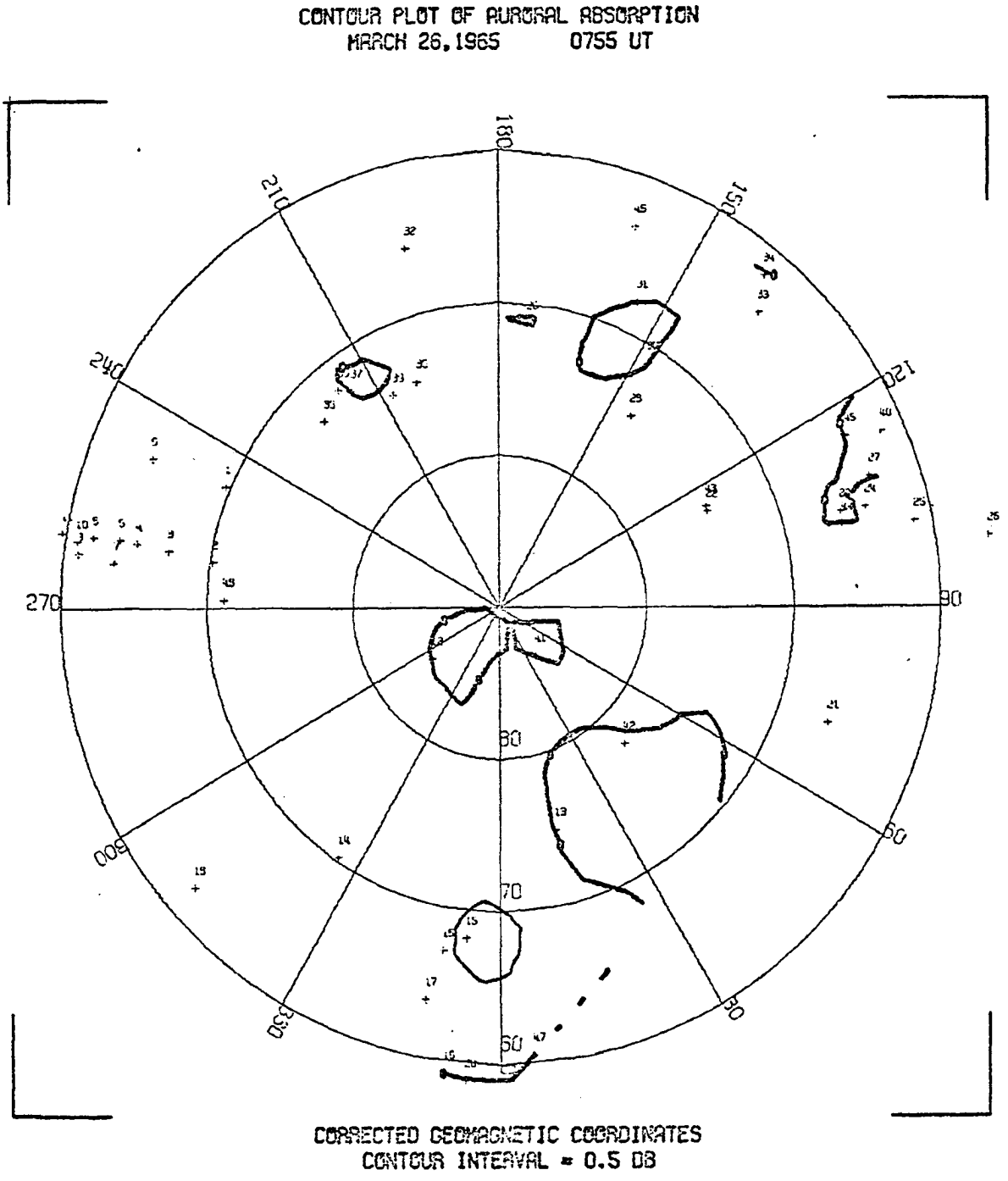

Figure (8.29) Contour map for 0755 UT on March 26, 1965.

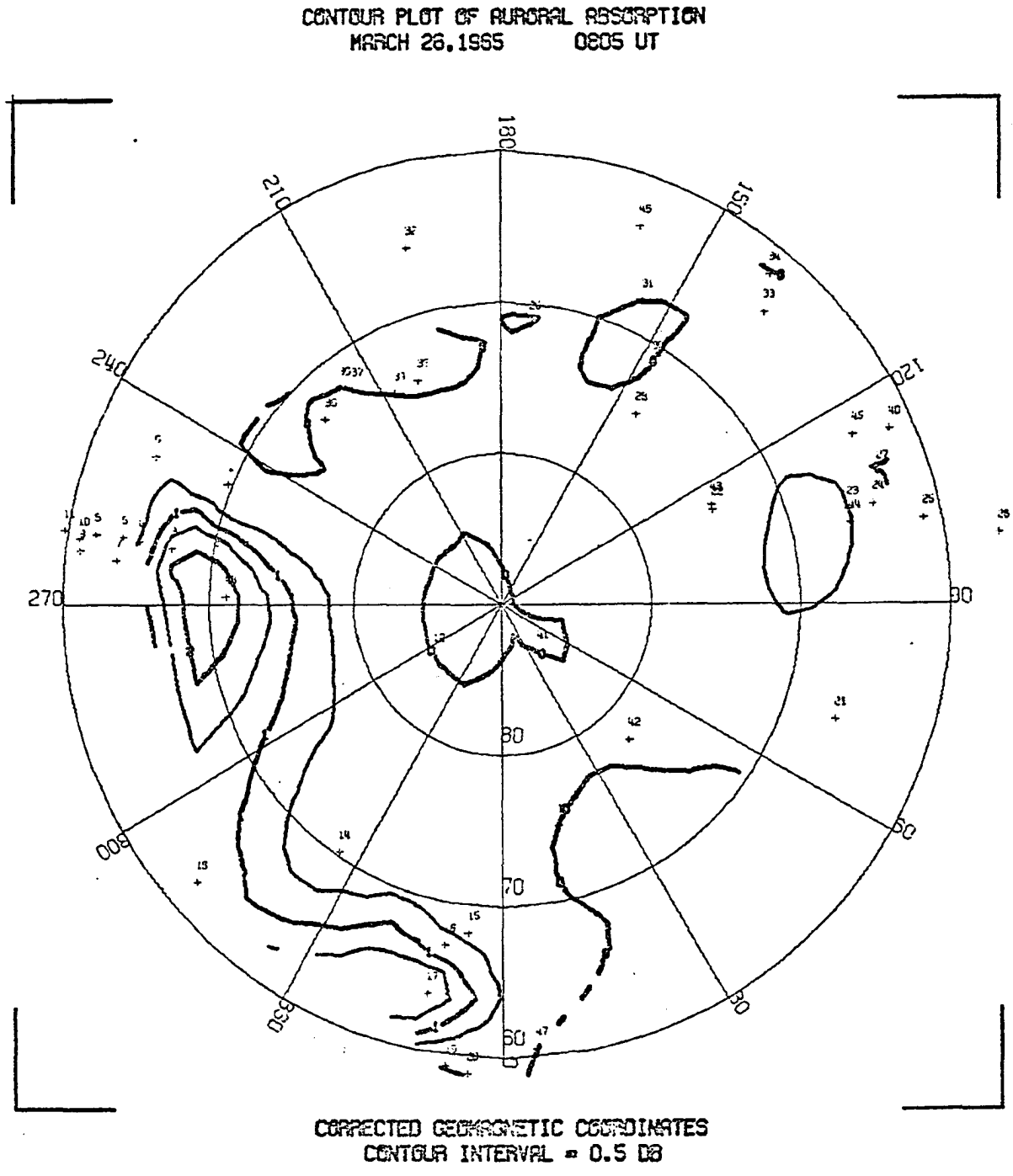

Figure (8.30) Contour map for 0805 UT on March 26, 1965.

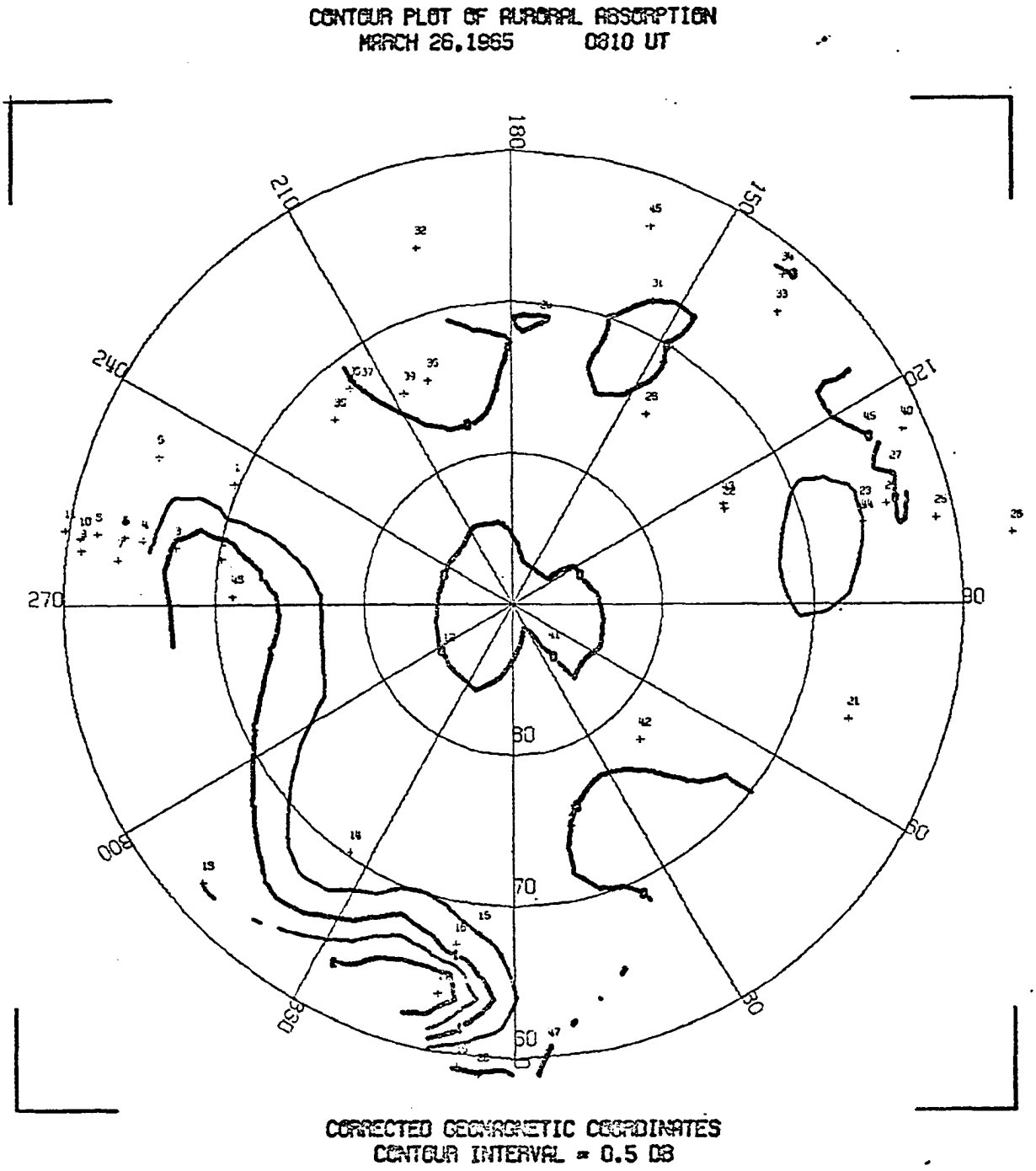

Figure (8.31) Contour map for 0810 UT on March 26, 1965.

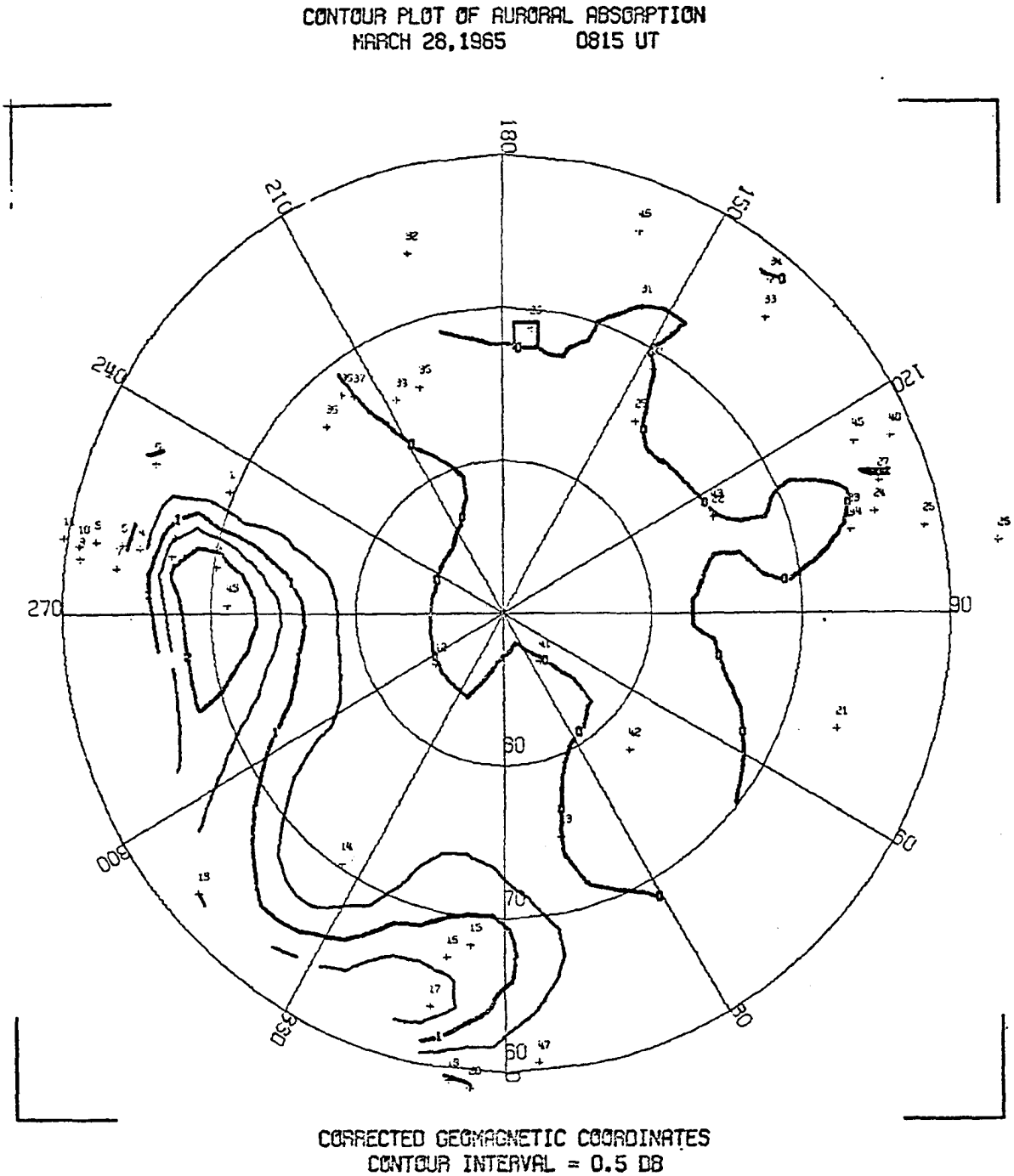

Figure (8.32) Contour map for 0815 UT on March 26, 1965.

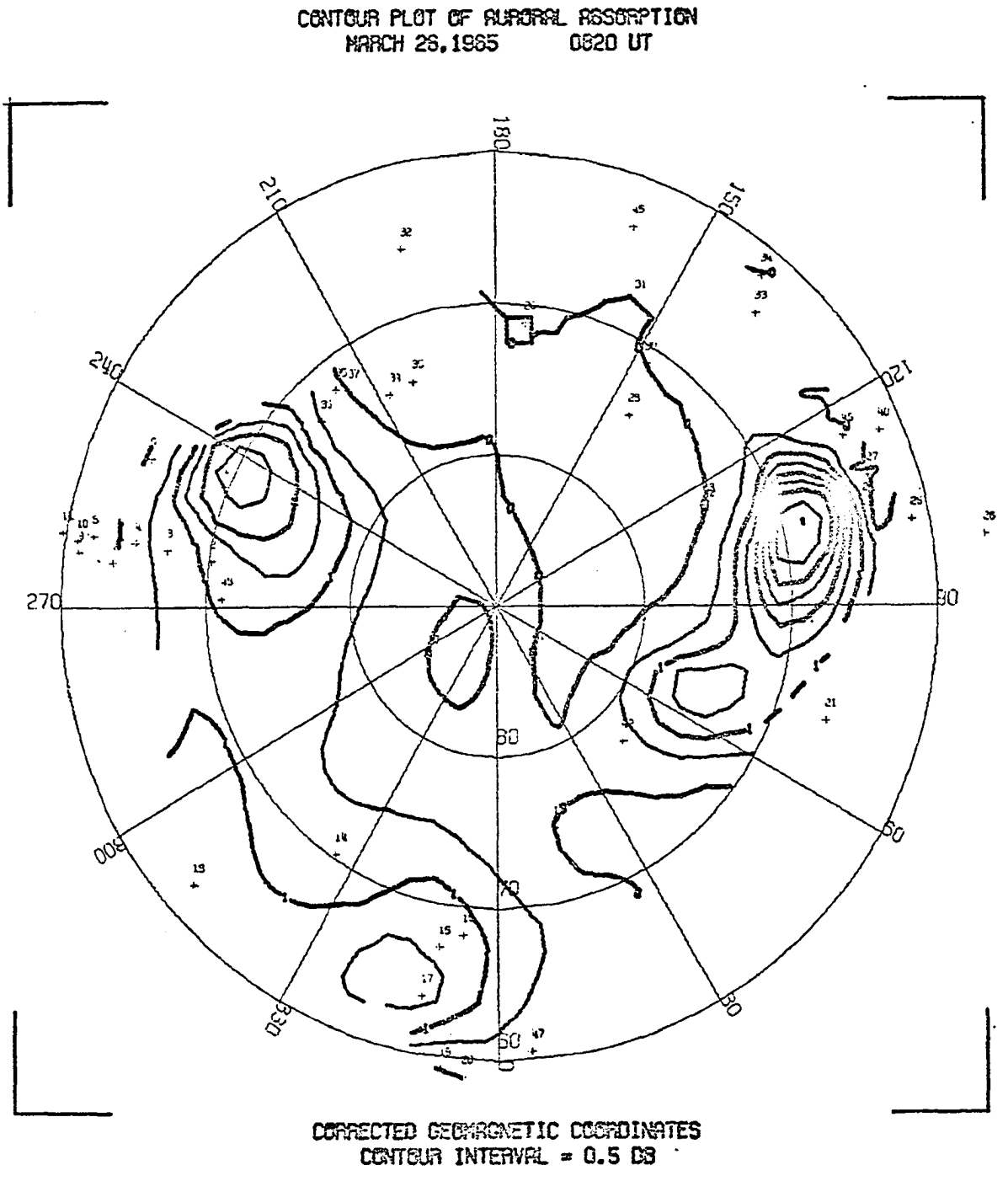

Figure (8.33) Contour map for 0820 UT on March 26, 1965.

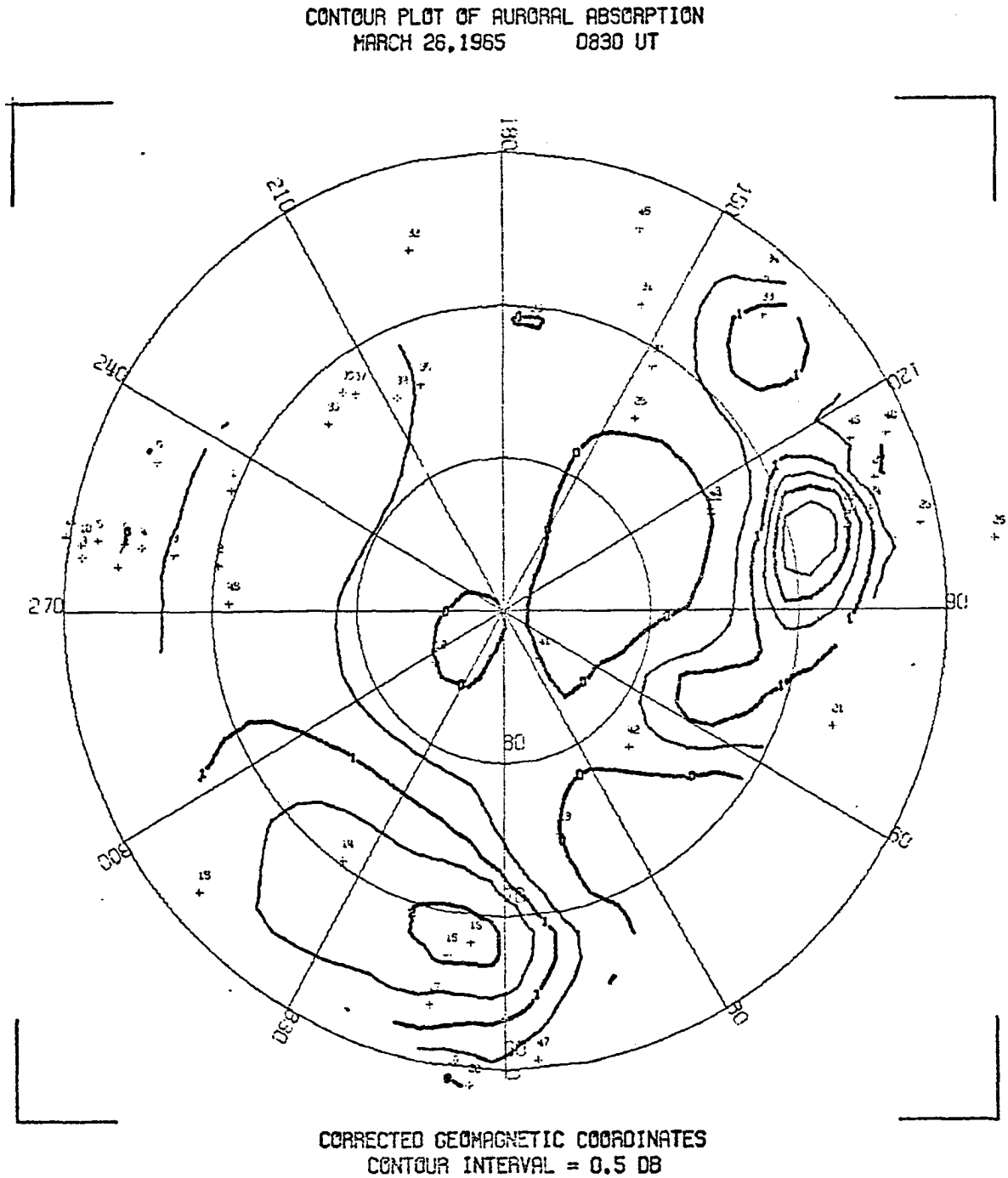

Figure (8.34) Contour map for 0830 UT on March 26, 1965.

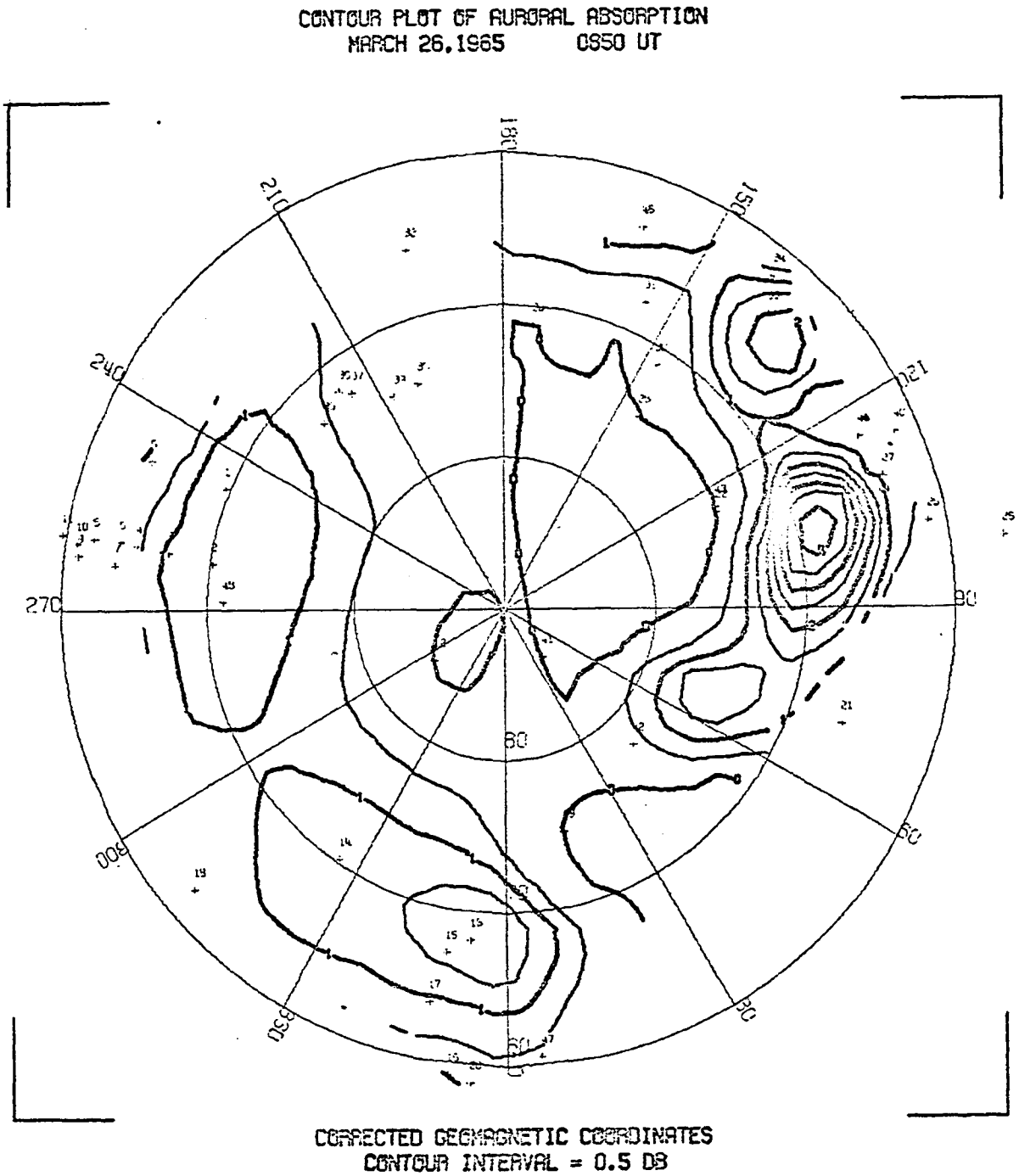

Figure (8.35) Contour map for 0350 UT on March 26, 1965.

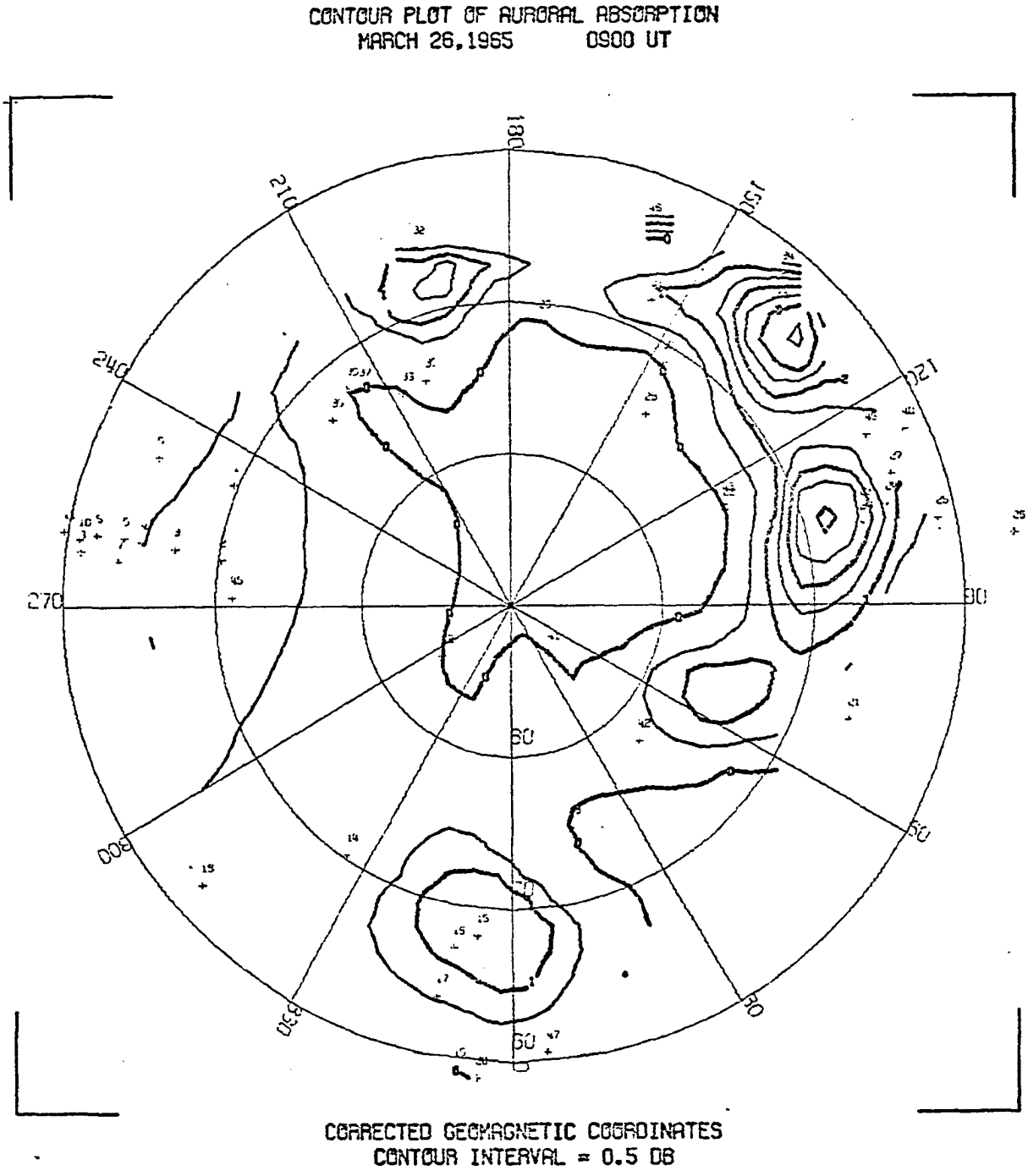

Figure (8.36) Contour map for 0900 UT on March 26, 1965.

(<1.0 db), while increasing at the noon meridian. At Amderma more than 3.0 db was recorded while absorption at Dixson reached nearly 1.0 db. In the afternoon sector, a maximum (1.35 db) was reached at Tixie. The pattern had changed very little by 0910 (Figure 8.37) UT although the maximum absorption occurred near Tromsø. Fifteen minutes later at 0925 UT (Figure 8.38), the intensity of absorption had decreased in all sectors, and by 0950 UT (Figure 8.39) absorption greater than 1 db occurred only at Amderma and Norilsk, located in the noon sector. At 1000 UT (see Figure 8.40), absorption began to increase at Isfjord and by 1015 UT had reached a maximum of 2.1 db while at the same time more than 1 db was recorded at Sodankiya, Dixson, Amderma, Norilsk, and Loparskaya (Figure 8.41). It is interesting to note that Isfjord is located within the auroral oval at this time. At Cape Zhelania, just equatorward of the oval, absorption maximized at 0915.

During this substorm absorption occurred at several high latitude stations: NP-13 (72.6°N) in the evening sector; Isfjord (74.6°N) in the noon sector; Cape Zhelania in the afternoon sector; and at Frobisher Bay (74.9°N) in the morning sector. However, no absorption was recorded at Cape Chelyuskin (71.3°N), Resolute Bay (84.3°N) or at Thule (86.0°N). At lower latitudes no absorption greater than 0.5 db was observed at Val D'or or Ottawa in the morning sector. However in the noon sector, nearly 1 db was recorded at Salekhard (61.8°N) and Lycksele (61.2°N).

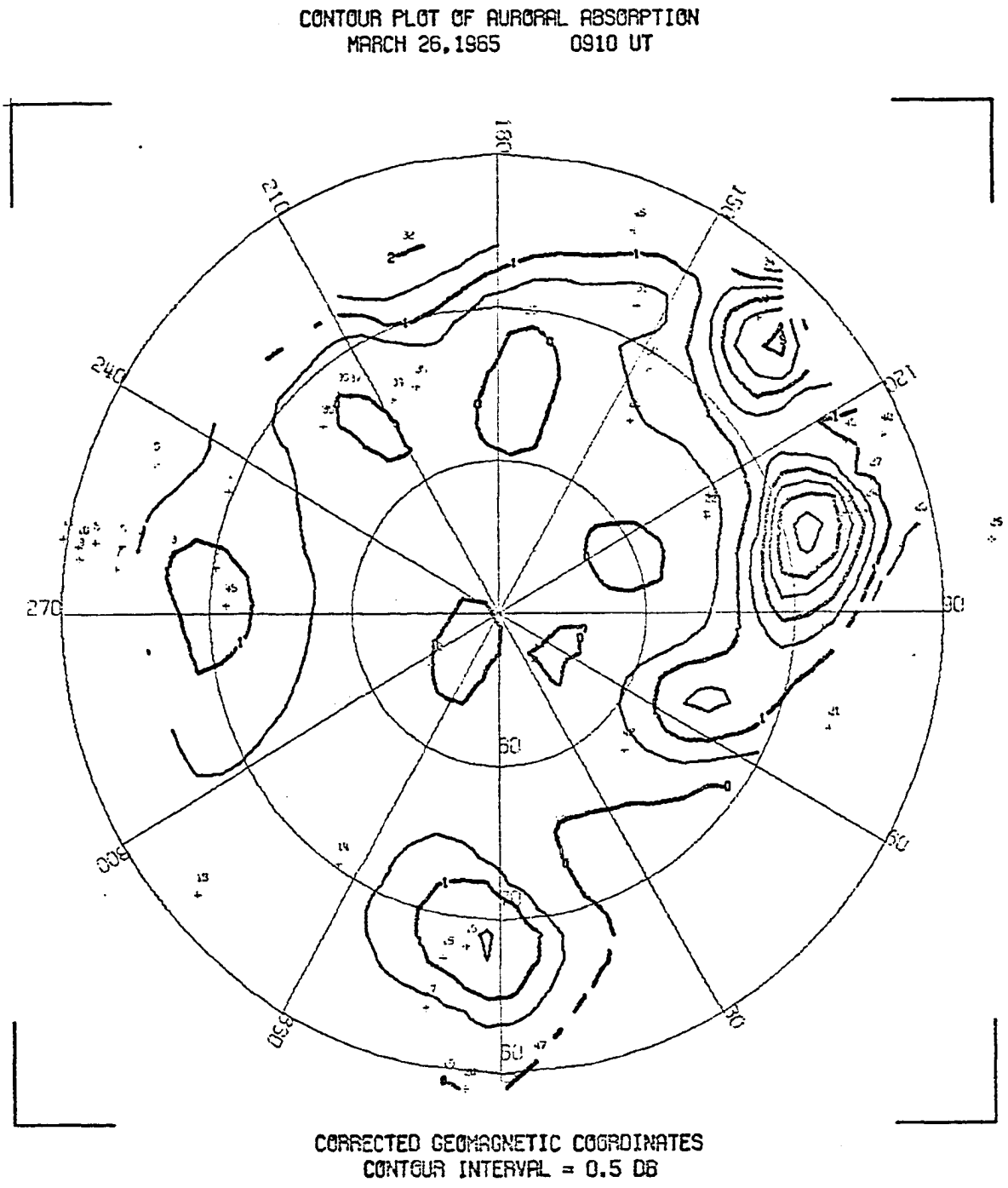

Figure (8.37) Contour map for 0910 UT on March 26, 1965.

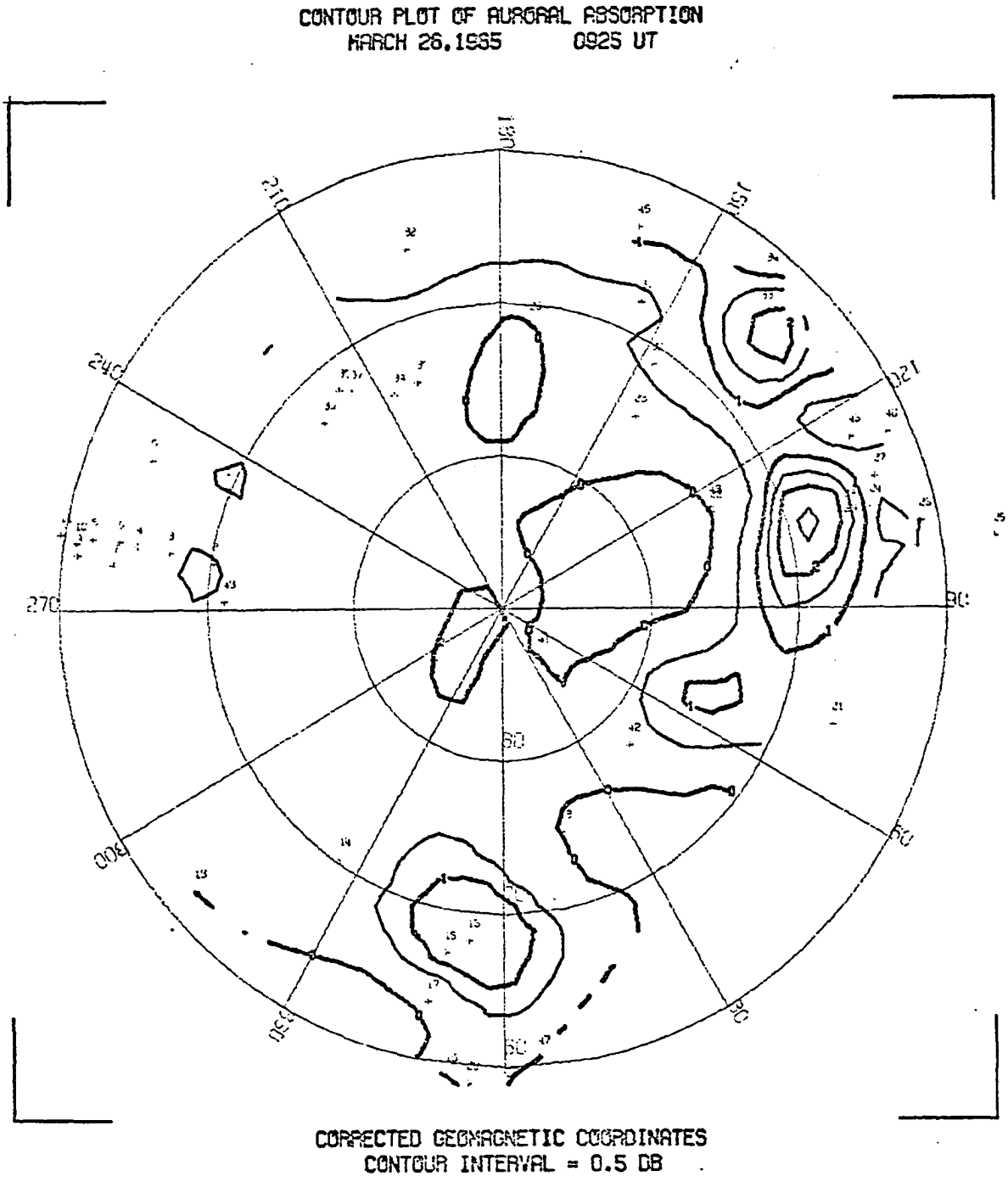

Figure (8.38) Contour map for 0925 UT on March 26, 1965.

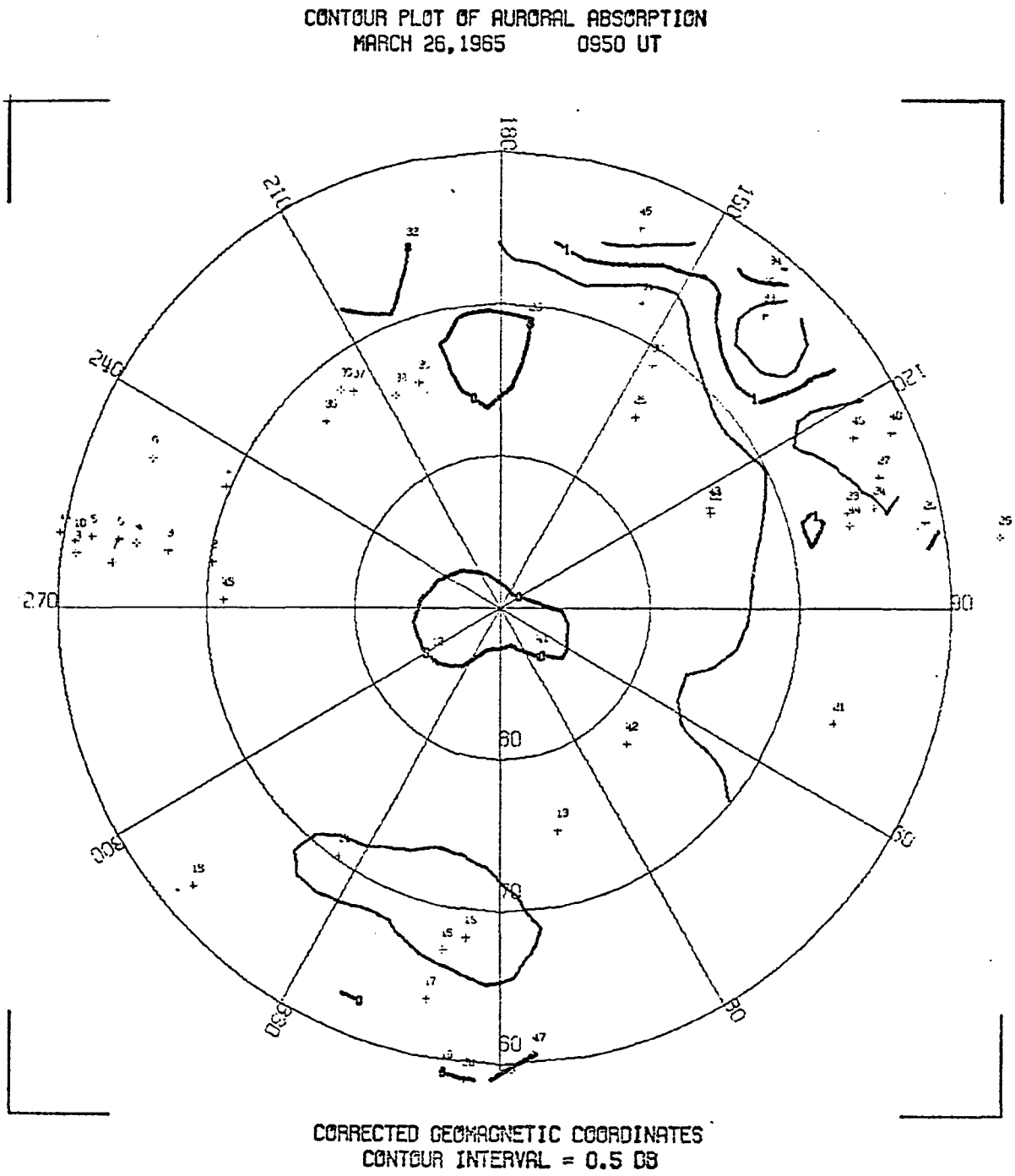

Figure (8.39) Contour map for 0950 UT on March 26, 1965.

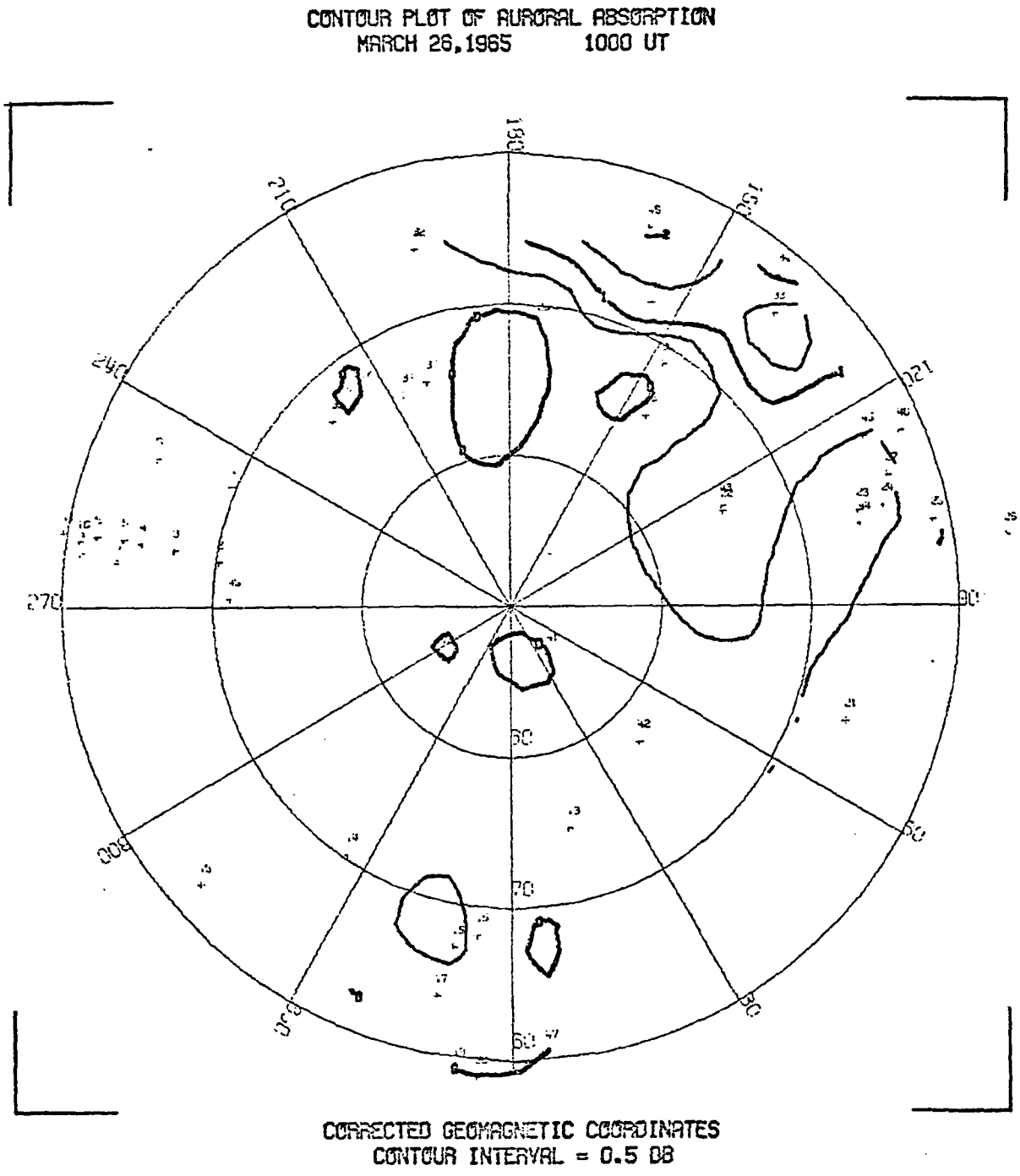

Figure (8.40) Contour map for 1000 UT on March 26, 1965.

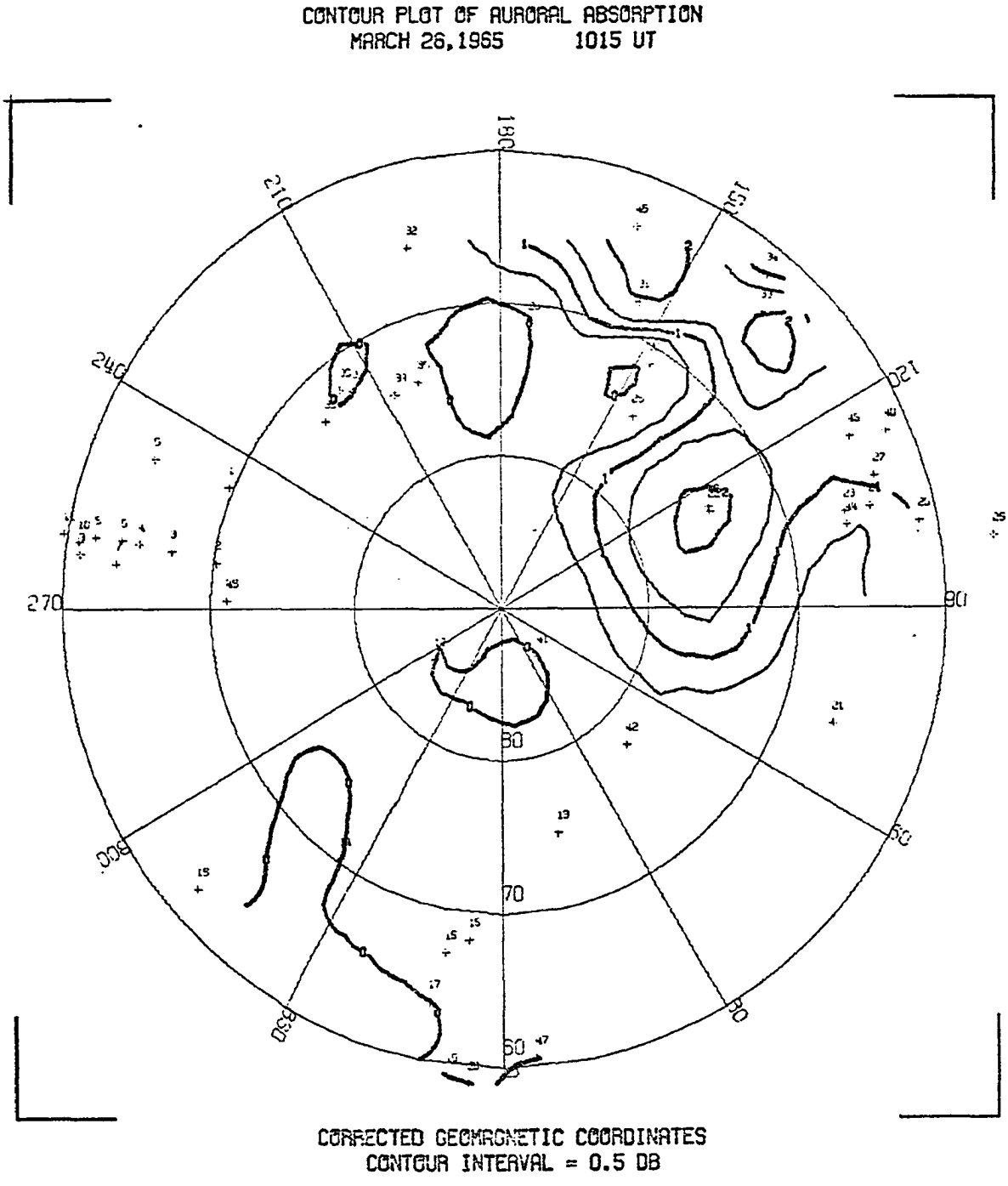

Figure (8.41) Contour map for 1015 UT on March 26, 1965.

8.5 The Substorm of January 14, 1965

Accompanying the polar substorm which commenced at approximately 11^h UT on January 14, 1965 was the lowest level of magnetic activity which occurred during the substorms studied herein; the Kp index was 2+ during the interval 09^h-15^h UT. At College, Barrow, Sitka, and Churchill, slowly decreasing negative bays of maximum amplitude 300 gamma were observed. No significant activity was seen at Meanook or Great Whale. In the midnight sector, an H-component decrease of 350 gamma was seen at NP-13 (72.0°N), situated near the poleward edge of the auroral oval at 1115 UT. At Cape Chelyuskin, ∿1500 kilometers west of NP-13 and also in the oval, an indented positive bay (Meng and Akasofu, 1967) occurred. A 250 γ positive bay was recorded at Heiss, located in the afternoon sector (see Figure 8.42).

The onset of the auroral absorption substorm is not accurately defined from the available data. From the magnetometer data presented in Figure 8.42 it is inferred that the onset of the substorm occurred between 1110 and 1115 UT, 30° -60° west of the College meridian.

Between 1115 and 1130 UT, the only absorption registered in the Northern Hemisphere was over Alaska (Figures 8.43, 8.44, and 8.45), although at Churchill and Cape Jones, an increase was noted by 1130 UT. At 1135 UT (Figure 8.45), absorption had reached 3.4 db at Fort Yukon, 2.8 db at College, and 1.9 db at Healy while 90° to the west, a sharp spike of 1.9 db was seen at Cape Chelyuskin. The event at Chelyuskin is coincident with the indented positive bay recorded in the H-component and provides evidence of an intense WTS passing near Chelyuskin.

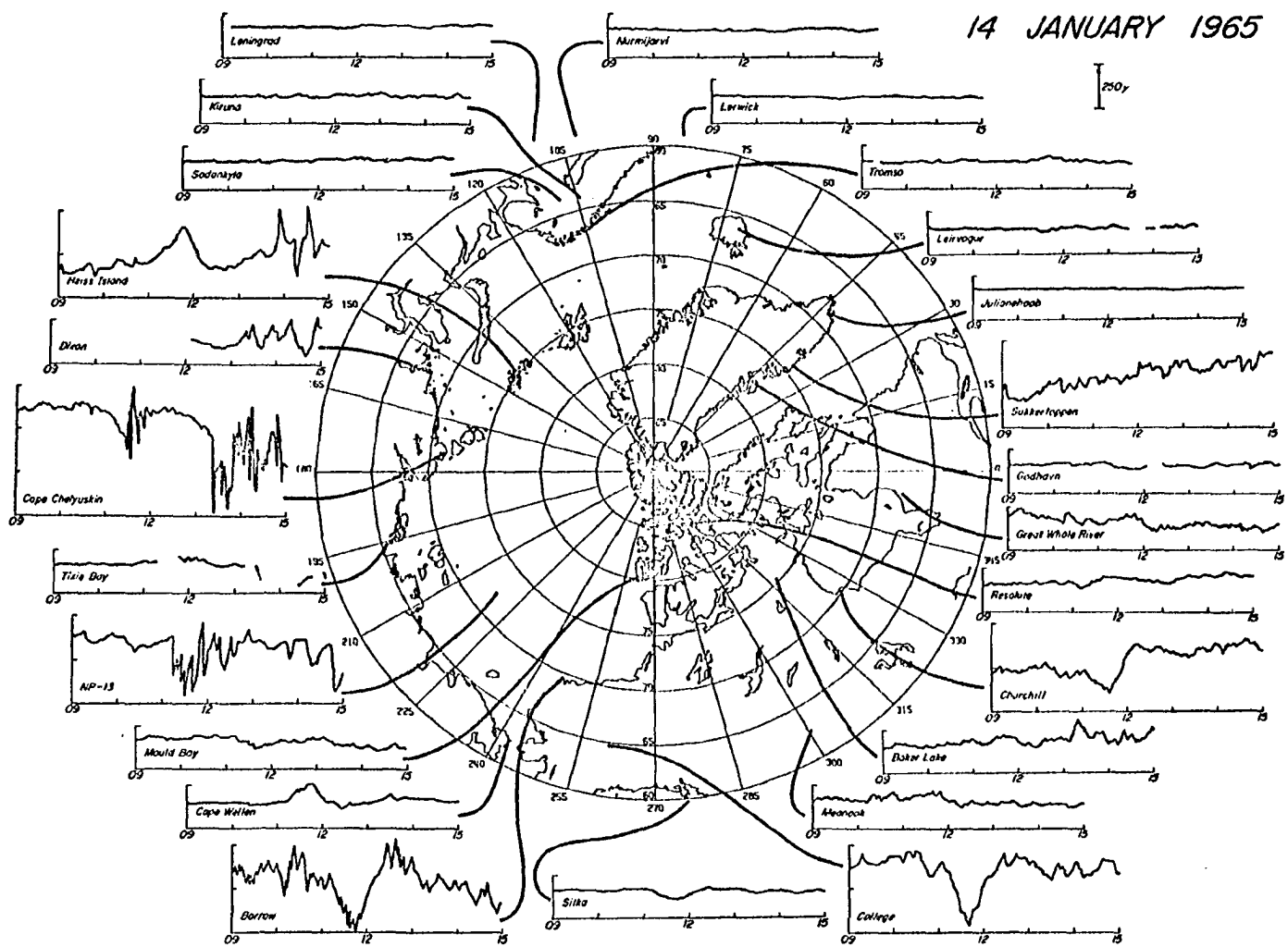

Figure (8.42) A collection of magnetic records (H or X component) from magnetic observatories in the Northern Hemisphere on January 14, 1965.

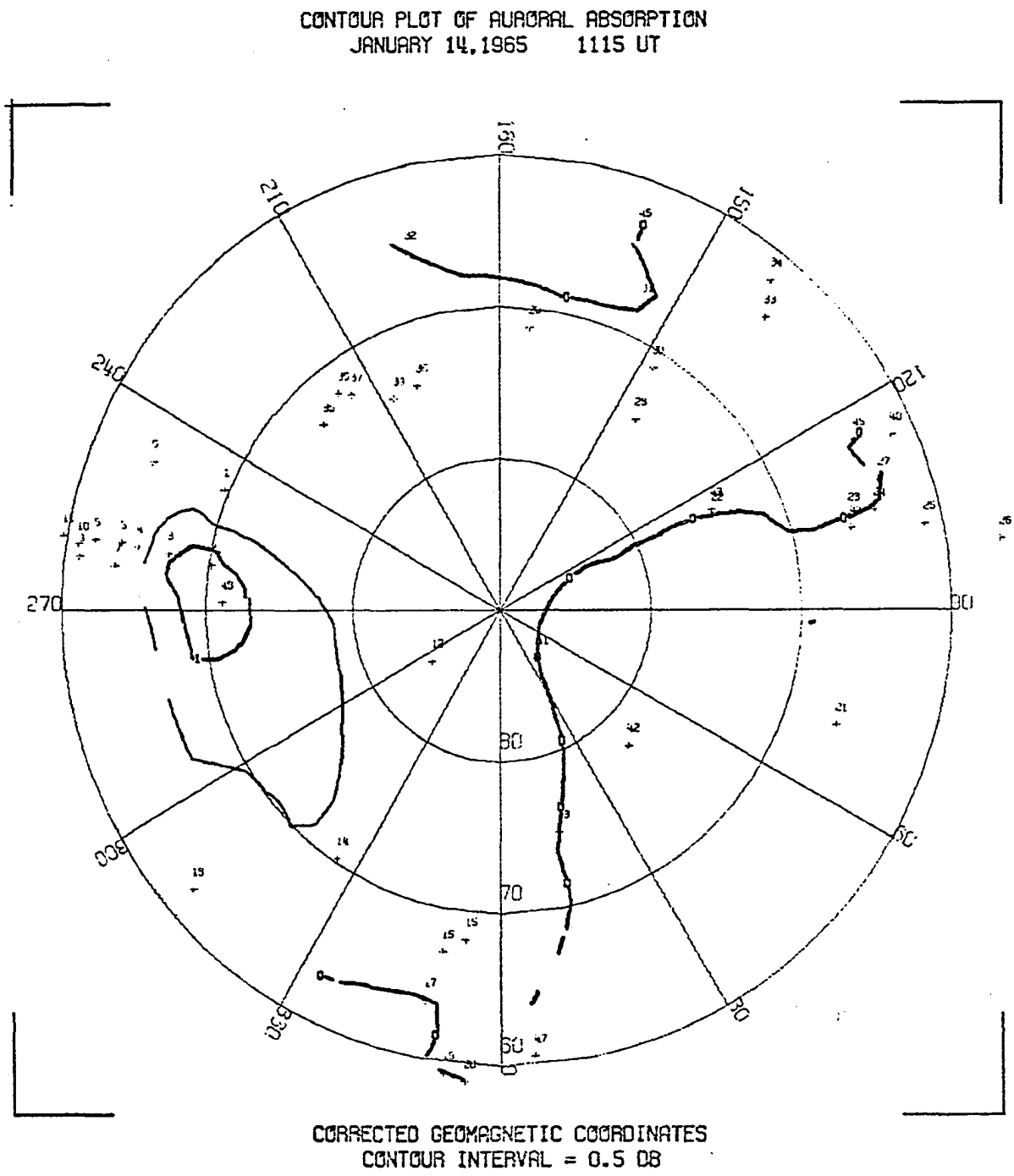

Figure (8.43) Contour map for 1115 UT on January 14, 1965.

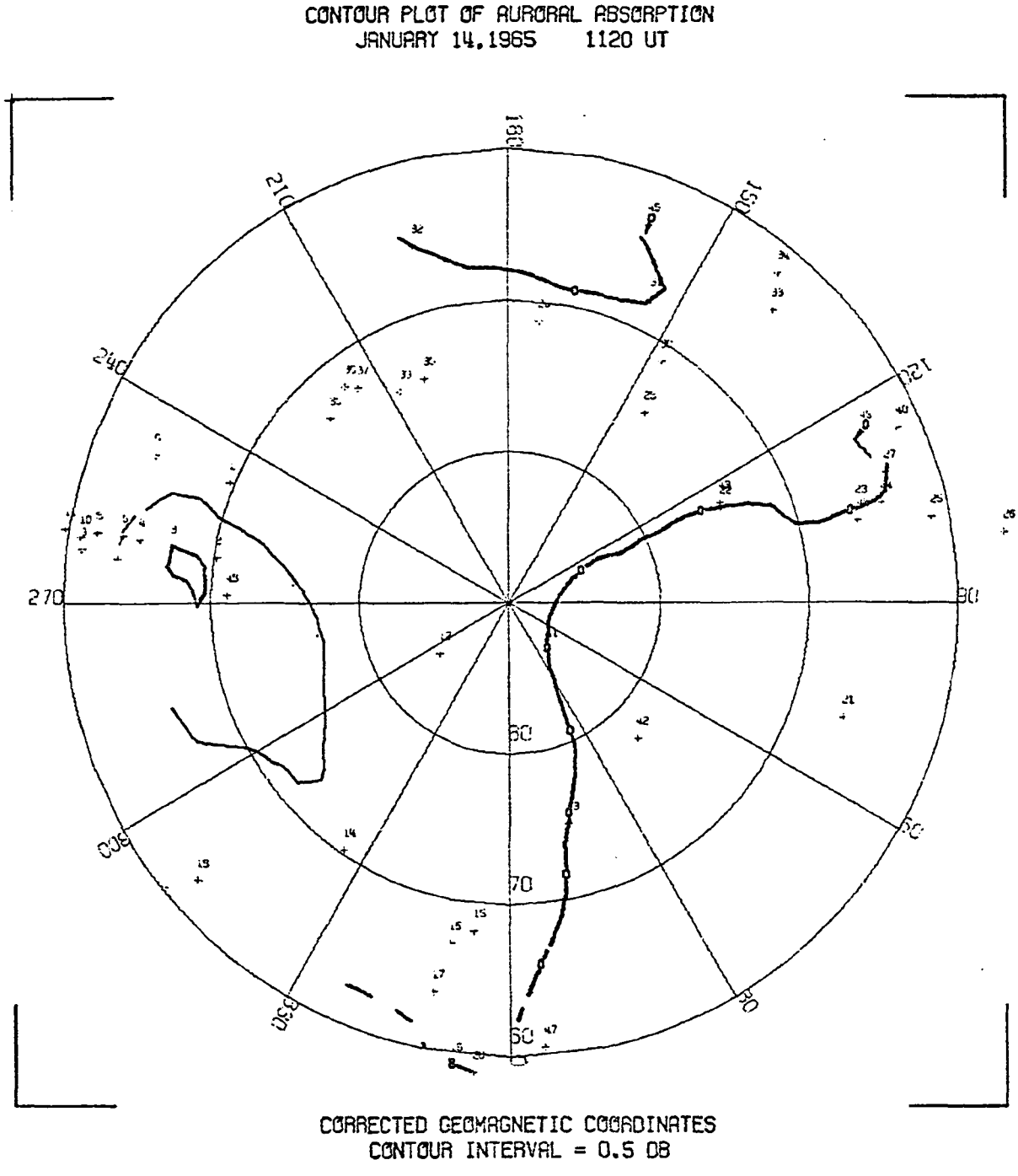

Figure (8.44) Contour map for 1120 UT on January 14, 1965.

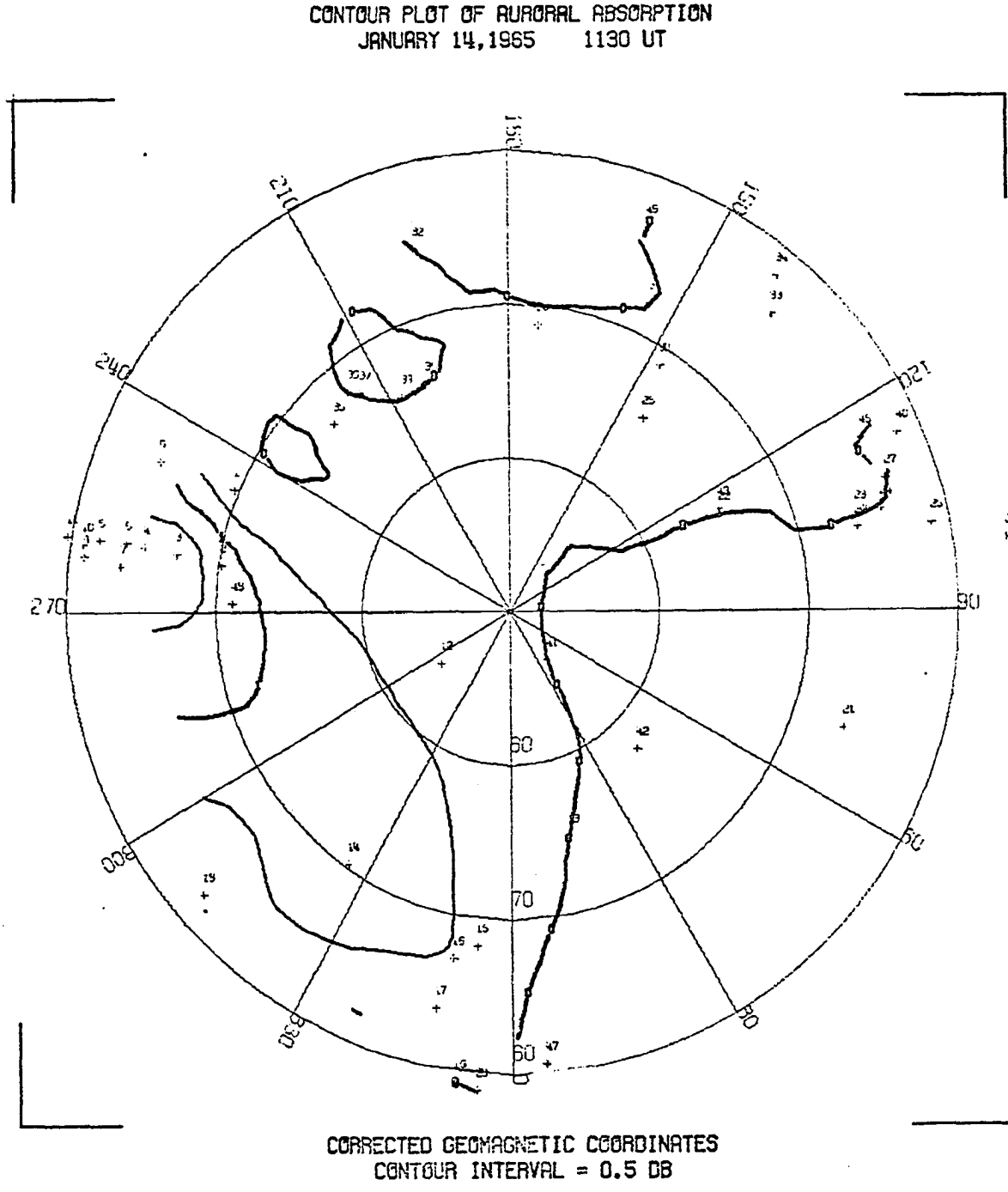

Figure (8.45) Contour map for 1130 UT on January 14, 1965.

Maximum absorption in the early morning sector occurred at 1140 UT when 3.7 db was observed at Fort Yukon, 2.8 db at College, and 2.2 db at Healy (see Figure 8.47). Simultaneously, in the late morning sector, approximately 1 db was seen at Cape Jones. By 1155 UT, (see Figure 8.48) the absorption intensity was increasing in the late morning sector (1.1 db at Cape Jones and Moosonee) while maximum absorption was reached at Great Whale, Moosonee, and Val D'Or. Little evidence of the substorm existed at 1210 UT (Figure 8.49); absorption was recorded only over Alaska and Canada at this time. At 1225 UT (Figure 8.50), no absorption greater than 1 db was registered at any station, but by 1240 UT (Figure 8.51) maximum absorption was reached in the noon sector.

A strong absorbing region persisted at Cape Jones at 1305 UT as illustrated in Figure 8.52. An interesting feature was observed at 1325 UT (Figure 8.53), when an enhancement of the absorption occurred throughout the entire polar region, coincident with a negative bay onset at Cape Chelyuskin. Shortly thereafter at 1335 UT (Figure 8.54), a secondary maximum in the absorption intensity was recorded in the Alaskan meridian. College and Fort Yukon, now located in the morning sector, observed more than 1 db of absorption. Again, this maximum could be interpreted as due to the gradient drift of electrons around the entire auroral zone. The drift period, from maximum to maximum, was approximately 115 minutes.

At College, Fort Yukon, and Healy, the nature of the event maximizing at 1140 UT characterized it as the type associated with pulsating, patchy auroral forms (Parthasarathy and Berkey, 1965). Although

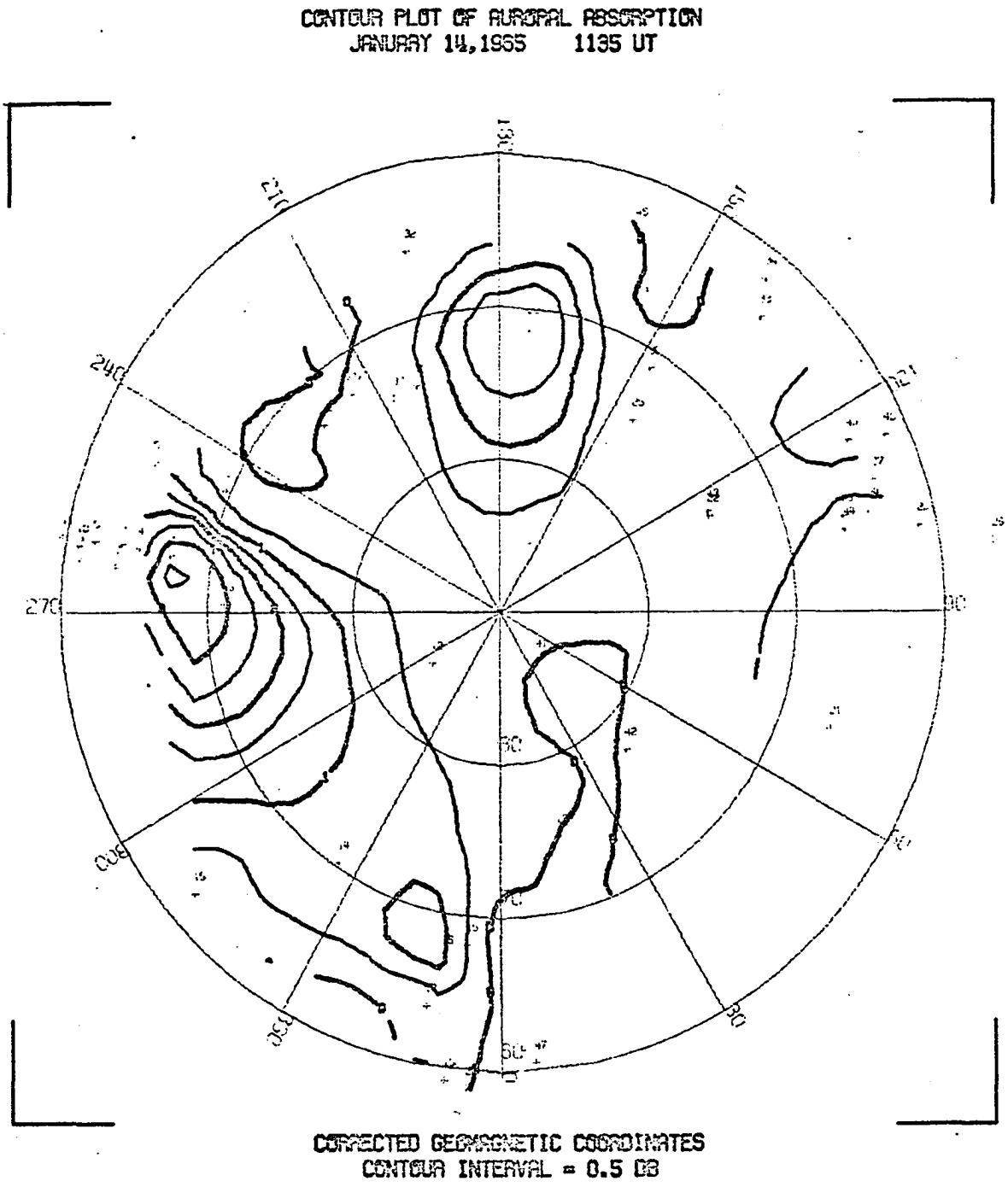

Figure (8.46) Contour map for 1135 UT on January 14, 1965.

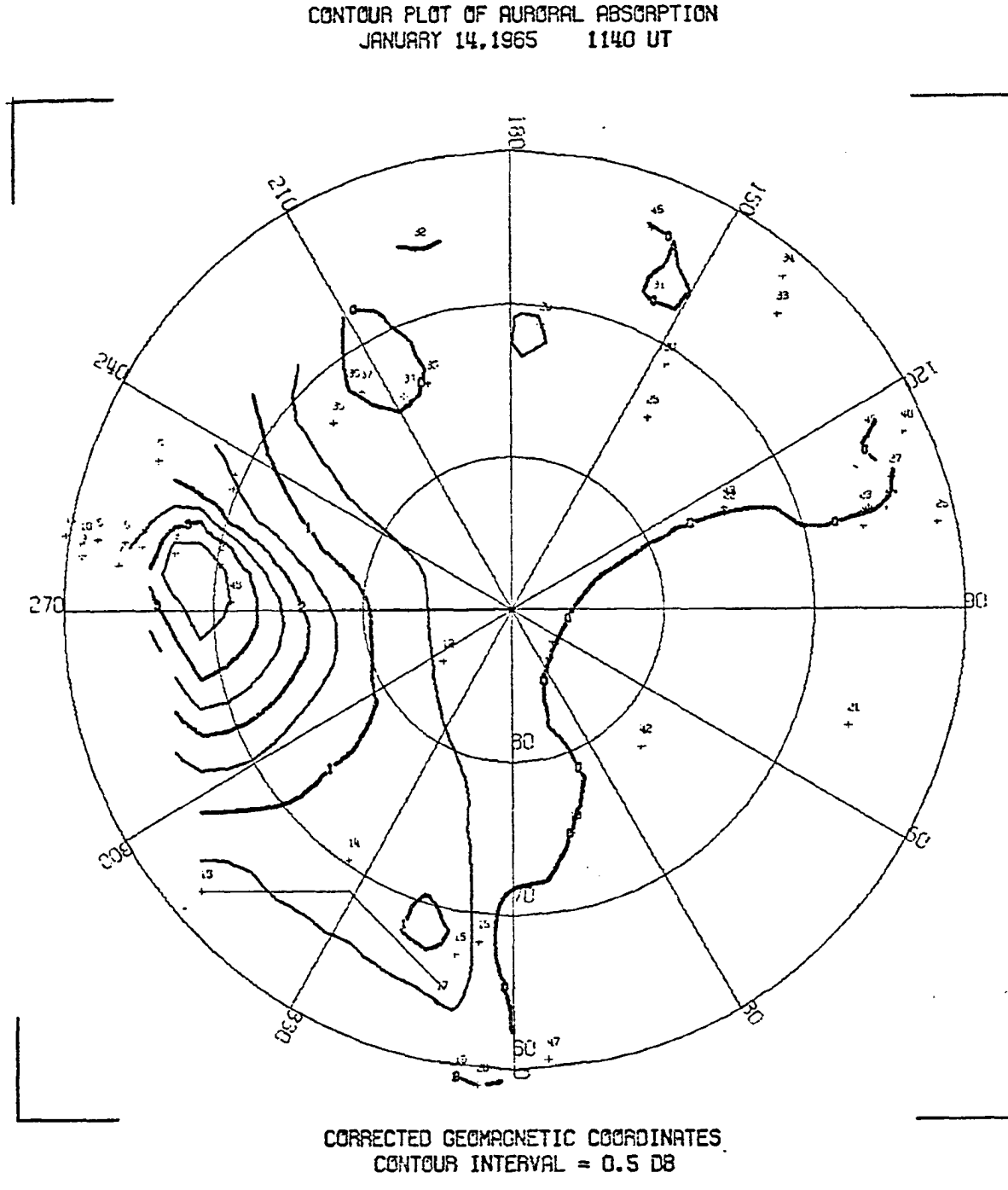

Figure (8.47) Contour map for 1140 UT on January 14, 1965.

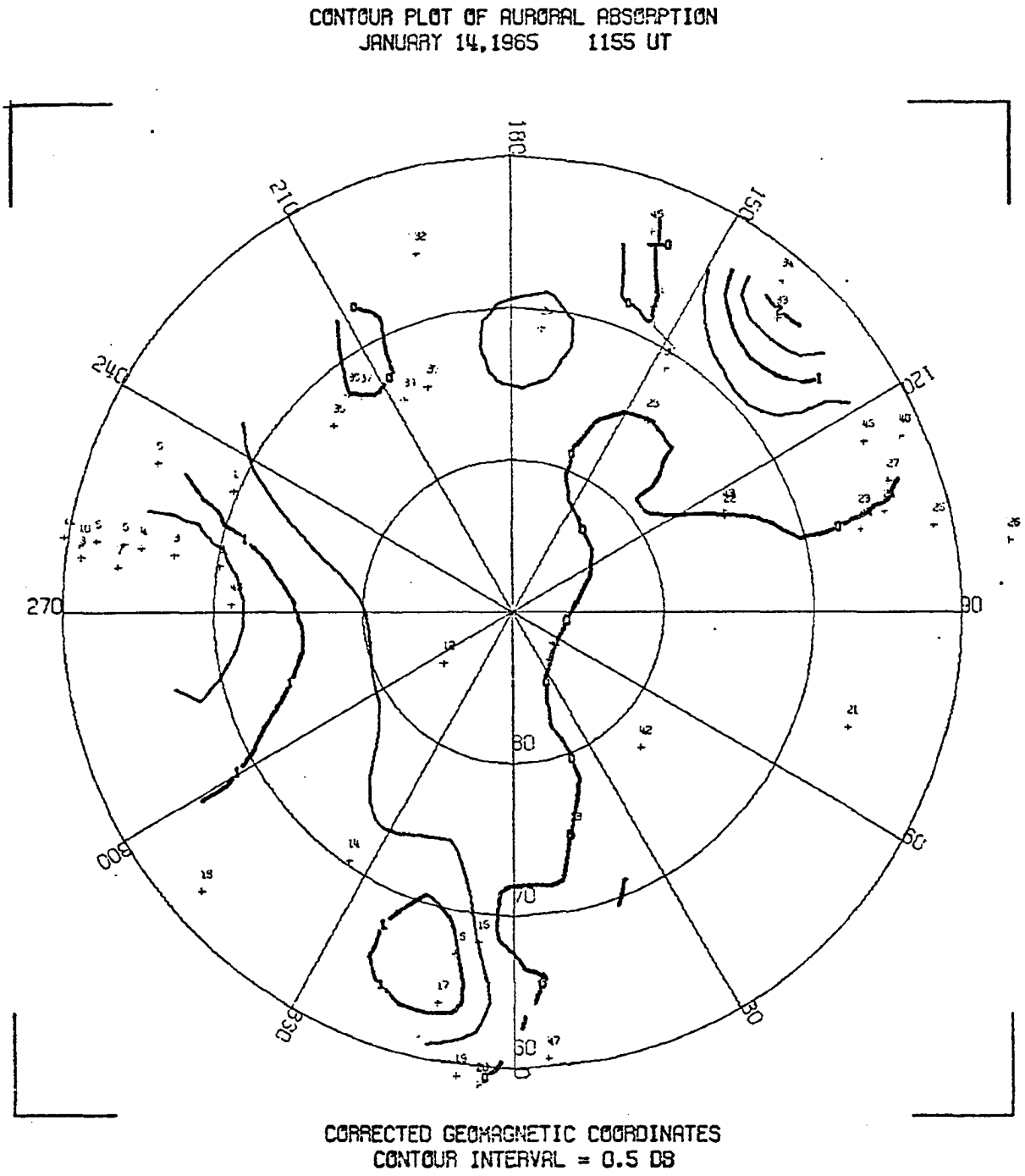

Figure (8.48) Contour map for 1155 UT on January 14, 1965.

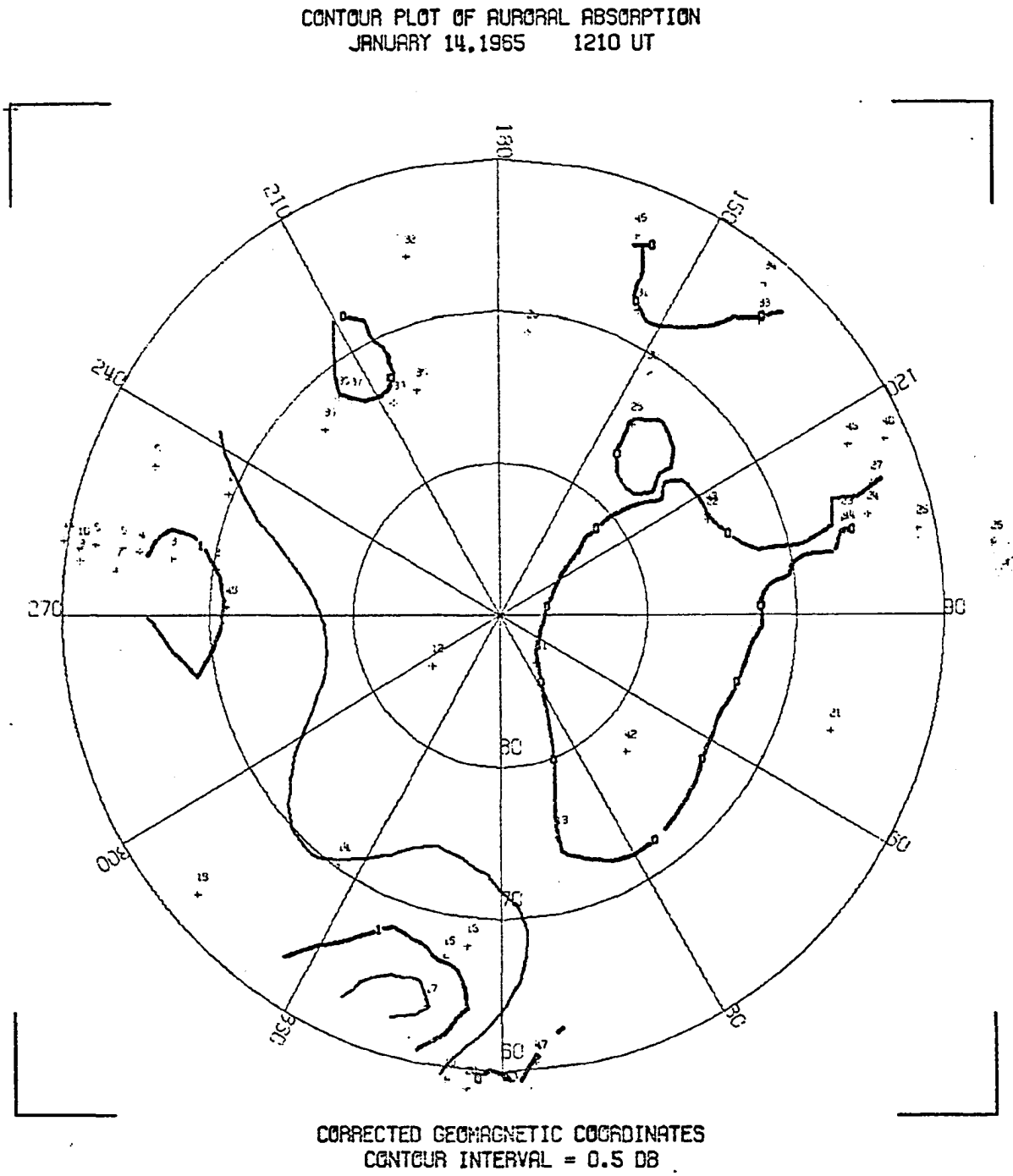

Figure (8.49) Contour map for 1210 UT on January 14, 1965.

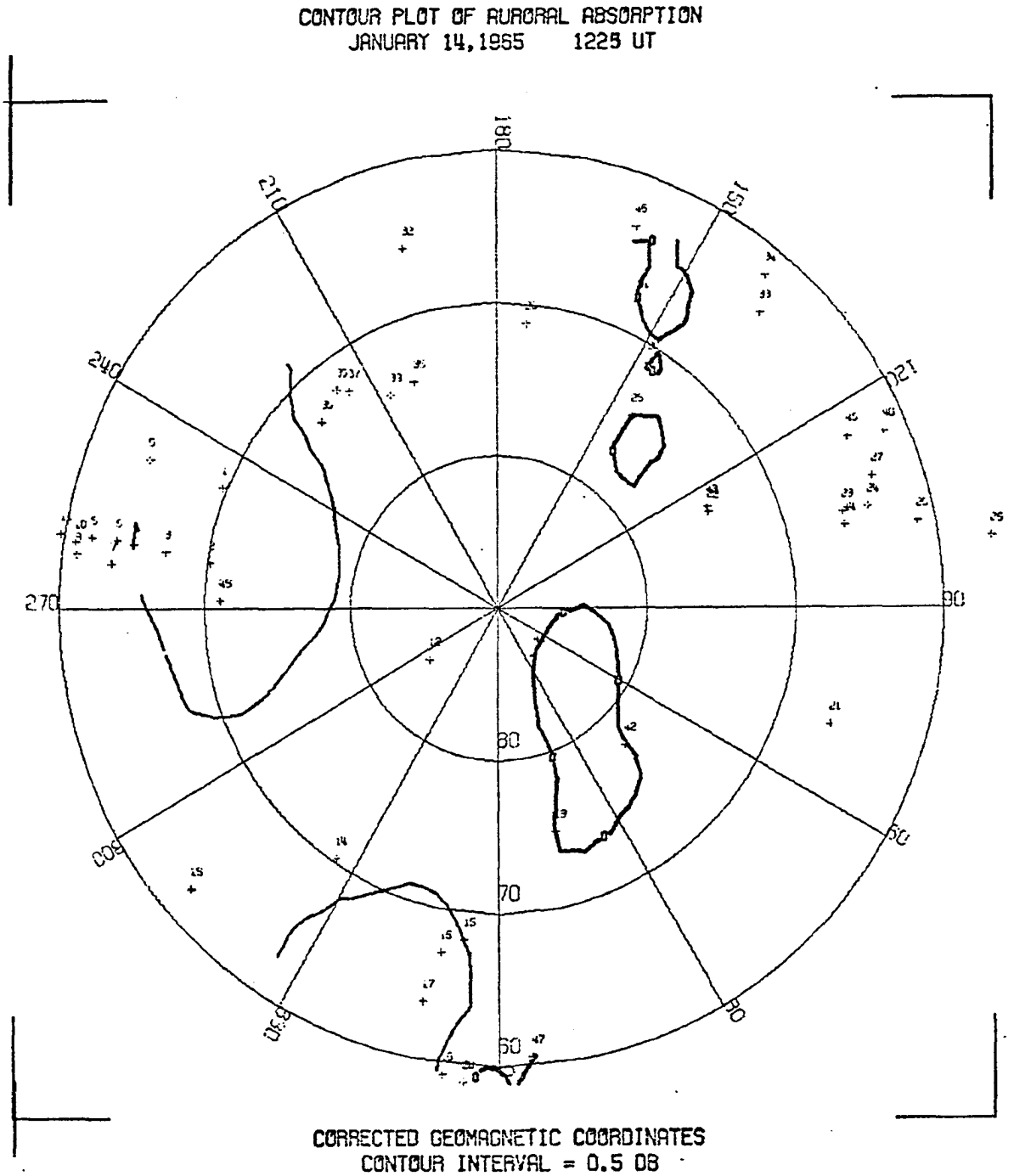

Figure (8.50) Contour map for 1225 UT on January 14, 1965.

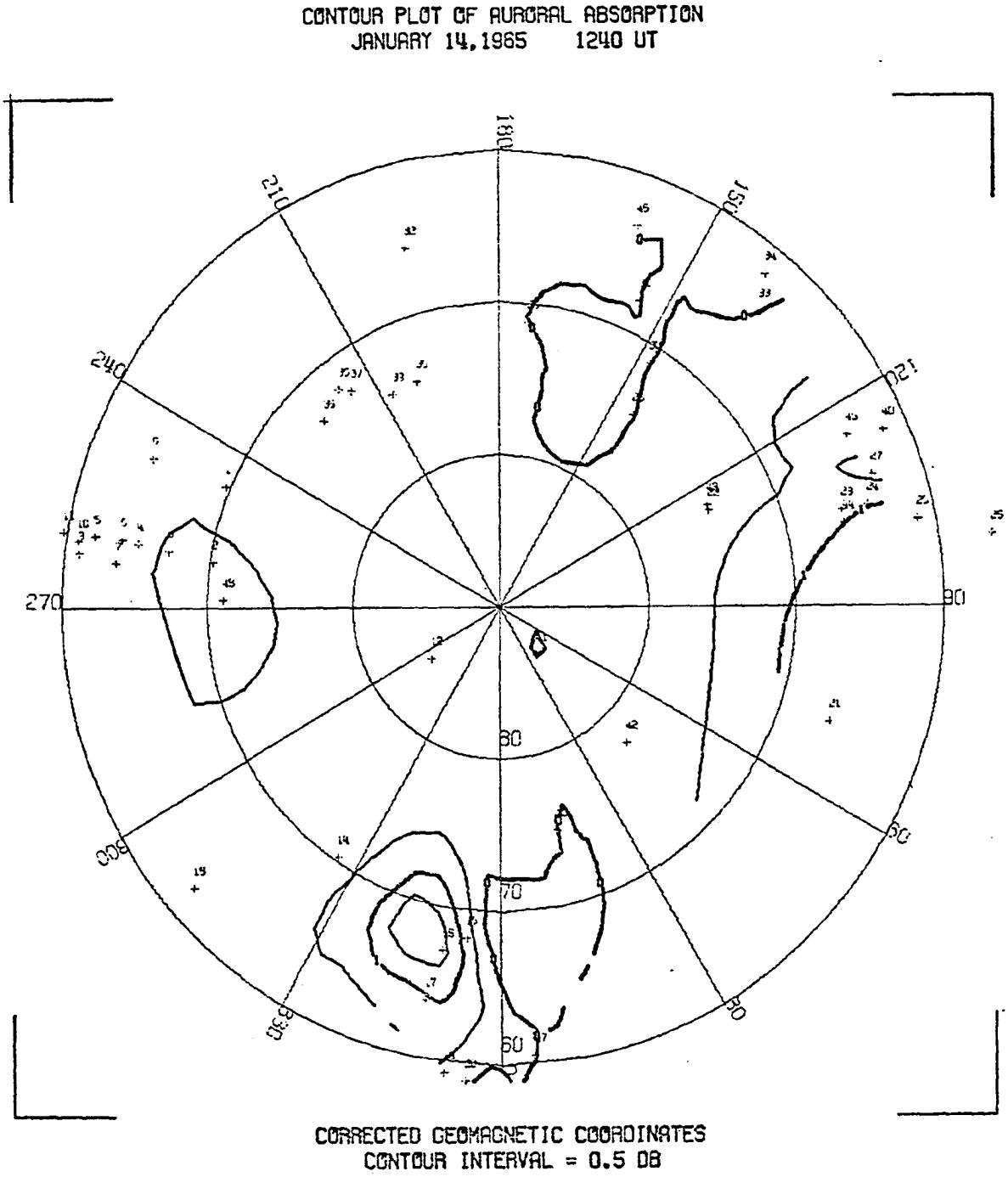

Figure (8.51) Contour map for 1240 UT on January 14, 1965.

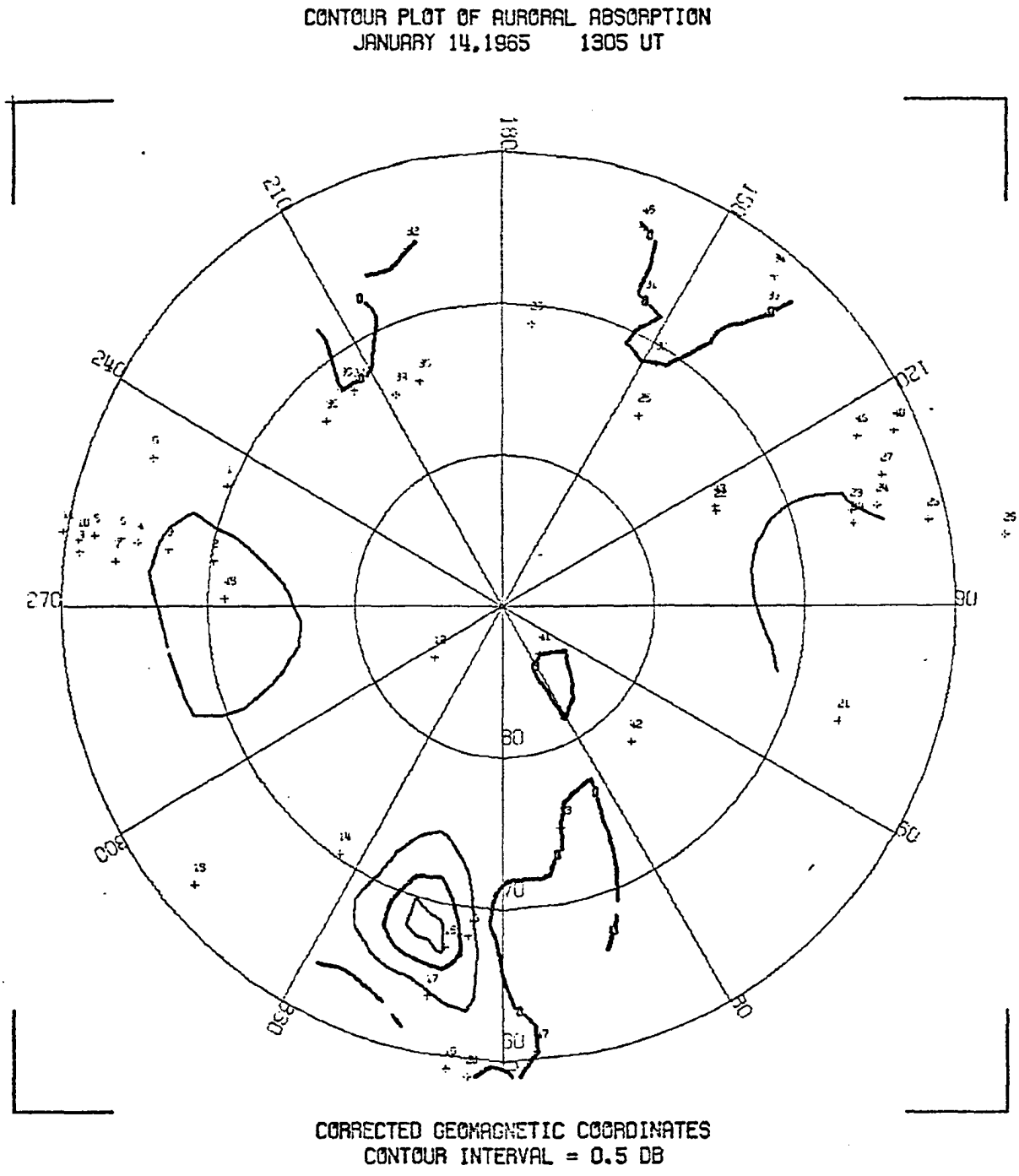

Figure (8.52) Contour map for 1305 UT on January 14, 1965.

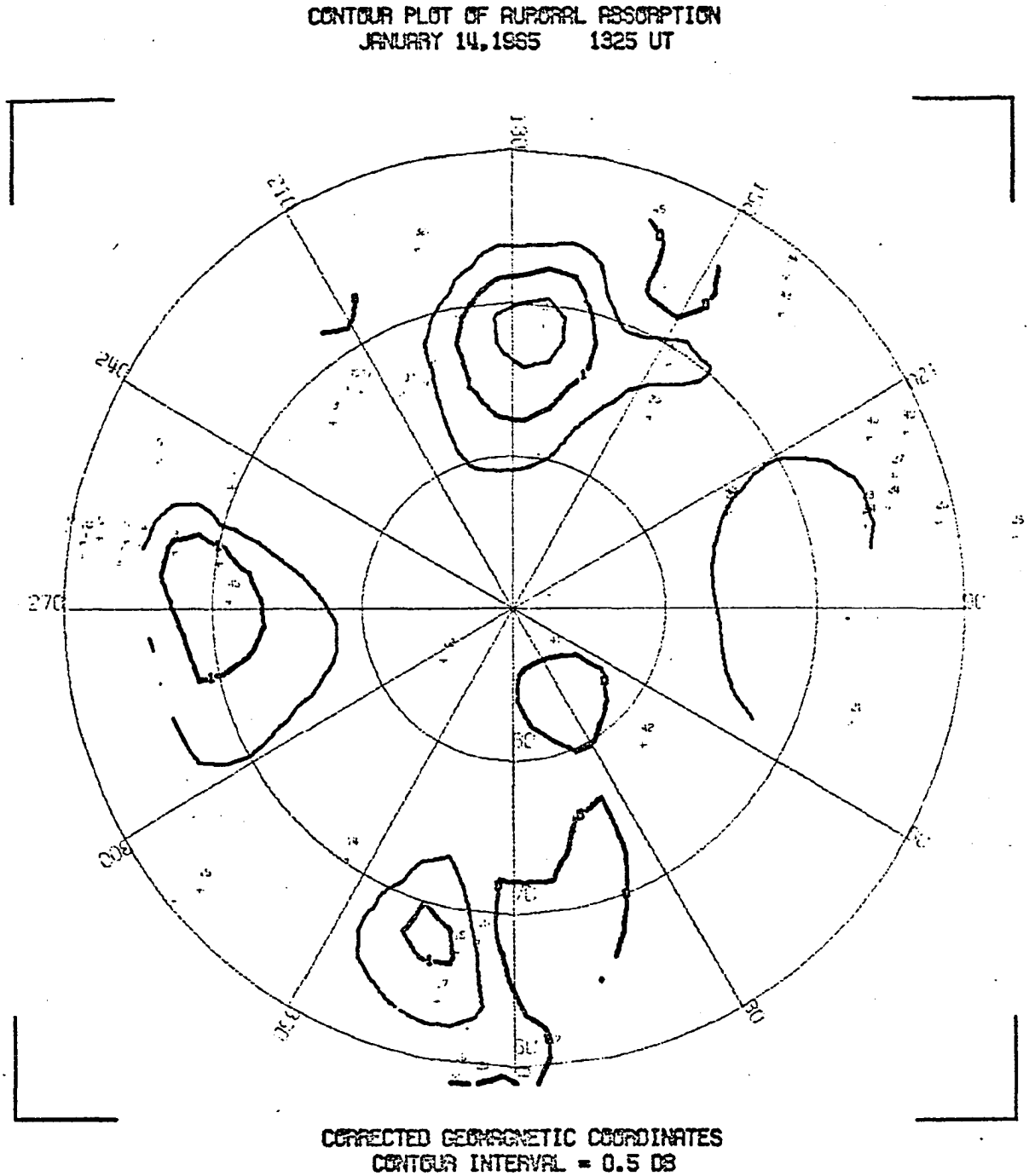

Figure (8.53) Contour map for 1325 UT on January 14, 1965.

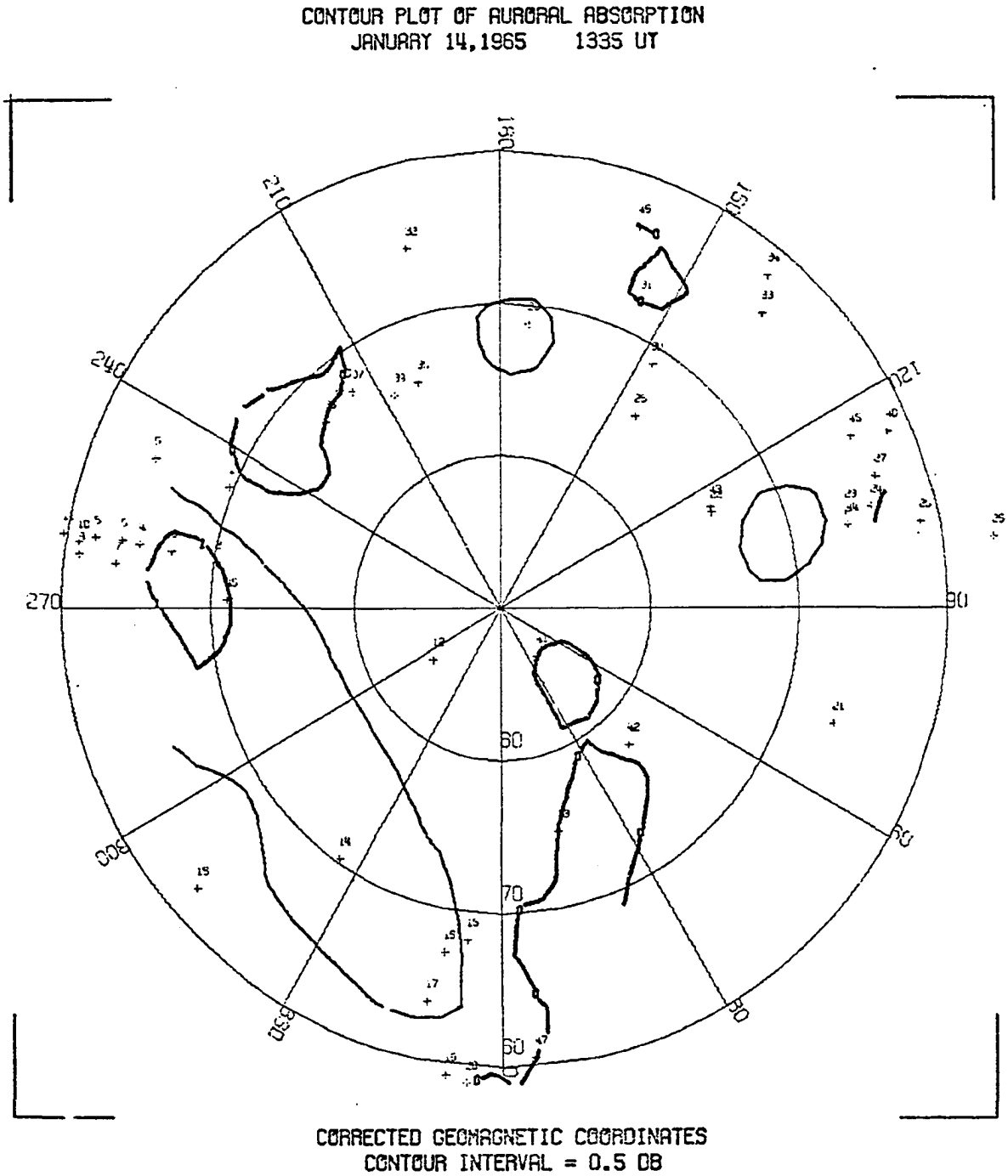

Figure (8.54) Contour map for 1335 UT on January 14, 1965.

moonlight severely contaminated the film, this relationship was confirmed using College all-sky camera film.

The association of intense absorption with the WTS was once again established, even though only one station recorded the associated absorption event. Interpolation from Chelyuskin toward the midnight meridian provides information concerning the location of the midnight meridian assuming an onset time of approximately 1110 UT (see Section 9.2).

From the analysis of this event, it is possible to infer that the auroral oval expands and contracts as a function of magnetic activity; during this event no absorption was recorded at Ottawa (58.9°N), Norilsk (63.4°N), Uppsala (56.4°N), and Baie St. Paul (60.6°N). Maximum absorption reached only 0.45 db at Val D'Or, 0.36 db at Sodanklya (63.4°N) and 0.75 db at Prince Albert. Note that Prince Albert was located in the morning sector where the oval has its greatest equatorward extent.

Maximum absorption was recorded at Fort Yukon (3.7 db) located in the morning sector; the absorption intensity exceeded 1 db only at Fort Yukon, Barrow, College, Healy, Cape Jones, Moosonee, Kiruna, and Cape Chelyuskin. Note that with the exception of Cape Jones, Moosonee, and Kiruna all the stations listed previously are situated within the auroral oval. Furthermore, at 12^h UT Cape Jones and Moosonee are located very near to the 06^h LT meridian and hence on the dayside. Kiruna is very obviously situated near the noon meridian. In the evening-midnight sector, NP-13 (72.0°N) and Cape Chelyuskin (71.3°N) represented the poleward extent of the absorbing region.

Prior to the onset of this substorm, absorption was recorded at Fort Yukon (1012 UT), Barrow (1020 UT), and Churchill (1035 UT). There did not seem to be a connection with the substorm which commenced at 1110 UT.

8.6 The Substorm of August 2, 1965

The level of magnetic activity was again very low, with Kp reaching 2+ during the interval 06^h - 09^h UT and 3- between 09^h and 12^h UT. No definite onset time could be established for the polar magnetic substorm; the largest H-component deflection was observed at College, where a 300 gamma negative decrease occurred between 09^h and 12^h UT. At Heiss and Chelyuskin, negative decreases were observed between 08^h and 11^h UT. At Meanook, a positive increase was observed at 0830 UT. Magnetic activity at other locations was essentially negligible.

Although the onset of the auroral absorption substorm was not well-defined, the development of the AAS was similar to those storms discussed previously. Figures 8.55 - 8.62 illustrate the growth of the substorm between 0815 and 1010 UT. Note that because of the smaller intensity of the storm, a contour interval of 0.25 db was used for the analysis. The absorption first appeared in the evening sector over Alaska (Figure 8.55). By 0830 UT, absorption was seen in the morning sector over Canada (Figure 8.56), reaching a maximum at 0930 UT (Figure 8.60) at Moosonee. At this point, the normal pattern of development stopped, and no increase in absorption attributable to the AAS was seen at either Kiruna or Tromsø. However, at 0935 UT an event of 2.2 db magnitude was recorded at Amderma, followed shortly by an increase of absorption at Tixie, which reached a maximum at 1000 UT (Figure 8.62).

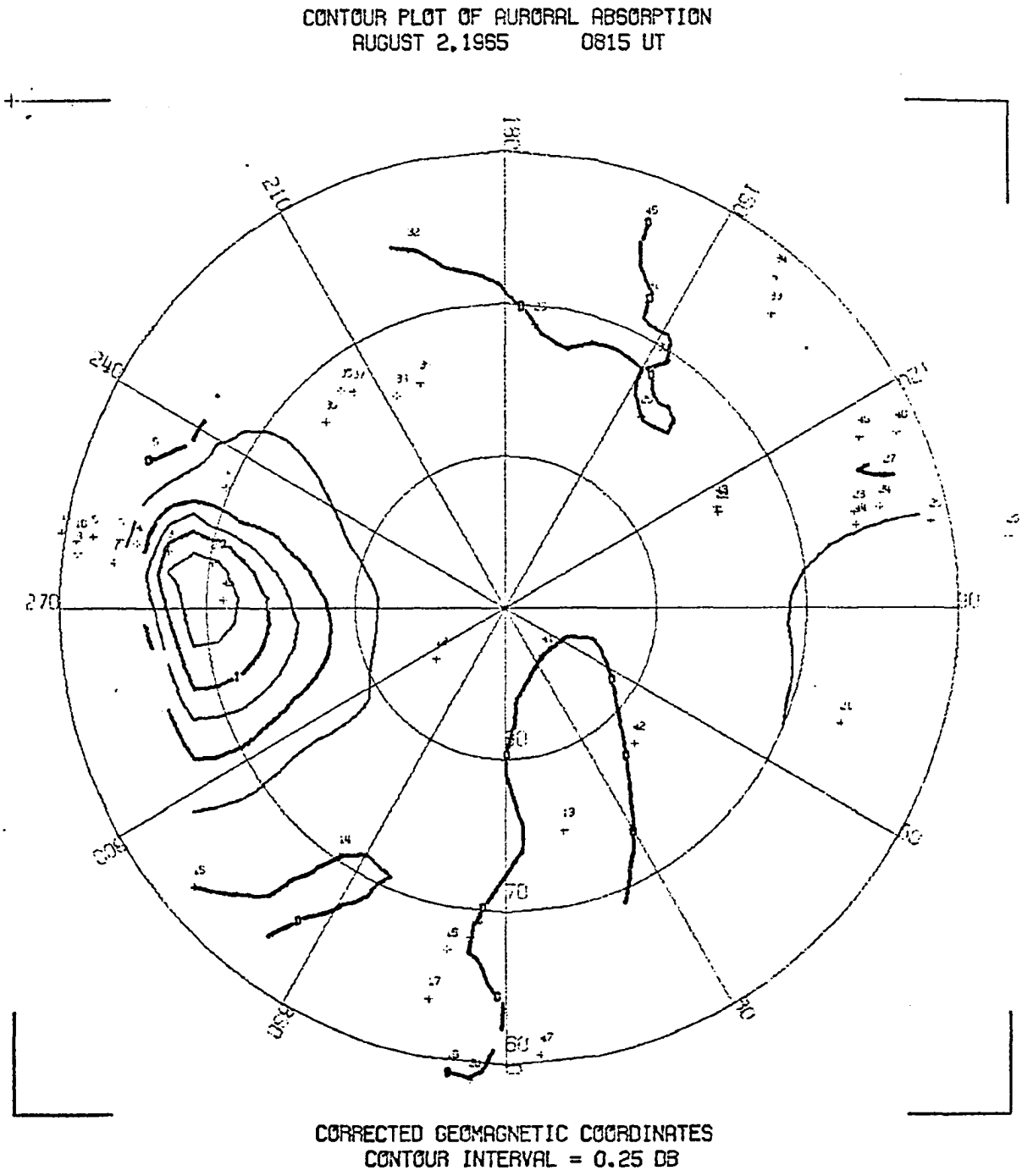

Figure (8.55) Contour map for 0815 UT on August 2, 1965.

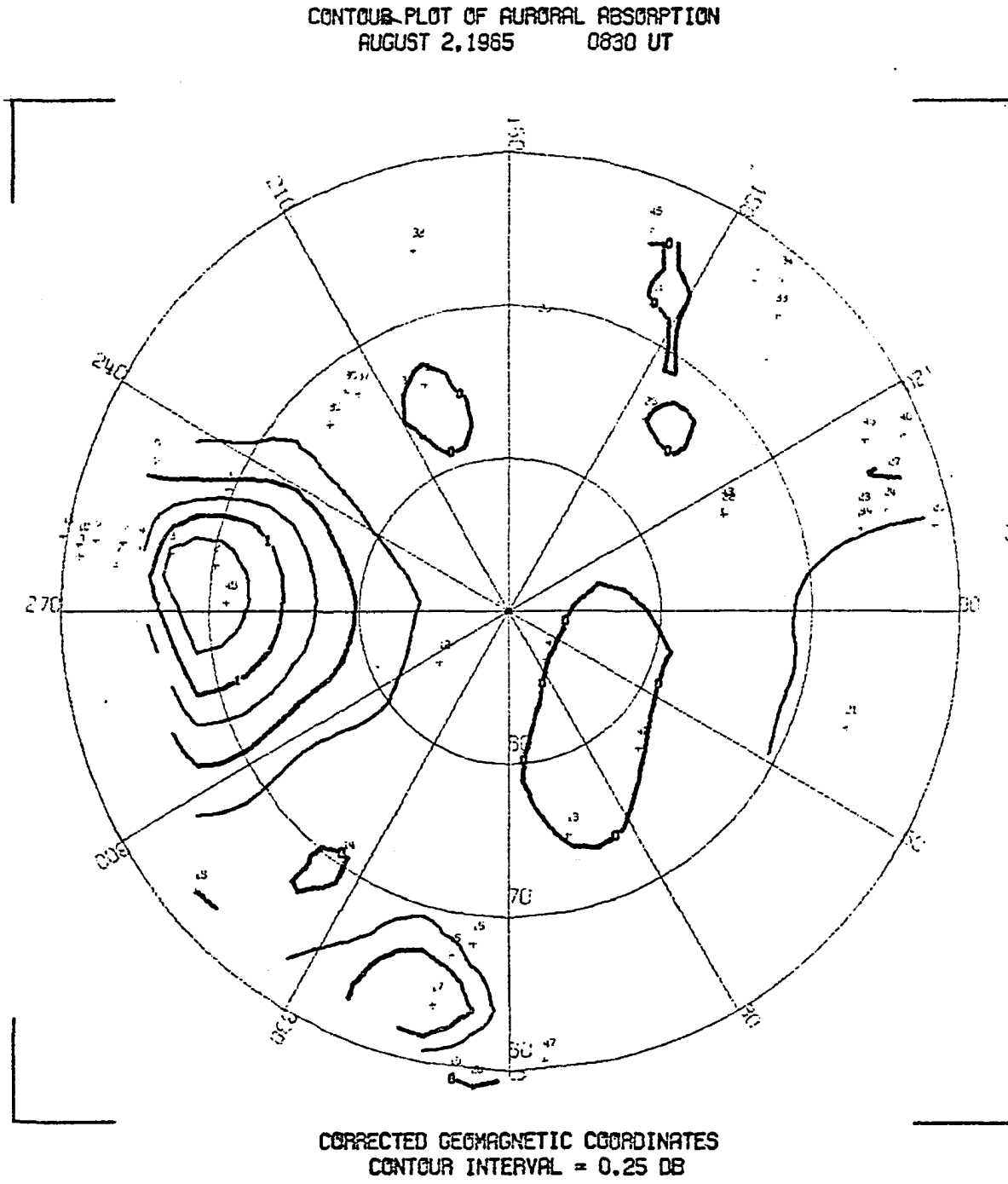

Figure (8.56) Contour map for 0830 UT on August 2, 1965.

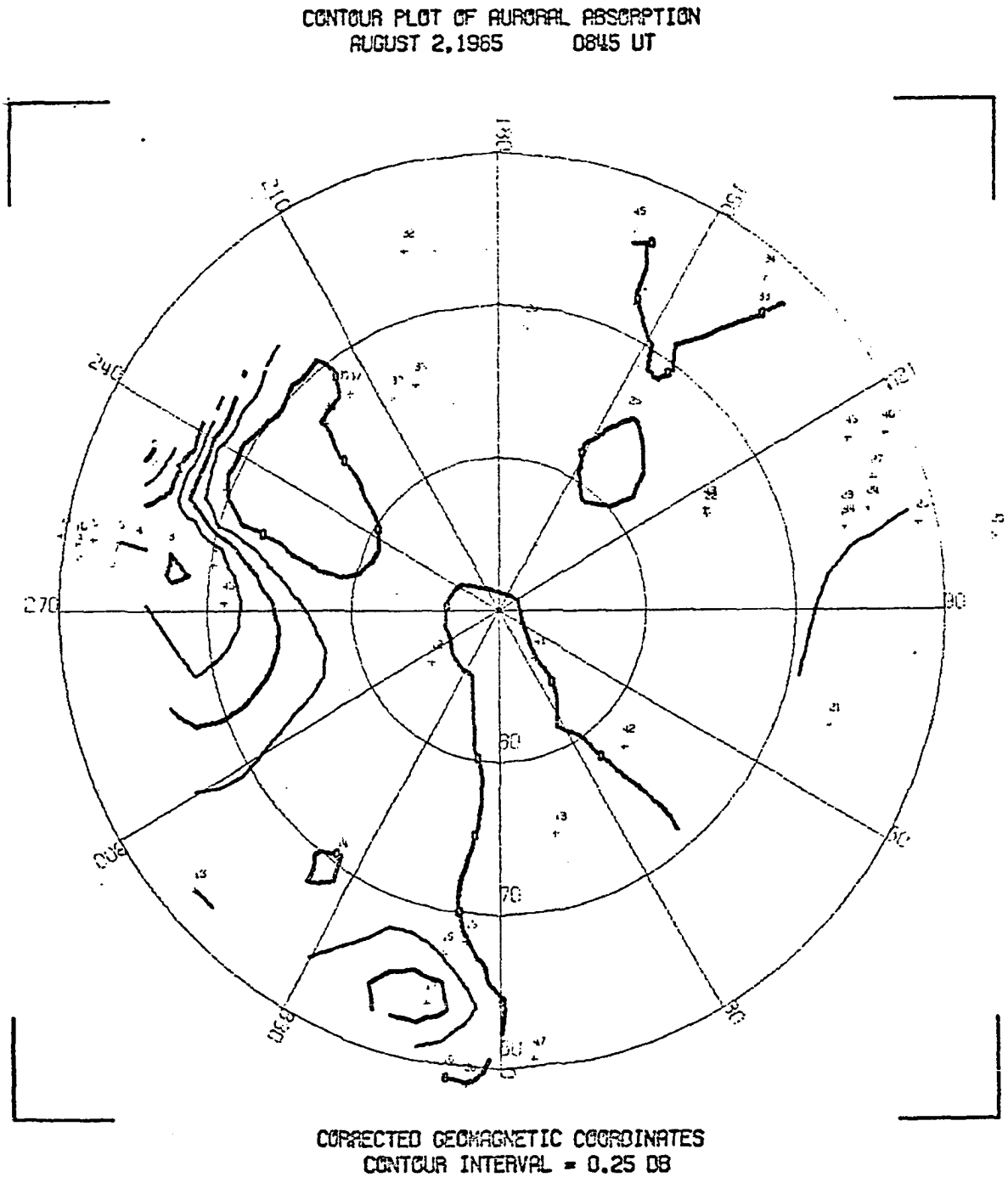

Figure (8.57) Contour map for 0845 UT on August 2, 1965.

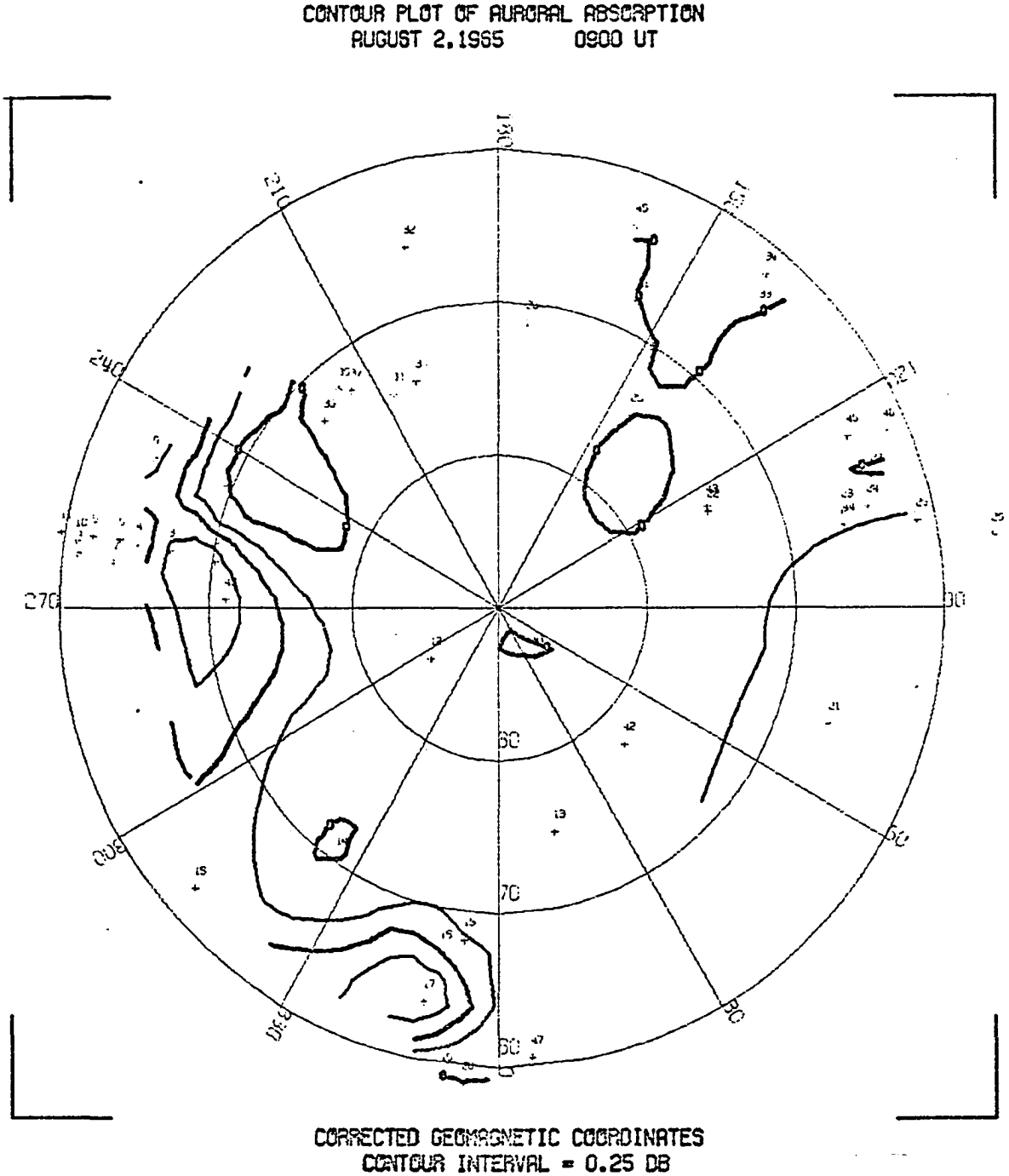

Figure (8.58) Contour map for 0900 UT on August 2, 1965.

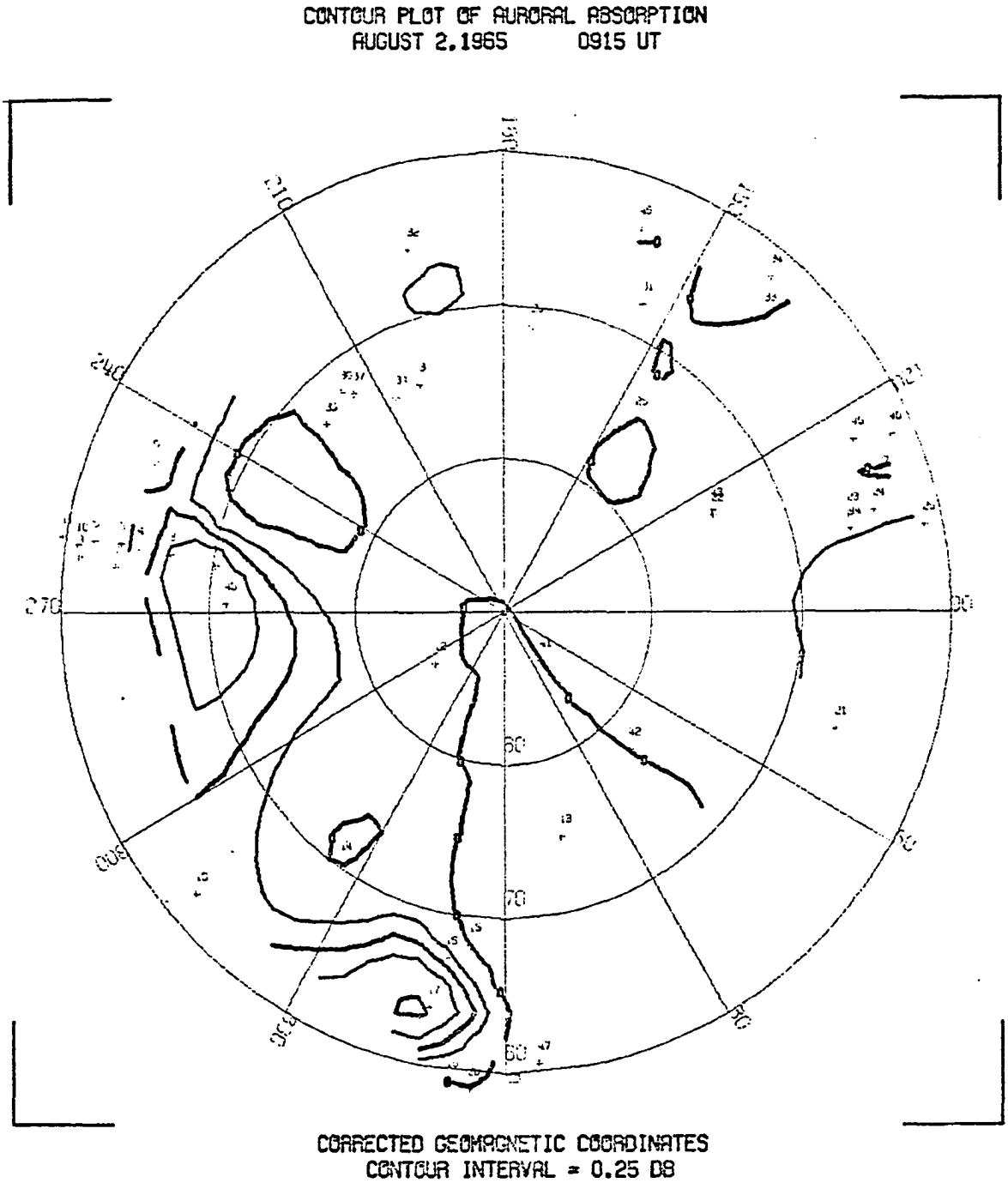

Figure (8.59) Contour map for 0915 UT on August 2, 1965.

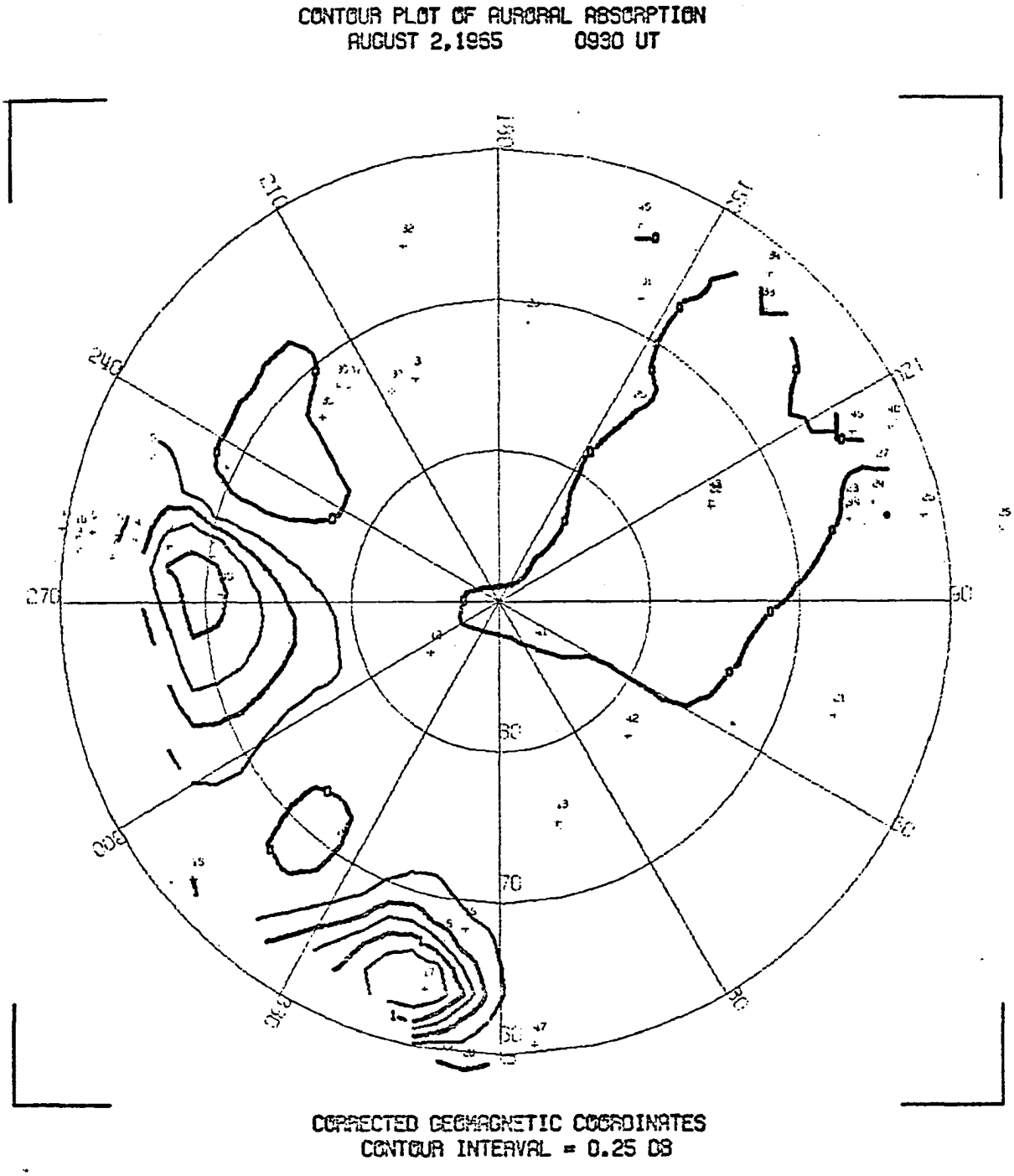

Figure (8.60) Contour map for 0930 UT on August 2, 1965.

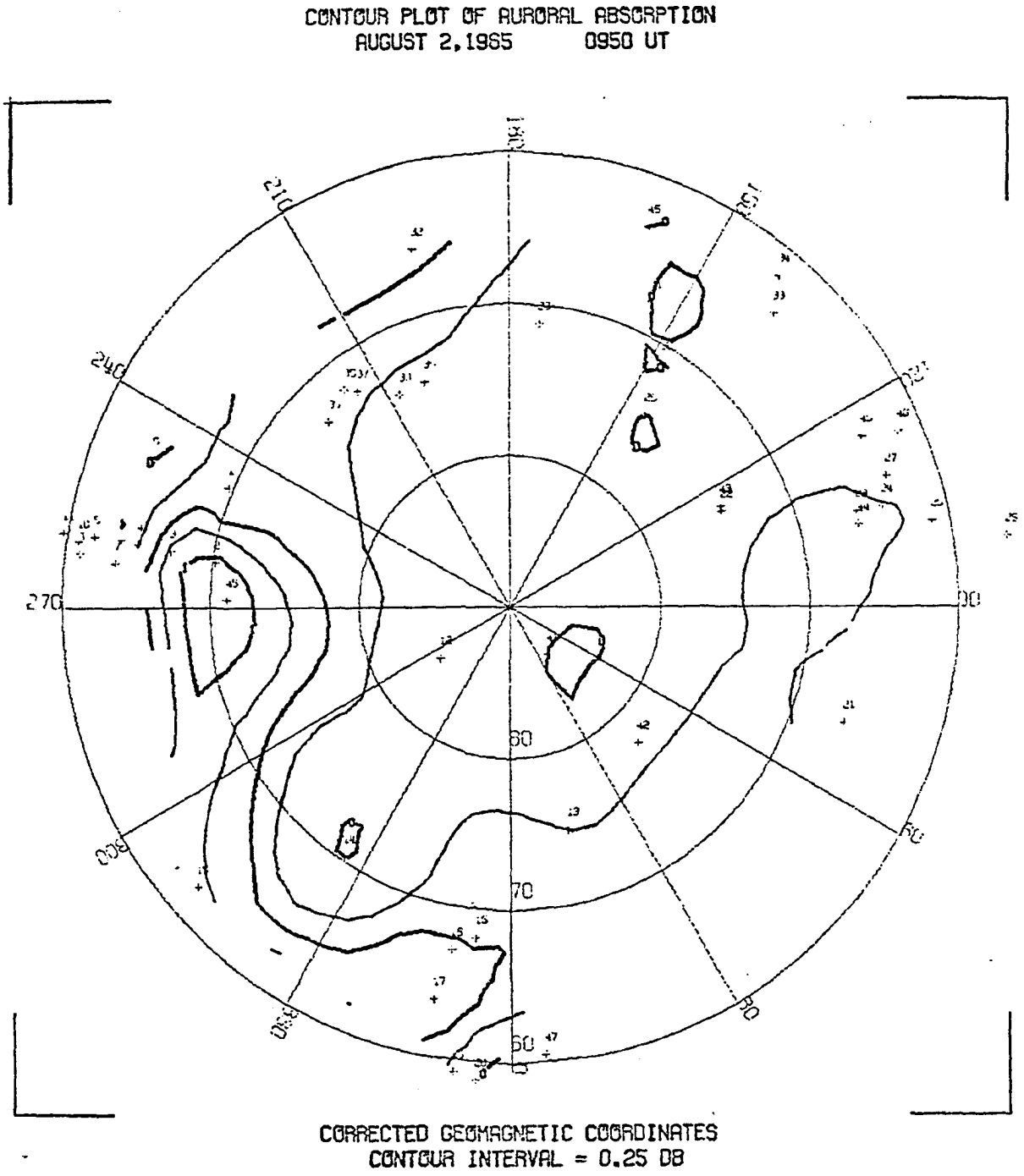

Figure (8.61) Contour map for 0950 UT on August 2, 1965.

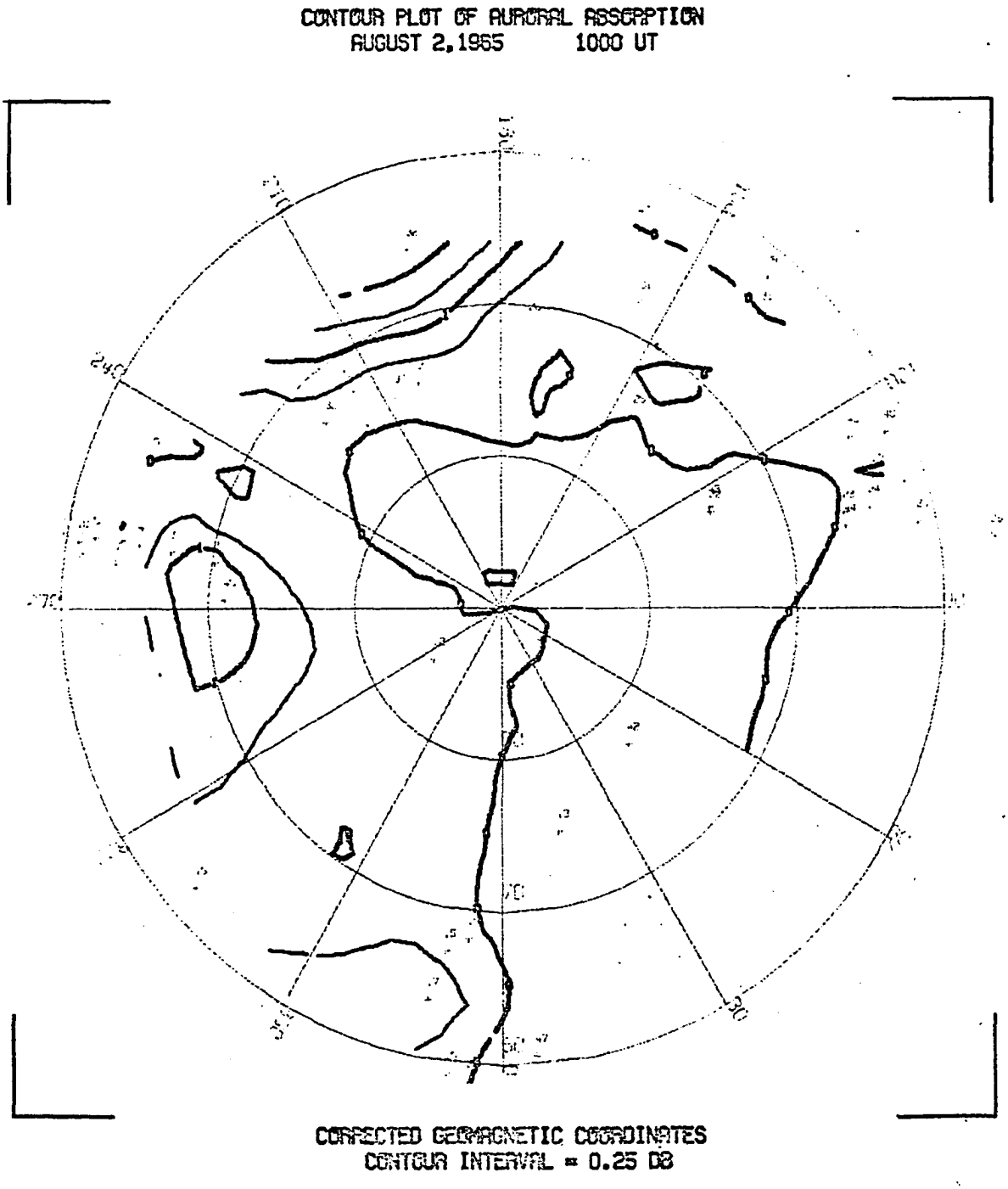

Figure (8.62) Contour map for 1000 UT on August 2, 1965.

This substorm differs from the previous storms in three significant ways: (1) the storm occurred during the Northern Hemisphere summer, when the 80 km level was sunlit in the midnight meridian; (2) the accompanying polar magnetic substorm variations were less than 300 gamma, and; (3) the development of the AAS was incomplete.

In terms of Kp and ΣKp, this storm was of greater intensity than both the November 7 and January 14 storms discussed previously. Thus it seems unlikely that the oval had contracted poleward beyond the range of the riometer network, particularly in view of the previously mentioned storms. A seasonal effect, noted at College by Hook (1968), is more than likely responsible for the smaller magnitude of absorption recorded during this event.

It has also been noted that auroral absorption is more intense in the Alaskan meridian than at other longitudes (Waite, 1965; Rapoport, 1970). It can then be argued that a small absorption event in Alaska may not even be detected near the noon meridian in Europe.

In interpreting this substorm, it is important to take into consideration two facts: (1) the occurrence of the storm during the summer months; (2) the lack of intense magnetic activity at high latitude.

8.7 Critique of contouring technique

A basic criticism of the application of the STAMPEDE technique to the contouring of auroral absorption data is the lack of sufficient data points to adequately define the contours. This is, of course, a valid criticism; as a result of the distribution of geophysical observatories, the data points tend to occur in clusters, with large gaps

between the clusters. For example, only one data source exists in the 60° of longitude between the Alaskan and Canadian meridian chains. Even more serious is the almost complete lack of data sources within the 90° interval between Canada and Europe.

However, in the course of the analysis, it was found that the program would derive contours in the region between Canada and Alaska even though only a single input point was provided in the region. Similarly, in the one example (November 7) for which data was available from Reykjavik, contours were drawn between Canada and Europe. On the other hand, when Reykjavik data was not available, no contours were drawn in the region.

More serious problems afflicting the contouring technique are: (1) the existence of an isolated station, or; (2) a single station near the boundary of the surface being contoured. Several examples of the effect of theses situations can be seen in the data discussed previously. As an example of the latter case, consider the contours drawn near Prince Albert (point 18): contour lines extend to the point, but never equatorward of it. The effect of an isolated point is illustrated in Figure 8.5. In this example an intense absorption event was recorded at NP-13 (point 35) on November 7, 1965. The program produced contours which extended over a large area, whereas in reality there is sufficient evidence that such absorption has a narrow latitudinal extent. In several of the maps, contours are developed which extend well into the polar region. For example in Figure 8.17 the 1 db contour is drawn at 85° N and the 2 db contour at 78°N. There is little doubt

that such an approximation is incorrect based on absorption recorded at high latitude stations such as Frobisher Bay, Thule, and Resolute.

As an experiment in modifying the map derived in Figure 8.17, the following modification was incorporated into the STAMPEDE program: after generating the grid intersections over the surface, those values falling in the interval 75° to 90° were assigned the value -1 db. This value was chosen since the lowest contour drawn on the map is at 0 db. At this point the grid values are used as input to the contour program and the contour map developed. The results are illustrated in Figure 8.63, which incorporates a smoothing polynomial as an attempt to smooth the 0 db contour at 75°N latitude. Modifications such as this permit one to control the approximations within the STAMPEDE program to a limited degree and thus to introduce the "human judgement" factor into the analysis.

It may also be possible to introduce more data points into the analysis by assuming a gaussian shape to the latitudinal distribution of the absorbing region, in the case where data for an isolated station is available. Such a modification was not tried.

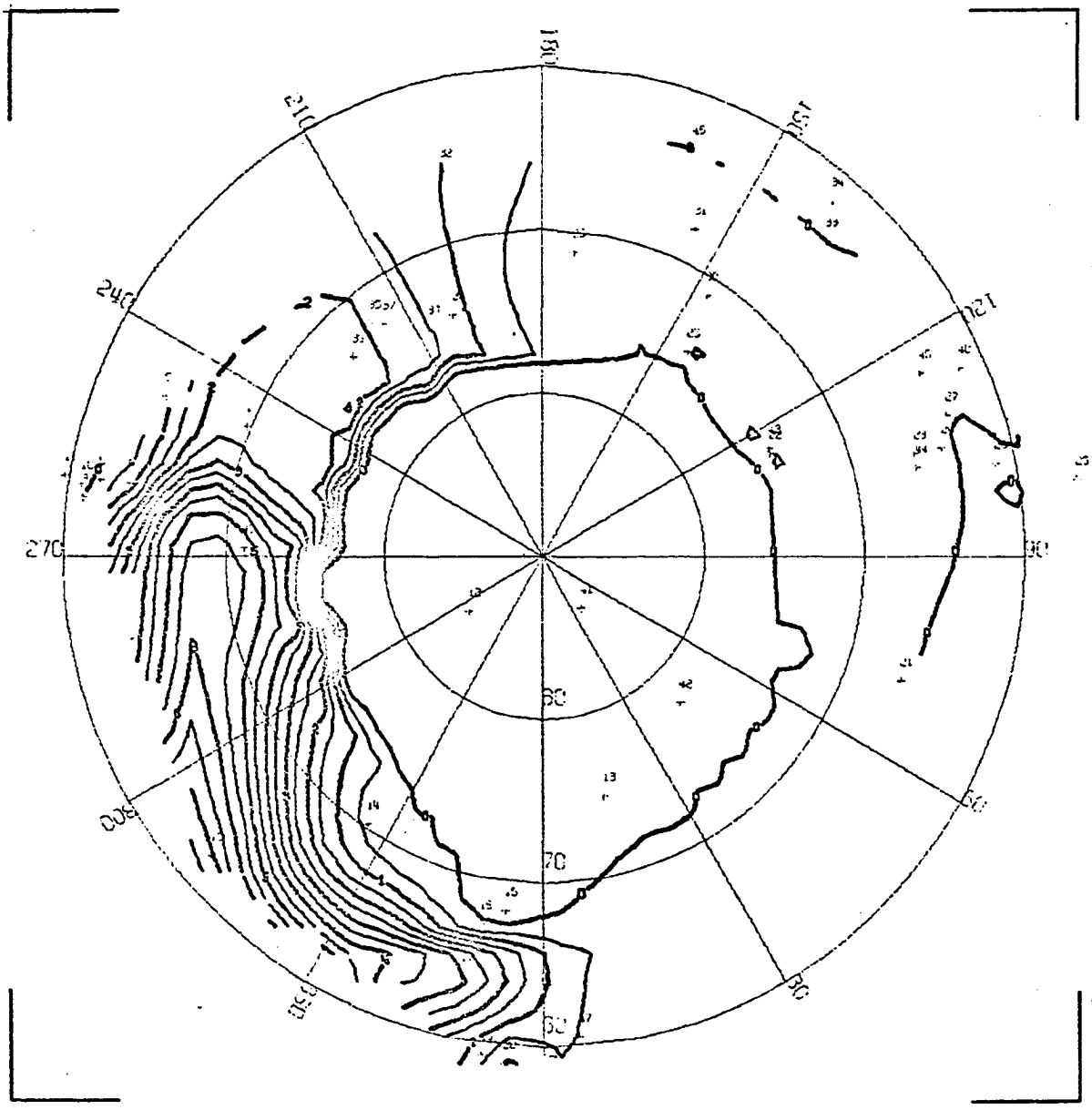

Figure (8.63) Modification of the contours of Figure 8.17.

CHAPTER 9

ANALYSIS OF THE MOTION OF PRECIPITATION REGIONS

9.1 Introduction

A regular pattern of development was observed in four of the five substorms studied; the predominant motions were eastward and westward. In general, poleward motions were not resolvable on the time scale used in this study; however, a poleward motion was inferred from one event which was studied in more detail. Equatorward motions per se were not observed.

While the eastward drift of auroral absorption has been extensively studied (Jelly, 1970; Driatsky, 1970), the westward expansion of absorption during an individual substorm has not been previously documented. In this study, the existence of westward drifting precipitation (WDP) has been demonstrated in four of the substorm events investigated. As will be shown later, the westward motion differs from the eastward motion in at least three significant respects: (1) occurrence at higher latitudes; (2) no dispersion of absorption with longitude, and; (3) lower average rate of propagation.

9.2 Westward Motions

During the March 26 and October 9 substorms, Fort Yukon, Point Barrow, and the floating ice island North Pole-13 were located within the auroral oval in the evening sector at 08^{h} UT. On November 7, the midnight meridian was located near the longitude of College while NP-13 was located 60° west of College, again within the auroral oval.

As the integrity of the WDP event is maintained during its lifetime, a relatively unambiguous determination of the propagation speed can be

made knowing the onset times at each station. At Fort Yukon and Point Barrow, the recording speed and time accuracy are such that onset times can be defined to within one minute. However, the onset times at NP-13 can only be determined to within three minutes. Using the onset times of absorption increases at Fort Yukon, Barrow, and NP-13, the velocities tabulated in Table XI were derived. A rate of expansion of the absorption maximum was also derived and is listed in Table XI as well.

Table XI

The Expansion Rates Derived for Westward Drifting Precipitation Events

	FYU - Barrow		Barrow - NP-13		FYU - NP-13	
	onset	maximum	onset	maximum	onset	maximum
3/26/65	842m/s	740m/s	1.72km/s	1.88km/s	1.25km/s	1.20km/s
10/9/64	2.96	2.15	2.14	3.75	2.44	2.98
11/7/65	--	--	--	--	3.56	2.80

Derived velocities range from less than 1 km/sec to more than 3 km/sec; moreover, differing expansion rates are found between Fort Yukon and Barrow than between Barrow and NP-13 for the same WPA event. No interpretation is made of the higher velocity found for the absorption maximum (i.e. Barrow - NP-13), except that such observations are not consistent with a particle drift theory, since a gradual dispersion of absorption would be expected if such were the case.

Using the average velocity of drift of the WDP, an estimate of the longitude of substorm origin can be made. Defining the substorm onset time as the time of the first negative deflection observed by magnetometers in the midnight sector, the distance along the auroral oval from

the first station observing the WDP to the midnight meridian can be found. Table XII summarizes these results:

Table XII

The Derivation of the Longitude of Substorm Origin For Three IQSY Substorms

	WDP onset time		WDP velocity	Distance along oval	Approximate longitude of substorm origin
Oct. 9	0803(FYU)	0758(MEA)	2.4km/sec	720 km	275°E
Mar. 26	0803(FYU)	0754(MEA)	1.2km/sec	648 km	275°E
Jan. 14	1130(CHEL)	1113(NP-13)	2.5km/sec	2550 km	225°E

The derivation of the midnight meridian will establish a reference to be used later in the determination of the eastward drift velocities.

The different velocities can be compared with the magnitude of the H-component decrease and intensity of absorption at the observing station. From Table XII it is apparent that the lower expansion rates are associated with the less intense absorption and H-component decrease.

Table XIII

A Comparison of the Magnitudes of Absorption Increase and H-component Decrease During WDP Events

	FYU	Barrow		NP-13		Chelyuskin	
	db	db	γ	db	γ	db	γ
Nov. 7	9.7	-	750	3.1	-		
Oct. 9	4.1	6.8	1375	2.2	325		
Mar. 26	2.9	3.75	750	0.7	225		
Jan. 14						1.9	500

During the substorms of November 7, October 9, and March 26 the WDP events were seen from 2250 to 2460 kilometers west of the substorm origin; these distances are the same order of magnitude as estimated by Akasofu et al. (1966) for the westward propagation of the WTS. It should also be noted that absorption was recorded at NP-13 from 11 to 35 minutes after the onset of the substorm. This corresponds with the duration of the expansive phase of the auroral substorm, during which time the WTS is observed.

Meng (1965) investigated a large number of WTS events, a summary of which is reported by Akasofu, Kimball and Meng (1965). He classified the surges as weak, medium, and intense according to their complexity in structure and their brightness. In general, higher propagation velocities were associated with the intense surges; more than 20 per cent of the surges investigated had speeds in excess of 1 km/sec. The greatest observed velocity was on the order of 2 km/sec (Kimball, private communication). It should be noted that, in contrast with the method used to find the speed of the WDP events, Akasofu and his co-workers projected successive all-sky camera frames from a single station onto a plane surface and computed the propagation speed from the resulting displacements as a function of time.

Meng (1965) also examined riometer records, where available, and based on a comparison of those records with the data investigated in this study, the WTS events assumed to be associated with the WDP events presented here may be classified as intense. Meng (1965) showed that the WTS is confined in a very narrow latitudinal region, generally less than 200 km in extent. The ground projection of an intense surge

recorded at Barrow on February 22, 1958 is shown in Figure 9.1. Sketched on this figure are the antenna patterns of three hypothetical stations located 100 kilometers apart and the location of the WTS at two successively later times. Assuming a propagation speed of 1 km/s, a station at B would observe the effect of the WTS (or WDP) on a riometer nearly four minutes prior to the time the same event would be seen if the station were situated at either A or C. Thus, the location of a station with respect to the surge may account for the differing propagation speeds found between the two pairs of stations used in this study. Referring to the same diagram, it should be noted that a station located at point B will observe a greater magnitude of absorption than a station at point A, since the beam pattern at point A is not completely filled. This assumes, of course, that the surge is uniformly intense and that the WDP corresponds spatially with the WTS.

Although the alignment of Fort Yukon, Barrow, and NP-13 within the auroral oval in the evening sector is rather fortuitous, it is possible to find other such alignments within the existing network of riometer stations. For example, the configuration of stations defined by Tixie, Cape Zhelania, and Bear Island or Tromsø, Reykjavik, and Narssarssuaq should be favorable for observing WDP events. Records from these stations should be examined for such events.

In several papers Jelly (Jelly, 1968, 1970; Jelly and Brice, 1967) has depicted a number of absorption events in the Canadian sector which were used to illustrate the poleward motion of absorption during a substorm. Examining the alignment of Cape Jones (or Great Whale) and Churchill with respect to the auroral oval in the evening and midnight

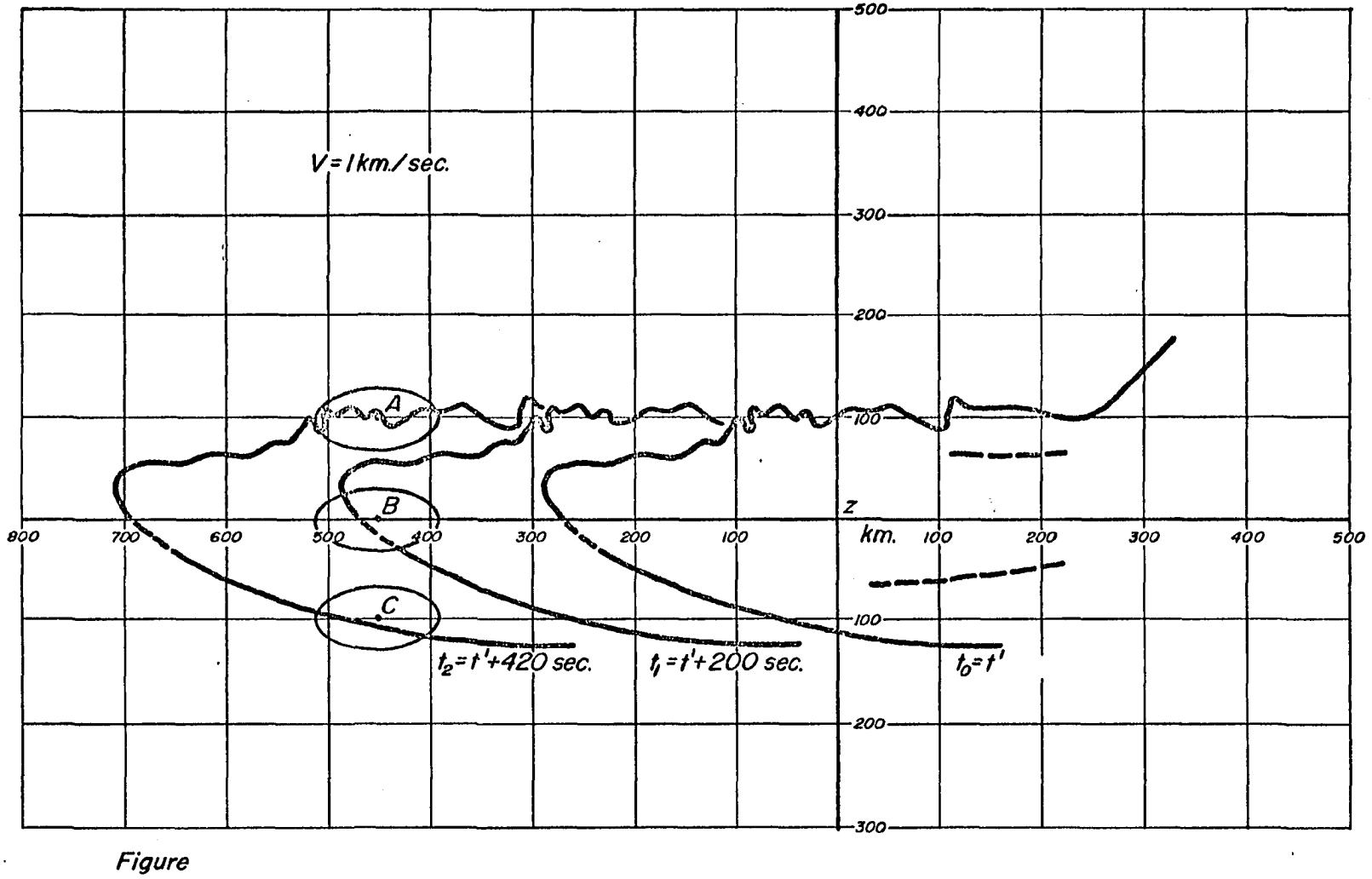

Figure

Figure (9.1) The ground projection of an intense surge (after Meng, 1965) at three successive time intervals. The ellipses A,B,C, represent the ground projections of the Yagi antenna patterns at stations located 100 km apart.

sector, it is immediately obvious that the consistent time delay between Cape Jones and Churchill noted by Jelly and Brice (1967) can be explained by the expansion speed of the WDP as well as by a poleward motion. Figure 9.2 (Jelly, 1970) graphically illustrates a WDP event and demonstrates the limited latitudinal extent of these events; maximum absorption is recorded at Cape Jones North slightly after appearing in the Great Whale River record (note that Great Whale is 155 km east of Cape Jones) while it is seen several minutes later only one degree (100 km) farther south. The ten minute time delay of onset times at Cape Jones North and Churchill implies a propagation speed of 1.5 km/sec. This would also explain the approximate 2 minute time delay between onsets at Great Whale and Cape Jones North.

The magnetogram from Baker Lake, located on approximately the same longitude as Churchill but 5° farther north and poleward of the oval, shows no activity at 0600 UT. However, at approximately 0620 UT a sharp onset negative bay is observed. This negative bay coincides in time with the second absorption maximum observed in the Churchill riometer record. At Resolute Bay (84.3°N) a positive increase of the X-component is seen, which infers that a WTS occurred at a lower latitude.

Further evidence of the WDP events could be gathered from a third station located west of Churchill. During the period 05^h - 07^h UT, a station at Yellowknife would be desirable. In conjunction with a riometer currently operating at Inuvik, four stations (including Cape Jones) would be favorably located with respect to the auroral oval to observe WDP events.

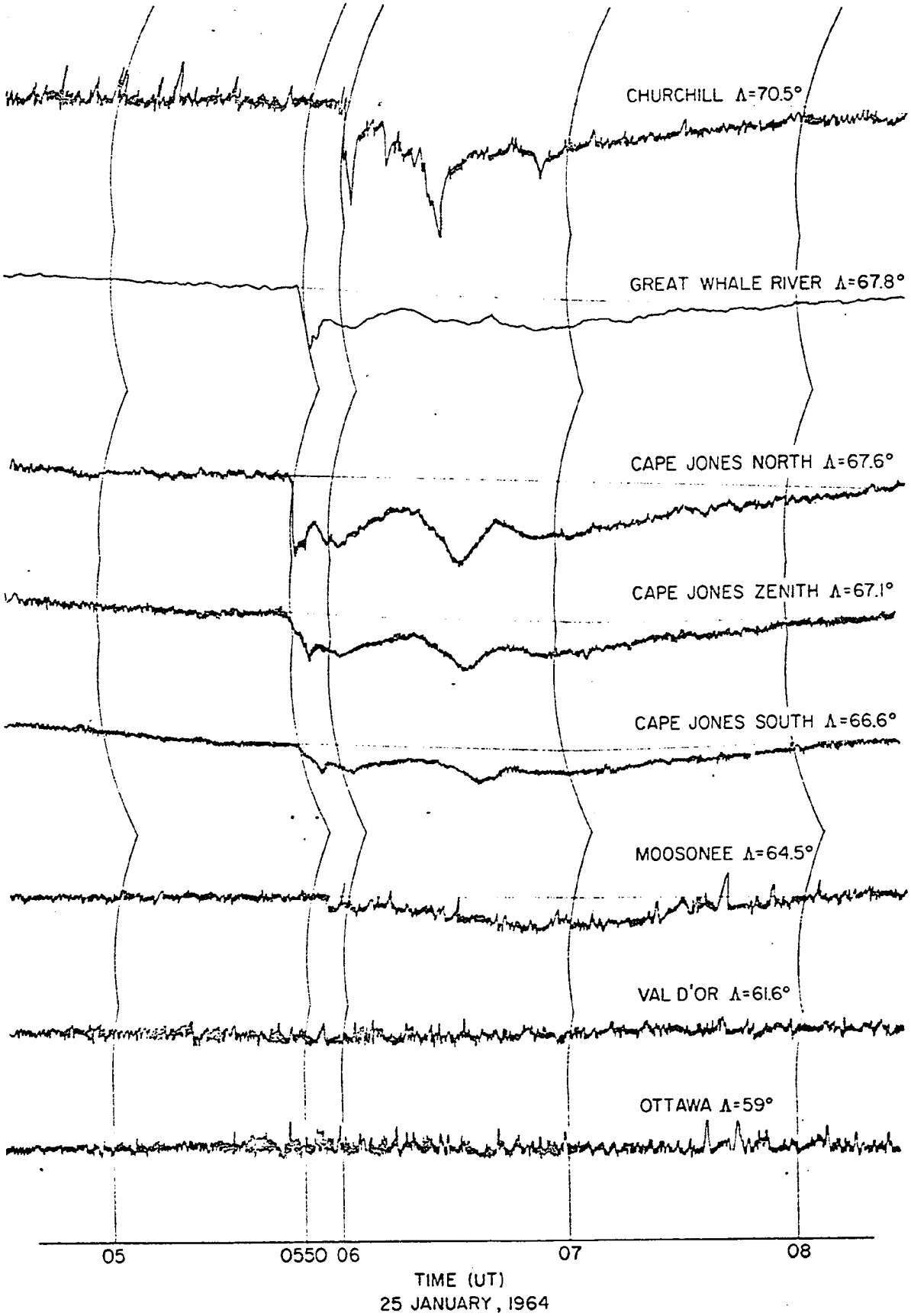

Figure (9.2) This example (from Jelly, 1970) is used to illustrate a WDP event observed in the Canadian data. Note the progression of the onset of the event between Great Whale River, Cape Jones and Churchill, all situated in the auroral oval at 06^{h} UT.

9.3 Eastward Motions

Eastward drifting precipitation (hereafter abbreviated EDP) occurred during all of the substorms investigated herein. However, the exact determination of onset times was made somewhat ambiguous because of the less rapid increase of absorption with increasing distance from the midnight sector. The time at which the rate of increase exceeded ∿0.2 db/minute was defined as the onset of the EDP event. Similarly, the time of absorption maximum was often difficult to define, but was normally defined by the first time maximum absorption was reached. As will be shown below, EDP was confined in an approximately circular zone, coinciding with the auroral oval on the night side of the earth and the auroral zone on the day side.

For all but the August 2 substorm, the times of absorption onset and maximum were determined for each station as a function of longitude from the substorm origin. Except for the November 7 substorm, the longitude of the substorm origin was estimated from a knowledge of the associated WDP event (the error of such an estimation is at least 5°). Plotting absorption onset and maxima time differences against latitude and degrees longitude from substorm origin, Figure 9.3 was prepared.

The onset of the EDP event is almost simultaneous with the onset of the substorm at longitudes up to 40° east of the substorm origin in the latitude range 62° - 68°, but maximum absorption occurs up to 30 minutes later. From 75° - 90° east of the origin, EDP events appear first at latitudes less than 66°, then 5 - 20 minutes later at both higher (>68°) and lower (<62°) latitudes (note, however, that there

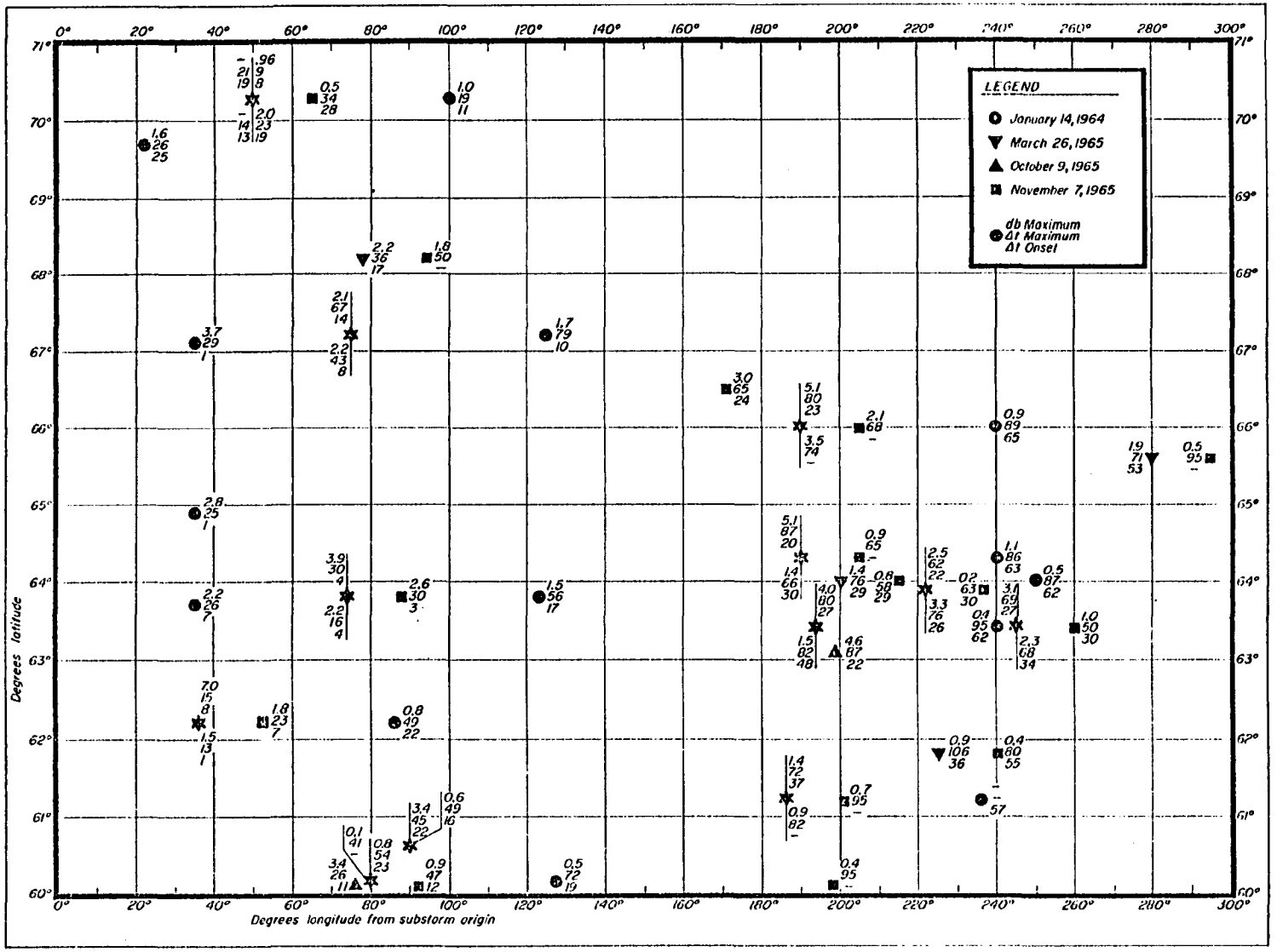

Figure (9.3) The time of onset, maximum and magnitude of EDP events for the substorms of January 14, 1965, March 26, 1965, October 9, 1964 and November 7, 1965 have been denoted in this diagram.

are no data in the range 64° - 67°). Maximum absorption is also delayed with respect to the onset in this longitude sector. From the longitude of substorm origin to 90°, in the 62° - 64° interval, the EDP_o (o for onset) travels at a rate of approximately 9.5°/minute (∿475 km/minute) and the EDP_m (m for maximum) at ∿2°/minute. In the 68° - 71° interval the EDP_o speed is ∿6°/minute and at latitudes less than about 62°, ∿5°/minute. For both these latitude intervals, the EDP_m speed is approximately 2°/minute.

While only one set of measurements falls in the interval 90° - 180° and relates to only one substorm, several sets of measurements can be found in the 170° - 210° sector. In this sector, there seems to be a tendency for EPA_o to be seen earlier in the 64° - 66° latitude range, whereas it appeared first in the 62° - 64° interval over the 30° - 90° longitude range. Further evidence for this trend is obtained by comparing the ratio of EDP_o at 66° - 68° to EDP_o at 62° - 64°; in the 30° - 90° range this ratio is 3, while the same ratio is less than 1 in the 170° - 210° sector. Ansari (1965) and Rosen (1969) have documented the earlier occurrence of absorption in the noon sector at ∿67° than at ∿63°. For latitudes 63° - 67°, the EDP_o drift rate to the 200° longitude is ∿7°/minute (330 km/min) and the EDP_m drift is ∿2.6°/minute. Between 90° and 200° the EDP_o drift rate is approximately 5°/minute, or slightly less than half of the speed derived for propagation to the 90° longitude. Note that the EDP_m is slightly higher than the corresponding value derived to the 90° meridian. At latitudes less than 64°, the EDP_o drift speed was ∿5°/minute and the EDP_m drift speed ∿2.6°/minute.

A number of measurements were available near 240° and two distinct onset times were evident; approximately 30 and 60 minutes, the latter value relating to a single substorm and the former to 3 separate substorms. An average value of the longer time was combined with the other values to derive an EDP_o drift rate of 6.2°/minute and EDP_m drift rate of ∿3°/minute for latitudes in the range 62° - 66°.

The drift velocity of the EDP event is of the same order of magnitude as Akasofu (1968) found for the process of disintegration of arcs from the midnight sector to the morning sector; he quotes a range of 3 - 10 km/sec (180-600 km/minute) for the propagation speed of this region of disintegration. Note the distinction between this velocity and that of individual patches in the morning sector; patches drift at a rate of ∿300 meters per second, which corresponds closely to the propagation speed of EDP_m in the morning sector. Akasofu (1964) indicates that the eastward drift motion tends to occur near the equatorward boundary of the auroral oval; this is also consistent with the observations of EDP presented here. From these observations, it can be concluded that the regions in which EDP events occur and that of eastward motion during the auroral substorm are coincident.

It is interesting to note that at latitudes >70°, in the midnight dawn sector, events structured similarly to those observed in the evening and midnight sectors are seen. These events appear to be associated with the maximum in absorption at lower latitudes.

It is postulated that these events are associated with the rapidly propagating Ω bands, so called due to their appearance in all-sky camera films. These bands are usually of greater intensity than other

forms appearing in the sky at the same time. A single intense Ω band may produce a sudden, sharp increase in absorption such as observed in this study. Akasofu (1964) observed these bands near the poleward boundary of the region of eastward drift motion; in this study the associated absorption events were in all cases observed at latitudes greater than 69°. There also appears to be an increase in the time between onset and maximum absorption as one progresses eastward from the midnight sector; this could be attributed to a decrease in propagation velocity of the Ω band. Note also that these events are not observed beyond about the 100° meridian and the latest time after a substorm onset was approximately 30 minutes. This observation is consistent with the duration of the expansive phase of the auroral substorm, during which time the Ω bands are observed.

9.4 Poleward Motions

During the substorm which commenced at approximately 0955 UT on November 7, 1965, 8 riometers were operating within Alaska covering a latitude range of 10° and 13° of longitude. The 30 minutes following the substorm onset were scaled at 1 minute intervals; these values are displayed in Figure 9.4. The striking feature of this figure is the spike-like increase of absorption at Fort Yukon, Allakaket and College. The magnitude of this spike increases dramatically with latitude, reaching more than 9.7 db at Fort Yukon. The secondary maximum, reached within 5 minutes of the time of the spike absorption, was seen at all stations except Farewell and Anchorage. Peak absorption during the secondary maxima was recorded almost simultaneously at College and Healy and then at Allakaket, Kotzebue, Fort Yukon and Bar-l.

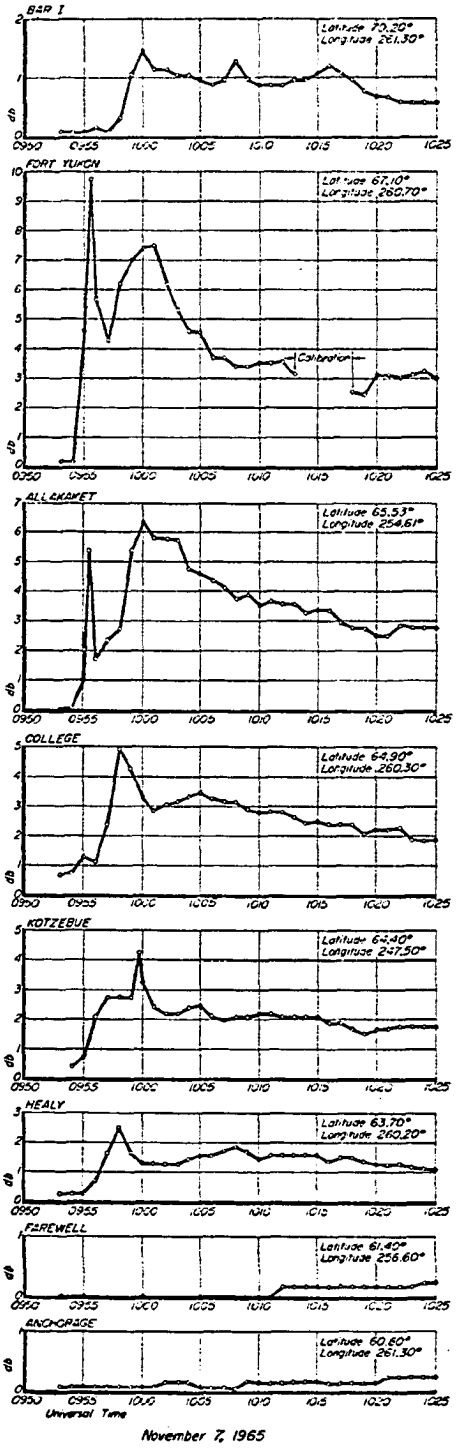

Figure (9.4) A detailed representation of the substorm event of November 7, 1965 at eight Alaskan stations.

Converting these time differences into propagation speeds, a 5 km/sec poleward and a 6 km/sec westward (from College) velocity can be derived. These speeds are consistent with the growth speeds derived for the expansion of the absorbing region.

It is suggested that the structure of the absorption as illustrated by the Allakaket and Fort Yukon records is typical of events recorded near the midnight meridian. It is postulated here that the spike absorption defines the location of the substorm origin in time and space.

9.5 Equatorward Motions

A purely equatorward motion was not observed; although the expansion of the substorm in the midnight sector appears to have a minor equatorward component, the other components are predominant. In the morning and day sectors, absorption occurs later at lower latitudes, but this can be attributed to the slower or differential eastward drift of absorption to these latitudes rather than an equatorward or meridional motion.

9.6 Anomalous Absorption Occurrences

During two of the substorms, significant departures from the overall pattern of development of the auroral absorption substorm were noted. On March 26 at Isfjord (74.6°N, 113.9°E) an absorption event of 2 db magnitude developed at approximately 0957 UT, some two hours after the onset of the substorm in the midnight sector. Isfjord was located within the auroral oval at this time as were both Heiss and Chelyuskin. Although there was no riometer data available from Heiss, there was no significant magnetic variation near 10^h UT. Thus, it is considered unlikely that

the absorption at Isfjord could have been caused by particles which migrated westward along the auroral oval from the midnight sector.

On October 9, two absorption events were recorded at Tixie, located well equatorward of the auroral oval at 08^h UT. The first event began at 0758 UT, coincident with the onset of the substorm in the midnight sector. No associated change was evident in the Tixie magnetogram. At 0807 UT the second event was initially recorded, reaching a maximum at 0820 UT. This event was coincident with a positive bay in the H-component at Tixie and also with a WDP event recorded at NP-13 (situated within the auroral oval) at 0814 UT. Projecting the WDP event along the oval, it reaches the longitude of Tixie in approximately six minutes, or at the time of maximum absorption at Tixie, 0820 UT. While such events need to be studied in more detail, it is suggested here that they are associated with moderate to intense magnetic substorms (K_p>4) during which a WTS occurs 6° - 7° poleward of the station. Such absorption may maximize during the expansive phase of the substorm and occurs preferentially within the auroral zone. It is interesting to note that during the March 26 substorm no magnetic activity was observed at Tixie (riometer data missing from 0800-0845 UT). However, during this storm the magnitude of both the magnetic activity and absorption was less than during the October 9 substorm.

9.7 A Model of the Auroral Absorption Substorm

A diagrammatic picture of the auroral absorption substorm development is given in Figure 9.5. This idealized picture is similar to that derived by Akasofu (1968) (see Figure 6.1) but is based on the analysis of the substorm events discussed previously. The onset of the auroral

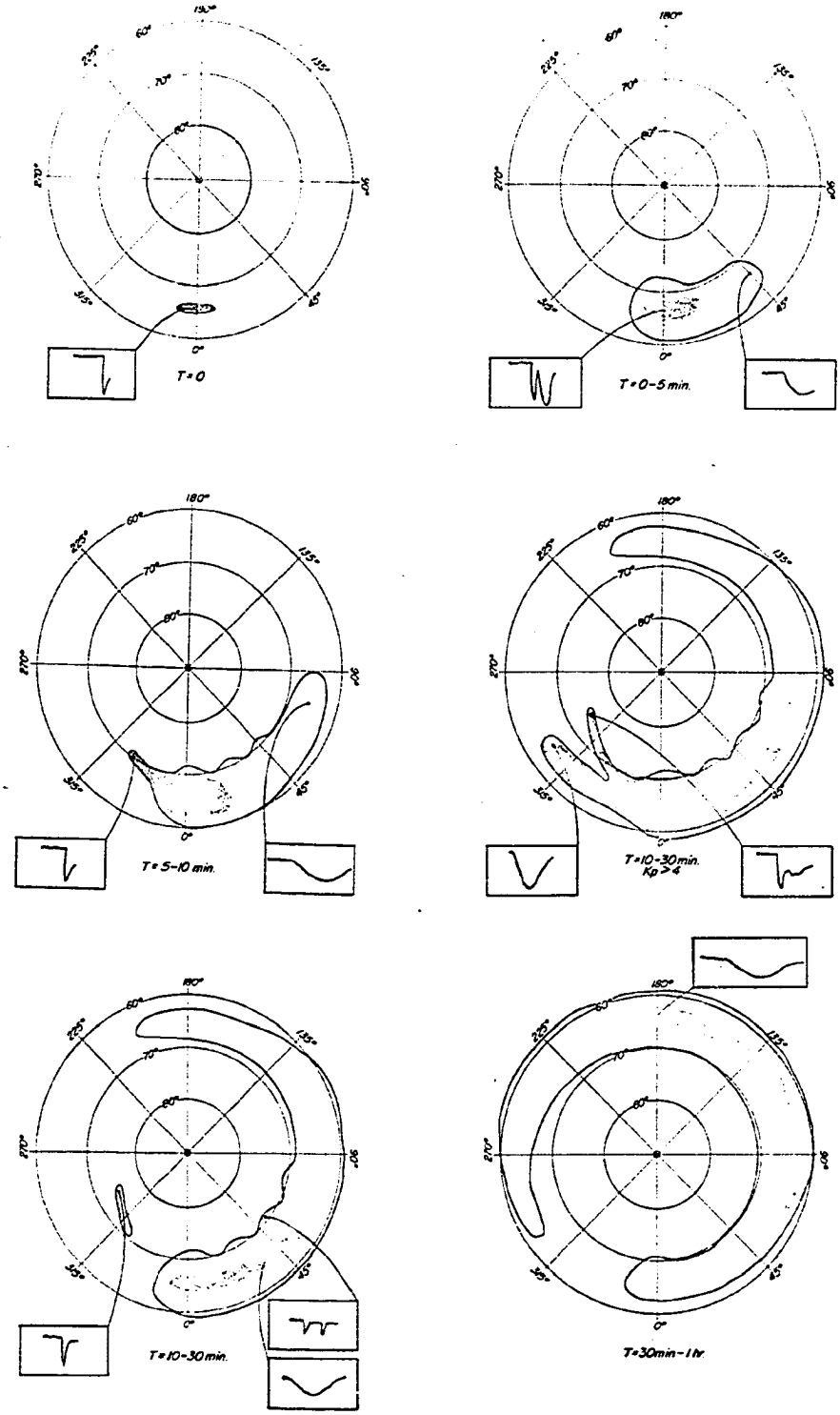

Figure (9.5) A model of the pattern of precipitation during the auroral absorption substorm. The shaded areas denote regions of most intense precipitation.

absorption substorm (T = 0) is defined by a sudden increase in absorption from a relatively quiet background level; the region in which this increase occurs is limited latitudinally, but probably extends over 15° - 30° of longitude. During the next five minutes (T = 0-5) the absorbing region expands rapidly and absorption occurs over 60° of longitude and 10° - 12° of latitude; in the midnight sector, intense absorption is associated with the motion of the poleward advancing bulge and the rate of increase of absorption is high. Absorption increases at a less rapid rate eastward of the midnight sector.

During the interval T = 5-10 minutes, rapid onset absorption events occur west of the midnight sector, along the auroral oval. At the same time absorption continues to expand eastward, reaching the dawn meridian by T = 10 minutes.

Two pictures have been derived for the interval T = 10-30 minutes; the one represents substorms during which the K_p index is greater than 4 and the other represents substorms of lesser magnitude. During this period absorption is still observed along the auroral oval west of the midnight meridian; if the substorm is particularly intense, the absorption along the auroral zone is of greater duration while occurring simultaneously with absorption in the auroral oval. By T = 30 minutes, absorption has propagated to the noon meridian; during the more intense substorms, the latitude of maximum absorption moves equatorward and the propagation speeds are higher. A non-uniform poleward boundary of the absorbing region is depicted because of the association of absorption with the propagation of eastward moving Ω bands.

The last diagram of Figure 9.5 represents the propagation of absorption during the interval T = 30 minutes - 1 hour; the region in which intense (>1 db) absorption occurs is now concentrated in the dawn-noon sector. No structured absorption is seen at this time since WDP events and Ω band absorption occurs only during the expansive phase of the auroral substorm. There is some evidence that absorption may extend back into the midnight sector, propagating along the auroral zone in an easterly direction.

9.7.1 Comparison with statistical auroral absorption zone

Statistical patterns of auroral absorption at high latitude (see Figure 9.6) are not entirely consistent with the pattern of absorption derived in this study. This is not an unexpected result, considering the analogy that can be made with visual auroral studies; the statistical measurements of visual aurora defined a circular auroral "zone" at approximately L = 5.5. However, the work of Akasofu (1964) and Feldstein (1963) showed that during the course of an individual substorm auroras exist within an oval shaped region. It is now recognized that the locus of the midnight region, where the brightest auroras occur, traces out what was previously defined as the auroral zone. Analogously, the most intense absorption occurs near L = 5.5, so that statistical studies which measure the percentage of time absorption exceeds a given level will yield a circular zone of absorption.

The statistical pattern derived by Driatsky (1966) suggests the occurrence of absorption near 80°N at 17^h GT. He found that "a secondary maximum is observed in the vicinity of midnight ($00\text{-}01^h$). It appears at all latitudes and shifts to late evening hours as we move north."

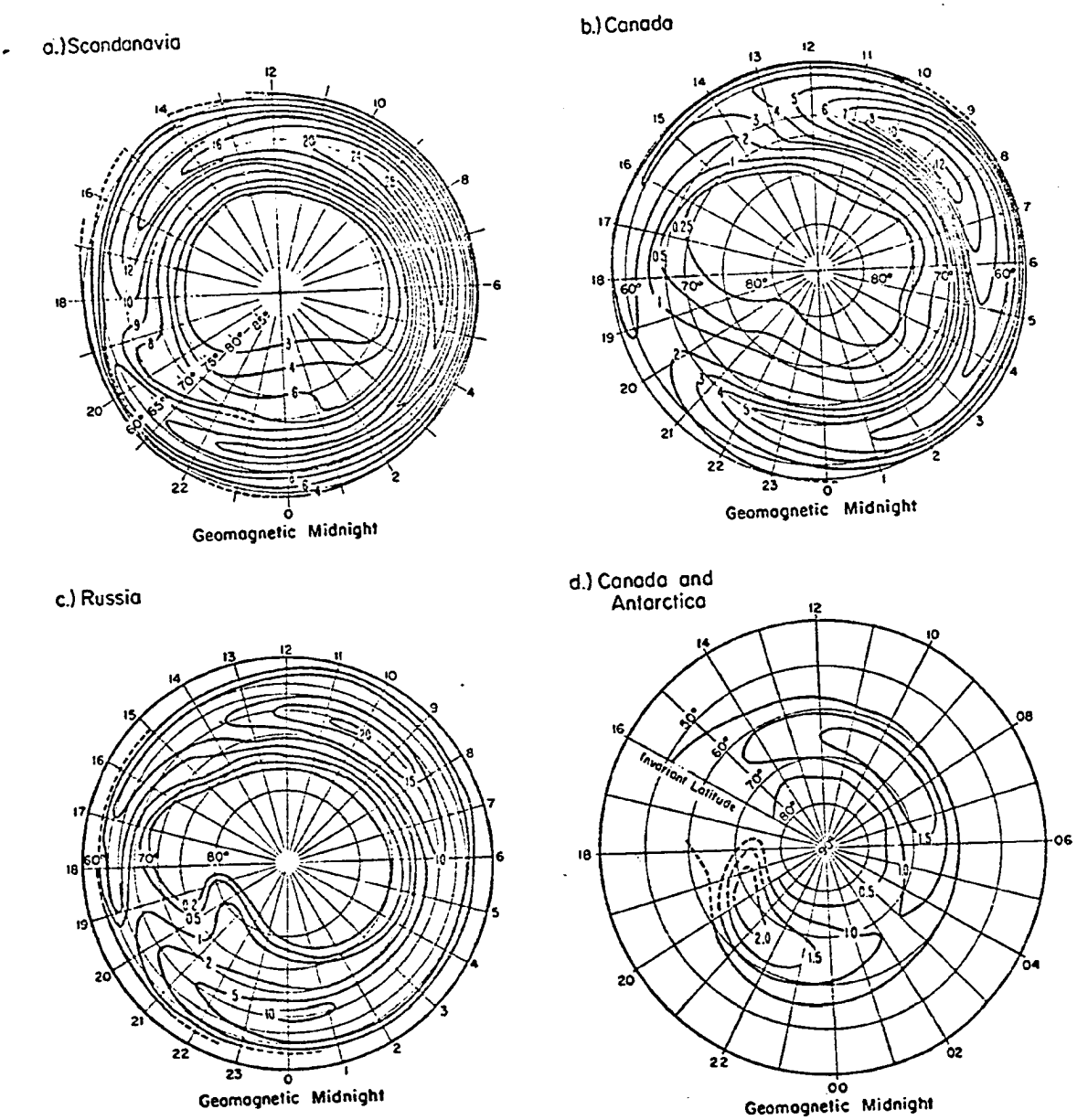

Figure (9.6) Occurrence of auroral absorption in latitude and time, measured at several longitudes (after Hargreaves, 1969).

Similarly, the pattern of Hargreaves and Cowley (1968) tends to confirm the pattern observed in this study. They found a maximum in absorption extending from approximately 73°N at 18^h GT to 64°N at 23^h GT. Discussing this feature of their pattern, Hargreaves and Cowley (1968) note that "the night events are shorter and more structured than day events so that they tend to be emphasized by the event technique and suppressed by methods based on a percentage of time." Additionally, they assumed a gaussian shape to the auroral absorption zone in deriving their pattern.

In this study, it has been shown that in the sector in which several statistical studies yield a minimum in absorption frequency (17^h-19^h GT), strong absorption occurs at high latitude (72° - 74°N). Those patterns which do not show this feature can be explained by: (1) lack of observing stations at high latitude (Hook); (2) the method of deriving the pattern (Holt et al., Hartz). It should be noted that with the exception of the evening sector, the results of this study agree with the patterns shown in Figure 9.6(a) and 9.6(b).

9.8 Magnetospheric Models

Through the use of magnetospheric models, it has become feasible to study a number of physical processes that occur within the magnetosphere and thereby to predict the results of such processes and to compare the results with experimental measurements. Roederer (1969) discusses six physical processes of this type:

(1) trapped particle motion;

(2) particle flux mapping in the outer magnetosphere;

(3) trapped-particle time variations;

(4) plasma convection and DC electric field;

(5) high-latitude conjugate-point phenomena;

(6) low-energy cosmic ray propagation.

In this study we will be concerned with the drift period of electrons trapped by the magnetic field.

Roederer (1969) succinctly describes the need for magnetospheric models: "the broad purpose of a magnetospheric model is to provide a mathematical description of the field (analytical or numerical) that is reasonably accurate within a given limited spatial and temporal domain and that can be used to study in a quantitative way any physical process influenced or governed by this field."

Two models are frequently referenced in the literature: the Mead-Williams model (Mead, 1964; Williams and Mead, 1965) and the Taylor-Hones model (Hones, 1963; Taylor and Hones, 1965; Taylor, 1966). The former is often referred to as a 'physical' model in that parameters of the model represent physical sources of the field, while the latter model is described as a 'mathematical' model since it is based on an image-dipole representation of the field, and variable parameters do not represent physical sources.

The Roederer computer program (Roederer, private communication) is a Fortran language program based on the Mead-Williams model of the magnetosphere. According to Roederer (1967), the "model considers two sources, in addition to the internal dipole; currents in the magnetopause and currents in the tail of the magnetosphere. Four adjustable parameters determine the field in Mead's model: (1) the distance R_s from the center of the earth to the magnetopause, in the solar direction; (2) and (3), the distances R_n and R_f from the center of the earth to the close and

far limit, respectively, of the neutral sheet in the anti-solar direction; and (4) the field intensity B_t near the neutral sheet. Most of the typical variations of the geomagnetic field can be simulated by appropriate variations of these parameters." According to Roederer (1970) typical quiet time values are: $R_s = 10\ R_e$, $R_n = 10\ R_e$, $B_t = 15$ gammas, $R_f = 200\ R_e$. To obtain the results discussed in the following sections, the values $R_s = 8\ R_e$, $R_n = 8.67\ R_e$, $B_t = 30$ gammas, $R_f = 200\ R_e$ were used in the program. This choice of parameters simulates the initial phase of a magnetic storm.

9.8.1 The mathematical formulation

Roederer (1970) outlines the basic operations which comprise the computer shell tracing code in the absence of external forces:

(a) magnetic field determination;

(b) field line tracing;

(c) determination of the integrals

$$I = \int_{s_m}^{s'_m} [1 - B(s)/B_m]\, ds, \quad S_b = \int_{s_m}^{s'_m} ds/[1 - B(s)/B_m]^{1/2}$$

(d) iteration to find the mirror point of a particle with parameters I, B_m, and;

(e) determination of the bounce-average drift velocity. The latter operation is the most pertiment here since drift times are to be calculated.

The expression used to determine the drift velocity is given by

$$\langle \bar{V}_o \rangle = \frac{mv^2 v_o I}{q\, S_b B_o} \times \bar{e}_o$$

where B_o is the field strength and S_b and I are defined above. Roederer

(1970) shows that this expression is the bounce-average of the gradient-curvature drift velocity and can be expressed in vector form as

$$\bar{V}_{cg} = [mv^2/2qB_s^2] (1 + \cos^2\alpha_s) \nabla_o I \times \bar{e}_o$$

where α_s is the particle pitch angle and $\bar{e}_o$ is a unit vector in the direction of the magnetic field.

9.8.2 Computation of trapped electron drift period and angular velocity

The original computer program (obtained from Roederer) was structured such that a drift period was derived from the summation of drift times to 10 longitudes between the midnight and noon meridians. The program was modified (see Appendix C) to derive drift times to 12 equatorial longitudes and to calculate the angular drift velocity to each longitude. At each of the 12 longitudes the intersection with the Earth of the field line which passed through that point was calculated. This information was used to plot the trajectories of the particles on a polar grid in invariant coordinates.

The calculations of drift period and angular drift velocity were made for electrons with equatorial pitch angles of 78°, 66°, 53°, 36°, 15°, 10°, and 6°. Several observations regarding the computational results are in order: (1) the drift rate at L = 4 is nearly symmetric with respect to the dawn meridian; (2) progressing outward from L = 4, the drift rate becomes increasingly more asymmetric with respect to the dawn meridian; (3) the shortest drift period is observed for particles injected in the midnight meridian at about L = 7, and (4) at L < 4, electrons with pitch angles of 6° or less are on open field lines in this model.

The drift rate of absorption onsets was derived from Figure 9.2 (see section 9.3) and plotted at five minute intervals on a polar grid (see Figure 9.7). It is concluded from this diagram that the drift rate is greatest within the range 64° - 67° invariant latitude. The computations of trapped particle motion will be used to show that the gradient and curvature drift of such particles is not inconsistent with the observed motion of precipitation events in the auroral regions.

The drift patterns shown in Figures 9.8a to 9.8d were derived assuming the injection of a test particle at the midnight meridian (0°) at L values of 4, 5, 6, 7 and 8 at time T = 0, simulating a line source. The location of this particle at five minute intervals was calculated using the angular drift velocity and contours of 'equal drift velocity' were drawn. As the largest drift rate of precipitation events was observed at about L = 5, it was assumed that the energy of the precipitated electrons was a function of L, peaking near L = 5. A four point spectrum having a sharp cut-off at the high energy end, near those energies whose drift period corresponded most closely with the observed drift times of absorption onset, was assumed. A continuous pattern of contours of equal drift velocity can be derived by combining Figures 9.8a through 9.8d; this would account for the dispersion in the precipitation events observed eastward of the midnight meridian. It can therefore be concluded that an accelerating mechanism which drifts in the equatorial plane at the same rate as electrons undergoing gradient and curvature drift, can produce a pattern of precipitation such as observed by the synoptic study of auroral absorption.

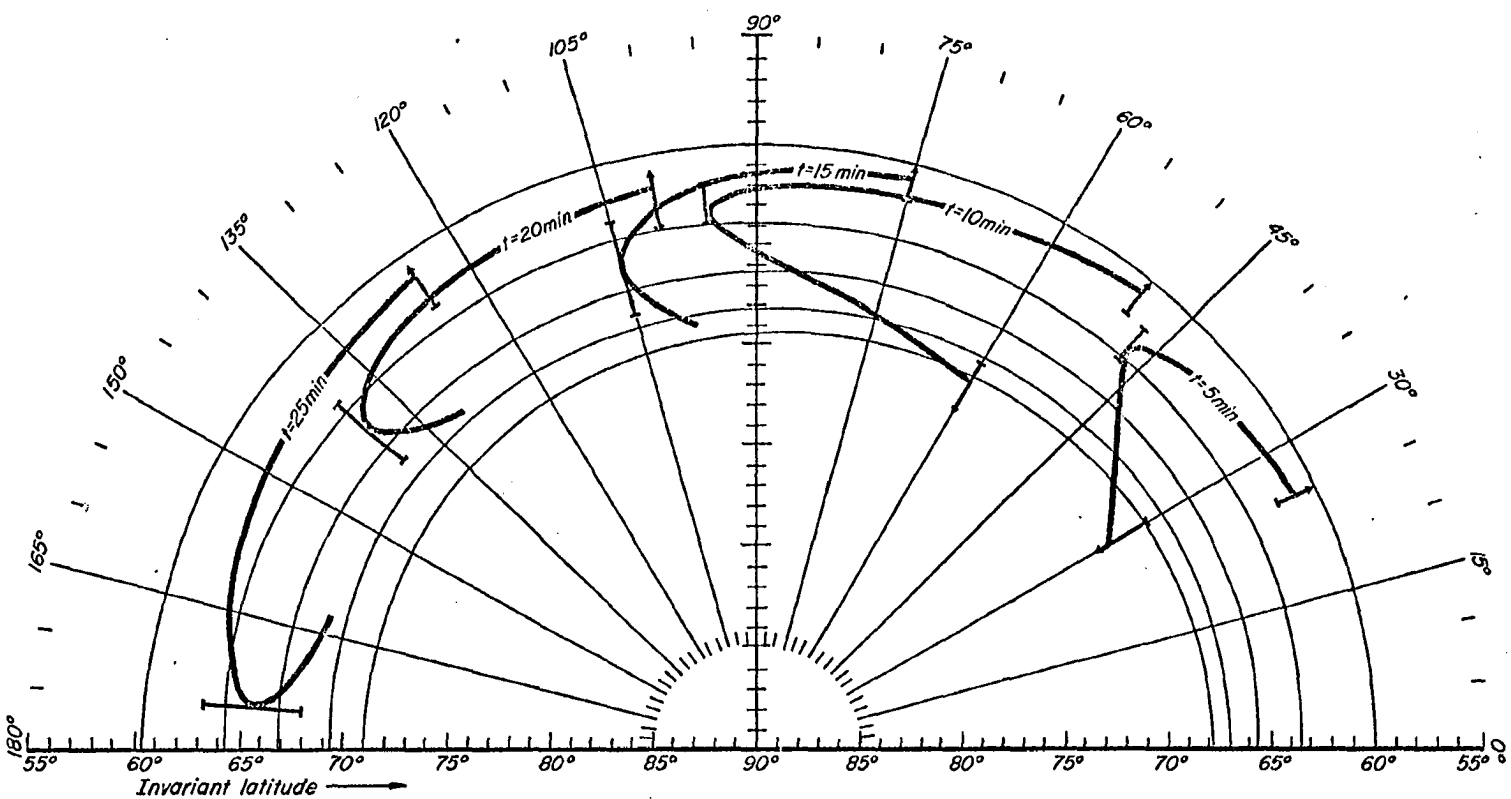

Figure (9.7) Progression of absorption onsets at five minute intervals.

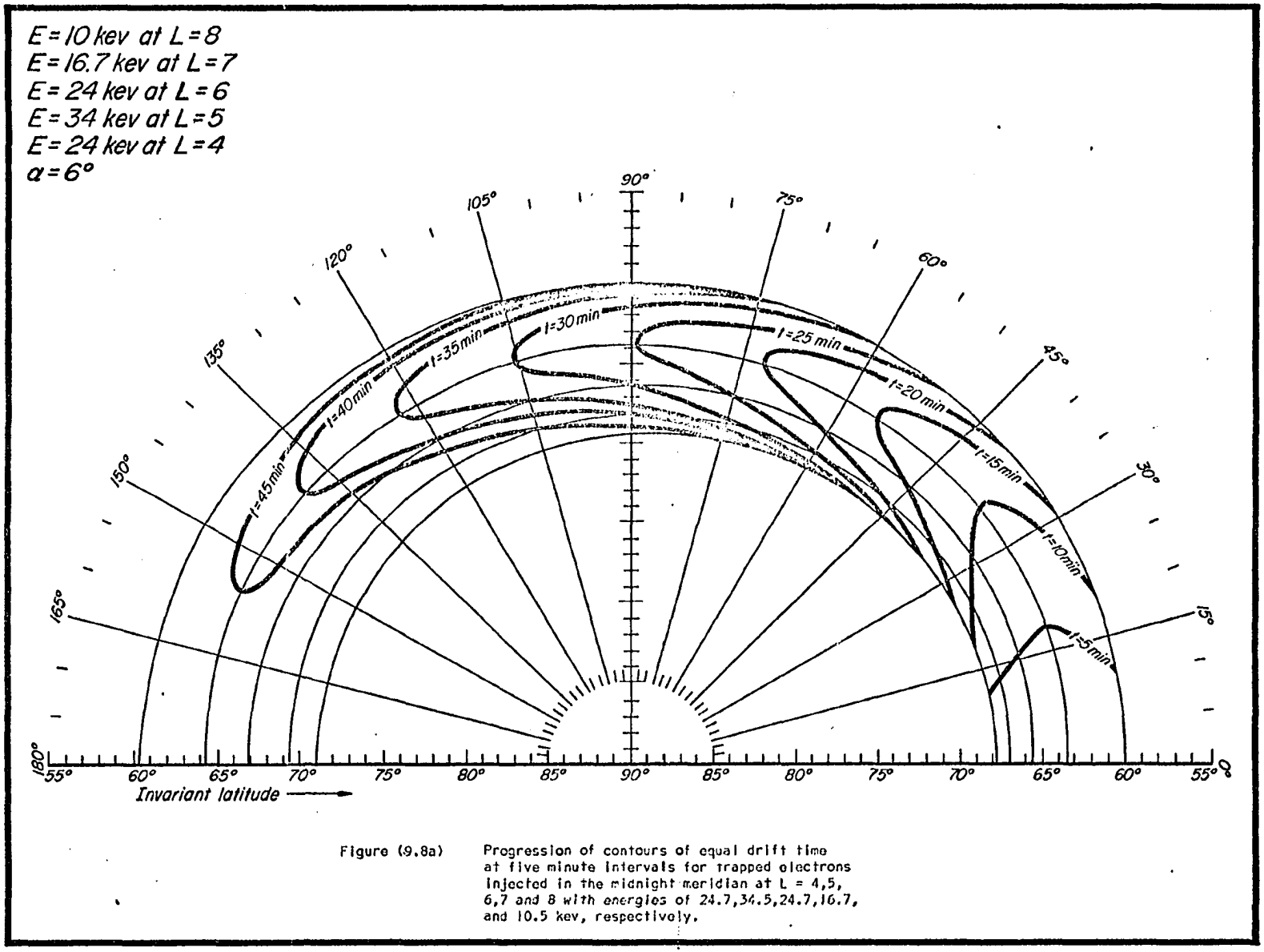

Figure (9.8a) Progression of contours of equal drift time at five minute intervals for trapped electrons injected in the midnight meridian at L = 4,5, 6,7 and 8 with energies of 24.7,34.5,24.7,16.7, and 10.5 kev, respectively.

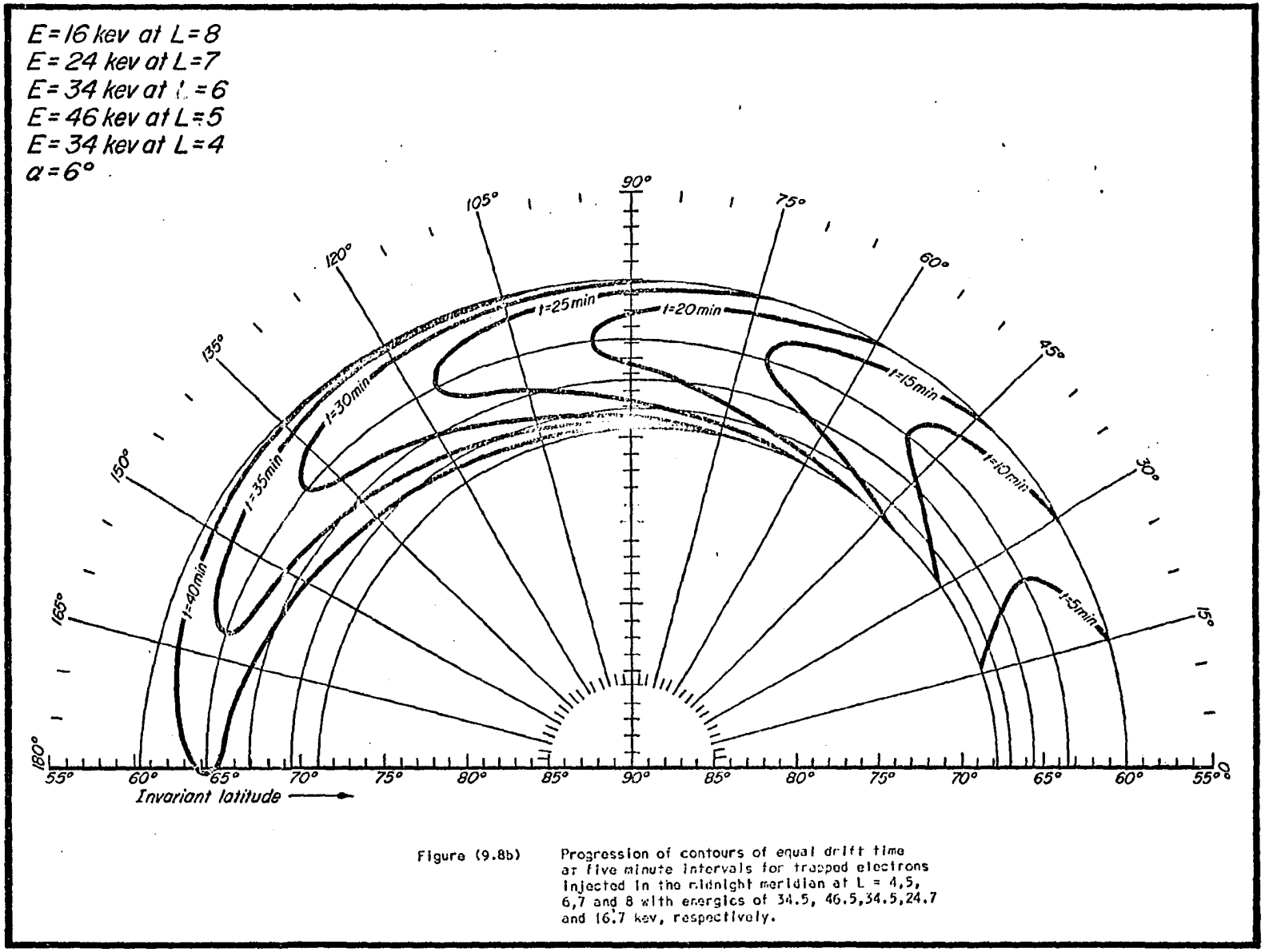

Figure (9.8b) Progression of contours of equal drift time at five minute intervals for trapped electrons injected in the midnight meridian at L = 4,5, 6,7 and 8 with energies of 34.5, 46.5,34.5,24.7 and 16.7 kev, respectively.

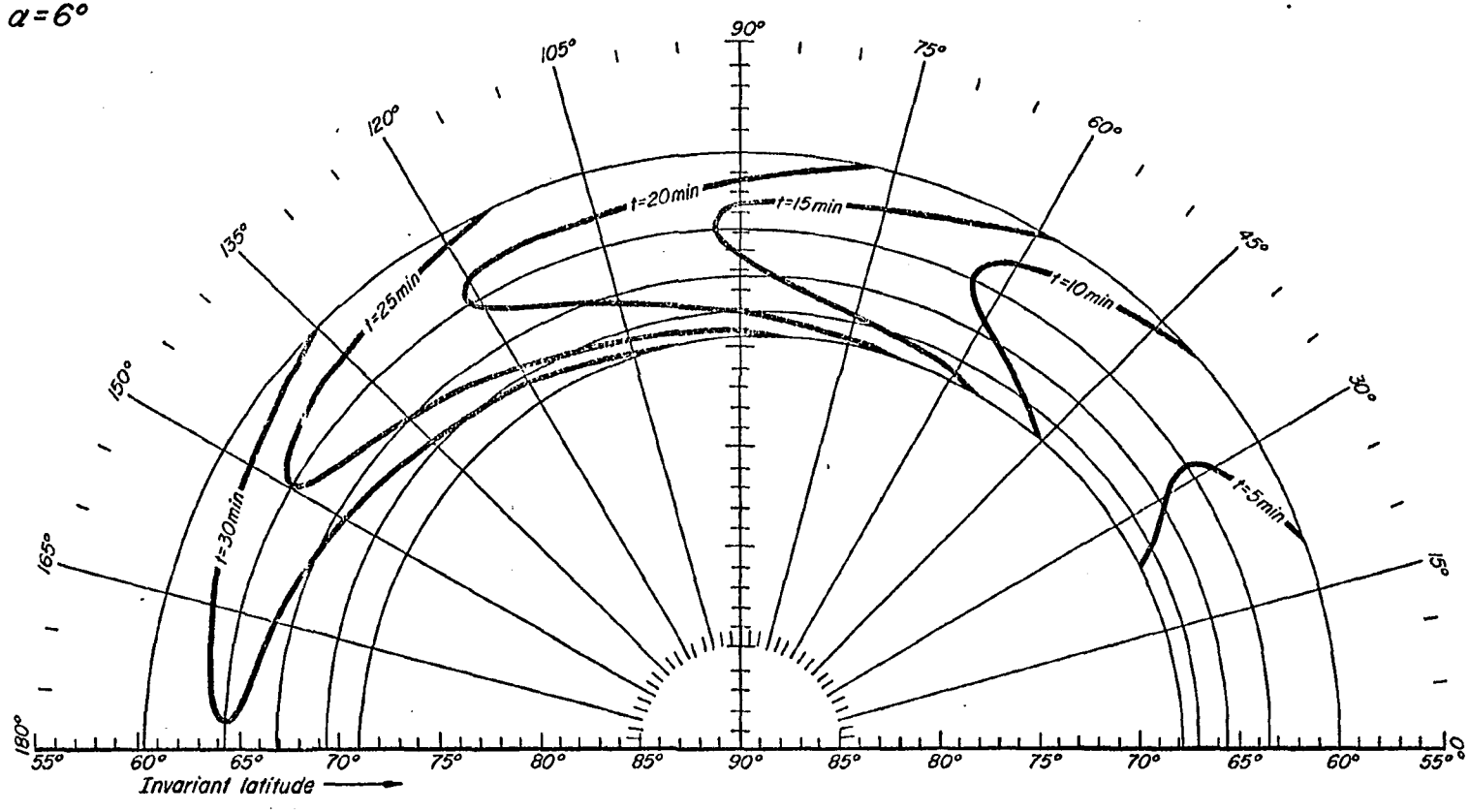

Figure (9.8c) Progression of contours of equal drift time at five minute intervals for trapped electrons injected in the midnight meridian at L = 4,5, 6,7 and 8 with energies of 46.5,61.2,46.5, 34.5 and 24.7 kev, respectively.

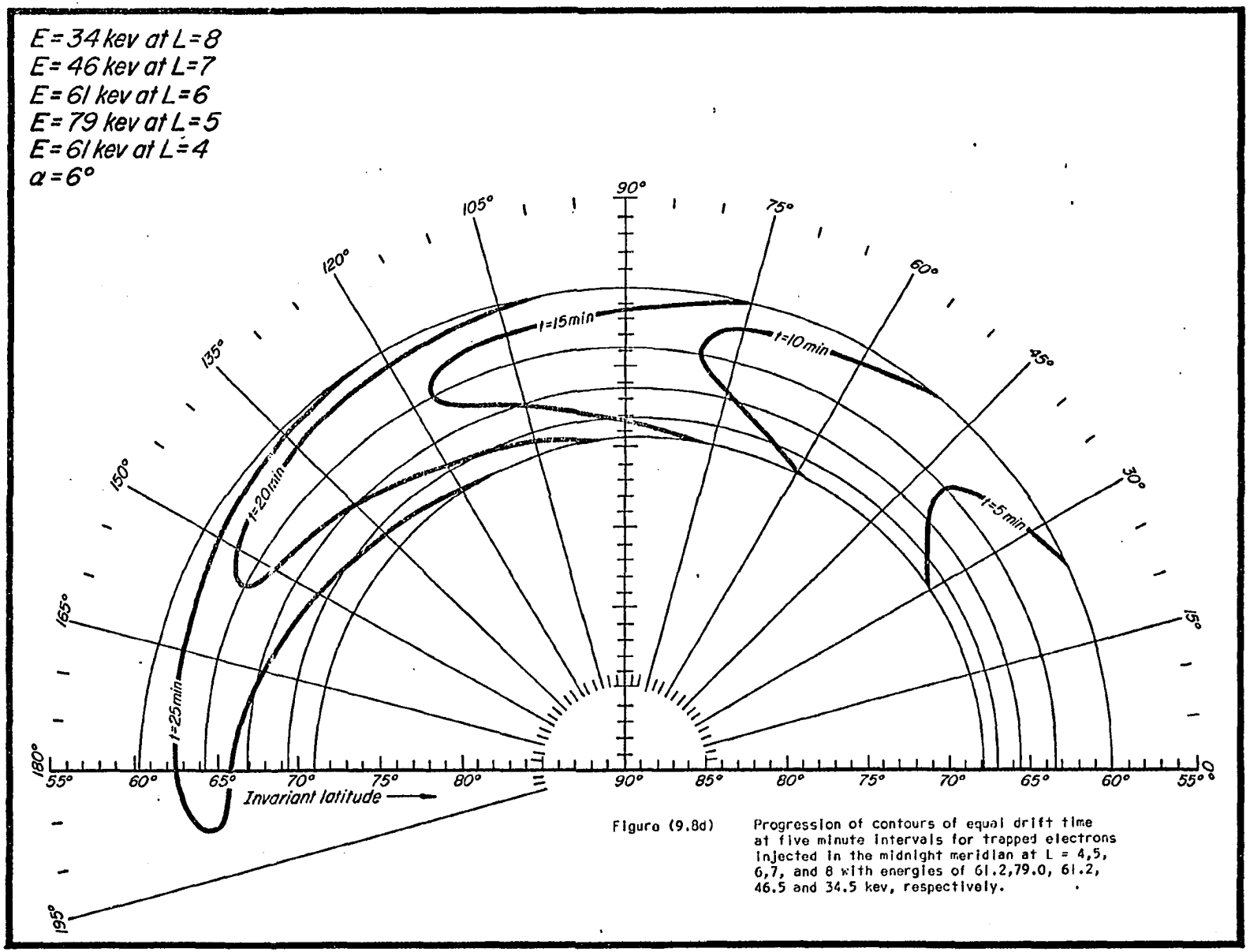

Figure (9.8d) Progression of contours of equal drift time at five minute intervals for trapped electrons injected in the midnight meridian at L = 4,5, 6,7, and 8 with energies of 61.2,79.0, 61.2, 46.5 and 34.5 kev, respectively.

The conclusion drawn here is in agreement with the results of Rosen (1969) (or Rosen and Winckler, 1970), who postulated a dribbling cloud model of electron precipitation. However, it was shown here that production region could be a line source in the midnight meridian whereas Rosen postulated a widespread production region, extending between the midnight and the 04^{h} meridian.

There is possibly an infinite combination of parameters such as pitch angle, energy, latitude or shape of injection source which could be made to account for the observations discussed here. No attempt was made to find more than one such combination as the purpose of this section was to show that the gradient and curvature drift can indeed account for the observations. Furthermore, the details pertaining to a precipitation mechanism have not been considered here; it has been tacitly assumed that such a mechanism could be found.

9.9 Summary and Conclusions

From a synoptic study of five substorms during the IQSY, it has been shown that auroral absorption expands away from a source region, which is located near the midnight sector, in both the eastward and westward directions. This result is consistent with previous studies of the longitudinal movement of absorption; however, a larger expansion rate than documented previously was found. Three factors distinguished the westward motion from the eastward motion: (1) occurrence at higher latitude; (2) lower drift rate, and; (3) no dispersion of the absorption with longitude. It was demonstrated that the westward expansion of the absorbing region occurs preferentially along the auroral oval; there was, however, some evidence to suggest that at the same time absorption may

drift westward along the auroral zone at possibly a higher rate. During the three substorms in which the westward motion along the oval was documented, drift rates varying from 48 km/min to 225 km/min were derived. These velocities are not inconsistent with the speed of the WTS observed by Akasofu et al. (1965).

For motion observed in the eastward direction, a drift rate for both the event onset and maximum was derived. It was shown that there was a differential drift rate, being greatest near L = 5.5 and smaller at both higher and lower latitudes. It was also found that the drift rate showed an asymmetry around the dawn meridian, being greater (∿9°/min or ∿425 km/min) in the midnight-dawn sector than in the dawn-noon sector (∿5°/min. or ∿240 km/min.). The drift rate in the midnight-dawn sector is consistent with the rate quoted by Akasofu (1968) for the propagation of the region in which the disintegration of arcs into patches occurs. Similarly, the drift rate of the absorption maximum is consistent with the drift rate of auroral patches in the morning sector (∿2°/min or ∿95 km/min). It was found that the eastward drift occurs at a nearly constant latitude, near that of the auroral zone maximum, which coincides with the auroral oval in the midnight-dawn sector and with the auroral zone in the dawn-dusk sector. It was shown that small events, in both magnitude and duration, occur near the poleward boundary of the region in which absorption occurs ($\lambda \simeq 70°$). These events seemed to move at the same rate as did the absorption maxima; they are assumed to be associated with the eastward propagating Ω bands identified by Akasofu (1964) from all-sky camera data.

The contour analysis suggests that there are two maxima in the longitudinal distribution of auroral absorption; one in the midnight sector, where the precipitation first occurs, and a second near the noon meridian. The noon maximum, although of greater duration, was observed to be of lesser intensity than the midnight maximum; however, this result may be biased due to the proximity of the midnight meridian to the Alaskan sector where an anomalously high frequency of occurrence and magnitude of absorption has been reported, relative to other longitudes (Waite, 1965; Rapoport, 1970). The results of the contour analysis also suggest that the secondary maxima often observed in the midnight sector approximately 2 hours after the onset of the substorm can be attributed to the electrons injected at the time of substorm onset. It is suggested that the energetic particles responsible for this precipitation are brought back into the midnight sector by the effect of gradient and curvature drift in the equatorial plane.

From a comparison of the observed drift rate of the precipitation events with the theoretical angular drift velocities of trapped electrons between the midnight and noon meridians, it was concluded that the observed precipitation drift rate could be accounted for by the gradient and curvature drift of trapped electrons with energies greater than about 25 kev. This implies that the precipitation mechanism moves with the same angular velocity as do the trapped electrons.

The nature of the absorption events observed to the west of the substorm origin (along the auroral oval) implies that proton drift is not sufficient to explain this precipitation; instead, the assumption

of a hydromagnetic mechanism or the application of an electric field are considered more likely explanations.

REFERENCES

Akasofu, S.-I., The development of the auroral substorm, Planet. Space Sci., 12, 273-282, 1964.

Akasofu, S.-I., D. S. Kimball and C.-I. Meng, Dynamics of the aurora-II; Westward travelling surges, J. Atmosph. Terr. Phys., 27, 173-187, 1965.

Akasofu, S.-I., D. S. Kimball and C.-I. Meng, Dynamics of the aurora-III; Westward drifting loops, J. Atmosph. Terr. Phys., 27, 189-196, 1965.

Akasofu, S.-I., C.-I. Meng and D. S. Kimball, Dynamics of the aurora-IV; Polar magnetic substorms and westward travelling surges, J. Atmosph. Terr. Phys., 28, 489-496, 1966.

Akasofu, S.-I., C.-I. Meng and D. S. Kimball, Dynamics of the Aurora-VI; Formation of patches and their eastward motion, J. Atmosph. Terr. Phys., 28, 505-511, 1966.

Akasofu, S.-I. and C.-I. Meng, Polar magnetic substorm in the evening sector, J. Atmosph. Terr. Phys., 29, 1127-1135, 1967.

Akasofu, S.-I., Polar and Magnetospheric Substorms, D. Reidel, Dordrecht, Holland, 1968.

American Radio Relay League, The ARRL Antenna Book, ARRL, 1968.

Ansari, Z. A., The spatial and temporal vibrations in high latitude cosmic noise absorption and their relation to luminous aurora, Scientific Report UAG-R138, Geophysical Institute, University of Alaska, 1963.

Ansari, Z. A., The aurorally associated absorption of cosmic noise at College, Alaska, J. Geophys. Res., 69, 4493, 1964.

Ansari, Z. A., A narrow-beam antenna array for radiowave absorption studies in the auroral zone, Proc. IEEE (Correspondence), 53, 530-532, 1965.

Appelton, E. V., R. Naismith and G. Builder, Ionospheric investigations in high latitudes, Nature, 132, 340, 1933.

Appelton, E. V., R. Naismith and L. J. Ingram, British radio ovservations during the second International Polar Year 1932-1933, Phil. Trans. Roy. Soc., A, 236, 191, 1937.

Barcus, J. R. and T. J. Rosenberg, Observations on the spatial structure of pulsating electron precipitation accompanying low frequency hydromagnetic disturbances in the auroral zone, J. Geophys. Res., 70, 1707, 1965.

Beach, R., G. R. Cresswell, T. N. Davis, T. J. Hallinan and L. R. Sweet, Flickering, A 10-cps fluctuation within bright auroras, Planet. Space Sci., 16, 1525-1529, 1968.

Berkey, F. T. and R. Parthasarathy, An investigation of selected types of radiowave absorption events in the auroral zone, Scientific Report, UAG-R151, Geophysical Institute, University of Alaska, 1964.

Berkey, F. T., Coordinated measurements of auroral absorption and luminosity using the narrow beam technique, J. Geophys. Res., 73, 319, 1968.

Brewersdorff, A., G. Kremser, W. Rielder and J. P. Legrand, Some properties of the slowly varying ionospheric absorption events in the auroral zone, Arkiv. Geofysik, 5, 115, 1967.

Broadfoot, A. L., Intensity of nitrogen band systems in faint aurora, Ph.D. Thesis, University of Saskatchewan, 1963.

Chamberlain, J. W., Physics of the Aurora and Airglow, Academic Press, New York, 1961.

Chapman, S. and J. Bartels, Geomagnetism, Clarendon Press, Oxford, 1940.

Cole, K. D., Eccentric dipole coordinates, Aust. J. Phys., 16, 423-429, 1963.

Cresswell, G. R., Fast temporal and spatial changes in auroras, Scientific Report, UAG R-206, Geophysical Institute, University of Alaska, 1968.

Cresswell, G. R., Flaming auroras, J. Atmosph. Terr. Phys., 31, 179-183, 1969.

Currie, B. W., Auroral heights over west-central Canada, Can. J. Phys., 33, 773-779, 1955.

Dicke, R. H., The measurement of thermal radiation at microwave frequencies, Rev. Sci. Instr. 17, 268-275, 1946.

Driatsky, V. M., Study of the space and time distribution of auroral absorption according to observations of the riometer network in the Arctic, Geomag. and Aeronomy, 6, 828, 1966.

Driatsky, V. M., On the drift of the auroral ionization, Geomag. and Aeronomy, 9, 398, 1969.

Driatsky, V. M. and O. I. Shumilov, Meridional movement of auroral absorption bays, Geomag. and Aeronomy, 10, 235, 1970.

Driatsky, V. M., O. I. Shumilov and A. V. Frank-Kamenetskiy, A drift model of auroral absorption, paper presented at International Symposium on Solar-Terrestrial Physics, Leningrad, May, 1970.

Dubatovko, O. Ye., M. I. Pudovkin and O. I. Shumilov, Some problems concerning auroral absorption, Geomag. and Aeronomy, 8, 240-243, 1968.

Eather, R. H. and F. Jacka, Auroral absorption of cosmic radio noise, Aust. J. Phys., 23, 170, 1966.

Eftestol, A. and A. Omholt, Studies on the excitation of N_2 and N_2^+ bands in aurora, Geophysica Norvegica, XXV, 1, 1966.

Evans, J. E., Newkirk, L. L. and B. M. McCormac, North polar, south polar, world maps and tables of invariant magnetic coordinates for six altitudes: 0, 100, 300, 600, 1000, and 3000 km (U), DASA 2347, Final Report, Lockheed Palo Alto Research Laboratory, 1969.

Evans, W. F. J. and A. Vallance-Jones, Some observations of type-B red aurora with a multichannel photometer, Can. J. Phys., 43, 697-704, 1965.

Feldstein, Y. I., Some problems concerning the morphology of auroras and magnetic disturbances at high latitudes, Geomag. and Aeronomy, 3, 183-192, 1963.

Feldstein, Y. I. and G. V. Starkov, Dynamics of auroral belt and polar geomagnetic disturbances, Planet. Space Sci., 15, 209-229, 1967.

Fritz, T. A., Energy spectral variations of electrons from 10 to 40 kev observed with satellite Injun 3 (abstract), Trans. Am. Geophys. Union, 47, 130, 1966.

Gadsen, M., Relative intensities of some nitrogen bands in auroral spectra, J. Atmosph. Terr. Phys., 22, 105-121, 1961.

Graf, K. A., A radio investigation of the structure of absorbing regions in the ionosphere, Thesis, University of Saskatchewan, 1960.

Gussow, D. W., R. J. Hunter, H. Korfage, and B. Pellant, Surface techniques, annotation and mapping programs for exploration, development and engineering, IBM Canada Laboratory, 1968.

Gustafsson, G., Spatial and temporal relations between auroral emission and cosmic noise absorption, Planet. Space Sci., 17, 1961-1975, 1969.

Gustafsson, G., A revised corrected geomagnetic coordinate system, Arkiv. for Geofysik, 5, 595-617, 1970.

Hakura, Y., Tables and maps of geomagnetic coordinates corrected by the higher order spherical harmonic terms, Rep. Ionosph. Space Phys., Japan, 19, 121, 1965.

Harang, L. and W. Bauer, Uber einen Nordlichtbogen in weniger als 80 km hohe uber der Erde, Gerl. Beitr. Geophys., 37, 109-115, 1932.

Harang, L., The luminosity curve of the aurorae, Geof. Publ. XVI, No. 6, 3, 1946.

Hargreaves, J. K. and F. C. Cowley, Studies of auroral radio absorption at three magnetic latitudes, I. Occurrence and statistical properties of the events, Planet. Space Sci., 15, 1571, 1967.

Hargreaves, J. K., Auroral motions observed with riometers: Movements between stations widely separated in longitude, J. Atmosph. Terr. Phys., 29, 1159, 1967.

Hargreaves, J. K., Auroral motions observed with riometers: latitudinal movements and a median global pattern, J. Atmosph. Terr. Phys., 30, 1461, 1968.

Hargreaves, J. K., Auroral absorption of HF radio waves in the ionosphere: A review of results from the first decade of riometry, Proc. IEEE, 57, 1348-1373, 1969.

Hartz, T. R. and N. M. Brice, The general pattern of auroral particle precipitation, Planet. Space Sci., 15, 301-329, 1967.

Heppner, J. P., E. C. Byrne, and A. E. Belon, The association of absorption and E_s ionization with aurora at high latitudes, J. Geophys. Res., 57, 121-134, 1952.

Holt, O. and A. Omholt, Auroral luminosity and absorption of cosmic radio noise, J. Atmosph. Terr. Phys., 24, 467, 1962.

Hones, E. W., Jr., Motion of charged particles trapped in the earth's magnetosphere, J. Geophys. Res., 68, 1209-1219, 1963.

Hook, J. L., Morphology of auroral zone radiowave absorption in the Alaska sector, J. Atmosph. Terr. Phys., 30, 1341, 1968.

Hultqvist, B., The geomagnetic field lines in higher approximation, Arkiv for Geofysik, 3, 63, 1958.

Hultqvist, B., Ionospheric absorption of cosmic radio noise, Space Sci. Rev., 3, 771-817, 1966.

Hunten, D. M., Some photometric observations of auroral spectra, J. Atmosph. Terr. Phys., 7, 141-151, 1955.

Jelly, D. and N. M. Brice, Changes in Van Allen radiation associated with polar substorms, J. Geophys. Res., 72, 1159, 1967.

Jelly, D., Apparent poleward motion of onsets of auroral absorption events, Can. J. Phys., 46, 33, 1968.

Johansen, O. E., Variations in energy spectrum of auroral electrons by simultaneous observation with photometer and riometer, Planet. and Space Sci., 13, 225, 1965.

Kavadas, J. W., Absorption measurements near the auroral zone, J. Atmosph. Terr. Phys., 23, 170, 1961.

Kraus, J. D., Antennas, McGraw-Hill, New York, 1950.

Lezniak, T. W. and J. R. Winckler, Experimental study of magnetospheric motions and the acceleration of energetic electrons during substorms, J. Geophys. Res., 7075-7097, 1970.

Little, C. G., High latitude ionospheric observations using extra-terrestrial radio waves, Proc. IRE (Correspondence), 42, 1700-1701, 1954.

Little, C. G. and H. Leinbach, Some measurements of high-latitude ionospheric absorption using extra-terrestrial radio waves, Proc. IRE, 46, 334-348, 1958.

Little, C. G. and H. Leinbach, The riometer - A device for the continuous measurement of ionospheric absorption, Proc. IRE, 47, 315-320, 1959.

Low, W., X-ray excitation of the second positive and first negative bands of nitrogen, J. Geophys. Res., 71, 1505, 1966.

Machin, K. E., M. Ryle and D. D. Vonberg, The design of an equipment for measuring small radio-frequency noise powers, Proc. IRE, 99, pt. 3, 127, 1952.

Maggs, J. E. and T. N. Davis, Measurements of the thickness of auroral structures, Planet. Space Sci., 205-209, 1968.

Major, G., The association of pulsating and flaming auroras with complete ionospheric absorption at Macquarie Island, Aus. J. Phys., 7, 471-476, 1954.

Malville, J. M., Type B aurorae in the Antarctic, J. Atmos. Terr. Phys., 16, 59-66, 1959.

Mayuad, P. N., Un nouveau systeme de coordonnees magnetiques pour l'etude de la haute atmosphere: les coordonnees de l'anneau equatorial, Ann. Geophys., 16, 278, 1960.

McIlwain, C. E., Direct measurement of particles producing visible auroras, J. Geophys. Res., 65, 2727-2747, 1960.

Mead, G. D., Deformation of the geomagnetic field by the solar wind, J. Geophys. Res., 69, 1181-1195, 1964.

Meng, C.-I., Polar magnetic and auroral substorms, M.S. Thesis, University of Alaska, 1965.

Meng, C.-I. and S.-I. Akasofu, Intense negative bays inside the auroral zone-II: indented positive bay, J. Atmosph. Terr. Phys., 29, 1305-1310, 1967.

Montbriand, L. E. J., Morphology of auroral hydrogen emissions during auroral substorms, Ph.D. Thesis, University of Saskatoon, 1969.

Moore, J. G., Lifetimes and heights of $O(^1S)$ in pulsating aurora, Planet. Space Sci., 19, 119-124, 1971.

Nash, R. T., Beam efficiency limitations of large antennas, IEEE Trans. Military Electron, MIL-8, 252-257, 1964.

Ortner, J. and A. F. Moore, Substorm events, Proceedings of an ESRO Colloquium held in Kiruna Sweden, March 1969, ESRO SP-38, September 1969.

Ospiv, N. K., N. B. Pivovarova and V. G. Pivovarov, Determination of electron fluxes in polar regions from synchronous photometric and riometric observations, Geomag. and Aeronomy, 8 , 844-847, 1968.

Parthasarathy, R. and V. P. Hessler, Periodic covariance of radiowave absorption, earth currents, and other associated phenomena in the auroral zone, J. Geophys. Res., 69, 2867, 1964.

Parthsarathy, R. and F. T. Berkey, Multiple-frequency investigations of radio wave absorption during the dawn breakup phase of auroras, Radio Sci., 69D, 415, 1965.

Parthasarathy, R. and G. C. Reid, Magnetospheric activity and its consequences in the auroral zone, Planet. Space Sci., 15, 917, 1967.

Rapoport, Z. A., Comparison of the variability of auroral radio wave absorption in the ionosphere at College and Loparskaya, Geomag. and Aeronomy, 10, 58, 1970.

Rees, M. H., Note on the penetration of energetic electrons into earth's atmosphere, Planet. Space Sci., 12, 722, 1964.

Reid, G. C. and R. Parthasarathy, Ionospheric effects of energetic electron bursts in the tail of the magnetosphere, J. Geophys. Res., 71, 3267, 1966.

Reid, J., Private communication, 1970.

Roederer, J. G., On the adiabatic motion of energetic particles in a model magnetosphere, J. Geophys. Res., 72, 981-992, 1967.

Roederer, J. G., Quantitative models of the magnetosphere, Rev. of Geophys., 7, 77-96, 1969.

Roederer, J. G., Dynamics of Geomagnetically Trapped Radiation, Springer-Verlag, New York, 1970.

Romick, G. J. and A. E. Belon, The spatial variation of auroral luminosity, II. Determination of volume emission rate profiles, Planet. Space Sci., 15, 1695-1710, 1967.

Rosen, L. H. and J. R. Winckler, Evidence for the large-scale azimuthal drift of electron precipitation during magnetospheric substorms, J. Geophys. Res., 75, 5576-5581, 1970.

Shemansky, D. E., Excitation of the N_2 first positive system in the aurora, Ph.D. Thesis, University of Saskatchewan, 1966.

Shemansky, D. E. and A. Vallance-Jones, Type-B red aurora; the O_2^+ first negative system and the N_2 first positive system, Planet. Space Sci., 16, 1115-1130, 1968.

Starkov, G. V. and Y. I. Feldstein, Change in the boundaries of the oval auroral zone, Geomag. and Aeronomy, 7, 48, 1967.

Sterling, T. D. and S. V. Pollack, Introduction to Statistical Data Processing, Prentice-Hall, Englewood Cliffs, 1968.

Størmer, C., The Polar Aurora, Clarendon Press, Oxford, 1955.

Taylor, H. E. and E. W. Hones, Jr., Adiabatic motion of auroral particles in a model of the electric and magnetic fields surrounding the earth, J. Geophys. Res., 70, 3605-3628, 1965.

Taylor, H. E., Adiabatic motion of outer-zone particles in a model of the geoelectric and geomagnetic fields, J. Geophys. Res., 71, 5135-5147, 1966.

Uda, S. and Y. Mushiake, Yagi-Uda Antenna, Sasaki, Sendai, 1954.

Vallance-Jones, A., Optical Measurements of Auroras, in Auroral Phenomena, Experiments and Theory, ed. Martin Walt, Stanford Univ. Press, 1965.

Waite, C. W., Auroral phenomena in an integral-invariant coordinate system, Can. J. Phys., 43, 2319-2330, 1965.

Williams, D. J. and G. D. Mead, Night-side magnetospheric configuration as obtained from trapped electrons at 1100 kilometers, J. Geophys. Res., 70, 3017-3029, 1965.

Wilson, C. R., Auroral infrasonic and ionospheric absorption substorms, J. Atmosph. Terr. Phys., 32, 293-301, 1970.

APPENDIX A

In the following tabulation, the values DB(2), DB(3) and DB(4) represent the attenuation necessary in each pair of rows of the 6 x 8 array (beginning with rows 3 and 6) to produce the sidelobe level given in Column 1. The resistance values RR1(2), RR3(2), etc., are the values of resistance which comprise symmetrical-pi attenuators for the given value of attenuation.

```
=  75.80 76.11 70.47 70.70 68.62 81.46 72.3

=  83.77 73.50 80.4 65. 150. 67.9 156.7
```

DIXSON

73.5001	80.4001		
73.7467	78.383	67.9	156.7
73.5851	78.4659	67.7501	156.7
73.592	78.7714	67.7501	156.95
73.5988	79.077	67.7501	157.2
73.6057	79.3826	67.7501	157.45
73.6126	79.6882	67.7501	157.7
73.6194	79.9936	67.7501	157.95
73.6262	80.2994	67.7501	158.2
73.6262	80.2994	67.7501	158.2
73.6262	80.2994	67.7501	158.2
73.6262	80.2994	67.7501	158.2
73.6262	80.2994	67.7501	158.2
73.6262	80.2994	67.7501	158.2
73.6262	80.2994	67.7501	158.2

```
←  #

←  SUBR IV

←  LI

          SUBR IV
          N=0
          ACCE A,B,C,D,AA,BB,CC
          ACCE DD,X,XX,SX,SY,XM,ML
          TYPE X,XX
     10   PH=(XM-SX)/5
     11   BE=(ML-SY)/10
          N=N+1
          IF (N-15) 12,2,2
     12   CONT
          FA=C+PH*(A-C)+BE*(D-C)+PH*BE*(B+C-A-D)
          FB=CC+PH*(AA-CC)+BE*(DD-CC)+PH*BE*(BB+CC-AA-DD)
          TYPE FA,FB,XM,ML
          IF (((FA-X)**2)-.225E-01) 5,5,50
     50   IF (FA-X) 20,5,30
     20   XM=XM+.25
          GO 10
     30   XM=XM-.15
          GO 10
      5   IF (((FB-XX)**2)-.225E-01) 10,2,60
     60   IF (FB-XX) 40,2,80
     40   ML=ML+.25
          GO 11
     80   ML=ML-.15
          GO 11
      2   CONT
          END

←  #

←  #

←  THE ABOVE LISTING IS THE THIRD VERSION (MOD III) OF TH
? IV
←  THE PROGRAM

?
←
```

APPENDIX B

The Tables of invariant latitude and longitude derived by Evans et al (1969) were found to be exceedingly cumbersome, if not impossible, to utilize with any degree of ease. The algorithm described in this Appendix resulted from an effort to use these Tables as the basis for the calculation of invariant coordinates.

The algorithm does an interpolation onto the geographic coordinates of the point in question, deriving the invariant coordinates from a first order estimate of the geomagnetic coordinates. The input parameters (A,AA), (B,BB), (C,CC) and (D,DD) are the geographic latitude and longitude of the points in the tabulation within which the point (X,XX) (whose invariant coordinates are to be derived) falls. The parameters SX and SY are the bounding values of latitude and longitude which pass through the points C, D and AA,DD, respectively. The quantities (XM,ML) are first order estimates of the invariant coordinates, for example the centered dipole coordinates of the point in question. The number of interpolations and the degree of accuracy are arbitrary parameters left to the user.

```
CSECT       BOASLOG     006FE8    006FE8
  ENTRY     ALOG10      006FF0
  ENTRY     ALOG        00700A

CSECT       BOAFIOCS    0070F8    0070F8
  ENTRY     RCBORG=     007710
  ENTRY     BUFORG=     00770C
  ENTRY     FIOCS=      0070F8
* ENTRY     FIOCD=      007132
* ENTRY     VDIOCS=     007714

CSECT       BOAUOPT     007738    007738
  ENTRY     USEROPT     007738

CSECT       BOAUNITB    007740    007740
  ENTRY     UNITAB=     007740

CSECT       BOASEXP     0077C8    0077C8
  ENTRY     EXP         0077CC
```

```
LINKAGE EDITOR HIGHEST SEVERITY WAS 0
```

// EXEC	B(2)	DB(2)	RR1(2)	RR3(2)	B(3)	DB(3)	RR1(3)	RR3(3)	B(4)	DB(4)	RR1(4)	RR3(4)
15	1.100	0.828	162.236	4.771	1.342	2.553	93.544	14.906	1.032	0.271	283.289	1.558
16	1.108	0.893	156.220	5.149	1.374	2.759	90.180	16.153	1.153	1.235	133.070	7.131
17	1.117	0.959	150.813	5.529	1.407	2.968	87.174	17.419	1.282	2.158	101.333	12.551
18	1.125	1.025	145.888	5.914	1.442	3.179	84.461	18.709	1.420	3.046	86.127	17.898
19	1.134	1.091	141.421	6.299	1.477	3.390	82.017	20.016	1.567	3.901	77.045	23.218
20	1.143	1.158	137.346	6.685	1.514	3.603	79.805	21.340	1.723	4.724	70.999	28.557
21	1.151	1.224	133.608	7.072	1.552	3.816	77.795	22.679	1.888	5.520	66.708	33.955
22	1.160	1.291	130.174	7.458	1.590	4.029	75.966	24.033	2.062	6.288	63.535	39.439
23	1.169	1.357	127.005	7.844	1.630	4.242	74.296	25.399	2.247	7.031	61.118	45.037
24	1.179	1.423	124.076	8.229	1.670	4.454	72.770	26.777	2.440	7.749	59.236	50.766
25	1.187	1.489	121.359	8.612	1.711	4.666	71.369	28.167	2.645	9.447	57.743	56.659
26	1.196	1.554	118.841	8.993	1.753	4.875	70.086	29.563	2.858	9.121	56.547	62.701
27	1.205	1.618	116.499	9.371	1.796	5.084	68.907	30.965	3.081	9.775	55.576	68.918
28	1.214	1.683	114.310	9.746	1.839	5.291	67.820	32.377	3.315	10.409	54.778	75.329
29	1.223	1.746	112.269	10.118	1.883	5.496	66.819	33.791	3.558	11.024	54.119	81.923
30	1.231	1.808	110.363	10.486	1.927	5.698	65.897	35.206	3.810	11.619	53.571	88.698
31	1.240	1.870	108.575	10.850	1.972	5.899	65.043	36.626	4.073	12.198	53.111	95.678
32	1.249	1.932	106.893	11.212	2.018	6.097	64.251	38.050	4.345	12.760	52.722	102.878
33	1.258	1.992	105.319	11.567	2.063	6.292	63.520	39.470	4.626	13.304	52.394	110.249
34	1.266	2.052	103.828	11.920	2.110	6.485	62.838	40.897	4.918	13.836	52.112	117.862
35	1.275	2.110	102.436	12.266	2.156	6.674	62.211	42.311	5.216	14.347	51.873	125.611
36	1.283	2.168	101.113	12.609	2.203	6.861	61.623	43.731	5.525	14.847	51.666	133.603
37	1.292	2.225	99.857	12.949	2.251	7.046	61.073	45.157	5.845	15.335	51.486	141.842
38	1.300	2.281	98.685	13.280	2.298	7.224	60.567	46.561	6.169	15.804	51.332	150.162
39	1.309	2.336	97.571	13.608	2.345	7.403	60.094	47.965	6.501	16.260	51.197	158.687
40	1.317	2.390	96.516	13.930	2.392	7.577	59.653	49.362	6.842	16.703	51.080	167.389
41	1.325	2.442	95.519	14.246	2.440	7.747	59.241	50.749	7.188	17.133	50.977	176.231
42	1.333	2.494	94.572	14.556	2.487	7.914	58.857	52.129	7.542	17.550	50.887	185.235
43	1.340	2.545	93.676	14.860	2.534	8.077	58.498	53.494	7.900	17.953	50.808	194.345
44	1.348	2.595	92.819	15.161	2.582	8.238	58.160	54.860	8.268	18.348	50.737	203.667
45	1.356	2.644	92.010	15.456	2.629	8.395	57.845	56.205	8.638	18.728	50.675	213.047
46	1.363	2.692	91.235	15.744	2.676	8.549	57.548	57.547	9.015	19.099	50.619	222.599
47	1.371	2.739	90.499	16.027	2.722	8.699	57.270	58.874	9.396	19.459	50.570	232.239
48	1.378	2.785	89.789	16.309	2.769	8.848	57.006	60.208	9.787	19.813	50.525	242.116
49	1.386	2.837	89.018	16.624	2.823	9.014	56.723	61.715	10.238	20.205	50.479	253.518
50	1.393	2.879	88.407	16.860	2.867	9.149	56.502	62.957	10.618	20.521	50.445	263.091

```
/&
IA58I   CUU  RW  RR  RN  PW  PR  PN
IA59I   181   1   0   0   0   0   0
```

APPENDIX C

The Roederer version of the Mead-Williams computer code had to be modified to a limited extent to obtain electron drift times and velocities as a function of longitude and energy. The subroutines in which these modifications were made are contained in this appendix. Subroutine DTIME is part of the original program; subroutine BERK is a subroutine added by the author.

```
UOS FORTRAN IV 360N-FO-479 3-1          DTIME              DATE   02/22/71     TIME    21.55.00       PAGE 0001

 0001                SUBROUTINE DTIME(RMIR,VM1,VM2,VM4,ENDV3,DR,ER2,ERR9,ERRI,RILIM,CHE
                    1CK,TAU,X)
                C
                C     COMPUTE DRIFT TIME BETWEEN LONG VM3 AND ENDV3 (IN RADIANS) OF A
                C     PARTICLE MIRRORING AT VM1,VM2,VM3. RETURNS MIRROR COORDINATES AT
                C     END LONG.
                C
                C     SUBROUTINE MODIFIED TO CALL SUBROUTINE BERK WHICH CALCULATES DRIFT
                C     PERIODS USING TAUI AND DTAU VALUES DERIVED HERE.
                C
 0002                COMMON /CONST/PAD,RADIN
 0003                COMMON/ENER/INT,IMAX,BETA(23),GAM(23),E(23),TIME(15,23),DRATE(15,2
                    1X3),PLAT(15),PLONG(15)
 0004                COMMON FRONT,SHEET1,SHEET2,FSHEET
 0005                DIMENSION TAUI(15),DTAU(15)
 0006                COMMON V(200),VI1(200),VM2(200),VM3(200),ARC(200),VNEAR(3),VBO(3),   0   3
                    1VSAVE(3),KK,KNEAR,JUP,VRM
 0007                COMMON VCOMJ(3),XLD
 0008                DIMENSION V01(12),V02(12),V03(12),VMM(18)
 0009                DO 9 I=1,IMT
 0010                TAUI(I)=0.
 0011              9 DTAU(I)=0.
 0012                TAUI(INT+1)=0.
 0013                CHECK=0.
 0014                VM3=VM4
 0015                FNT=INT
 0016                M=INT
 0017                DV=(ENDV3-VM3)/FMT
 0018                IF(ABS(DV).LT.0.01)GO TO 30
 0019                CALL DRIFT(RMIR,VM1,VM2,VM3,DR,ERR,RILIM,SPEED1,BOUNCE,FIM)
 0020             10 VM3=VM3+DV
 0021                CALL SEARCH(VM1,VM2,VM3,RMIR,FIM,BB,FI,ER2,ERR9,ERRI,CHECK)
 0022                IF(CHECK.GT.0.5)GO TO 20
 0023                CALL DRIFT(RMIR,VSAVE(1),VSAVE(2),VM3,DR,ERR,RILIM,SPEED2,BOUNCE,F
                    1IM)
 0024                DTAU(M)=(VM1+VSAVE(1))/(SPEED1+SPEED2)*DV
 0025                TAUI(M)=TAUI(M+1) + DTAU(M)
 0026                VMM(M)=VM3*RAD
 0027                SPEED1=SPEED2
 0028                VM1=VSAVE(1)
 0029                VM2=VSAVE(2)
 0030                V01(M)=VSAVE(1)
 0031                V02(M)=VSAVE(2)
 0032                V03(M)=VM3
 0033                TAU=TAUI(1)
 0034                J=(INT+1) - M
 0035                IF(J.EQ.6) WRITE(15,101)
 0036                IF(M .LE. 1) GO TO 30
 0037                M=M-1
 0038                GO TO 10
 0039             20 VM3=VM3*RAD
 0040                WRITE(3,100) VM3
 0041                RETURN
 0042             30 L=INT
```

```
DOS FORTRAN IV 360N-FO-479 3-1          DTIME              DATE  02/22/71      TIME    21.55.00      PAGE 0002

0043          40    CALL INSECT(VQ1(L),VQ2(L),VQ3(L),ERR,1)
0044                PLAT(L)=ABS(90.-(VCONJ(2)*RAD))
0045                PLONG(L)=VCONJ(3)*RAD
0046                IF(L.EQ.1) GO TO 50
0047                L=L-1
0048                GO TO 40
0049          50    CALL PERM(PLAT,PLONG,VQ3,VMN,TAUI,DV,K)
0050                RETURN
0051          101   FORMAT(1X,'PROGRAM DOING LONG ITERATIONS, JOB RUNNING NORMALLY')
0052          100   FORMAT(1H0,5X,42HPARTICLE LEFT TRAPPING REGION AT F10.2, 11H DEG. L
                    1ONG.)
0053                END
```

```
OOS FORTRAN IV 360N-FO-470 3-1          BERK              DATE   02/22/71      TIME    21.55.44      PAGE 0001

0001            SUBROUTINE BERK(VM1,VM2,VM3,VM4,TAUI,DV,K)
                C
                C     IN THIS SUBROUTINE, THE DRIFT PERIOD TO VARIOUS LONGITUDES IS
                C     CALCULATED USING TAUI AND DTAU.  THE LONGITUDE AND LATITUDE OF
                C     FIELD LINE INTERSECTIONS IS ALSO COMPUTED.  THE SUBROUTINE CALLS
                C     THE SUBROUTINE EDIT TO ALLOW FOR STORAGE OF DATA ON TAPE.
                C
0002                COMMON /PRINTV/ SALT,SLA1,SLONG,PITCH,AS,ELS,SE24,SEVL,AMIR,ELVAL,
                   1EVEVAL,ERMIN1,ERMIN2,V2MIN1,V2MIN2,RMIN1,RMIN2,TAU,NOTAU,NTREE,VM,
                   2L1MIN,LMIN2,KMAX
0003                COMMON /CONST/PAI,RADIN
0004                COMMON/ENER/IPI,VMAX,BETA(24),GAM(24),E(24),TIME(15,23),ORATE(15,2
                   X3),PLST(15),PLONG(15)
0005                DIMENSION V1I(15),V2I(15),VM3(15),VM4(15),TAUI(15),DTAU(15)
0006                TAUI(1,1) =0.
0007                DV=DV*PAI
0008                DO 40 M=1,INT
0009                DO 40 N=1,24
0010                GAM=(1./(BETA(N)*GA3(N)))
0011                FAC=((7.566E03*GAM)/60.)
0012                IPI(M,N) =(ABS((TAUI(1)) - TAUI(M+1)))*FAC)
0013           40   ORATE(M,N) =(DV*( 1))/IPI(M,N)
0014                DO 45 J=1,INT
0015                VM1(J)=VM1(J) + SLONG
0016           45   VM4(J)=VM4(J) + 1%. + SLONG
0017                PRINT 100
0018                PRINT 104, (VM4(J),J=1,INT)
0019                WRITE(3,101) (E(N),(TIME(M,N),M=1,INT),N=1,23)
0020                PRINT 103
0021                PRINT 104, (VM4(J),J=1,INT)
0022                WRITE(3,101) (E(N),(ORATE(M,N),M=1,INT),N=1,23)
0023                PRINT 105
0024                PRINT 102,((VM1(KT),KT=1,INT),(VM2(KT),KT=1,INT))
0025                CALL EDIT(4,K)
0026           100  FORMAT('0',37X,'DRIFT PERIOD (IN MINUTES) OF ELECTRONS IN EQUATORI
                   XAL PLANE')
0027           101  FORMAT(3X,F7.2,12F9.3)
0028           102  FORMAT(1X,12E10.3/1X,12E10.3,//)
0029           103  FORMAT('1',37X,'DRIFT VELOCITY (DEGREES/MINUTE) OF ELECTRONS')
0030           104  FORMAT(5X,'KEV',2X,12F9.2,//)
0031           105  FORMAT('0',20X,'LATITUDE AND LONGITUDE OF FIELD LINE INTERSECTION
                   XWITH THE EARTH',/)
0032                RETURN
0033                END
```

APPENDIX D

The compilation of data graphs contained in this Appendix comprises an atlas of events for the winter of 1966-1967. For the sake of continuity and completeness, some of the events described in Chapter 4 are reproduced again here. It is hoped that the reproduction of the entire set of observations will prove to be useful to other investigators who gathered data during that period.